




**7<sup>th</sup> South African Conference on Photonic Materials**

**27 - 31 March 2017**

**Amanzi Game Reserve, South Africa**



**Programme and Abstracts**

TIME	Monday	Tuesday	Wednesday	Thursday	Friday	
7:00 to 8:00		BREAKFAST (Conference Hall)	BREAKFAST (Conference Hall)	BREAKFAST (Conference Hall)	BREAKFAST (Conference Hall)	
		Chair: Nel	Chair: Vorster	Chair: Vinod Kumar		
8:00 to 8:20		INVITED 1: Ashutosh Tiwari	INVITED 4: Susanne Siebentritt	INVITED 8: S. J. Dhoble	<b>Booking out &amp; Departure</b>	
8:20 to 8:40						
8:40 to 9:00		Oral 1: J. A. A. Engelbrecht	Oral 9: Vinod Kumar	Oral 20: Vinay Kumar		
9:00 to 9:20		Oral 2: R. A. Harris	Oral 10: R. M. Dix-Peek	Oral 21: P. P. Mokoena		
9:20 to 9:40		Oral 3: Eric N. Maluta	Oral 11: Edward Lee	Oral 22: Ashwini Kumar		
9:40 to 10:00		INVITED 2: Peter Deák	INVITED 5: Vladimir Dyakonov	INVITED 9: Lucas C. V. Rodrigues	10:00 to 10:20	
10:00 to 10:20						
10:20 to 10:40		TEA (Conference Hall)	TEA (Conference Hall)	TEA (Conference Hall)	10:20 to 10:40	
		Chair: Ntwaeaborwa	Chair: van Dyk			
10:40 to 11:00		INVITED 3: David J. Rogers	INVITED 6: Vladimir Kolkovsky	 <b>POSTER SESSION B:</b> <b>posters 39 - 74</b> (Conference Hall upstairs)	10:40 to 11:00	
11:00 to 11:20					11:00 to 11:20	
11:20 to 11:40		Oral 4: Trilok K. Pathak	Oral 12: Matshisa J. Legodi		11:20 to 11:40	
11:40 to 12:00		Oral 5: Katekani Shingange	Oral 13: Joachim Bollmann		11:40 to 12:00	
12:00 to 12:20		Oral 6: Vijay Kumar	Oral 14: Ivan G. Ivanov		12:00 to 12:20	
12:20 to 12:40		Oral 7: Jitendra Sharma	Oral 15: D. D. Ramteke	12:20 to 12:40		
12:40 to 13:00		Oral 8: V. Craciun	Oral 16: Muburak Y. A. Yagoub	CONFERENCE PHOTO	12:40 to 13:00	
13:00 to 14:00		LUNCH (Conference Hall)	LUNCH (Conference Hall)	LUNCH (Conference Hall)	13:00 to 14:00	
			Chair: Venter	Chair: Swart		
14:00 to 14:20	<b>Arrival &amp; Registration</b>  (settle in to accommodation)	<b>POSTER SESSION A:</b> <b>posters 1 - 38</b>  (Conference Hall upstairs)	INVITED 7: Martin Geller	INVITED 10: Philippe F. Smet	14:00 to 14:20	
14:20 to 14:40					14:20 to 14:40	
14:40 to 15:00				Oral 17: Magnus C. Wagener	Oral 23: Vishal Sharma	14:40 to 15:00
15:00 to 15:20				Oral 18: M. E. Lee	Oral 24: Jorma Hölsä	15:00 to 15:20
15:20 to 15:40			Oral 19: P. O. Holtz	Oral 25: Iorkyaa Ahemen	15:20 to 15:40	
15:40 to 16:00			TEA (Conference Hall)	TEA (Conference Hall)	15:40 to 16:00	
16:00 to 16:30			GAME DRIVE (option 1)	GAME DRIVE (option 2)	(free time)	16:00 to 16:30
16:30 to 17:00						
17:00 to 17:30						17:00 to 17:30
17:30 to 18:00					17:30 to 18:00	
18:00 to 20:30	WELCOME DINNER (Wild Olive Restaurant)	DINNER (Mountain Lodge)	DINNER (Boma)	CONFERENCE DINNER (Mountain Lodge)	18:00 to 20:30	

# Table of Contents

Organising Committee .....	ii
List of Sponsors .....	ii
Message from SAIP President.....	iii
Invited Speakers.....	iv
Ashutosh Tiwari .....	iv
Peter Deák.....	v
David Rogers.....	v
Susanne Siebentritt .....	vi
Vladimir Dyakonov.....	vi
Vladimir Kolkovsky .....	vii
Martin Geller .....	vii
Sanjay J. Dhoble .....	viii
Lucas C. V. Rodrigues.....	ix
Philippe Smet .....	ix
Programme Overview .....	xi
Scientific Programme and Abstracts.....	1
Tuesday 28 March .....	1
Wednesday 29 March .....	13
Thursday 30 March .....	29
Posters .....	39
Abstract number index.....	117

## Organizing Committee

Prof Danie Auret	UP	Sponsors
Prof Reinhart Botha	NMMU	Proceedings guest co-editor
Prof Japie Engelbrecht	NMMU	NRF KIC grant application, sponsors
Dr Richard Harris	UFS	Accompanying persons programme
Mr Johan Janse van Rensburg	UP	Website
Prof Ted Kroon (Chairperson)	UFS	Proceedings guest co-editor, Venue, Accommodation, Registrations, Programme book, Finances
Mr Matshisa Legodi	UP	Website
Prof Walter Meyer	UP	Sponsors, Finances
Dr Jackie Nel	UP	Proceedings guest co-editor
Prof Martin Ntwaeaborwa	UFS	Conference bags, Transport
Prof Hendrik Swart	UFS	Invited speakers liaison & gifts, Finances
Prof Koos Terblans	UFS	On-site Registration, Computers and audiovisual equipment, WIFI, Poster boards
Prof Ernest van Dyk	NMMU	Sponsors, Finances
Prof Andre Venter	NMMU	Abstract review (convenor)
Dr Freddie Vorster	NMMU	Sponsors

**NMMU:** Nelson Mandela Metropolitan University **UFS:** University of the Free State **UP:** University of Pretoria

The committee was assisted by the Office of the South African Institute of Physics, particularly Mr Brian Masara (logistics and finances) as well as Mr Juan Grey (IT support).

## Sponsors

National Research Foundation: Knowledge, Interchange and Collaboration – KIC (Local Events support grant 105353)	<a href="http://www.nrf.ac.za">www.nrf.ac.za</a>
Exhibitor: Chemetrix	<a href="http://www.chemetrix.co.za">www.chemetrix.co.za</a>
Exhibitor: Comtest	<a href="http://www.comtest.co.za">www.comtest.co.za</a>
Advertiser: Horiba	<a href="http://www.horiba.com">www.horiba.com</a>
Advertiser: Hitech Lasers	<a href="http://www.hitechlasers.co.za">www.hitechlasers.co.za</a>
Poster session sponsor: Vacutec	<a href="http://www.vacutec.co.za">www.vacutec.co.za</a>
Sponsor: Dean of the Faculty of Science and Agriculture, University of the Free State	<a href="http://www.ufs.ac.za/natagri">www.ufs.ac.za/natagri</a>
Sponsor: Dean of the Faculty of Science, Nelson Mandela Metropolitan University	<a href="http://science.nmmu.ac.za">science.nmmu.ac.za</a>
Selected prizes: International Association of Advanced Materials	<a href="http://www.iaaonline.org">www.iaaonline.org</a>

## Message from the SAIP President

Dear colleagues and the international photonic materials community:

The forthcoming 7<sup>th</sup> South African Conference on Photonic Materials will be held from 27 to 31 March, 2017 in Amanzi Private Game Reserve, South Africa. I am delighted to welcome you for what is sure to be an exciting week of oral and poster presentations as well as discussions on the current issues related to photonic materials. This year's conference follows on the success of six previous conferences in the series. The chosen venue for this year's conference is at a new and unique location.

South African Institute of Physics (SAIP) is proud of this initiative by the Division for Physics of Condensed Matter and Materials and the Applied Physics Forum to host this excellent conference series. This falls within SAIP's strategy which encourages and supports Divisions and Forums to organize their activities outside the annual SAIP Conference.

Photonics as the science of light is a challenging and very productive research field. It underpins technologies of daily life: consumer electronics, telecommunications, health manufacturing industry, defense and security, entertainment, etc. All around the world, scientists, engineers and technicians perform cutting edge research surrounding the field of Photonics. South African researchers are playing an active leading role in the photonics and photonic materials research.

I am excited by the prospect of more interactions between the local and international delegates. I also encourage students to take this opportunity to interact with our international delegates. This will ensure sustainable capacity development within SAIP's Division for Physics of Condensed Matter and Materials, the Applied Physics Forum, and the Photonics Division.

On behalf of the South African Institute of Physics, it is my honour to welcome you to this momentous event. I am confident that with the help of your contributions and participation, it will be an unforgettable experience.

Azwinndini Muronga  
SAIP President

## Invited Speakers



Ashutosh Tiwari

*Linköping University (Sweden) and Tekidag AB*

### **“Programmable bioelectronic devices and systems” (p. 2)**

Prof Ashutosh Tiwari is Chairman and Managing Director of Tekidag AB (AAA Innotech); Associate Professor and Group Leader, Smart Materials and Biodevices at the world premier Biosensors and Bioelectronics Centre, Linköping University; Director, Vinoba Bhave Research Institute; Editor-in-Chief, Advanced Materials Letters and Advanced Materials Proceedings;

Secretary General, International Association of Advanced Materials; a materials chemist and docent in the Applied Physics with the specialisation of Biosensors and Bioelectronics from Linköping University, Sweden. Dr. Tiwari has several honorary and visiting positions worldwide including visiting professor at the National Institute for Materials Science, Japan; University of Jinan, University of Jiangsu, China; and DCR University of Science and Technology, and Chairman (Academics) of Dr. G. P. Law College, India. Just after completed his PhD, he joined as young scientist at National Physical Laboratory, India and later moved to University of Wisconsin, USA for postdoctoral research. He obtained various prestigious fellowships including Marie Curie, The European Commission; JSPS (regular and bridge fellow), Japan; SI, Sweden; and from INSA, CSIR & DST, India. His research focus is on the design and advanced applications of cutting edge stimuli-responsive materials for smart biodevices. He is actively involved in the undergraduate, post graduate and PhD teaching in the field of intelligent materials, nanomaterials and atom-thick materials for biomedical, biosensing and bioenergy devices. Dr. Tiwari is recipient of prestigious ‘The Nano Award’, ‘Innovation in Materials Science Award’ and ‘Advanced Materials Medal’ for his notable contributions to smart materials and biomedical nanotechnology. He has more than 300 peer-reviewed publications in the field of materials science and nanotechnology with h-index of 33. He has edited/authored over 40 books on advanced materials and technology for esteemed publishers in USA. He is the editor of the Advanced Materials series that is published by Scrivener Publishing and co-published with John Wiley & Sons; and a founder member and chair of Advanced Materials World Congress, American Advanced Materials Congress, European Advanced Materials Congress, Asian Advanced Materials Congress, Smart materials and surfaces, Smart Energy Technologies, European, American, Asian and Global Graphene Forum and World Technology Forum famous international events of materials science and technology and also bilateral events such as Sweden-Japan Nano, Indo-Swedish Advanced Materials Forum, etc. Prof. Tiwari serves as scientific evaluator and member of panels of experts to various governmental and non-governmental agencies; member of PhD committee, and have been invited for plenary, keynote and invited lectures in the more than 20 countries. His current research on zipper-like bioelectronics, nanobioreactors, programmable super-thin bioelectronics, smart theranostics, and affinity/MIP surfaces realised by the integration of smart architecting has emerged as a versatile platform for building a new age technological outlets to tackle key challenges in medical, energy supply and environmental issues.



**Peter Deák**

*University of Bremen (Germany)*

**“Calculating the optical properties of defects and surfaces in diamond and TiO<sub>2</sub>” (p. 6)**

Prof Peter Deák is professor of theoretical semiconductor physics at University Bremen and is head of the Electronic Materials Group at the Bremen Center for Computational Materials Science. He has obtained his Ph.D. in Physics from the Lóránd Eötvös University Budapest in 1984 and the Doctor of Science title from the Hungarian Academy of Science in 1993. After research at SUNY/Albany and a Humboldt Fellowship at MPI Stuttgart, he became Professor at the Budapest University of Technology and Economics in 1993, heading an applied surface physics laboratory. He has organized a European PhD program in Applied Physics, with the support of companies like Siemens, General Electric Lighting and Thales. In 2003 he moved to Germany. His research experience is in computer simulation of atomic processes in electronic materials and in surface related materials problems. He is (co)author and editor of several scientific collections and university textbooks and published ~190 scientific papers. He is member of the editorial board of *physica status solidi (a)*.



**David Rogers**

*Nanovation (France)*

**“Zinc oxide based photonics” (p. 7)**

Dr. David Rogers (CTO) received his PhD from the University of Glasgow (Scotland) and his MBA from the Open University (England). His early research career was involved with the growth and characterization of magnetic materials for data storage. This was first of all at Philips Research Laboratories (Netherlands), Carnegie Mellon University (US) and Nippon Telephone and Telegraph (Japan). Dr. ROGERS was later Project Manager of a cuprate superconductor start-up company based in Paris. In 2001 he co-founded Nanovation, which is a French start-up specialised in the development, fabrication and commercialisation of ZnO thin films and nanostructures tailored for energy conversion applications. Dr. Rogers is the author/co-author of 15 patents and 96 publications and has received numerous prizes (including the NTT Distinguished Research Award & the Magnetism Society of Japan award). He is also an organiser and a regular invited speaker at numerous international conferences. In parallel with developing Nanovation, Dr. Rogers has also been a lecturer at the University of St Andrews (UK), an Associate Professor at the Université de Technologie de Troyes (France), a visiting professor at the Indian Institute of Technology (Jodhpur) and a visiting Professor at the University of Technology of Sydney.



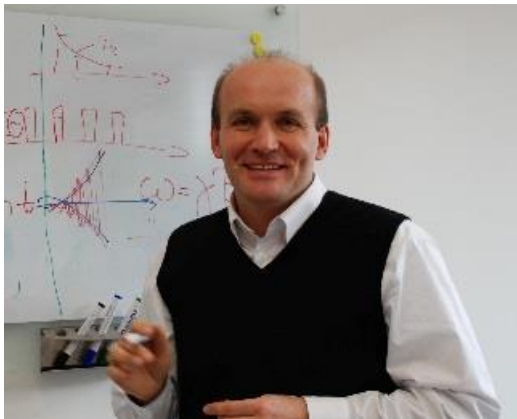
Susanne Siebentritt

*University of Luxembourg (Luxembourg)*

**“Why do we make CIGS solar cells off-stoichiometric?” (p. 14)**

Susanne Siebentritt is a physics professor and heads the laboratory for photovoltaics at the University of Luxembourg since 2007. Her research interest is twofold:

the development of new thin film solar cells and the semiconductor physics of the materials used in these cells. She studied physics at the University of Erlangen and received her doctoral degree from the University of Hannover. After several postdoc positions at the University of Los Angeles, the Free University of Berlin and the Hahn-Meitner-Institute (now Helmholtz-Zentrum Berlin), she led a group at Hahn-Meitner-Institute for nearly 10 years, which focused on the physics of chalcopyrite solar cells, before building the laboratory in Luxembourg. She is the author of nearly 160 peer reviewed publications, with more than 2900 independent citations. In 2014 she received the FNR Outstanding Publication Award, together with three co-authors. In 2015 she was awarded the "Grand Prix en Sciences Physique - Prix Paul Wurth" of the Luxembourgish Institut Grand Ducal. She is a regular topical organiser at the international photovoltaics conferences in Europe and the US. She is vice chair of the scientific council of Science Europe and a board member for the Kopernikus projects, a 10 year research programme for the energy transition of the German Ministry of Education and Research.



Vladimir Dyakonov

*University of Würzburg (Germany)*

**“Charge carrier recombination in perovskite solar cells” (p. 18)**

Professor Vladimir Dyakonov holds the Chair of Experimental Physics (Energy research) on the Faculty of Physics and Astronomy of Julius-Maximilian University of Würzburg, Germany since 2004 and he is the Scientific Director of the Bavarian Centre of Applied Energy

Research (ZAE Bayern) since 2005. He studied physics at the University of St. Petersburg and received his doctorate at the A. F. Ioffe Physico-Technical Institute in 1996. Since 1990, he has been a visiting researcher at the universities of Bayreuth (Germany), Antwerp (Belgium) and Linz (Austria). He finished his habilitation in experimental physics at the University of Oldenburg (Germany) in 2001. In 2007-2009 he was the Vice-dean of the Faculty of Physics and Astronomy, in 2010-2011 the managing director of Institute of Physics and in 2013-2015 he was the Dean of the Faculty of Physics and Astronomy at the University of Würzburg. Dyakonov's main research interests are in the fields of thin-film photovoltaics, semiconductor spectroscopy and functional energy materials, in general. He is a member of several committees including the Board of Directors of German Renewable Energy Research Association (FVEE), the Advisory Board of Bavarian Energy Technology Cluster and the Board of Trustees at German Plastics Centre (SKZ).





Vladimir Kolkovsky

*Fraunhofer Institute IPMS in Dresden (Germany)*

**“Carbon-hydrogen-related complexes in Si” (p. 19)**

Dr. Vladimir Kolkovsky has received his Ph. D. degree at the Institute of Physics, Polish Academy of Sciences in Warsaw. Afterwards he spent two years as a post-doc in the group of Prof. A. N. Larsen in Aarhus. In 2009 he joined the group of Prof. Weber at the Technical University of Dresden where he spent three more years. At the moment he is a member of the scientific staff at the Fraunhofer Institute IPMS in Dresden. His research interests are mainly focused on: characterization and identification of point and extended defects in semiconductors and isolators; large lattice relaxation effects (the negative-U effect); transport in low-dimensional systems (quantum dots and nanowires), photovoltaic materials and their application, MEMS and MOEMS, bipolar and ion sensitive field effect transistors. He has published more than 50 papers in peer reviewed international journals.



Martin Geller

*University of Duisburg-Essen (Germany)*

**“Spectroscopy on self-assembled quantum dots: transport meets optics” (p. 25)**

Martin Paul Geller received his PhD degree from the Technical University of Berlin in 2007 in the group of Dieter Bimberg. After a Post-doc at the University of Duisburg-Essen in the group of Axel Lorke and a research visit at the ETH Zurich (Switzerland) he joined as a Post-doc the group of Mete Atatüre at the University of Cambridge. Since 2012 he is back at the University of Duisburg-Essen working on transport and optical on low-dimensional quantum systems. He is mainly interested in quantum phenomena in such quantum systems, using time-resolved transport and high-resolution resonance fluorescence measurements on ensembles and single self-assembled quantum dots. He has authored more than 50 papers in physical journals and conference proceedings, has two patents and published two book chapters. He received the Carl-Ramsauer-Preis from the “Physikalischen Gesellschaft zu Berlin” and the Nanoscience award from the “Working group of the Centers of Competence of Nanotechnology”.



Sanjay J. Dhoble

*R.T.M. Nagpur University (India)*

**“Luminescence behaviour of lanthanide ions in different host lattices and their application in LED for lighting” (p. 30)**

Dr. S. J. Dhoble obtained his M.Sc. degree in Physics from Rani Durgavati University, Jabalpur, India in 1988. He obtained his Ph.D. degree in 1992 on Solid State Physics from Nagpur University, Nagpur. He is presently working as an Associate Professor in Department of Physics, R.T.M. Nagpur University, Nagpur, India.

During his research career, he has been involved in the synthesis and characterization of solid state lighting nanomaterials as well as development of radiation dosimetry phosphors using thermoluminescence, mechanoluminescence and lyoluminescence techniques. Dr. Dhoble has published more than 553 research papers in international and national reviewed journals on solid-state lighting, LEDs, radiation dosimetry and laser materials. He has 3116 research papers citations, an h-index of 25 and a patent. He recently received the Prof. B.T. Deshmukh Research Award 2016 and Prof. B.P. Chandra Research Award 2016 in NCLA-2016, Nagpur. He also received Outstanding Scientist-2015 award in outstanding research contribution in Solid State Physics at Chennai from Venus International Foundation and he has received Advanced Materials Scientist Letter Awards-2011 for outstanding contribution in Advanced Materials Letter presented by VBRI Press in International Conference on Nanomaterials and Nanotechnology, Delhi University, 2011. His academic achievement includes best research paper awards for 37 research papers in conferences and reviewer of 29 international and national journals. He has a teaching experience of 26 years and has served as a Principal of a College for five years. He visited abroad to the countries viz. Italy, Egypt, Greece, Australia, China, South Africa, South Korea, Sweden, Japan and Malaysia for research and education purpose and as a participant in the conferences and other activities. He has successfully guided 28 students for Ph.D. degree, 5 submitted Ph.D. thesis and 5 are currently registered for Ph.D. degree with him. He has successfully completed 4 research projects of BRNS, DAE, IUAC and UGC to his credit. He is co-author of 22 books/chapters. He is life member of Society for Materials Chemistry, Luminescence Society of India, Indian Association for Radiation protection, Indian Laser Association, Indian Physics Association, International Association of Advanced Materials (IAAM), Vidarbha Environment Society, Nuclear Track Society of India, Society for Technologically Advanced Material of India (STAMI) and Indian Physics Teachers' Association. He is Vice President of the Luminescence Society of India and Director of the Inter Institutional Computer Centre, R.T.M. Nagpur University. He is editor of Luminescence: The Journal of Biological and Chemical Luminescence.



Lucas C.V. Rodrigues  
*University of São Paulo (Brazil)*

**“Designing infrared persistent luminescence materials” (p. 34)**

Prof. Lucas C.V. Rodrigues obtained his Bachelor in Chemistry from the Universidade de São Paulo (2006) and Ph.D. in Chemistry from Universidade de São Paulo (2012). Worked as Senior Researcher at the Department of Chemistry of University of Turku, Finland during 2012-2013 and occupies a professor position at the Department of Fundamental Chemistry of the Universidade de São Paulo. His main research interest is rare earth doped materials, in special those presenting persistent luminescence and up- and down-conversion properties for application in solar converters.



Philippe Smet  
*Ghent University (Belgium)*

**“Enhancing the performance of persistent phosphors: focus on the trapping defects and detrapping processes” (p. 35)**

Prof Philippe Smet obtained his PhD in Physics at Ghent University (Belgium) in 2005 in the field of thin film electroluminescence, based on impurity doped sulfide compounds. Between 2007 and 2010 he was a post-doctoral fellow of the FWO-Flanders. Research then focused on the photo- and thermoluminescence of rare earth doped compounds and research stays were performed at the Otto-von-Guericke Universität in Magdeburg and at TU Delft. In 2010 he was admitted to a tenure track position in the field of “Physics and chemistry of condensed matter”. In 2015, he was appointed as associate professor at Ghent University. Currently, the main research topics include persistent and mechanoluminescent phosphors, cathodoluminescence spectroscopy and LED conversion phosphors. He is coordinating a SBO-IWT project on remote phosphors (2013-2017). Together with Dirk Poelman he heads the LumiLab research group (<http://lumilab.ugent.be>) at the Department of Solid State Sciences. The research group is currently formed by seven PhD students, one post-doc and five master thesis students. Philippe Smet is author of 110 peer-reviewed, international publications, with an h-index of 27. In the past five years, he gave 10 invited presentations at international conferences, including two keynote lectures. Since end 2013 he is associate editor for the open access journal ‘Optical Materials Express’. He is involved in the physics teacher training programme, as well as in regular Bachelor (‘Waves and optics’, ‘Material Physics’, ‘Introduction to atomic and molecular physics’) and elective Master courses (‘Luminescence’). In 2014 he obtained the first prize in the Belgian heat of the Famelab competition on science communication. He is involved in many science communication events, such as lectures for ‘Children University’, Science Fairs and during the past Ghent Light Festival, for which he received the UGent Hermes award in 2015.

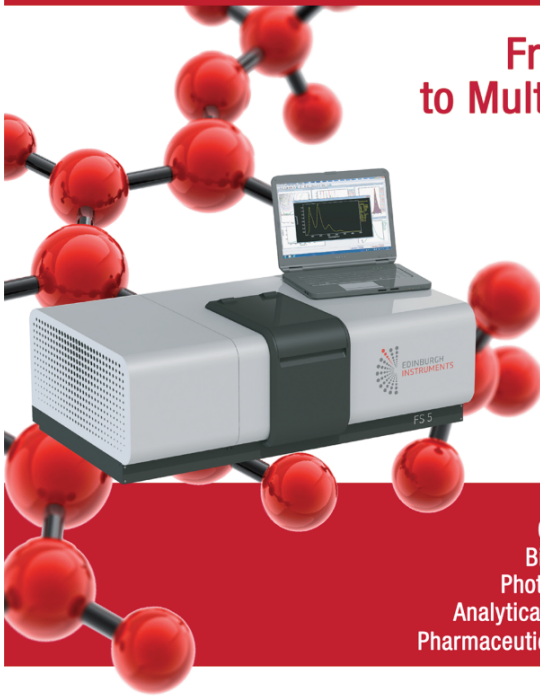
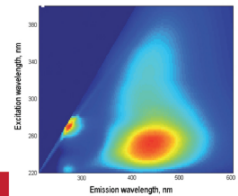
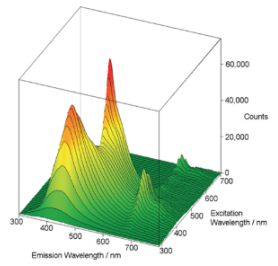


# FS5

## Spectrofluorometer

### From Single Photons to Multitude of Measurements

An unprecedented, modern fluorescence spectrometer designed and engineered to the highest standards of sensitivity, acquisition speed, ease of use and sampling flexibility

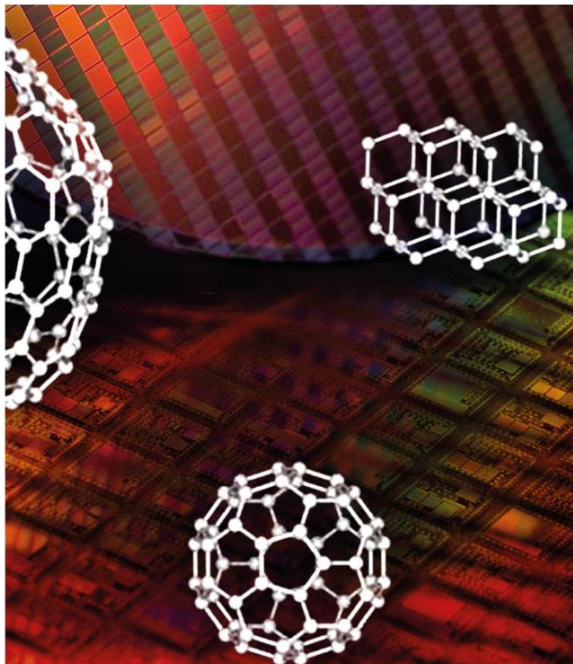


#### Applications

Cell Biology  
Biochemistry  
Photochemistry  
Analytical Chemistry  
Pharmaceutical Industry

Medicine  
Manufacturing  
Material Research  
Environmental Science  
Food Science and Agriculture

T: +2712 349 1250 E: [hitech@hitechlasers.co.za](mailto:hitech@hitechlasers.co.za) W: [www.hitechlasers.co.za](http://www.hitechlasers.co.za) F: [www.facebook.com/hitechgroupsa](https://www.facebook.com/hitechgroupsa)



## Your Partner for Photonic Materials Study

HORIBA Scientific proposes a full range of instruments for photonic materials study, from nano-object to wafer scale analysis:

- Atomic Force Microscope
- Raman and NanoRaman Spectroscopy
- Spectrofluorometry
- Spectroscopic Ellipsometry
- Custom design platforms

Raman Spectrometer



Atomic Force Microscope



Spectrofluorometer



Ellipsometer



[www.horiba.com/scientific](http://www.horiba.com/scientific)


[info-sci.fr@horiba.com](mailto:info-sci.fr@horiba.com)

Explore the future

Automotive Test Systems | Process & Environmental | Medical | Semiconductor | Scientific



# Programme Overview

TIME	Monday	Tuesday	Wednesday	Thursday	Friday	
7:00 to 8:00		BREAKFAST (Conference Hall)	BREAKFAST (Conference Hall)	BREAKFAST (Conference Hall)	BREAKFAST (Conference Hall)	
		Chair: Nel	Chair: Vorster	Chair: Vinod Kumar		
8:00 to 8:20		INVITED 1: Ashutosh Tiwari	INVITED 4: Susanne Siebentritt	INVITED 8: S. J. Dhole	<b>Booking out &amp; Departure</b>	
8:20 to 8:40						
8:40 to 9:00		Oral 1: J. A. A. Engelbrecht	Oral 9: Vinod Kumar	Oral 20: Vinay Kumar		
9:00 to 9:20		Oral 2: R. A. Harris	Oral 10: R. M. Dix-Peek	Oral 21: P. P. Mokoena		
9:20 to 9:40		Oral 3: Eric N. Maluta	Oral 11: Edward Lee	Oral 22: Ashwini Kumar		
9:40 to 10:00		INVITED 2: Peter Deák	INVITED 5: Vladimir Dyakonov	INVITED 9: Lucas C. V. Rodrigues		
10:00 to 10:20					10:00 to 10:20	
10:20 to 10:40		TEA (Conference Hall)	TEA (Conference Hall)	TEA (Conference Hall)	10:20 to 10:40	
		Chair: Ntwaeaborwa	Chair: van Dyk			
10:40 to 11:00		INVITED 3: David J. Rogers	INVITED 6: Vladimir Kolkovsky	 <b>POSTER SESSION B:</b>  <b>posters 39 - 74</b>  (Conference Hall upstairs)	10:40 to 11:00	
11:00 to 11:20					11:00 to 11:20	
11:20 to 11:40		Oral 4: Trilok K. Pathak	Oral 12: Matshisa J. Legodi		11:20 to 11:40	
11:40 to 12:00		Oral 5: Katekani Shingange	Oral 13: Joachim Bollmann		11:40 to 12:00	
12:00 to 12:20		Oral 6: Vijay Kumar	Oral 14: Ivan G. Ivanov		12:00 to 12:20	
12:20 to 12:40		Oral 7: Jitendra Sharma	Oral 15: D. D. Ramteke		12:20 to 12:40	
12:40 to 13:00		Oral 8: V. Craciun	Oral 16: Muburak Y. A. Yagoub	CONFERENCE PHOTO	12:40 to 13:00	
13:00 to 14:00		LUNCH (Conference Hall)	LUNCH (Conference Hall)	LUNCH (Conference Hall)	13:00 to 14:00	
			Chair: Venter	Chair: Swart		
14:00 to 14:20	<b>Arrival &amp; Registration</b>  (settle in to accommodation)	<b>POSTER SESSION A:</b>  <b>posters 1 - 38</b>  (Conference Hall upstairs)	INVITED 7: Martin Geller	INVITED 10: Philippe F. Smet	14:00 to 14:20	
14:20 to 14:40						14:20 to 14:40
14:40 to 15:00				Oral 17: Magnus C. Wagener	Oral 23: Vishal Sharma	14:40 to 15:00
15:00 to 15:20				Oral 18: M. E. Lee	Oral 24: Jorma Hölsä	15:00 to 15:20
15:20 to 15:40			Oral 19: P. O. Holtz	Oral 25: Iorkyaa Ahemen	15:20 to 15:40	
15:40 to 16:00			TEA (Conference Hall)	TEA (Conference Hall)	15:40 to 16:00	
16:00 to 16:30					16:00 to 16:30	
16:30 to 17:00			GAME DRIVE (option 1)	GAME DRIVE (option 2)	(free time)	16:30 to 17:00
17:00 to 17:30					17:00 to 17:30	
17:30 to 18:00					17:30 to 18:00	
18:00 to 20:30	WELCOME DINNER (Wild Olive Restaurant)	DINNER (Mountain Lodge)	DINNER (Boma)	CONFERENCE DINNER (Mountain Lodge)	18:00 to 20:30	

## Scientific Programme and Abstracts Tuesday 28 March

Time	Activity
7:00-8:00	Breakfast (Conference Hall)
<b>ORAL SESSION 1: Chairperson – Jackie Nel</b>	
8:00-8:40	Invited Talk 1: <b>Ashutosh Tiwari</b> (p. iv) <i>p. 2: Programmable bioelectronic devices and systems</i>
8:40-9:00	Oral 1: <b>J. A. A. Engelbrecht</b> <i>p. 3: An assessment of theoretical models for the calculation of the refractive index of <math>In_xGa_{1-x}As</math></i>
9:00-9:20	Oral 2: <b>R. A. Harris</b> <i>p. 4: Surface enhanced Raman scattering through selective substitution of thiolated coumarin derivatives on gold nanoparticles</i>
9:20-9:40	Oral 3: <b>Eric N. Maluta</b> <i>p. 5: Density functional theory study of <math>TiO_2</math> brookite (100), (110) and (210) surfaces doped with ruthenium (Ru) and calcium (Ca) for application in dye-sensitized solar cell</i>
9:40-10:20	Invited Talk 2: <b>Peter Deák</b> (p. v) <i>p. 6: Calculating the optical properties of defects and surfaces in diamond and <math>TiO_2</math></i>
10:20-10:40	Tea (Conference Hall)
<b>ORAL SESSION 2: Chairperson – Martin Ntwaeaborwa</b>	
10:40-11:20	Invited Talk 3: <b>David J. Rogers</b> (p. iv) <i>p. 7: Zinc oxide based photonics</i>
11:20-11:40	Oral 4: <b>Trilok K. Pathak</b> <i>p. 8: Structural and plasmonic properties of noble metal doped ZnO nanomaterials</i>
11:40-12:00	Oral 5: <b>Katekani Shingange</b> <i>p. 9: Microwave-assisted synthesis of Au nanoparticles incorporated ZnO rose-like hierarchical structures and their gas sensing properties</i>
12:00-12:20	Oral 6: <b>Vijay Kumar</b> <i>p. 10: Recent advances in plasmon enhanced luminescence upconversion of lanthanide-doped <math>NaYF_4</math> core-shells for solar cell applications</i>
12:20-12:40	Oral 7: <b>Jitendra Sharma</b> <i>p. 11: Optical properties of <math>Sr_3B_2O_6:Dy^{3+}/PMMA</math> polymer nanocomposites</i>
12:40-13:00	Oral 8: <b>V. Craciun</b> <i>p. 12: Radiation effects in amorphous optical films</i>
13:00-14:00	Lunch (Conference Hall)
14:00-16:00	POSTER SESSION A: posters 1 – 38 (p. 43 – 80) (Conference Hall upstairs)
16:00-18:00	GAME DRIVE (option 1)
18:00-20:30	DINNER (Mountain Lodge)

# Programmable bioelectronic devices and systems

**Ashutosh Tiwari<sup>1,2\*</sup>**

<sup>1</sup>Institute of Advanced Materials, UCS, Teknikringen 4A, Mjärdevi Science Park, Linköping 583 30, Sweden

<sup>2</sup>Biosensors and Bioelectronics Centre, IFM, Linköping University, 581 83 Linköping, Sweden

\*Corresponding author e-mail address: director@iaam.se and ashutosh.tiwari@liu.se

## 1. Introduction

Biodigital devices are emerged an interdisciplinary field of research in the biosensors and bioelectronics [1, 2]. Today, smart bio-interfaces are applying a renewed influence on bioelectronics beyond the incorporation of few or single atom(s)-thick two dimensional (2D) materials, which fuses the benefits of extraordinary stimuli-controlled interior and exterior catalytic atomic surfaces with those of super-thin digital biotechnology [3, 4]. The development of switchable and/or tunable interfaces of 2D materials endowed with desirable functionalities, and incorporation of these interfaces into on/off-switchable bio-devices [5-7], fig. 1. The aim of talk is to demonstrate various strategies of stimuli-enabled programming of enzymatic super-thin digital systems answer by a considerable control in their biochemical behavior with uni- and multi-model triggering of interfaces via temperature, pH, light, etc. These smart bioengineered atom-thick approaches are being formulated that sense specific biochemical changes and regulate in a liable manner, making them useful super-thin biotechnological tools. The progress in this field would make significant contributions to new age biodigital energy and medical technologies.

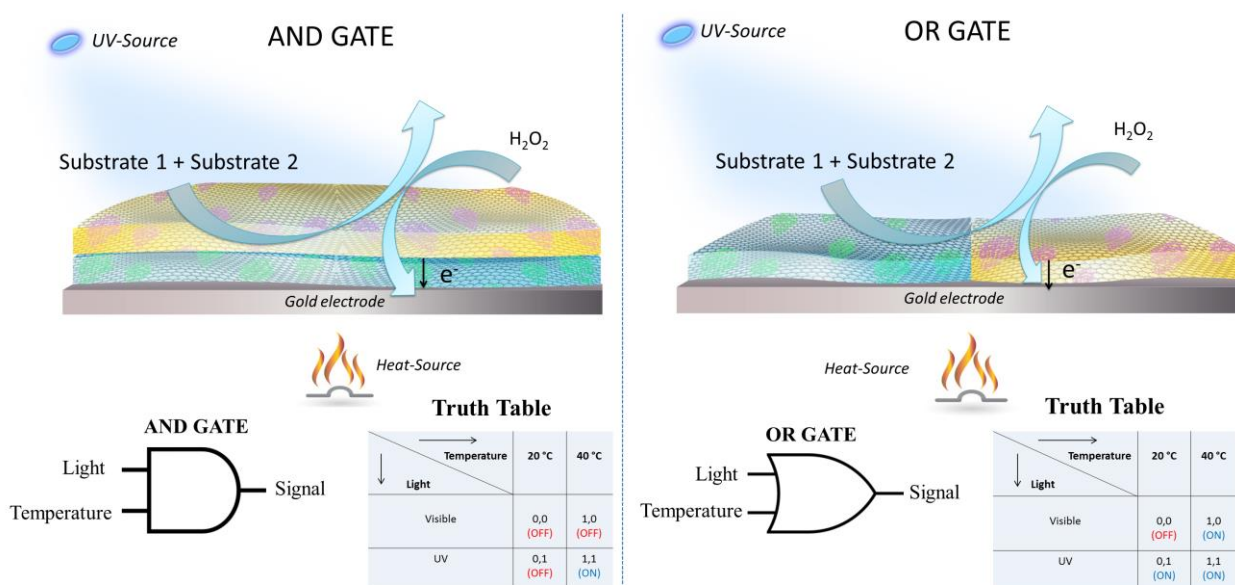


Fig. 1: Stimuli-enabled 'built-in' super-thin smart digital bioelectronic devices.

## 2. References

- [1] A. Tiwari, A.P.F. Turner, (Eds.), *In Biosensors Nanotechnology*, Wiley - Scrivener, USA, MA, (2014).
- [2] O. Parlak, S. Beyazit, M.J. Jafari, B.T.S. Bui, K. Haupt, A. Tiwari, A.P.T. Turner, *Advanced Materials Interfaces*, (2015).
- [3] O. Parlak, A.P.F. Turner, A. Tiwari, *Advanced Materials*, **26** (2014) 482.
- [4] A. Tiwari, M. Syväjärvi, (Eds.), *In Graphene Materials: Fundamentals and Emerging Applications*, Wiley - Scrivener, USA, MA, (2015).
- [5] H. Patra, R. Imani, M. Pazoki, A. Iglie, A.P.F. Turner, A. Tiwari, A.; *Nature – Scientific Reports*, **5** (2015) 14571.
- [6] Onur Parlak, Selim Beyazit, Bernadette Tse-Sum-Bui, Karsten Haupt, Turner Anthony P. F., Ashutosh Tiwari, *Nanoscale*, **8** (2016) 9976.
- [7] Sachin Mishra, Md. Ashaduzzaman, Prashant Mishra, Hendrik C. Swart, Anthony P.F. Turner, Ashutosh Tiwari; *Biosensors and Bioelectronics*, **89**(1) (2017) 305.

# An assessment of theoretical models for the calculation of the refractive index of $\text{In}_x\text{Ga}_{1-x}\text{As}$

J. A. A. Engelbrecht<sup>1\*</sup>

<sup>1</sup>CHRTEM, NMMU, Port Elizabeth, South Africa

\*Corresponding author e-mail address: Japie.Engelbrecht@nmmu.ac.za

## 1. Introduction

The binary  $\text{In}_x\text{Ga}_{1-x}\text{As}$  alloy finds application as HEMT transistors, laser and photodiodes, triple-junction photovoltaic devices and infrared detectors, due to its advantageous band gap, which varies from 0.36 to 1.425 eV [1, 2]. In particular, the band gap is advantageous for use of the alloy in optical fibre communication systems. A knowledge of the optical parameters of the alloy, in particular the refractive index  $n$ , is thus a requirement for the design of the required optical devices. While the refractive index for  $\text{In}_x\text{Ga}_{1-x}\text{As}$  is known in the visible and ultraviolet regions ( $0.5 - 6 \text{ eV} = 2480 - 207 \text{ nm} = 4033 - 48\,395 \text{ cm}^{-1}$ ) of the electromagnetic spectrum, a literature survey revealed only four papers referring to work done in the mid-infrared region of the spectrum.

The current investigation reports on an assessment of the refractive index of  $\text{In}_x\text{Ga}_{1-x}\text{As}$ . Four theoretical models for the calculation of the refractive index will be reviewed, viz. single [3] and modified oscillator [4, 5], the Sellmeier [5] and the dielectric function [6] model. The single and modified oscillator equations contain terms related to the energy of the oscillator,  $E_o$ , and the dispersion energy  $E_d$ . The latter is a function of the band gap energy  $E_g$ , which in turn depends on the doping concentration  $x$ . Various different expressions have also been proposed to calculate  $E_o$ . Problems experienced with some of the models will be reported, and a comparison will be made of the refractive indices obtained by these various models. The models were also extended into the mid-infrared region ( $4\,000 - 400 \text{ cm}^{-1} = 0.5 - 0.05 \text{ eV}$ ) of the electromagnetic spectrum. A comparison will be made between refractive index values published for the mid-infrared region, and values calculated values from the various theoretical models.

## 2. Results

The influence of the various parameters ( $E_o$ ,  $E_d$ ) contained in the expression for the band gap of  $\text{In}_x\text{Ga}_{1-x}\text{As}$  as function of composition  $x$ , is depicted in Fig. 1. Clearly three of the models reflect a reverse trend than the others. The values for  $E_g$  from the various models have a maximum deviation at  $x = 0$ , viz. from 0.77 to 0.89, with least variations for  $0.8 < x < 0.2$ . In Fig. 2, the variation of the refractive index  $n$  as calculated from the model by Afromowitz [7] is shown.

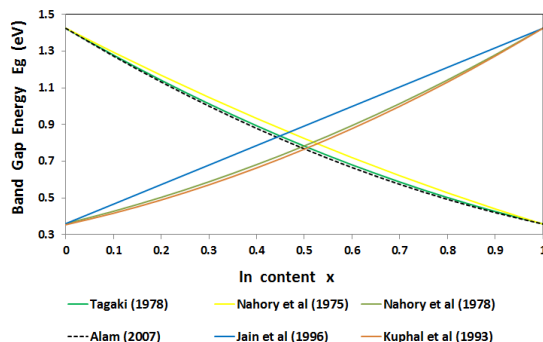


Fig. 1: Variation of the band gap energy  $E_g$  for  $\text{In}_x\text{Ga}_{1-x}\text{As}$  as obtained from the various theoretical models proposed.

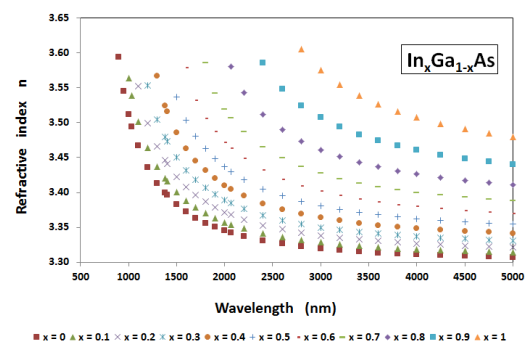


Fig. 2: Variation of the refractive index  $n$  with wavelength and composition, according to the model by Afromowich [4]

## 3. References

- [1] S.L. Geelhaar, R.A. Bartynski, F. Ren, M. Schnoes and D.N. Buckley. *J. Appl. Phys.* **80** (1996) 3075.
- [2] J.C. Woolley, M. B. Thomas and A.G. Thompson. *Can. J. Phys.* **46** (1968) 157.
- [3] S.H. Wemple and M. DiDomenico Jr. *Phys. Rev. B* **3** (1971) 1338.
- [4] M.A. Afromowitz. *Solid State Comm.* **15** (1974) 59.
- [4] T. Takagi. *Jap. J. Appl. Phys.* **17** (1978) 1813.
- [5] W. Sellmeier. *Annalen der Physik und Chemie* **219.6** (1871) 272.
- [6] M.S. Alam, M.S. Rahman, M.R. Islam, A.G. Bhuiyan and M. Yamada. *Conference Proceedings 19th IPRM*, 14-18 July 2007, Matsue, Japan, p. 343..



# Surface enhanced Raman scattering through selective substitution of thiolated coumarin derivatives on gold nanoparticles

R. A. Harris<sup>1\*</sup>, M. Mlambo<sup>2</sup>, P. M. Mdluli<sup>3</sup>

<sup>1</sup>Department of Physics, University of the Free State, Bloemfontein, 9301, South Africa

<sup>2</sup>Department of Physics, University of Pretoria, Hatfield, Pretoria, 0002, South Africa

<sup>3</sup>Department of Chemistry, Durban University of Technology, Durban, 4000, South Africa

\*Corresponding author e-mail address: harrisra@ufs.ac.za

## 1. Introduction

Surface enhanced Raman spectroscopy (SERS) is greatly dependent on the optical properties of nanostructured materials. Known to enhance weaker Raman signals by a factor of  $10^4$  to  $10^6$  through surface plasmon resonance (SPR) in metallic nanostructures, SERS may be employed to detect and identify molecules up to single molecule detection levels. Thus, this technique holds great promise for *in vitro* early cancer detection devices [1].

However, understanding how this enhancement is obtained, is no trivial task [2]. Metal nanoparticles exhibit a SPR adsorption that is dependent on many factors including the dielectric constant of metals and their surfaces, the inter-particle, distances as well as the size and shape of the nanoparticles, to name a few. The excitation of the SPR absorption results in a strong, local electromagnetic field enhancement in the vicinity of the NPs, as it is responsible for the major enhancement in the Raman spectra of molecules near or attached to the surface of metal nanoparticles.

In this investigation, we report on the effect of changing the HS-(CH<sub>2</sub>)<sub>11</sub>-NHCO coumarin to stabilizing surfactant HS-PEG(CH<sub>2</sub>)<sub>11</sub>COOH ratio on the Raman signal intensity. We draw our conclusions from both an experimental as well as a theoretical simulation investigation. We report further on the theoretical investigation of the interaction of a cancer causing mutagen molecule such as benzo(a)pyrene with gold and paramagnetic nanoparticles.

## 2. Results

Figure 1 shows the experimentally calculated enhancement factors for Au nanoparticles coated with different ratios of HS-(CH<sub>2</sub>)<sub>11</sub>-NHCO coumarin and HS-PEG(CH<sub>2</sub>)<sub>11</sub>COOH. The effect of different sized nanoparticles is also clear from this figure. This was obtained after nanoparticles were synthesised and a ligand exchange facilitated. The experimental data was compared to similar, modelled and dynamically simulated Au nanoparticles, (figure 2) where it can clearly be seen that, for much smaller nanoparticles, a severe overlap of electromagnetic hotspots occur whereas these hotspots are fairly spread out in physical space for larger nanoparticles. It was also observed that the positions in both energy and physical space of the highest occupied molecular orbital (HOMO) and lowest unoccupied molecular orbital (LUMO) greatly affect the Raman signal intensity.

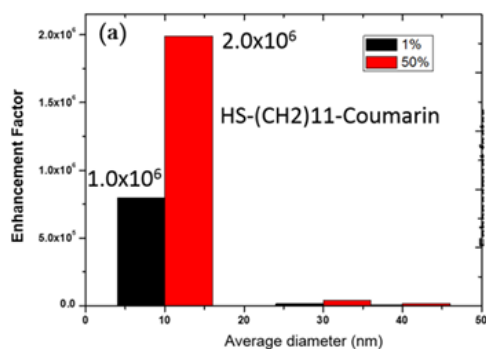


Fig. 1: Experimentally calculated enhancement factors for Au nanoparticles coated with HS-(CH<sub>2</sub>)<sub>11</sub>-NHCO coumarin.

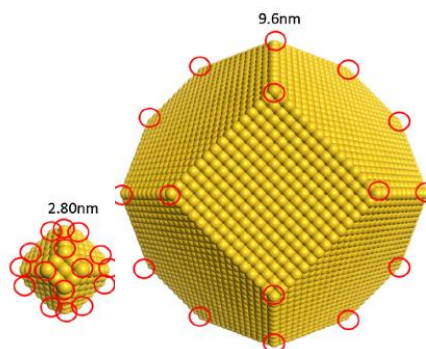


Fig. 2: Simulated Au nanoparticles of 2.80 and 9.60 nm respectively showing overlapping electromagnetic "hotspots".

## 3. References

- [1] R. A. Harris, M. Mlambo and P. S. Mdluli. *RSC Advances* **6** (2016) 12131.
- [2] J. Prakash, R. A. Harris, H. C. Swart. *Int. Rev. Phys. Chem.* **35** (2016) 353.

# Density functional theory study of TiO<sub>2</sub> brookite (100), (110) and (210) surfaces doped with ruthenium (Ru) and calcium (Ca) for application in dye-sensitized solar cell

**Eric N. Maluta<sup>1,2\*</sup>, Steve R. Dima<sup>1,2</sup>, Rapela R. Maphanga<sup>2,3</sup>**

<sup>1</sup>The University of Venda, Department of Physics, P/Bag X 5050, Thohoyandou, 0950

<sup>2</sup>National Institute for Theoretical Physics (NITheP), Gauteng, South Africa

<sup>3</sup>Material Modelling Centre, University of Limpopo, Turfloop Campus, P/Bag X 5050, Sovenga, 0950.

\*Corresponding author e-mail address: Eric.Maluta@univen.ac.za

## 1. Introduction

Energy crisis in the world is causing a lot of problems for every one and it has a negative impact on the growth of developing country economy. There is a dire need to implement and harness the renewable energy. For South Africa as a developing country, there is a dire need to implement the 2020 strategies to harness renewable energy and the country need evident of the knowledge of the amount of solar energy falling in different areas of SA. Since the discovery of dye sensitized solar cells, which uses TiO<sub>2</sub> as a semiconductor, TiO<sub>2</sub> has attracted extensive attention as an ideal photocatalytic material because of its excellent properties such as high activity, good stability, nontoxicity and low cost. However, as a wide band gap oxide semiconductor ( $E_g = 3.14$  eV), brookite TiO<sub>2</sub> can only show photocatalytic activity under UV light irradiation that accounts for only a small portion of solar energy, in contrast to visible light for a major part of the solar energy. Therefore, how to effectively utilize sunlight is the most challenging subject for the extensive application of TiO<sub>2</sub> as a photocatalyst.

Transition metal doping is one of the most effective approaches to extend the absorption edge of TiO<sub>2</sub> to the visible light region, which either inserts a new band into the original band gap, improving the photocatalytic activity of TiO<sub>2</sub> to some degree.

In this work, the structural optimizations, band structure, and electronic density of states of doped and undoped TiO<sub>2</sub> brookite surfaces were performed using the first-principles calculations based on Density Functional Theory (DFT) using a plane-wave pseudopotential method. The generalized gradient approximation (GGA) was employed in the scheme of Perdew-Burke-Ernzerhof (PBE) to describe the exchange-correlation functional. All calculations were carried out with CASTEP (Cambridge Sequential Total Energy Package) code in Materials Studio of Accelrys Inc. From the doping of the transitional element Ruthenium, we observed that the absorption of TiO<sub>2</sub> to be tuned into the visible-light range with high stability.

# Calculating the optical properties of defects and surfaces in diamond and TiO<sub>2</sub>

**Peter Deák<sup>1\*</sup>**

<sup>1</sup>University of Bremen, Bremen Center for Computational Materials Science, PoB 330440, D-28334 Bremen, Germany

\*Corresponding author email address: deak@uni-bremen.de

## 1. Introduction

Defects and surfaces modify the electronic and optical properties of non-metallic solids, so these effects have to be known and taken into account in materials engineering for optical applications. Since both the bulk and the surface contain many defects, disentangling the consequences requires the help of quantum mechanical model calculations. Theoretical defect physics, using the standard local or semi-local approximations of density functional theory, has been quite successful in traditional semiconductors, however, wide band gap materials are a serious challenge. In this talk I show how range-separated non-local hybrid functionals can be used to overcome earlier problems, leading to an unprecedented accuracy in describing optical excitations [1,2]. Two examples will be considered: the single photon emitter NV(-) center in diamond [3,4] and photocatalytic watersplitting by TiO<sub>2</sub> [5,6].

## 2. Results

The photoluminescent NV(-) center of diamond is being under intense investigation lately due to its potential in quantum information technology, for nano-sensing and bio-labeling. Since these applications require the NV(-) center to be near the diamond surface, the effect of the latter can be critical. Based on calculations using a screened hybrid functional on a (001) slab of diamond, I show that the completely hydrogenated or hydroxylated surface leads to bleaching, while a much too strong oxygenation to blinking of the luminescence. Ideally, the surface should be terminated by a mixture of H, OH and bridging O, which can be achieved by mild oxidation of a hydrogenated surface or by oxidation with an acid.

TiO<sub>2</sub> is a typical oxide used in energy-related applications. By far the most important is photocatalysis, where efficiency depends on the separation of the photo-generated electron-hole pairs. One possibility for that is offered by the staggered band-alignment between rutile and anatase in mixed TiO<sub>2</sub> powders. The direction of the charge transfer depends on the sign of the band-offset, which is hotly debated in the literature. Based on theoretical studies I show that, in case of a direct rutile/anatase interface, both band edges of the former lie higher in energy. However, in for rutile and anatase, both in contact with an aqueous electrolyte, the relative position may be reversed due to the absorption of OH<sup>-</sup> and H<sup>+</sup> ions. This phenomenon also explains the observed differences in the efficiency of water splitting, and our results show how the latter can be improved.

## 3. References

- [1] P. Deák, B. Aradi, T. Frauenheim, E. Jánzn, and A. Gali, *Phys. Rev B* **81** (2010) 153203.
- [2] P. Deák, Quoc Duy Ho, F. Seemann, B. Aradi, M. Lorke, and T. Frauenheim, *Phys. Rev. B* submitted.
- [3] P. Deák, B. Aradi, M. Kaviani, T. Frauenheim, and A. Gali, *Phys. Rev. B* **89** (2014) 075203.
- [4] M. Kaviani, P. Deák, B. Aradi, T. Frauenheim, J.-P. Chou, and A. Gali, *Nano Letters* **14** (2014) 4772.
- [5] J. Kullgren, B. Aradi, T. Frauenheim, L. Kavan, and P. Deák, *J. Phys. Chem. C* **119** (2015) 21952.
- [6] P. Deák, J. Kullgren, B. Aradi, T. Frauenheim, and L. Kavan, *Electrochim. Acta* **199** (2016) 27.

# Zinc oxide based photonics

David J. Rogers<sup>1\*</sup>, Ferechteh H. Teherani<sup>1</sup>, Eric V. Sandana<sup>1</sup>, Philippe Bove<sup>1</sup>

<sup>1</sup>Nanovation, 8 route de Chevreuse, 78117 Chateaufort, France  
\*Corresponding author e-mail address: rogers@nanovation.com

## 1. Introduction

Zinc oxide (ZnO) is a remarkable, multifunctional semiconducting material with a direct, wide bandgap ( $E_g \sim 3.4$  eV), intrinsically high transparency over the whole visible range, and a resistivity that can be tuned from semi-insulating right through to semi-metallic by doping. It also presents one of the highest piezoelectric responses of any semiconductor and has a relatively high thermoelectric figure of merit. Moreover, it has been judged to be biocompatible and has been approved for human consumption (in products such as vitamin pills) by the U.S. Food and Drug Administration.

The figure below shows that ZnO is currently one of the hottest topics in materials science, with over 8000 publications in 2015:

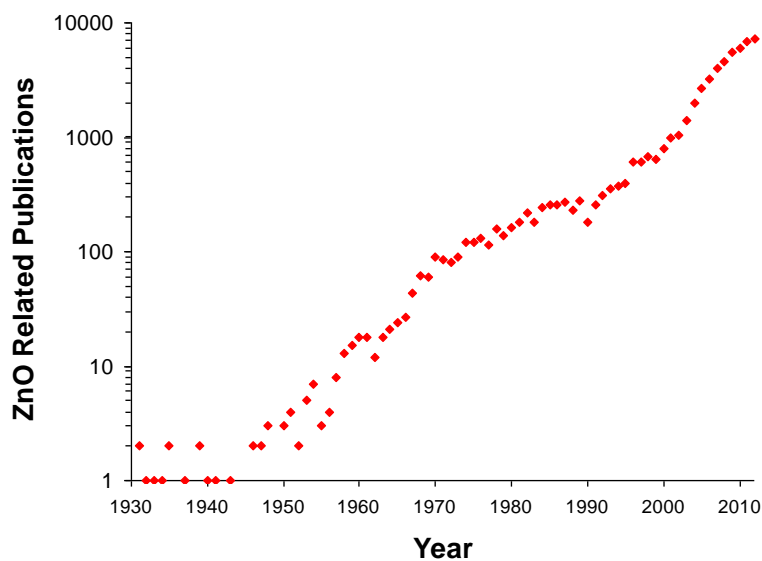


Fig. 1. Number of annual publications vs. year according to a search of the [www.scopus.com](http://www.scopus.com) database for the term “ZnO” in the abstract, title, or keywords.

ZnO has become a hot topic because of its’ distinctive property set plus a number of recent breakthroughs. Also of note is that a recent Thomson-Reuters study, recorded more publications dedicated to nanostructured ZnO than to carbon nanotubes. This was attributed to the multifunctional nature of ZnO, the ease of fabricating nanostructures by various techniques (including wide-area, low cost chemical growth) and the extremely large family of nanostructure shapes that can be obtained. In this talk, we will give an overview of the advances in the field and present some of the wide range of ZnO-related photonics devices and applications being researched at the moment with illustrations from the work of the French ZnO start-up, Nanovation ([www.nanovation.com](http://www.nanovation.com)).

# Structural and plasmonic properties of noble metal doped ZnO nanomaterials

Trilok K. Pathak<sup>1\*</sup>, H. C. Swart<sup>1</sup>, R. E. Kroon<sup>1\*</sup>

<sup>1</sup>Department of Physics, University of the Free State, Bloemfontein, South Africa  
\*Corresponding author e-mail address: tpathak01@gmail.com, KroonRE@ufs.ac.za

## 1. Introduction

Zinc oxide (ZnO) is a multifunctional material having unique physical properties as well as chemical and photo-stability. It has a large bandgap (3.27 eV) and large exciton binding energy (60 meV) at room temperature, giving it great importance in the field of optoelectronic devices and solar cell applications [1]. The effect of noble metal (Ag, Au and Pd) nanoparticles (NPs) on the structural and optical properties of ZnO has been investigated in this study, due to the localized surface plasmon resonance (LSPR) which may occur for such metallic NPs. LSPR is an optical phenomena generated by light when it interacts with metal nanoparticles (NPs) that are smaller than the incident wavelength [2]. Samples of pure and noble metal doped ZnO (2 mol%) were synthesized by the combustion method. Zinc nitrate, silver nitrate, chloroauric acid and potassium tetrachloropalladate were used as the source materials for Zn, Ag, Au and Pd respectively, while urea was used as the fuel.

## 2. Results

X-ray diffraction patterns for the samples are presented in Fig.1. For the undoped ZnO all the diffraction peaks matched the hexagonal wurtzite structure of ZnO (PDF 01-075-0576). For the doped samples the additional peaks marked with asterisks (\*) matched the expected positions of the doped noble metals. Scanning electron microscopy results (not shown) revealed spherical NPs of the noble metals. Diffuse reflectance spectra (Fig. 2) were measured in the range 300-800 nm using a UV-vis spectrophotometer in combination with an integrating sphere. In the doped samples dips in the reflectance spectra centred at 468 nm, 483 nm and 566 nm were attributed to LSPR absorption of the Ag, Au and Pd NPs, respectively [3, 4]. The doping also affected the optical bandgap of ZnO which varied from 3.02 to 3.14 eV as calculated using Tauc plots. Photoluminescence measurements were made using a He-Cd laser emitting at 325 nm as the excitation source. For pure ZnO the near-band-edge (NBE) exciton recombination peak was observed at 384 nm as well as visible luminescence in the range 500-750 nm attributed to oxygen and zinc related defects [5]. The NBE was significantly enhanced in the presence of Pd NPs comparatively to Ag and Au NPs. The visible emission was most enhanced by the addition of Au NPs. The experimental results show that the addition of noble metals (Ag, Au and Pd) may enhance the NBE and visible emissions of ZnO which is generally attributed to transfer of energetic electrons from the metallic NPs to the ZnO as a result of plasmonic effects, even when excited at 325 nm far from their LSPR absorption bands.

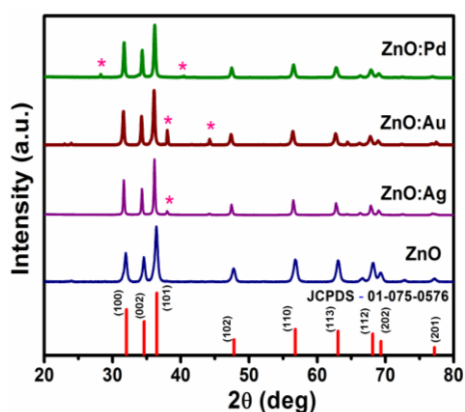


Fig.1: X-ray diffraction pattern of noble metal doped ZnO.

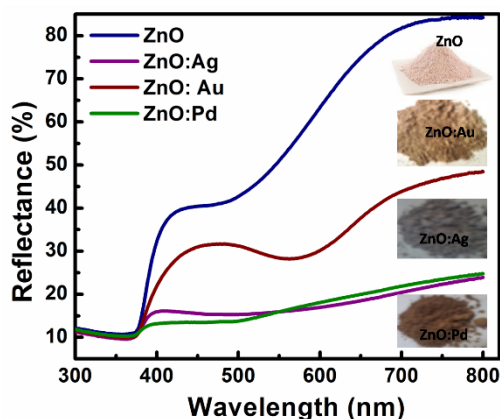


Fig. 2: Diffuse reflectance spectra of noble metal doped ZnO.

## 3. References

- [1] A. Janotti and C. G. Van de Walle. *Rep. Prog. Phys.* **72** (2009) 126501.
- [2] E. Petryayeva and U. J. Krull. *Analytica Chimica Acta* **706** (2011) 8.
- [3] C. Karunakaran, V. Rajeswari and P. Gomathisankar. *Superlattices and Microstructures* **50** (2011) 234.
- [4] M. Ahmad, S. Yingying, A. Nisar, H. Sun, W. Shen, M. Wei and J. Zhu. *J. Mater. Chem.* **21** (2011) 7723.
- [5] J. R. Heath, J. J. Shiang. *Chemical Society Reviews* **27** (1998) 65.

# Microwave-assisted synthesis of Au nanoparticles incorporated ZnO rose-like hierarchical structures and their gas sensing properties

**Katekani Shingange<sup>1,2\*</sup>, Gugu Mhlongo<sup>1</sup>, Hendrik Swart<sup>2</sup>**

<sup>1</sup>DST/CSIR National Centre for Nanostructured Materials, Council for Scientific and Industrial Research, Pretoria 0001, South Africa

<sup>2</sup>Department of Physics, University of Free State, Bloemfontein 9300, South Africa

\*Corresponding author e-mail address: kshingange@csir.co.za

## 1. Introduction

Nanostructured zinc oxide is one of the mostly used metal oxides in gas sensing applications. This is due to its high electron mobility, good chemical and thermal stability and also sensitivity to wide variety of oxidizing and reducing gases [1]. ZnO is one of the historically earliest materials used for the detection of several gases; it however has some shortcomings such as high operating temperatures, poor sensitivity and selectivity [2]. Researchers have devoted determined attempts such as doping with other metal oxides, incorporating noble metals on the surface of the ZnO nanostructures and post annealing treatment to overcome such challenges. Amongst the attempts to improve the sensing performance of the ZnO nanostructures, the loading of noble metals on the surface of the nanostructures have been proved to be effective. It has been established through research that different sizes and morphologies has profound influence on the sensing performance of the ZnO nanostructures [1]. Hierarchical ZnO nanostructures have recently receiving tremendous attention due to them possessing a high surface area which provides a larger surface where the reactions can take place [3].

In this study, ZnO roses-like hierarchical structures obtained through the microwave-assisted method were successfully prepared. Their crystallinity, morphology and optical properties were studied using X-ray diffraction (XRD), scanning electron microscopy (SEM) and Photoluminescence (PL) respectively. The interest was to also study the influence of Au nanoparticles on the gas sensing properties of these hierarchical nanostructures .to different concentrations of CH<sub>4</sub>, CO, NH<sub>3</sub> and H<sub>2</sub> at different temperatures.

## 2. Results

Fig.1 presents the XRD patterns of the as prepared ZnO and ZnO loaded with Au nanoparticles. All peaks correspond to the hexagonal wurtzite phase of ZnO (JCPDS no. 36-1451), with new diffraction peaks belonging to the face centred cubic Au (JCPDS no. 01-1172) appearing as soon as Au was introduced. Fig.2 shows the SEM image of the ZnO rose-like structures.

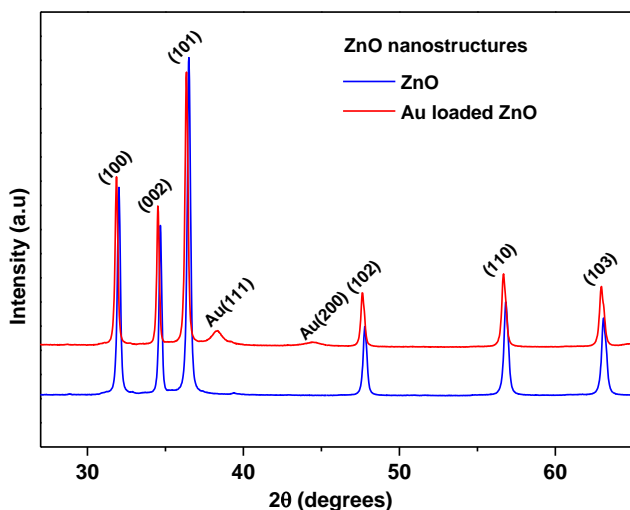


Fig. 1: XRD patterns of the ZnO and Au/ZnO nanoroses structures.

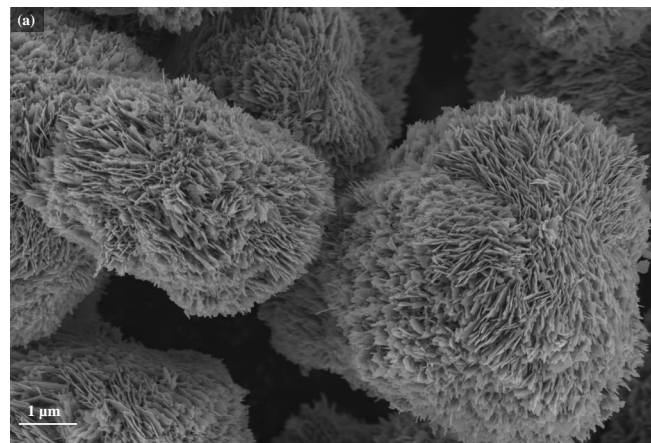


Fig. 2: SEM image of the ZnO nanoroses structures.

## 3. References

- [1] K.Shingange, Z.P. Tshabalala, B.P. Dhonge, O.M.Ntwaeaborwa, D.E. Motaung and G.H. Mhlongo. *Mater.Res.Bull.* **85** (2017) 52.
- [2] G.K.Mai and J.B.B. Rayappan, *Mater.Lett* **158** (2015) 373.
- [3] S.T.Kochuveedu, J.H.Oh, Y.R.Do and D.H.Kim. *Chem.Eur.J.***18** (2012) 7467.

# Recent advances in plasmon enhanced luminescence upconversion of lanthanide-doped NaYF<sub>4</sub> core-shells for solar cell applications

Deepak Kumar<sup>1</sup>, Kartikey Verma<sup>1</sup>, Shefali Verma<sup>1</sup>, Sudipta Som<sup>2</sup>, Vishal Sharma<sup>3</sup>, Vijay Kumar<sup>1,2\*</sup>, Hendrik C. Swart<sup>2\*</sup>

<sup>1</sup>Department of Applied Physics, Chandigarh University, Gharuan, Mohali (Punjab), India

<sup>2</sup>Department of Physics, University of the Free State, Bloemfontein, South Africa

<sup>3</sup>Institute of Forensic Science & Criminology, Panjab University, Chandigarh, India

\*Corresponding author e-mail address: vj.physics@gmail.com; swarthc@ufs.ac.za

## 1. Introduction

Lanthanide doped upconversion (UC) nanophosphors through decades, have been used in various fields of science and technology [1]. The technological advancements in upconversion nanophosphors are shaping the boundaries shared by the various fields of physics, chemistry, engineering and materials science. Recently, much interest has been focused on core-shell upconversion nanophosphors based on different materials because their properties noticeably differ from their bulk counterparts [2]. One motivation for using core-shell nanostructures is to achieve multiple functions. Another important motivation for utilizing core-shell is to enhance the photoluminescence by protecting the luminescent ions in the core from non-radiative decay due to the surface defects, vibrational deactivation attributed to solvent molecules and ligands captivated on the nanocrystals surface. Among all the rare earth fluorides, cubic and hexagonal phases of NaYF<sub>4</sub> are considered to be excellent luminescent host materials for UC because of low phonon energy, which is very favourable for high UC. However, one of the major obstacles lies in the poor absorption and emission efficiency of such nanocrystals. This problem can be overcome if one can concentrate the local electromagnetic field around them by means such as plasmonic nanostructures. The core-shell nanoparticles can also be combined with Ag/Au nanoparticles. The addition of Ag/Au nanoparticles improved excitation rates through local field magnification and amplify emission efficiency by enhanced radiative decay rates, both of which add to the overall increase in emission intensities [3]. Information on the progress made in the plasmon enhanced UC luminescence of lanthanide-doped NaYF<sub>4</sub> core-shells for solar cell applications is given. It also provides a couple of interesting features of these materials that have meticulous significance in the performance of these materials in the various fields of science and technology. We bring to light recent advances in general synthetic approaches, prospect for fabricating core-shell upconversion nanoparticles, their properties, the characterizations and applications in a single platform. It offers a short overview of cutting-edge research on plasmon enhanced upconversion luminescence of lanthanide-doped NaYF<sub>4</sub> core-shells. We also convey the primary challenges for the upcoming study.

## 2. Results

Remarkably, the intensity of UC emission from the NaYF<sub>4</sub>:Yb,Er/NaYF<sub>4</sub> core-shell nanocrystals is 16 times greater than that of the core-only nanoparticles, which lead to their applications in bioimaging and bio-analysis [4]. It is reported that the UC intensity of NaYF<sub>4</sub>:Yb,Er/SiO<sub>2</sub>/Ag core-shell nanocomposites was 14.4 times higher than that of only NaYF<sub>4</sub>:Yb,Er/SiO<sub>2</sub> core-shell nanocomposites [3]. Yin and co-workers compared the UC luminescence spectra between the NaYF<sub>4</sub>:Yb<sup>3+</sup>,Er<sup>3+</sup> nanoparticles deposited on the molybdenum trioxide/ gold nanorods and the molybdenum trioxide/gold nanorods film hybrid and NaYF<sub>4</sub>:Yb<sup>3+</sup>, Er<sup>3+</sup> nanoparticles deposited directly on the glass substrate (Fig. 1) [5]. They have been found that the UC intensity of NaYF<sub>4</sub>:Yb<sup>3+</sup>,Er<sup>3+</sup>/MoO<sub>3</sub>/gold nanorods arrays hybrids have increased more than 35 folds after 980 nm excitation.

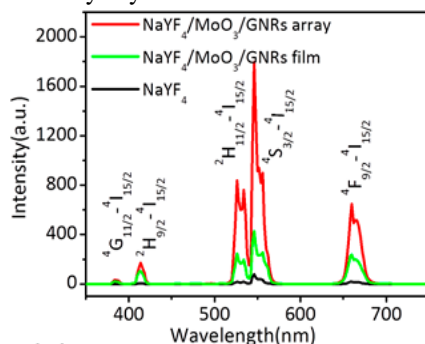


Fig. 1: The UC emissions of NaYF<sub>4</sub>:Yb<sup>3+</sup>, Er<sup>3+</sup> films, NaYF<sub>4</sub>/molybdenum trioxide/gold nanorods array hybrids and NaYF<sub>4</sub>/molybdenum trioxide/gold nanorods film hybrids under 980 nm excitation.

## 3. References

- [1] F. Wang and X. Liu, *Chem. Soc. Rev.* **38** (2009) 976.
- [2] R. G. Chaudhuri and S. Paria, *Chem. Rev.* **112** (2012) 2373.
- [3] P. Yuan, Y. H. Lee, M. K. Gnanasamandhan, Z. Guan, Y. Zhang, Q.-H. Xu, *Nanoscale* **4** (2012) 5132.
- [4] W. Ren, G. Tian, S. Jian, Z. Gu, L. Zhou, L. Yan, S. Jin, W. Yina, Y. Zhao, *RSC Advances* **2** (2012) 7037.
- [5] Z. Yin, D. Zhou, W. Xu, S. Cui, X. Chen, H. Wang, S. Xu, *ACS Appl. Mater. Interfaces* **8** (2016) 11667.

# Optical properties of $\text{Sr}_3\text{B}_2\text{O}_6:\text{Dy}^{3+}/\text{PMMA}$ polymer nanocomposites

Sumara Khursheed<sup>1</sup>, Vinay Kumar<sup>1,2</sup>, Vivek K. Singh<sup>1</sup>, Jitendra Sharma<sup>1,\*</sup>, H. C. Swart<sup>2,\*</sup>

<sup>1</sup>Department of Physics, Shri Mata Vaishno Devi University, Sub Post office Katra -182320 J&K (India)

<sup>2</sup>Department of Physics, University of the Free State, Bloemfontein, ZA 9600 South Africa

\*Corresponding author email: [jitendra.sharma@gmail.com](mailto:jitendra.sharma@gmail.com), [swarthc@ufs.ac.za](mailto:swarthc@ufs.ac.za)

## 1. Introduction

Nanocomposites are considered as a different form of composite materials, involving the inclusion of nano sized particles into organic polymer, metal or ceramic matrix materials[1-2]. Embedding of these nanoparticles in the matrices creates a great change in the mechanical, electrical, optical or magnetic properties of these materials. Since, a large number of polymers are available, but poly (methyl-methacrylate) (PMMA) represents a particularly suitable matrix for embedding nanophosphors because of its outstanding mechanical, chemical, and physical properties. Alkaline earth borates are cost effective, easy to handle, possesses long duration phosphorescence characteristics, high quantum efficiency and hence have a wide range of applications in the field of luminescence. In the present work, a detailed study of structural and optical properties of the  $\text{Sr}_3\text{B}_2\text{O}_6:\text{Dy}^{3+}/\text{PMMA}$  has been carried out. Solution casting method has been employed for the synthesis of the  $\text{Sr}_3\text{B}_2\text{O}_6:\text{Dy}^{3+}/\text{PMMA}$ . It has been observed that the embedding of the nanoparticles in the PMMA matrix preserves their typical phosphorescence emission.

## 2. Results

From the PL emission spectra (figure 1) the  $\text{Sr}_3\text{B}_2\text{O}_6:\text{Dy}^{3+}/\text{PMMA}$ , it is clear that the emission peak corresponding to 486nm and 546nm wavelength give a bluish and yellowish emission peak due to the characteristic emission of the  $\text{Dy}^{3+}$  ion, respectively. The photoluminescence (PL) spectra showed less intense phosphorescence, but no shift in the wavelength of the emission peak for all the composites. The optical properties of the composite were studied using UV-VIS Spectrophotometer. A band gap of 4.91 eV was calculated from the diffused reflectance spectrum using K-B function (figure 2). FTIR studies confirm the presence of functional groups in the nanocomposite and also it is confirmed that mixing the nanophosphors with PMMA does not change the properties of the host polymer.

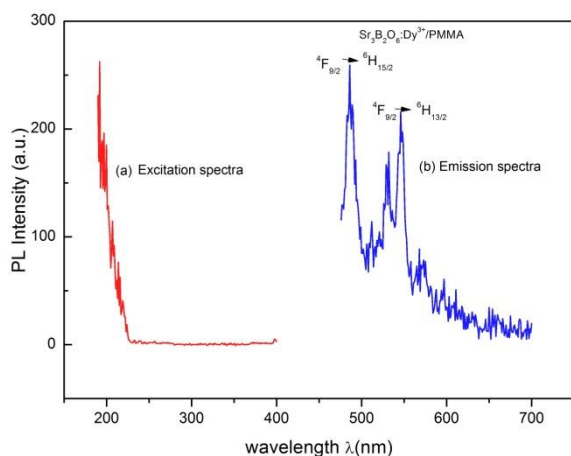


Fig. 1: Photoluminescence excitation and emission spectra  $\text{Sr}_3\text{B}_2\text{O}_6:\text{Dy}^{3+}/\text{PMMA}$  nanocomposite.

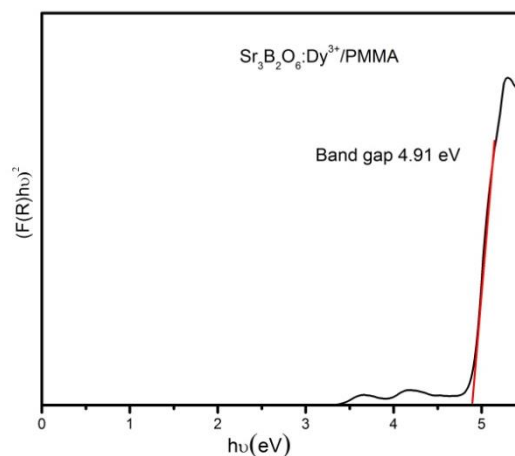


Fig. 2: Band gap determination of  $\text{Sr}_3\text{B}_2\text{O}_6:\text{Dy}^{3+}/\text{PMMA}$  nanocomposite.

## 3. References

- [1] K. Park, J. Kim, P. Kung and S.M. Kim. *J. Lumin.* **130** (2010) 1292.
- [2] F. Xiao, Y.N. Xue, Y.Y. Ma and Q.Y. Zhang. *Physica B* **405** (2010) 891.
- [3] Z.J. Wang, Z.P. Yang, P.L. Li, Q.L. Guo and Y.M. Yang. *J. Rare Earths* **28** (2010) 30.



# Radiation effects in amorphous optical films

D. Craciun<sup>1</sup>, G. Dorcioman<sup>1</sup>, O. Fufa<sup>1</sup>, G. Socol<sup>1</sup>, A. C. Galca<sup>2</sup>, H. C. Swart<sup>3</sup>, L. J. B. Erasmus<sup>3</sup>, R. E. Kroon<sup>3</sup>, C. Martin<sup>4</sup>, V. Craciun<sup>1\*</sup>

<sup>1</sup>National Institute for Lasers, Plasma and Radiation Physics, Măgurele, Romania

<sup>2</sup>National Institute for Materials Physics, Măgurele, Romania

<sup>3</sup>Department of Physics, University of the Free State, Bloemfontein, South Africa

<sup>4</sup>Ramapo College, New Jersey, USA

\*Corresponding author e-mail address: valentin.craciun@inflpr.ro

## 1. Introduction

Amorphous indium zinc oxide (IZO) films have excellent opto-electronic properties and smoothness ( $R_{\text{RMS}} < 0.5$  nm) [1]. Pulsed laser deposition (PLD) is one technique that can be used to easily grow thin films of IZO with  $\text{In}/(\text{In}+\text{Zn})$  values from 0.1 to 0.9,  $\text{In}_{1-x}\text{Ga}_x\text{ZnO}_4$ , and  $\text{HfO}_2$  that are used to fabricate thin films transistors. We deposited by the PLD technique films on Si and glass substrates from room temperature up to 200 °C. The grown films were irradiated by gamma and UV radiation to investigate the effects of radiation on the structure and properties of the films.

## 2. Results

The surface morphology of the deposited films, investigated by atomic force microscopy, was very smooth with rms values below 1 nm, allowing for the use of surface sensitive characterization techniques such as X-ray reflectivity, X-ray diffuse scattering, and grazing incidence X-ray diffraction. In addition, we also used optical reflectometry and photoluminescence (PL) to characterize the optical properties of the irradiated films. The results showed that after gamma irradiation, the surface morphology changes, the rms values increased to 2-3 nm. Also, the density decreased by a few percentage points, which resulted in a small thickness increase. The refractive index also decreased by 1-2 percentage points, consistent with the changes in density. The optical band gap values, extracted from Tauc plots, slightly decreased by few tenths of eV, while the resistivity was almost unchanged. PL measurements for different ratios of  $\text{In}/(\text{In}+\text{Zn})$  showed that the light emission increased dramatically due to defect formation after gamma radiation. The emission peaks, however, deviated from the normal expected defect emission peaks. For example, Figure 1 shows the PL emission of the 0.3 value sample excited with a He-Cd laser at 325 nm, (a) as deposited and (b) gamma irradiated. Interesting was that a regular shift in the wavelength of peak positions was also observed during measurements at different spots on the films due to changing film thickness. PL can heavily be distorted by interference. One reason for the pronounced interference may be the low reabsorption of the PL emission that typically occurs below the band gap. Figure 1 shows possible (c) wide angle interference and (d) multiple beam interference that may occur in the samples [2]. The results showed that these amorphous transparent oxide films could tolerate a high level of various radiation without adverse effects upon their structure, stoichiometry or optical and electrical properties.

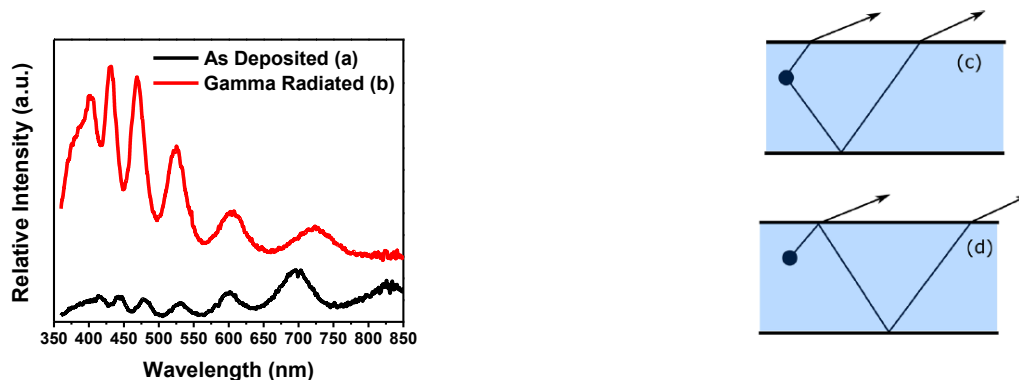


Fig. 1: (a) As deposited and (b) gamma irradiated InZnO thin films with  $\text{In}/(\text{In}+\text{Zn})$  ratio of 0.3 and a schematic of the (c) wide angle interference and (d) multiple beam interference that may occur in the thin films [2].

## 3. Acknowledgement

This work was supported by grants of the Romanian Space Agency, ROSA STAR project number 65, project IDEI 52, NUCLEU program and Romania/South Africa Research collaboration program UID: 104027 and 6 BM/2016.

## 4. References

- [1] J. Perkins, T. Gennett, M. Galante, D. Gillaspie, D. Ginley. Presented at the 37th IEEE Photovoltaic Specialists Conference (PVSC 37), Seattle, Washington, June 19-24, 2011.
- [2] J.K. Larsen, S.-Y. Li, J.J. S. Scragg, et al. *J Appl. Phys.* **118** (2015) 035307.

## Scientific Programme and Abstracts

### Wednesday 29 March

Time	Activity
7:00-8:00	Breakfast (Conference Hall)
<b>ORAL SESSION 3: Chairperson – Freddie Vorster</b>	
8:00-8:40	Invited Talk 4: <b>Susanne Siebentritt</b> (p. vi) <i>p. 14: Why do we make CIGS solar cells off-stoichiometric?</i>
8:40-9:00	Oral 9: <b>Vinod Kumar</b> <i>p. 15: Rare earth doped up conversion nanophosphor for solar cell application</i>
9:00-9:20	Oral 10: <b>R. M. Dix-Peek</b> <i>p. 16: Identification of defects in poly-crystalline Si solar cells</i>
9:20-9:40	Oral 11: <b>Edward Lee</b> <i>p. 17: Synthesis and characterisation of Y<sub>2</sub>O<sub>3</sub> phosphor co-doped with bismuth and ytterbium ions for application in solar cells</i>
9:40-10:20	Invited Talk 5: <b>Vladimir Dyakonov</b> (p. vi) <i>p. 18: Charge carrier recombination in perovskite solar cells</i>
10:20-10:40	Tea (Conference Hall)
<b>ORAL SESSION 4: Chairperson – Ernest van Dyk</b>	
10:40-11:20	Invited Talk 6: <b>Vladimir Kolkovsky</b> (p. vii) <i>p. 19: Carbon-hydrogen-related complexes in Si</i>
11:20-11:40	Oral 12: <b>Matshisa J. Legodi</b> <i>p. 20: Deep Level Transient Spectroscopy and Admittance Spectroscopy of methylammonium lead-bromide (CH<sub>3</sub>NH<sub>3</sub>PbBr<sub>3</sub>) perovskite solar cells</i>
11:40-12:00	Oral 13: <b>Joachim Bollmann</b> <i>p. 21: Admittance Spectroscopy or DLTS: a contrasting juxtaposition</i>
12:00-12:20	Oral 14: <b>Ivan G. Ivanov</b> <i>p. 22: Doping and defects in fluorinated SiC CVD</i>
12:20-12:40	Oral 15: <b>D. D. Ramteke</b> <i>p. 23: Structure and photoluminescence properties of Ba<sub>(1-x)</sub>Si<sub>4</sub>O<sub>10</sub>:xSm<sup>3+</sup></i>
12:40-13:00	Oral 16: <b>Mubarak Y. A. Yagoub</b> <i>p. 24: Low temperature photoluminescence study of Ce<sup>3+</sup> and Eu<sup>2+</sup> ions doped SrF<sub>2</sub> nanocrystal</i>
13:00-14:00	Lunch (Conference Hall)
<b>ORAL SESSION 5: Chairperson – André Venter</b>	
14:00-14:40	Invited Talk 7: <b>Martin Geller</b> (p. vii) <i>p. 25: Spectroscopy on self-assembled quantum dots: transport meets optics</i>
14:40-15:00	Oral 17: <b>Magnus C. Wagener</b> <i>p. 26: Electronic structure and optical properties of GaSb/GaAs and GaSb/Al<sub>x</sub>Ga<sub>1-x</sub>As quantum rings</i>
15:00-15:20	Oral 18: <b>M. E. Lee</b> <i>p. 27: Optical and microanalytical characterization of Al<sub>x</sub>Ga<sub>1-x</sub>N epilayers for photonic applications</i>
15:20-15:40	Oral 19: <b>P. O. Holtz</b> <i>p. 28: Single polarized-photon emitters from elongated III-nitride pyramidal quantum dots</i>
15:40-16:00	Tea (Conference Hall)
16:00-18:00	GAME DRIVE (option 2)
18:00-20:30	DINNER (Boma)

# Why do we make CIGS solar cells off-stoichiometric?

**Susanne Siebentritt<sup>1\*</sup>**

<sup>1</sup>Laboratory for Photovoltaics, Physics and Materials Science Research Unit, University of Luxembourg, 41, rue du Brill, 4422 Belvaux, Luxembourg

\*Corresponding author e-mail address: susanne.siebentritt@uni.lu

## 1. Cu-poor and Cu-rich Cu(In,Ga)Se<sub>2</sub>

Cu(In,Ga)Se<sub>2</sub> is an alloy of CuInSe<sub>2</sub> and CuGaSe<sub>2</sub> based on the chalcopyrite structure. It is used as absorber in thin film solar cells, which present a new generation of photovoltaic technologies. The advantages of thin film solar cells are low cost based on their low material and energy consumption, short energy pay back times, flexibility in design and light weight (see e.g. the White Paper on <http://cigs-pv.net>). Solar cells have reached 22.6% of certified power conversion efficiency [1], commercial modules reach 16% efficiency (see [2] and the websites of various producers).

Cu(In,Ga)Se<sub>2</sub> solar cells are usually based on Cu-poor material, i.e. material with a sub-stoichiometric Cu content. simply, because solar cells based on Cu-poor material always show better efficiencies [3-5]. However, Cu-rich material shows the better semiconductor properties with lower defect concentrations and better transport properties [6]. It has been long understood that the lower efficiency is due to recombination at or near the interface, which limits the open-circuit voltage [3]. This recombination can be suppressed by an In-Se surface treatment [4] or by a potassium treatment [7]. In pure CuInSe<sub>2</sub> solar cells (without Ga) the surface treatment leads to efficiencies of Cu-rich solar cells equal to Cu-poor ones [8], whereas in Ga-containing absorbers the surface treatment leads to an improvement of the open-circuit voltage, but not to a complete recovery of the values obtained in Cu-poor absorbers [5]. It was only recently understood that this difference is not in the first place due to a difference in interface properties, but to bulk properties of Cu(In,Ga)Se<sub>2</sub>: in pure CuInSe<sub>2</sub> the quasi-Fermi level splitting, which is a measure of the open-circuit voltage an absorber could achieve, is higher in Cu-rich material than in Cu-poor [9], whereas in Cu(In,Ga)Se<sub>2</sub> (with Ga) the quasi-Fermi level splitting is lower in Cu-rich material than in Cu-poor, already in the absorber without any interface [10]. It has been proposed that the difference is due to a deep Ga<sub>Cu</sub> antisite defect [11, 12], which forms a less detrimental pair with copper vacancies in Cu-poor material. A deep defect with the expected composition dependence has been observed [12].

## 2. References

- [1] P. Jackson, R. Wuerz, D. Hariskos, E. Lotter, W. Witte, M. Powalla, *physica status solidi (RRL) – Rapid Research Letters* **10** (2016) 583.
- [2] M. A. Green, K. Emery, Y. Hishikawa, W. Warta, E. D. Dunlop, *Progress in Photovoltaics: Research and Applications* **24** (2016) 905.
- [3] M. Turcu, O. Pakma, U. Rau, *Appl. Phys. Lett.* **80** (2002) 2598.
- [4] Y. Aida, V. Depredurand, J. K. Larsen, H. Arai, D. Tanaka, M. Kurihara, S. Siebentritt, *Progress in Photovoltaics* **23** (2015) 754.
- [5] L. Choubrac, T. Bertram, H. Elanzeery, S. Siebentritt, *Phys. stat. sol. a* (2016) DOI: 10.1002/pssa.201600482.
- [6] S. Siebentritt, L. Gütay, D. Regesch, Y. Aida, V. Depredurand, *Solar Energy Mat. Solar Cells* **119** (2013) 18.
- [7] H. Elanzeery, F. Babbe, M. Melchiorre, E. Robert, A. Zelenina, S. Siebentritt, submitted 2016.
- [8] T. Bertram, V. Depredurand, S. Siebentritt, in *40th IEEE Photovoltaic Specialist Conference*, IEEE, Denver (2014) 3633.
- [9] L. Gütay, D. Regesch, J. K. Larsen, Y. Aida, S. Siebentritt, *Appl. Phys. Lett.* **99** (2011) 151912;
- [10] D. Regesch, L. Gütay, J. K. Larsen, V. Depredurand, D. Tanaka, Y. Aida, S. Siebentritt, *Appl. Phys. Lett.* **101** (2012) 112108.
- [11] F. Babbe, L. Choubrac, S. Siebentritt, *Appl. Phys. Lett.* **109** (2016) 082105.
- [12] B. Huang, S. Chen, H.-X. Deng, L.-W. Wang, M. A. Contreras, R. Noufi, S.-H. Wei, *IEEE J. Photovolt.* **4** (2014) 477.
- [13] C. Spindler, D. Regesch, S. Siebentritt, *Appl. Phys. Lett.* **109** (2016) 032105.

# Rare earth doped up conversion nanophosphor for solar cell application

Vinod Kumar<sup>1,2\*</sup>, H. C. Swart<sup>2</sup>, O. M. Ntwaeaborwa<sup>3</sup>, Viresh Dutta<sup>1</sup>

<sup>1</sup> Photovoltaic Laboratory, Centre for Energy Studies, Indian Institute of Technology Delhi, New Delhi 110016, India

<sup>2</sup> Department of Physics, University of the Free State, P.O. Box 339, Bloemfontein, ZA 9300, South Africa

<sup>3</sup> School of Physics, University of the Witwatersrand, Private Bag X3, Wits, 2050, South Africa

\*Corresponding author e-mail address: vinod.phy@gmail.com

## 1. Introduction

The global energy consumption is increasing and is expected to double by the year 2050. Most of our energy supply comes from fossil fuels; however, their exhaustibility and the environmental concerns associated with fossil fuels have triggered the search for alternative renewable energy sources. The sun is the largest source of renewable energy on earth. It freely provides 120,000 TW of solar power to the Earth's surface. It has been reported that the Earth's surface receives nearly 10,000 times more solar power than the global power consumption. There is an urgent need for cheap energy from clean and abundant sources. As a result, research efforts are underway to find low cost and high efficiency photovoltaic devices to convert sunlight to electricity. In recent years, wavelength dependent spectral converters have been explored for enhanced energy conversion in solar cells [1]. The up-conversion (UC) of sunlight has two possible routes for improving energy harvesting over the whole solar spectrum. Via such processes it could be possible to enhance the efficiency of solar cells. One of the materials more extensively studied for this purpose have been the rare earth (RE) materials, due to the suitability of their discrete energy levels for photon conversion inside a wide variety of host materials. Semiconductors doped with RE elements such as Eu, Er, Yb, and Tb have been intensively pursued for the synthesis of UC solar cells. There are two main factors leading to the stable and sharp luminescence in RE elements: one is that the 4f orbital of RE ions is shielded by the outer 6s, 5p and 5d orbitals, which weakens its coupling with the surrounding ligands; the other is that the f-f transitions are parity forbidden. In this work, UC nanophosphors (NPrs) were prepared by different synthesis technique for solid state lighting and solar cell application. The effect of the dopant concentration on the structural, morphological, chemical and photoluminescence properties of doped UC NPr is reported. The optimized up conversion nanophosphors are investigated to improve the performance of solar cells. The effect of coating up conversion layers (etc - TiO<sub>2</sub>:Eu NPr) onto the front and inside of a solar cell is evaluated. So up conversion nanophosphors based material can be used as a new future approach for solar cell.

## 2. Results

The current density-voltage (J-V) curves of the dye sensitized solar cells (DSSCs) with and without UC NPr for the solar cell are shown in Fig. 1. Short-circuit current density ( $J_{SC}$ ) of 17.56 mA/cm<sup>2</sup>, an open-circuit voltage ( $V_{OC}$ ) of 0.68 V, a fill factor (FF) of 0.70 and an overall PCE of 8.29% were recorded for the cell without UC layer and a  $J_{SC}$  of 18.55 mA/cm<sup>2</sup>,  $V_{OC}$  of 0.68 V and FF of 0.70 with a PCE of 8.76% were recorded for the cell with UP layer. A DSSC with UP layer shows the higher  $J_{SC}$  due to the increase in the number of photo-generated photons in the visible region converted from NIR region due to the doping of RE materials [2]

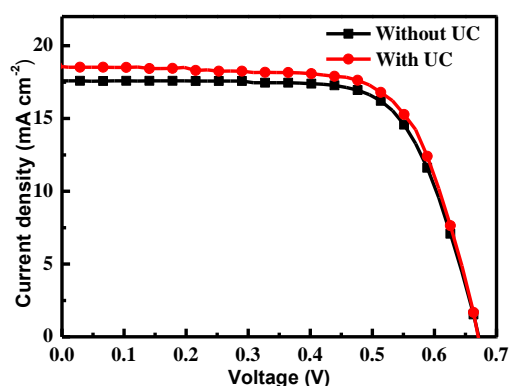


Fig. 1: J-V characteristics of with and without UC NPr based solar cell.

## 3. References

- [1] H. Ennen, G. Pomrenke, A. Axmann, K. Eisele, W. Haydl and J. Schneider. *Appl. Phys. Lett.* **46** (1985) 381.
- [2] Y. Shang, S. Hao, C. Yang and G. Chen. *Nanomaterials* **5** (2015) 1782.

# Identification of defects in poly-crystalline Si solar cells

**R. M. Dix-Peek<sup>1\*</sup>, E. E. van Dyk<sup>1</sup>, F. J. Vorster<sup>1</sup>, C. J. Pretorius<sup>2</sup>**

<sup>1</sup>Department of Physics, Nelson Mandela Metropolitan University, Port Elizabeth, 6031,

<sup>2</sup>Department of Mathematics and Applied Mathematics, Nelson Mandela Metropolitan University, Port Elizabeth, 6031,

\*Corresponding author e-mail address: s212286552@nmmu.ac.za

## 1. Introduction

Device material quality plays an important role in the efficiency and longevity of photovoltaic (PV) cells. During operation of a PV module, local shading of the module can cause shaded PV cells to be reverse biased. This can lead to localised heating and therefore possibly leading to irreversible damage to the PV module [1]. Cells under reverse bias experience localised heating through sites of junction breakdown [2] and shunting [3].

In this study, a combination of spatially-resolved, non-destructive techniques, electroluminescence (EL), infrared thermography and light beam induced current (LBIC) measurements, were used to identify specific defects and features of a poly-crystalline (p-c) Si PV cell. EL is the technique associated with electrically stimulated emission of light from the PV cell. The EL emitted under forward bias is related to recombination, optical, resistive and material properties of the cell [4]. The EL emitted under reverse bias is related to various breakdown mechanisms [5]. Dark IR thermography (electrically stimulated) is used in the identification and characterisation of shunts [6], and that of breakdown sites [2] of p-c Si PV cells. LBIC measurements are used to spatially resolve local cell parameters [7, 8].

## 2. Results

Fig. 1 shows the reverse biased EL (ReBEL) image of a p-c Si cell at -17.901 V and -2 A. Fig. 2 shows reverse modulated dark IR thermal image of the same cell at the same bias and current. Features A and B appear in both the Fig. 1 and Fig. 2, indicating there is an optically active, thermally responsive site of the cell. These features are most likely due to localised junction break down. Features C and D appear Fig. 2 and not in Fig. 1, indicating there is an optically inactive, thermally responsive site of the cell. These features are most likely due to localised shunting.

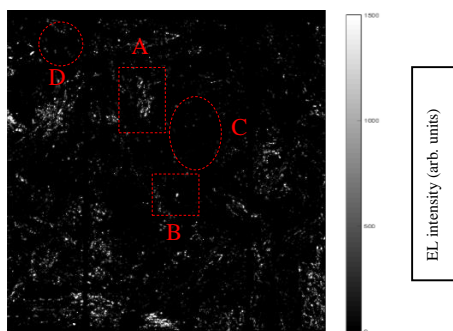


Fig. 1: ReBEL image of p-c Si cell

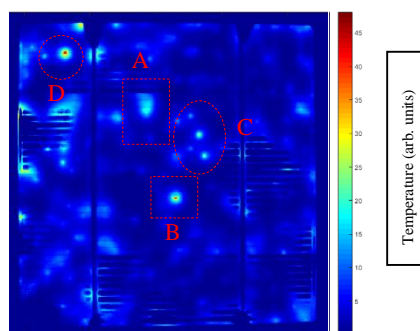


Fig. 2: IR thermal image of p-c Si cell:

## 3. References

- [1] M. C. Alonso-García et al., 'Experimental study of mismatch and shading effects in the I-V characteristic of a photovoltaic module' *Sol. Energy Mater. Sol. Cells*, **90** (2006) 329.
- [2] J. Bauer, J.-M. Wagner, A. Lotnyk, H. Blumtritt, B. Lim, J. Schmidt, O. Breitenstein 'Hot spots in multicrystalline silicon solar cells: avalanche breakdown due to etch pits', *Phys. Status Solidi RRL* **3** 2 (2009) 40.
- [3] A Kaminski, O Breitenstein, J P Boyeaux, P Rakotoniaina, A Laugier, 'Light beam induced current and infrared thermography studies of multicrystalline silicon solar cells', *J. Phys.: Condens. Matter* **16**, (2004).
- [4] M Okullo, F Vorster, E van Dyk, J Crozier, 'Analysis of homogeneity in thin film photovoltaic modules using large area light beam induced current (LA-LBIC) measurements', *Proceedings of South African Institute of Physics 2015*, (2015).
- [5] B. Y. Zhang, C. Yang, W. F. Liu, A. M. Liu, 'Origin of breakdown mechanism in multicrystalline silicon solar cells', *Applied Physics Letters* **101** (2012) 093903.
- [6] O. Breitenstein, J.P. Rakotoniaina, M. Kaes, S. Seren, T. Pernau, G. Hahn, W. Warta, and J. Isenberg. 'LOCK-IN THERMOGRAPHY - A UNIVERSAL TOOL FOR LOCAL ANALYSIS OF SOLAR CELLS', *Proceedings of 20<sup>th</sup> European Photovoltaic Solar Energy Conference*, (2005) 590.
- [7] J. Carstensen, G. Popkurov, J. Bahr, H. Föll, 'CELLO: an advanced LBIC measurement technique for solar cell local characterization', *Sol. Energy Mater. Sol. Cells*, **90**, (2006) 329.
- [8] Bezuidenhout, L 2015, 'On the characterization of photovoltaic device parameters using light beam induced current measurements', MSc thesis, Nelson Mandela Metropolitan University

# Synthesis and characterisation of $\text{Y}_2\text{O}_3$ phosphor co-doped with bismuth and ytterbium ions for application in solar cells

Edward Lee<sup>1\*</sup>, R. E. Kroon<sup>1</sup>, J. J. Terblans<sup>1</sup>, H. C. Swart<sup>1\*</sup>

<sup>1</sup>Department of Physics, University of the Free State, Bloemfontein, South Africa

\*Corresponding author e-mail address: LeeE@ufs.ac.za, SwartHC@ufs.ac.za

## 1. Introduction

Silicon based solar cells are currently the most common form of photovoltaic cells used to convert solar energy to electrical energy. Unfortunately silicon solar cells suffer from low conversion efficiencies, due to the mismatch between the solar spectrum and the maximum absorption spectrum of silicon [1]. This may be improved by coating the solar cell with a down-converting phosphor such as  $\text{Y}_2\text{O}_3:\text{Bi}^{3+}, \text{Yb}^{3+}$  that absorbs the sun's ultraviolet light and emits in the infrared where the silicon solar cell is most efficient. The effect of  $\text{Yb}^{3+}$  ion concentration on the morphological and luminescent properties of these co-doped phosphors was investigated. The samples were prepared using the co-precipitation technique where yttrium oxide ( $\text{Y}_2\text{O}_3$ , 99.99%), bismuth oxide ( $\text{Bi}_2\text{O}_3$ , 99.9%) and ytterbium oxide ( $\text{Yb}_2\text{O}_3$ , 99.995%) were used as starting materials. These were dissolved in nitric acid and diluted with ammonium hydroxide in order to control the pH during synthesis. After annealing the samples at 1000 °C, they were characterised using X-ray diffraction and photoluminescence spectroscopy.

## 2. Results

The X-ray diffraction spectra for the  $(\text{Y}_{0.98-x}\text{Bi}_{0.02}\text{Yb}_x)_2\text{O}_3$  samples ( $x = 0.01, 0.02, 0.03, 0.04$  and  $0.05$ ) shown in Fig. 1 revealed that they had a simple cubic structure with a  $Ia\bar{3}$  space group which matched the JCPDS file number 83-0927. The crystallite size for the prepared nanophosphors varied between 20 nm to 35 nm with the  $x = 0.04$  sample having the smallest crystallite size. The luminescence spectra shown in Fig. 2 were obtained using excitation with a 325 nm He-Cd laser. The results show a broad near-infrared emission band with a sharp maximum situated at 976 nm due to the  $\text{Yb}^{3+}: {}^2\text{F}_{5/2} \rightarrow {}^2\text{F}_{7/2}$  transition, accompanied by several other weaker emission peaks due to Stark splitting of the  ${}^2\text{F}_{5/2}$  and  ${}^2\text{F}_{7/2}$  levels [2]. A sample doped only with  $\text{Bi}^{3+}$  ions shows no emission in the NIR region. This result demonstrates UV to near-infrared down-conversion optimised in the phosphor with  $x = 0.03$  (maximum emission intensity) which may be used to modify the solar spectrum with the aim of improving the efficiency of silicon solar cells.

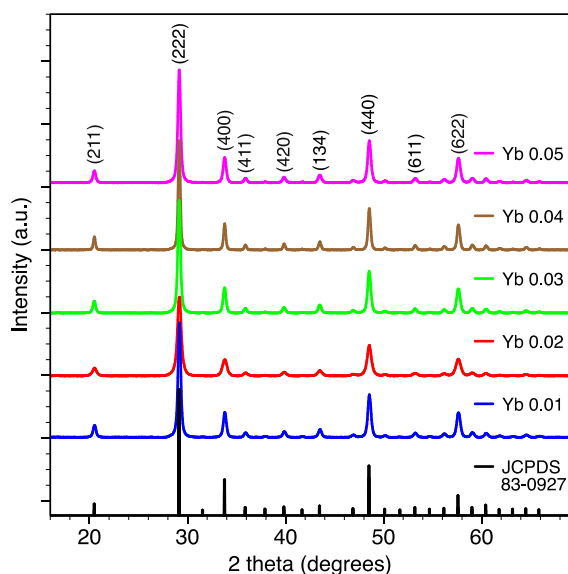


Fig. 1: X-ray diffraction spectra of  $(\text{Y}_{0.98-x}\text{Bi}_{0.02}\text{Yb}_x)_2\text{O}_3$  phosphors ( $x = 0.01, 0.02, 0.03, 0.04$  and  $0.05$ ).

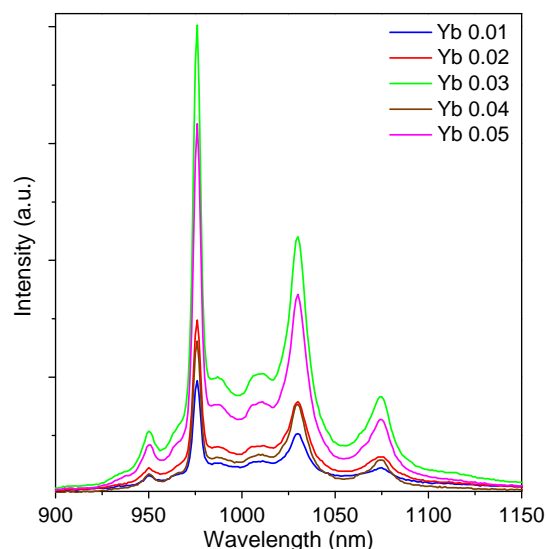


Fig. 2: Near-infrared emission of  $(\text{Y}_{0.98-x}\text{Bi}_{0.02}\text{Yb}_x)_2\text{O}_3$  phosphors ( $x = 0.01, 0.02, 0.03, 0.04$  and  $0.05$ ).

## 3. References

- [1] B. M. Van Der Ende and A. Meijerink. *Phys. Chem. Chem. Phys.* **11** (2009) 11081–11095.
- [2] R. Simura et al. *Opt. Mater.* **30** (2007) 18–21.

# Charge carrier recombination in perovskite solar cells

Vladimir Dyakonov<sup>1,2\*</sup>, David Kiermasch<sup>1</sup>, Philipp Rieder<sup>1</sup>, Kristofer Tvingstedt<sup>1</sup>, Andreas Baumann<sup>2</sup>

<sup>1</sup> Experimental Physics 6, University of Würzburg, 97074 Würzburg, Germany

<sup>2</sup> Bavarian Center for Applied Energy Research, 97074 Würzburg, Germany

\*Corresponding author e-mail address: dyakonov@physik.uni-wuerzburg.de

## 1. Introduction

Perovskite solar cells are progressing very fast, showing extraordinary performance exceeding 22%. The charge carrier lifetime is an important parameter in solar cells as it defines, together with the mobility, the diffusion length of the charge carriers, thus directly determining the optimal active layer thickness of a device. Here, we address the recombination dynamics in planar solar cells made of methylammonium lead iodide perovskites MAPbI<sub>3</sub> and compare them with bromine-containing perovskites.

## 2. Results

Most of the recombination studies presented so far have been focused on perovskite films or crystals but only a few have studied the charge carrier lifetime in complete devices. [1] We report on charge carrier lifetime values in bromine containing planar perovskite solar cells with varying the bromine content by using different precursor materials. The lifetime and corresponding charge carrier density has been derived from transient photovoltage (TPV) and charge carrier extraction (CE) experiments. To study the impact of different bromine-to-iodine ratios, we varied the precursors in the well-established *interdiffusion* approach. Starting from PbI<sub>2</sub> and methylammonium iodine (MAI), bromine was introduced in the perovskite lattice by replacing the salts with MABr or PbBr<sub>2</sub> (MAPb(I<sub>1-x</sub>Br<sub>x</sub>)<sub>3</sub>).

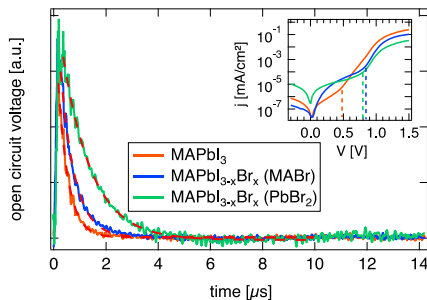


Fig. 1: TPV decays at a background illumination intensity of 1 sun for the three different devices measured at 300 K. The single exponential fits are shown as dashed lines. Inset shows dark J-V.

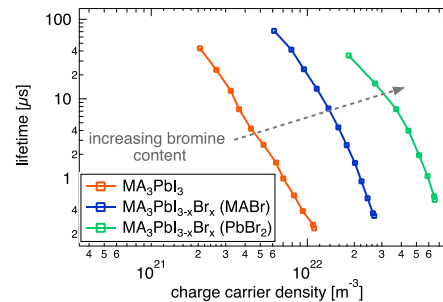


Fig. 2: TPV lifetime plotted versus the charge carrier density determined with CE for the three investigated devices.

Normalized TPV transients for the three devices are plotted in Fig. 1, measured under illumination conditions equivalent to 1 sun. To determine the small perturbation decay lifetime, the signal was fitted with a single exponential function. It is also important to note that TPV experiments should be conducted in the exponential diode regime of a solar cell to correctly study the bulk material properties of the active layer, instead of recombination losses via parasitic shunt pathways (see inset to Fig.1). Here, we conducted measurements in the range of 0.0056 up to 2 suns accordingly by changing the current of the LED and using different neutral density filters. This light intensity span resulted in corresponding  $V_{oc}$  values ranging from 692 mV to 856 mV for the MAPbI<sub>3</sub> device, clearly being in the exponential diode regime. From these measurements, we calculated charge carrier lifetime values  $\tau$  in dependence on the applied illumination intensity. Performing CE experiments at the same conditions as TPV allows us to determine the corresponding charge carrier density  $n$  at each background illumination intensity, and subsequently correlate it with the charge carrier lifetimes  $\tau$ . The obtained charge carrier lifetimes from TPV plotted versus the carrier density from CE is shown for the three perovskites in Fig. 2.

To summarize, we observed an increased charge carrier lifetime from 0.39  $\mu$ s for the MAPbI<sub>3</sub> device to 1.07  $\mu$ s for MAPb(I<sub>0.46</sub>Br<sub>0.54</sub>)<sub>3</sub> at an illumination intensity of 1 sun. We discuss the increased lifetime in a picture, in which bromine act as dopants introducing shallow defects to the MAPbI<sub>3</sub> lattice which may lead to a reduced second order recombination and hence increased carrier lifetime due to carrier trapping-and-release events. [2]

## 3. References

- [1] A. Baumann, K. Tvingstedt, M. C. Heiber, S. V ath, C. Momblona, H. J. Bolink, V. Dyakonov, *APL Mater.* **2** (2014) 081501.
- [2] D. Kiermasch, P. Rieder, K. Tvingstedt, A. Baumann, V. Dyakonov, *Sci. Reps.* **6** (2016) 39333.

# Carbon-hydrogen-related complexes in Si

Vladimir Kolkovsky<sup>1\*</sup>

<sup>1</sup>Technische Universität Dresden, 01062 Dresden, Germany

\*Corresponding author e-mail address: kolkov@ifpan.edu.pl

## 1. Introduction

The performance of electronic devices is greatly influenced by the presence of unintentionally introduced electrically active defects in silicon. Some impurities such as carbon or oxygen which are electrically inactive in Si can create electrically active complexes only after interaction with other crystal imperfections and impurities. Nowadays the technological processing of devices often includes heat treatments of Si wafers in hydrogen (H) containing atmosphere in order to reduce the density of interface states or to passivate the electrical activity of the surface. As a result hydrogen also penetrates into the bulk of Si wafers and this can lead to the appearance of a number of H-related defects in the active region of Si devices. Among those traps the electrical and structural properties of CH-related defects attract significant attention since carbon is always present in Czochralski (Cz) and float-zone (FZ) Si. The presence of oxygen in high concentrations in such samples could also result in the appearance of novel defects compared to hydrogenated samples with a low oxygen content. In this study our recent findings, which shed light on the origin of carbon-hydrogen related complexes in *n*-type and *p*-type Si samples with different oxygen concentrations, are presented.

## 2. Results

Figs. 1 and 2 show deep level transient spectroscopy (DLTS) spectra recorded in *n*- and *p*-type Cz Si after hydrogenation by a dc H plasma treatment. Several DLTS peaks (E42, E65, E75, E90, E262, and H180) are observed in these samples. The concentrations of E65 and E75 are below the detection limit of our DLTS setup (around  $5 \times 10^{11} \text{ cm}^{-3}$ ) in hydrogenated FZ Si whereas E42, E90, and E262 also appear in these samples. Until now the charge states and the origin of the defects presented in Figs. 1-2 are unknown or controversial in the literature. We employ the high-resolution Laplace DLTS technique in order to study the activation enthalpy, the capture cross section, the charge state, and the annealing properties of these traps. By analysing the depth profiles of these defects in samples with different carbon, oxygen, hydrogen, and doping concentrations we conclude that all these traps belong to carbon-hydrogen related defects that contain one carbon and one hydrogen atom. The origin of these defects is discussed. Our results on the carbon-hydrogen-related complexes give a first conclusive explanation of some previously reported controversial experimental data.

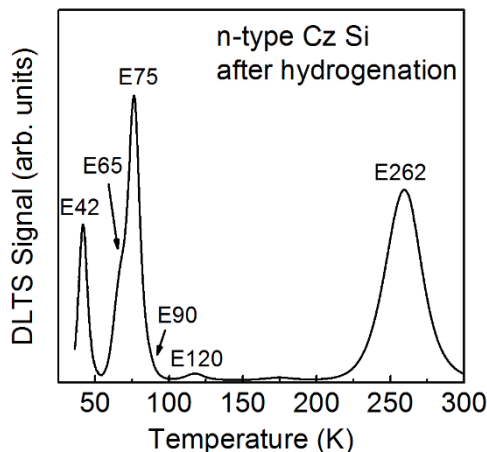


Fig. 1: DLTS spectrum recorded in *n*-type Cz Si subjected to hydrogenation by a dc H-plasma treatment

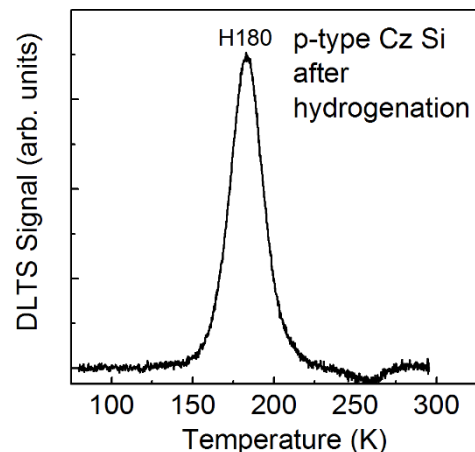


Fig. 2: DLTS spectrum recorded in *p*-type Cz Si subjected to hydrogenation by a dc H-plasma treatment



# Deep Level Transient Spectroscopy and Admittance Spectroscopy of methylammonium lead-bromide ( $\text{CH}_3\text{NH}_3\text{PbBr}_3$ ) perovskite solar cells

Matshisa J. Legodi<sup>1\*</sup>, Mmantsae W. Diale<sup>1</sup>, Francois D. Auret<sup>1</sup>, John W. Rosenberg<sup>2</sup>, David Cahen<sup>2</sup>

<sup>1</sup>Physics Department, University of Pretoria, Private Bag X20, Pretoria, 0028, South Africa

<sup>2</sup>Department of Materials and Interfaces, Weizmann Institute of Science, Rehovoth 76100, Israel

\*Corresponding author e-mail address: matshisa.legodi@up.ac.za

## 1. Introduction

Significant progress has been recorded in the power conversion efficiency (PCE) and device stabilization of organoplumbate-trihalide ( $\text{MAPbX}_3$ , (MA = methylammonium, X = I, Br, Cl) perovskite solar cells. From the humble 4% reported in 2009 to a certified [1] 22% efficiency in 2015; these developments are spectacular. Interest in the transport properties of the  $\text{MAPbX}_3$ 's was triggered as soon as the first high efficiency devices appeared. A remarkable feature in  $\text{MAPbX}_3$  devices is the low diffusion coefficients and mobility:  $0.05\text{--}0.2\text{ cm}^2\text{ s}^{-1}$  and  $1\text{--}30\text{ cm}^2\text{ V}^{-1}\text{ s}^{-1}$ , respectively, in polycrystalline material [2]. Mobilities in single crystalline material are marginally higher than  $100\text{ cm}^2\text{ V}^{-1}\text{ s}^{-1}$  [2]. This is in spite of the low effective masses that are comparable to those in prototypical Si and GaAs solar cells. Structural defects and not impurities are thought to be responsible for the low mobility figures. Defects are also implicated in the hysteresis typical of these materials and in the intrinsic doping. Bandgap engineering has been demonstrated by introducing Sn and Ge to partially substitute the Pb in this materials system. Again, the effect of defects introduced in this manner on the transport properties is still unknown. Knowledge about defects is critical for further improvements in materials properties.

We have studied highly resistive single crystal lightly p-type methylammonium lead-bromide using admittance spectroscopy and current-mode deep level transient spectroscopy (I-DLTS). Multi-frequency capacitance-temperature ( $C\text{--}T$ ) scans reveal a phase transition around 150 K and the presence of a defect with activation energy,  $E_V+0.60\text{ eV}$ , around 275 K (Fig. 1); the same defect does not appear in the  $C\text{--}T$  spectra when the sample is cooled and measured under forward bias. The  $C\text{--}T$  spectra also reveal anomalous capacitances profiles: capacitance decreases with increasing temperature, suggesting deeper acceptor-like defects. Light on/off  $C\text{--}T$  measurements support the acceptor-like characterization. Using I-DLTS, we detect a trap at  $E_V+0.80\text{ eV}$  (Fig. 2) but are unsuccessful in splitting it using Laplace-DLTS. This defect becomes almost un-detectable by I-DLTS post vacuum-annealing at 380 K.

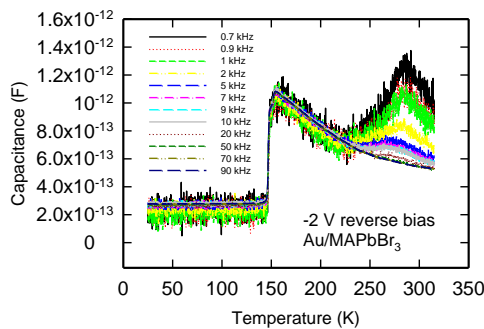


Fig. 1:  $C\text{--}T$  scans showing phase transition at 150 K, anomalous  $C\text{--}T$ 's at  $T > 150\text{ K}$  and frequency dispersion around 275 K.

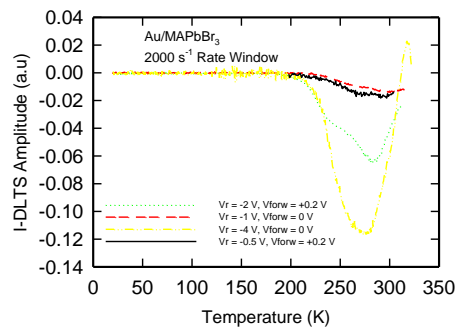


Fig. 2: I-DLTS spectra showing the  $E_V+0.7\text{ eV}$  hole trap recorded at various biases at  $2000\text{ s}^{-1}$  rate window.

## 3. References

[1] [http://www.nrel.gov/pv/assets/images/efficiency\\_chart.jp](http://www.nrel.gov/pv/assets/images/efficiency_chart.jp), accessed 19 November 2016.

[2] Thomas M. Brenner, David A. Egger, Leeor Kronik, Gary Hodes and David Cahen, *Nature Reviews, Materials*, **1** (2016) 1.

# Admittance Spectroscopy or DLTS: a contrasting juxtaposition

**Joachim Bollmann<sup>1\*</sup>, André Venter<sup>2</sup>**

<sup>1</sup>Technische Universität Bergakademie Freiberg, 50937 Freiberg, Germany

<sup>2</sup>Nelson Mandela Metropolitan University, University Way Port Elizabeth, South Africa

\*Corresponding author e-mail address: joachim.bollmann@esm.tu-freiberg.de

## 1. Introduction

Arguably the most commonly used electrical defect spectroscopic techniques in condensed matter physics are Admittance Spectroscopy (AS) and the Deep Level Transient Spectroscopy (DLTS). Based on Shockley Read Hall statistics, the thermal activation energies, the capture cross sections (for both minority and majority charge carriers), as well as the densities of deep level centres could be obtained using these techniques. AS measures the frequency (and temperature) dependence of both the real (conductance) and the imaginary component (susceptance) of the complex admittance of the space charge region of a  $p-n$  junction or a Schottky device [1] while in DLTS, the capacitance transient due to the thermal emission of trapped carriers in the space charge region, is recorded.

In DLTS, empty traps within the space charge region of a reverse biased junction are filled up to a point, defined by the magnitude of a periodically applied filling pulse. The time constant (inverse thermal emission rate) of the thermally induced relaxation (to equilibrium) is then measured. It should be clear that accurate determination of the defect parameters (i.e. defect density, depth profiles, and electrical field dependence of activation energy) requires particular knowledge of the bias dependent space charge properties. AS evaluates the energy levels of majority carrier traps, in close proximity to the point where the energy level intersects the Fermi level, the so called cross-over point [2]. In contrast to DLTS, the underlying observed physical effect is not the thermal emission of trapped carriers but rather a frequency dependent variation in the admittance of the device due the charging and discharging of traps, a consequence of the applied ac voltage, located at the cross-over point. Depending on the junction temperature, and for a given energy level, the trap occupation could adiabatically follow the ac test frequency [3]. Similar to the dielectric relaxation response of an ideal, no interacting population of dipoles to an alternating external electric field (Debye relaxation model) the conductance shows a maximum for  $\omega\tau = 1$ ; with  $\omega = 2\pi f$ , with  $f$ , the ac test frequency and  $\tau$ , the characteristic time constant of the defect. In parallel the capacitance changes by  $\Delta C = C(\omega\tau \ll 1) - C(\omega\tau \gg 1)$ .

## 2. Results

In this paper AS and DLTS measurements on SiC diodes will be used to address the following critical questions:

- (1) Are the detection limits of AS and DLTS comparable?
- (2) What is the spectroscopic resolution of AS?
- (3) How does one estimate defect densities from AS measurement? (i.e., is depth profiling of deep level defects possible using AS?)
- (4) How should one interpret results if the defect densities approach or exceed the doping densities?
- (5) What is the emission rate limit for AS?
- (6) Should the activation energies obtained from AS and DLTS be similar?
- (7) How does the field effect, critical in DLTS, impact the thermal emission rate of defect states as determined by AS?

One remarkable result is that in AS the sensitivity depends on both the cross-over point position ( $w_\lambda$ ) and the total space charge width ( $w_c$ ). Consequently, the smaller the applied bias the higher the sensitivity of the measurement. For low defect densities:

$$\frac{\Delta C}{C_0} \cong \left(1 - \frac{w_\lambda}{w_c}\right) \frac{N_T}{N_{d,a}} \cong \frac{\lambda}{w_c} \frac{N_T}{N_{d,a}}$$

where,  $N_T$  is the trap density,  $N_{d,a}$ , the shallow doping density and  $C_0 = C(\omega\tau \gg 1)$ , the junction capacitance without trap response.

## 3. References

- [1] D. L. Losee, *J. Appl. Phys.* **46** (1975) 2204.
- [2] V. G. Karpov, D. Shvydka, U. Jayamaha and A. D. Compaan, *J. Appl. Phys.* **94** (2003) 5809.
- [3] J. Barbolla, S. Dueñas and L. Bailón, *Solid-State Electron.* **35** (1992) 285.

# Doping and defects in fluorinated SiC CVD

Pontus Stenberg<sup>1</sup>, Ivan G. Ivanov<sup>1\*</sup>, Robin Kahru<sup>1</sup>, Henrik Pedersen<sup>1</sup>, Erik Janzén<sup>1†</sup>

<sup>1</sup>Department of Physics, Chemistry and Biology, Linköping University, 581 83 Linköping, Sweden

\*Corresponding author e-mail address: ivani@ifm.liu.se

†Erik Janzén would originally have presented this work, but sadly passed away shortly before the conference

## 1. Introduction

Fluorinated chemistry in chemical vapor deposition (CVD) of silicon carbide (SiC) using SiF<sub>4</sub> as Si precursor has been shown to fully eliminate formation of silicon clusters in the gas phase [1] making SiF<sub>4</sub> an interesting Si precursor. Before a fluorinated CVD chemistry can be adopted, the effect of fluorine on the both defects and dopant incorporation must be understood since this is of great importance for the performance of semiconductor devices. Here, we present defects and dopant incorporation studies for n-type doping with N using N<sub>2</sub> and p-type doping with Al using TMA in fluorinated CVD of homoepitaxial SiC characterized by capacitance-voltage (CV) measurements for doping incorporation and photoluminescence (PL) and deep level transient spectroscopy (DLTS) for defect studies.

## 2. Results

We find that it is possible to control the doping in SiC epitaxial layers when using a fluorinated CVD chemistry for both n- and p-type material using the C/Si ratio as in standard SiC CVD as the site competition theory suggests [2] and no stagnation in dopant incorporation was seen (Fig. 1). However, large area doping uniformity seems challenging for the fluorinated CVD chemistry, most likely due to the very strong Si-F and Al-F bonds. We also find that some epitaxial p-type layers show no Q<sub>0</sub> line at 3821 Å from N in their PL spectra (Fig. 2).

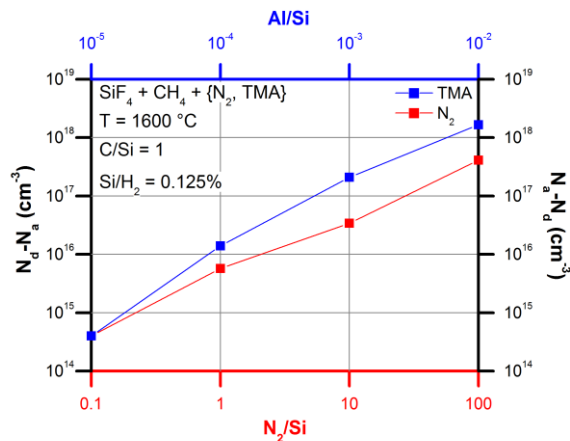


Fig. 1: Net carrier concentration by CV measurements from Al and N doping using N<sub>2</sub> and TMA. No stagnation in dopant incorporation was observed.

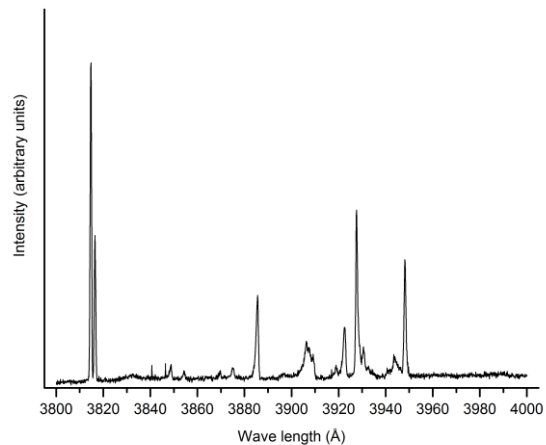


Fig. 2: PL spectrum from a p-type epitaxial layer doped to ~10<sup>16</sup> with Al. No Q<sub>0</sub> line at 3821 Å from N is observed in the spectrum.

## 3. References

- [1] T. Rana, M. V. S. Chandrashekar and T. S. Sudarshan, Phys. Status Solidi A **209**, 2455 (2012).
- [2] D.J. Larkin, P.G. Neudeck, J. A. Powell, and L.G. Matus, Appl. Phys. Lett. **65**, 1659 (1994).

# Structure and photoluminescence properties of $\text{Ba}_{(1-x)}\text{Si}_4\text{O}_{10}:x\text{Sm}^{3+}$

D. D. Ramteke<sup>1</sup>, H. C. Swart<sup>1\*</sup>

<sup>1</sup>Department of Physics, University of the Free State, P.O. Box 339, Bloemfontein 9300, South Africa

\*Corresponding author e-mail address: swarthc@ufs.ac.za

## 1. Introduction

In the recent years there is a sudden increase in the use of phosphors in the field of light emitting diode (LEDs), cathode ray tubes (CRTs) display panels and in field emission displays (FEDs). This developments demand new phosphors with high efficiency, a stable chemical and thermal stability, easy preparation method with practical applications [1]. Various scientific groups are struggling to get a red emitting phosphor which meets the above conditions. Among all phosphors silicate phosphor shows a high chemical and thermal stability with good photoluminescence properties. Thus in the present study we synthesized a red emitting  $\text{Ba}_2\text{Si}_4\text{O}_{10}$  [2] phosphor that contained  $\text{Sm}^{3+}$  ions by the solid state reaction method. We investigate the structure, the photoluminescence (PL) spectra, fluorescence lifetime and quantum yield as a function of the concentration of the  $\text{Sm}^{3+}$  ions.

## 2. Results

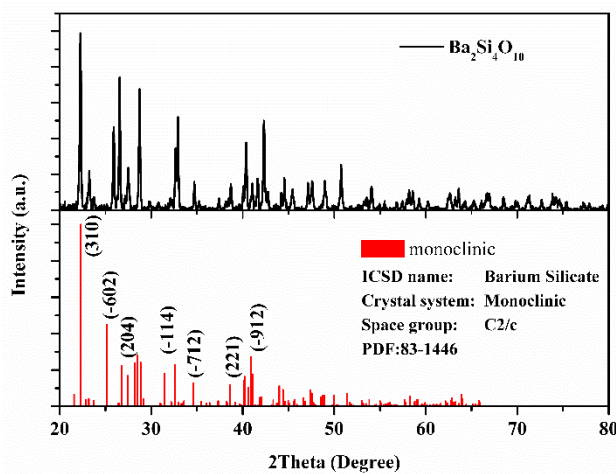


Fig. 1: XRD pattern of  $\text{Ba}_2\text{Si}_4\text{O}_{10}$  phosphor prepared at  $1200^\circ\text{C}$  for 10 hrs

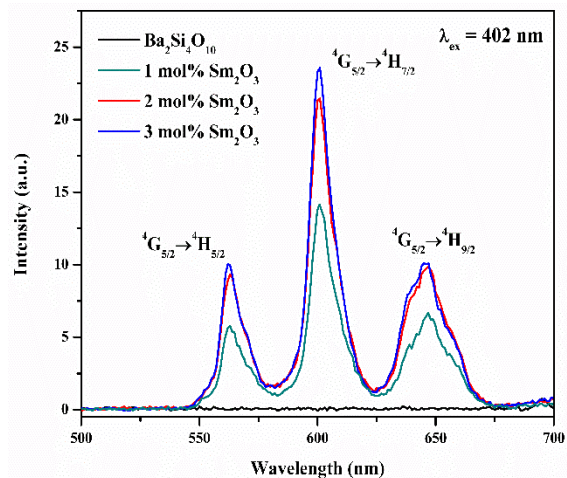


Fig. 2: Emission spectra of  $\text{Ba}_{(1-x)}\text{Si}_4\text{O}_{10}:x\text{Sm}^{3+}$  phosphor

Fig. 1 shows the X-ray diffraction (XRD) patterns of the  $\text{Ba}_2\text{Si}_4\text{O}_{10}$  phosphor prepared at  $1200^\circ\text{C}$  for 10 hrs and the ICSD standard. All the diffraction patterns were well indexed as monoclinic  $\text{Ba}_2\text{Si}_4\text{O}_{10}$  with space group of C2/c, and the lattice parameter values were  $a=23.202\text{ \AA}$ ,  $b=4.661\text{ \AA}$  and  $c=13.613\text{ \AA}$  (PDF: 83-1446) [3]. Fig. 2 shows the emission spectra of the  $\text{Ba}_2\text{Si}_4\text{O}_{10}$  containing different concentration of  $\text{Sm}^{3+}$  ions at an excitation wavelength of 402 nm. As expected the host samples did not show any emission at this excitation wavelength.  $\text{Sm}^{3+}$  ions containing phosphor shows three emission bands at 561 nm, 601 nm and at 646 nm. These transitions correspond to  $^4\text{G}_{5/2}\rightarrow^6\text{H}_{5/2}$ ,  $^4\text{G}_{5/2}\rightarrow^6\text{H}_{7/2}$  and  $^4\text{G}_{5/2}\rightarrow^6\text{H}_{9/2}$ . The  $^4\text{G}_{5/2}\rightarrow^6\text{H}_{7/2}$  transition was the strongest transition in the present study. The synthesized glasses emitted an intense reddish orange color because of the  $^4\text{G}_{5/2}\rightarrow^6\text{H}_{7/2}$  and  $^4\text{G}_{5/2}\rightarrow^6\text{H}_{9/2}$  transitions, respectively. The emission intensity has also increased with the addition of more  $\text{Sm}^{3+}$  ions in the  $\text{Ba}_2\text{Si}_4\text{O}_{10}$  matrix. These results show that the  $\text{Ba}_2\text{Si}_4\text{O}_{10}$  phosphor is quite useful for display applications.

## 3. References

- [1] V. Pankratov, A.I. Popov, L. Shirmane, A. Kotlov, C. Feldmann, J. Appl. Phys. **110** (2011) 053522–053528.
- [2] H. Katscher, G. Bissert and F. Liebau, Zeitschrift für Kristallographie, **137** (1973) 146–158.
- [3] Y. Yao, Z. Zhou, J. Lumin., **179** (2016) 408–412

# Low temperature photoluminescence study of Ce<sup>3+</sup> and Eu<sup>2+</sup> ions doped SrF<sub>2</sub> nanocrystal

Mubarak Y. A. Yagoub<sup>1,2\*</sup>, Hendrik C. Swart<sup>1</sup>, R. E. Kroon<sup>1</sup>, Elizabeth Coetsee<sup>1\*</sup>

<sup>1</sup>Department of Physics, University of the Free State, Bloemfontein, South Africa.

<sup>2</sup>Department of Physics, Sudan University of Science and Technology, Khartoum, Sudan.

\*Corresponding author e-mail address: coetsee@ufs.ac.za, mubarakayagoub@gmail.com

## 1. Introduction

Lanthanide ions with 5d-4f transition including Ce and Eu ions are interesting ions owing to their high absorption strength compared to their 4f-4f counterpart. They have great impact on the field of phosphor application in solar cells [1]. In a previous investigation done by the authors, Ce<sup>3+</sup> doped SrF<sub>2</sub> was found to emit broadband emission due to the 5d level decay to <sup>2</sup>F<sub>7/2</sub> and <sup>2</sup>F<sub>5/2</sub> of the 4f state. It was also reported that Eu exhibited two oxidation states that enhance the emission of the system. In this work, the study of the photoluminescence (PL) of these ions at low and room temperature were studied. The Ce and Eu doped SrF<sub>2</sub> material were synthesis by hydrothermal method. In the synthesis procedure, all the chemical reagents were of analytical grade and were used without further purification. The phosphors were characterized by X-ray diffraction (XRD) to identify the crystalline structure of the samples. The PL at low and room temperature analysis are discussed.

## 2. Results

Figure 1 shows the XRD patterns of un-doped and doped SrF<sub>2</sub> as well as the standard data for SrF<sub>2</sub> from card 00-086-2418. Doping with Eu- and Ce ions (up to 10 mol%) did not change the structure of the SrF<sub>2</sub> host in this study. The calculated SrF<sub>2</sub> lattice parameter was found to be (5.785 ± 0.005) Å and this agrees well with the reported value in the literature. The XRD peaks broadened with increasing the dopants ions. The broadening of the XRD peaks were also observed by other groups [2, 3]. Therefore we assigned the XRD broadening as a result of a decrease in crystallite size of the matrix, which agrees well with F. Wang et al. [3]. The emission and excitation spectra at room temperature of the Eu<sup>2+</sup> doped SrF<sub>2</sub> nanophosphor are shown in figure 2. The emission of Eu<sup>2+</sup> consisted of a broad emission band which is a characteristic of the Eu<sup>2+</sup> ion in the SrF<sub>2</sub> crystal. From the inset graph of figure 3 the decay lifetime of Eu<sup>2+</sup> was significantly altered during the low temperature measurement.

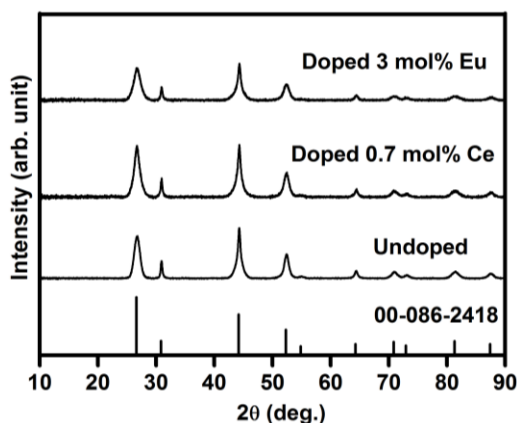


Fig. 1: XRD patterns of Ce and Eu doped SrF<sub>2</sub> crystal. In the bottom the standard data of SrF<sub>2</sub> crystal (ICSD 00-086-2418).

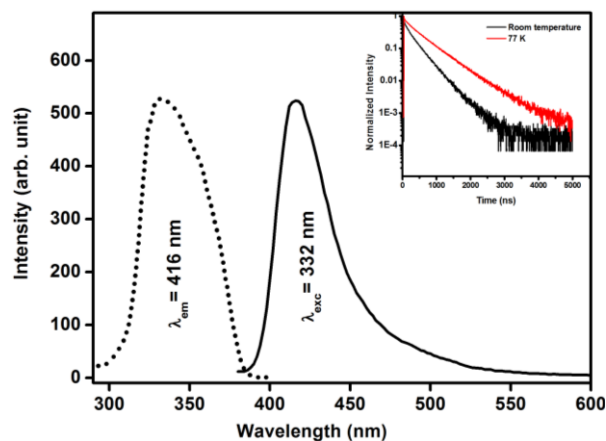


Fig. 2: The excitation and Emission of Eu<sup>2+</sup> doped SrF<sub>2</sub> crystal. The insert graph is the decay lifetime of Eu<sup>2+</sup> in SrF<sub>2</sub> at low and room temperature.

## 3. References

- [1] B. M. Van der Ende, L Aarts, A. Meijerink, *Phys. Chem. Chem. Phys.* **11** (2009) 11081.
- [2] M. Y. A. Yagoub, H. C. Swart, L. L. Noto, P. Bergman, E. Coetsee, *Materials* **8** (2015) 2361.
- [3] F. Wang, Y. Han, C. S. Lim, Y. Lu, J. Wang, J. Xu, H. Chen, C. Zhang, M. Hong, X. Liu, *Nature* **463** (2010) 1061.

# Spectroscopy on self-assembled quantum dots: transport meets optics

Martin Geller<sup>1\*</sup>

<sup>1</sup>Faculty of Physics and Cenide, University of Duisburg-Essen, Lotharstr. 1, 47048 Duisburg, Germany,

\*Corresponding author e-mail address: martin.geller@uni-due.de

## 1. Introduction

Self-assembled quantum dots (QDs) are nanoscopic semiconductor islands inside a crystalline GaAs matrix and the “workhorse” for zero-dimensional nanostructures. Like an atom, self-assembled QDs show energy quantization, direct and indirect (exchange) Coulomb interaction as well as angular momentum and spin dependent optical and electrical properties. I will summarize the transport (like capacitance-voltage spectroscopy) and optical methods (like  $\mu$ -Photoluminescence) to investigate the atomic-like structure in self-assembled InAs QDs and show recent new results on high-resolution resonance fluorescence (RT) measurements and time-resolved transport spectroscopy.

## 2. Results

The most-established methods to study the level structure of electrons and holes independently are based on capacitance (C-V) measurements. C-V spectroscopy allows studying the many-particle ground states for electrons and holes. However, the static C-V measurements cannot resolve the excited, i.e. non-equilibrium many-particle charge and spin states. In a newly-developed all-electrical spectroscopy technique on an ensemble of self-organized InAs QDs we use the Coulomb coupling to a nearby two-dimensional electron gas (2DEG) to detect and prepare excited charge and spin configurations and observe their evolution in a time-resolved measurement scheme [1,2], see Fig. 1(a). We demonstrate a controlled initialization of excited spin states and measure their relaxation time; which is in the order of tens of microseconds.

Furthermore, we combined “transport and optics” in an optical detection scheme to observe single electron tunneling into a single self-assembled QD. The detection scheme is based on driving the excitonic transition in resonance fluorescence [3]. The time-resolved resonance fluorescence signal is measured, while non-equilibrium tunneling between the charge reservoir and the QD is switch on and off. We are able to tune optically the relaxation rate [4] and observe in a real-time measurements quantum jumps of electrons tunneling into and out of the dot, see Fig. 1(b) and (c).

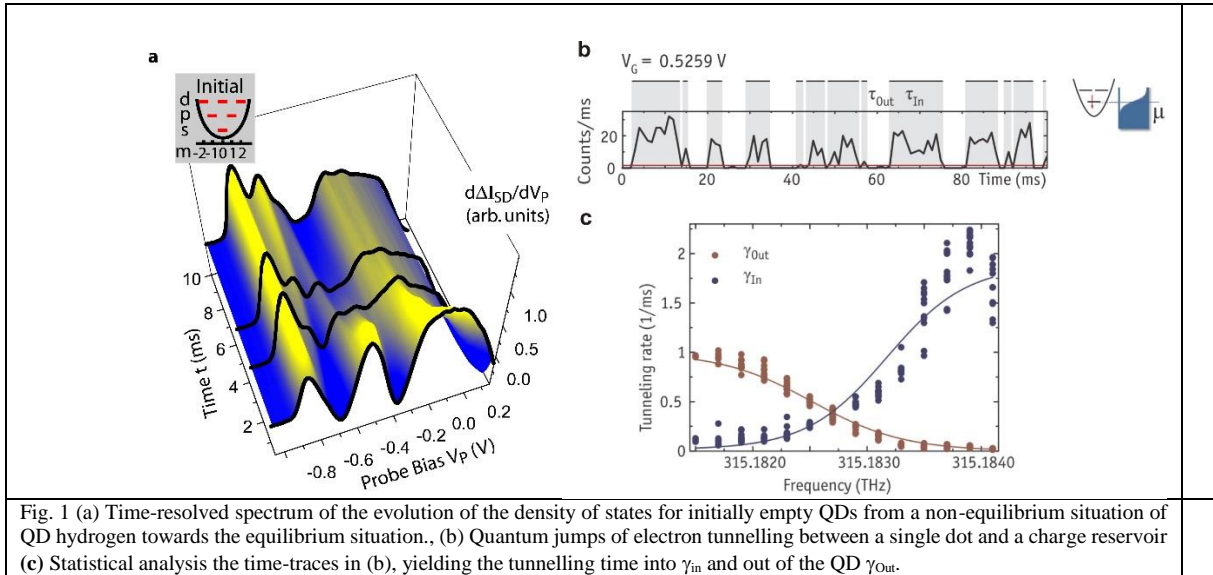


Fig. 1 (a) Time-resolved spectrum of the evolution of the density of states for initially empty QDs from a non-equilibrium situation of QD hydrogen towards the equilibrium situation., (b) Quantum jumps of electron tunnelling between a single dot and a charge reservoir (c) Statistical analysis the time-traces in (b), yielding the tunnelling time into  $\gamma_{in}$  and out of the QD  $\gamma_{Out}$ .

## 3. Acknowledgements

I have to acknowledge many people. At the University of Duisburg-Essen, I am especially grateful to Axel Lorke, Andreas Beckel, Bastian Marquardt, Annika Kurzmann, Benjamin Merkel and Amran Al-Ashouri. For providing samples, I am very thankful to Dirk Reuter, Arne Ludwig, Patrick Labud and Andreas Wieck at the Ruhr-University of Bochum.

## 4. References

- [1] B. Marquardt, M. Geller, B. Baxevanis, D. Pfannkuche, A. D. Wieck, D. Reuter & A. Lorke, Nature Commun. **2**, 209 (2011).
- [2] A. Beckel, A. Ludwig, A.D. Wieck, A. Lorke, and M. Geller, Phys. Rev. B **89**, 155430 (2014).
- [3] C. Matthiesen, Martin Geller, Carsten H.H. Schulte, Claire Le Gall, Jack Hansom, Zhengyong Li, Maxime Hugues, Edmund Clarke, and Mete Atatüre, Nature Commun. **4**, 1600 (2013).
- [4] A. Kurzmann, B. Merkel, P. A. Labud, A. Ludwig, A. D. Wieck, A. Lorke, and M. Geller, Phys. Rev. Lett. **117**, 017401 (2016).
- [5] A. Kurzmann, A. Ludwig, A. D. Wieck, A. Lorke, and M. Geller, Nano Lett. **16**, 3367-3372 (2016).

# Electronic structure and optical properties of GaSb/GaAs and GaSb/Al<sub>x</sub>Ga<sub>1-x</sub>As quantum rings

**Magnus C. Wagener<sup>1\*</sup>, Peter J. Carrington<sup>2</sup>, S. Hatch<sup>2</sup>, Huiyun Liu<sup>2</sup>, J. R. Botha<sup>1</sup>, J. O'Connell<sup>3</sup>**

<sup>1</sup>Department of Physics, Nelson Mandela Metropolitan University, Port Elizabeth, South Africa

<sup>2</sup>Department of Electronic & Electrical Engineering, University College London, Torrington Place, London, WC1E 7JE, UK

<sup>3</sup>Centre for High Resolution Transmission Electron Microscopy, Nelson Mandela Metropolitan University, South Africa

\*Corresponding author e-mail address: magnus.wagener@nmmu.ac.za

## 1. Introduction

Incorporating quantum structures such as quantum dots into the active region of a conventional solar cell junction has been successfully demonstrated as a means of extending the spectral response beyond the absorption edge of the host material. Depending on the band structure, these structures could localise both electrons and holes within the region of the nanostructures, *i.e.* type-I heterostructures, or localise one carrier type, leaving the other only weakly bound by Coulomb forces *i.e.* type-II structures. The unique stress relaxation mechanism whereby GaSb island structures transform into nano-rings also facilitate the incorporation of a large density of nanostructures without the need for strain compensation. This report sets out to relate the unusual ring geometry of embedded GaSb nanostructure to their strain and associated optoelectrical characteristics. Generally, the strain produced by a flat in-plane profile, such as a disk or flat island produces little mixing of the heavy and light hole states, as compared to significant mixing in structures with a tapered profile, *i.e.* pyramidal shaped [1]. The optical absorption characteristics of embedded quantum structures is therefore closely related to the geometry and localised strain. In addition to the in-plane orbital angular momentum associated with the lateral confinement within quantum dots, the coupling between heavy and light hole states also directly impacts the spectral characteristics of the quantum structures [2].

## 2. Results

The electronic characteristics of the quantum ring (QR) were simulated using the software package, nextnano. The quantum mechanical determination of the electronic structure was realised using an effective mass and 6-band **k** $\times$ **p** model for the conduction and valance bands, respectively. The local strain was obtained by minimizing the total elastic energy within the structure, with the resulting strain tensor used to obtain the piezoelectric charge density and local deformation potentials present within the ring structure. The geometry of the three-dimensional model of the quantum rings was based on high resolution scanning transmission electron microscopy performed on structures used for the solar cell device fabrication. For our simulations, the model consisted of an outer ring diameter of 24 nm, a thickness of 2 nm and ring band width of 2.5 nm. Figure 1 depicts the simulated hole and electron probability distributions for the quantum ring ground state. As anticipated for the type-II GaSb/GaAs bandstructure, the hole distribution is localised within the GaSb quantum ring, whereas the electron distribution is localised within the GaAs filled ring center. In the case of quantum rings embedded within a GaAs barrier layer, the electron-hole interband transition energy is found to be 1.03 eV, which coincides with the observed photoluminescence and absorption spectra of these structures. Increasing the aluminium content of the barrier layer raises the hole confinement energy and the associated transition energies of the hole states.

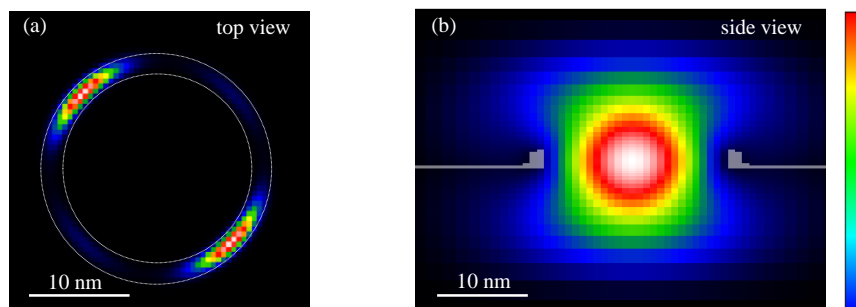


Fig. 1: False colour map of (a) the simulated hole (b) and electron probability densities. The planar hole distribution in (a) is found to be aligned with the [110] direction of the piezoelectric field within the ring.

## 3. References

- [1] A. Schliwa, M. Winkelkemper, and D. Bimberg. *Phys. Rev. B* **76** (2007) 205324.
- [2] G.A. Narvaez and A. Zunger. *Phys. Rev. B* **75** (2007) 085306.

# Optical and microanalytical characterization of $\text{Al}_x\text{Ga}_{1-x}\text{N}$ epilayers for photonic applications

M. E Lee<sup>1\*</sup>, B. C. Sephton<sup>2</sup>, J. A. A. Engelbrecht<sup>1</sup>, J. E. Westraadt<sup>1</sup>

<sup>1</sup>Centre for HRTEM, Nelson Mandela Metropolitan University, Port Elizabeth, South Africa

<sup>2</sup>National Laser Centre, CSIR, Pretoria, South Africa

\*Corresponding author e-mail address: michael.lee@nmmu.ac.za

## 1. Introduction

$\text{Al}_x\text{Ga}_{1-x}\text{N}$  tertiary alloys have unique material properties, causing the material to be useful in a range of electronic and UV optoelectronic devices due to the variation of the band gap of the alloy with varying aluminium content [1,2]. In particular, AlGa<sub>N</sub> has a large direct band gap, ranging between 3.39 and 6.0 eV which covers the UV spectrum UVA (340-400nm), UVB (290-340nm) and UVC (200-290nm) [3,4]. Mechanical hardness, chemical stability at high temperatures, high thermal conductivity and good carrier mobility additionally make material especially useful [4]. Prominent applications fueling much of the research include UV light emitting diodes, high field effect transistors, diode laser cladding as well as deep visible and solar blind UV detectors [3,4]. Determination of the physical, optical and electrical properties of the material is therefore important in achieving optimum material parameters. In this work we will report on the characterization of the grown  $\text{Al}_x\text{Ga}_{1-x}\text{N}$  epilayers grown by the metal organic chemical vapour deposition (MOCVD) technique on sapphire substrates. The epilayers having Al composition varied from  $x=0.15$  to 0.78. The characterization techniques used in this study include photoluminescence (PL) and infrared (FTIR) spectroscopy to determine optical properties and microanalysis by transmission electron microscopy (TEM) coupled to an energy dispersive spectrometer (EDS) to determine the thickness, crystalline quality and composition of the layers.

## 2. Results

The epilayer thickness and the band gap for different Al compositions were obtained by infrared reflectance spectra as shown in figure 1. The values for the band gap, measured in the range 3.6eV to 5.1eV, using FTIR, will be shown to be in good agreement with PL measurements and theoretical calculations for Al content in the range  $x=0.15$ -0.78. Optical measurements for the epilayer thickness calculated from the infrared reflectance spectra are in good agreement with high angular annular dark field (HAADF) STEM measurements (Figure 2), as well as calculated values using the formula proposed by Engelbrecht et al [5]. TEM characterization as shown in figure 2 revealed a columnar type growth morphology for all the epilayers. Cracks in the epilayers are also observed (indicated by red ellipse) and can possibly be attributed to strain in the layers. However, it is observed that the top surface of the epilayer become faceted for Al content greater than  $x=0.5$  which is not observed in layers of lower Al content having smooth surface layers.

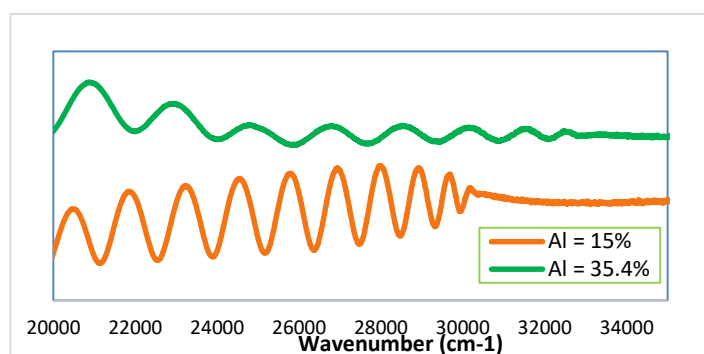


Fig 1: Infrared reflectance spectra for  $\text{Al}_x\text{Ga}_{1-x}\text{N}$  epilayers of varying Al content and thickness

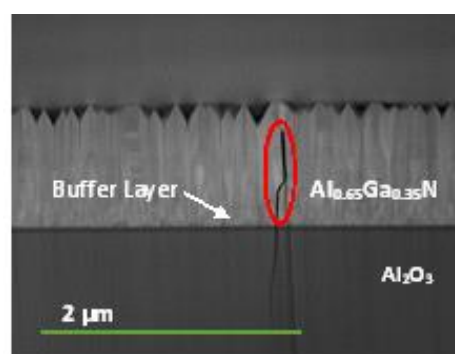


Fig 2: HAADF STEM image of epilayer grown on sapphire substrate

## 3. References

- [1] N. Maeda, T. Saitoh, K. Tsubaki, T. Nishida and N. Kobayashi. *Jap. J. Appl.Phys.* **38** (1999) L 987.
- [2] T.Takano, Y. Narita, A. Horiuchi and H. Kawanishi. *Appl. Phys. Let.* **84** (2004) 3567.
- [3] G. James, *PhD Thesis (2005)* Port Elizabeth: Nelson Mandela Metropolitan University.
- [4] T. D. Moustakas, Y. Liao, C. Kao, C. Thomidis, A. Bhattacharyya, D. Bhattarai, and A. Moldawer, *Proc. SPIE 8278* (2012) 82780L-1.
- [5] J.A.A Engelbrecht, B. Sephton, E. Minnaar, M.C Wagener. *Physica B*, **480** (2016) 181.



# Single polarized-photon emitters from elongated III-nitride pyramidal quantum dots

P. O. Holtz<sup>1\*</sup>, M. Eriksson<sup>1</sup>, H. Machhadani<sup>1</sup>, C. W. Hsu<sup>1</sup>, T. Jemson<sup>1</sup>, K. F. Karlsson<sup>1</sup>, E. Janzén<sup>1</sup>

Department of Physics, Chemistry and Biology (IFM), Linköping University, S-581 83, Linköping, Sweden

\*Corresponding author e-mail address: poh@ifm.liu.se

## 1. Introduction

There is a strong global need for secure communication as recently reflected by the vast media and political attention given to eavesdropping. Quantum cryptography, if established, is a form of secure communication that is conjectured to be impossible to intercept, in contrast to classical cryptography. Based on the global need, there have been significant efforts over the last decades to realize quantum cryptography schemes experimentally. For such a realization of quantum cryptography, there is a need to generate a flow of single photons to forward the information, where the message by each photon, in terms of *wavelength and polarization coding*, has to be well controlled. Further, for an efficient high capacity communication, i.e. a flow of a large number of individual photons per time unit and area, one needs *multiplexing* combined with a *high frequency* photon generation. Another crucial parameter for efficient and high-capacity communication is a *low loss factor* for the flow of single photons.

## 2. Results

In our approach, elongated nanopylramids of III-N materials are employed (Fig. 1). These nanopylramids are fabricated by means of a patented method using a unique hot-wall CVD technique developed at Linköping University. Highly controlled mask etching, combined with the nature of III-N crystalline growth, make the fabrication a highly deterministic process, allowing custom arrays to be grown with high precision and material quality across whole wafers. On top of the buffer layer and the thin SiN film with etched circular holes, GaN pyramids with six equal facets are grown by Selective Area Growth (SAG). Subsequently, the pyramids are overgrown by a thin optically active InGaN quantum well and finally capped with a thin GaN layer. On top of the slightly truncated GaN pyramids, InGaN quantum dots (QDs) will evolve due to the accumulated strain caused by the lattice mismatch between the GaN and InGaN well. In the next step, the circular holes are replaced by elongated holes. As a result, elongated pyramids with six unequal facets are formed. From extended QDs on top of the elongated pyramid, an excitonic emission with a FWHM down to 0.3 meV and a strong degree of linear polarization, about 85% in the direction of the elongation, is monitored (Fig. 1). The exciton lifetimes have been studied in  $\mu$ -PL set-up with a high spatial resolution equipped with a streak-camera detector for recording of ultra-fast emission decays (down to 7 ps). The exciton lifetimes were measured to be 320 ps and 130 ps for the neutral excitons and the negatively charged excitons, respectively, i.e. consistent with theoretical predictions of a ratio close to 2 between the lifetimes for a QD size close to the exciton Bohr radius. In addition, the lifetimes remain essentially constant with increasing excitation power, consistent with a weak effect of the built-in field, as predicted for small QDs.

For demonstration of the single photon characteristics of the QDs, temporal photon correlation spectroscopy has been performed. The ultimate proof of QD formation on these pyramidal microstructures has been demonstrated, as evidenced by photon antibunching with  $g^{(2)}=0.24$  confirming the sound single photon properties of these QDs.

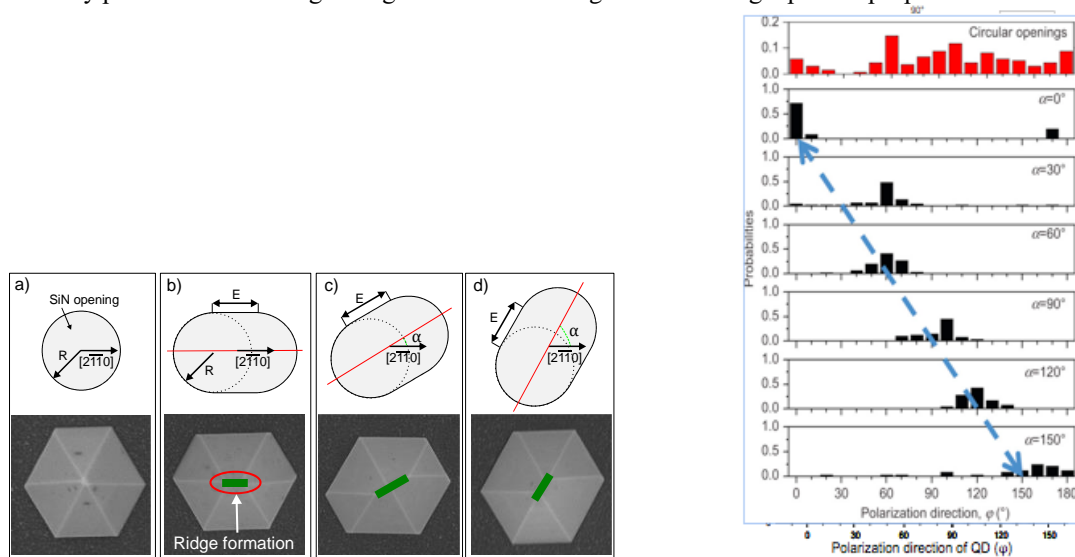



Fig. 1. An illustration of the elongated pyramidal quantum structures (lefthand figure). The resulting polarization dependence for pyramidal quantum structures elongated in different directions (righthand figure)

## Scientific Programme and Abstracts

### Thursday 30 March

Time	Activity
7:00-8:00	Breakfast (Conference Hall)
<b>ORAL SESSION 6: Chairperson – Vinod Kumar</b>	
8:00-8:40	Invited Talk 8: <b>S. J. Dhoble</b> (p. viii) <i>p. 30: Luminescence behaviour of lanthanide ions in different host lattices and their application in LED for lighting</i>
8:40-9:00	Oral 20: <b>Vinay Kumar</b> <i>p. 31: Potential of Sm<sup>3+</sup> doped LiSrVO<sub>4</sub> nanophosphor to fill amber gap in LEDs</i>
9:00-9:20	Oral 21: <b>P. P. Mokoena</b> <i>p. 32: Up-conversion luminescence of Er<sup>3+</sup>/Yb<sup>3+</sup> doped Sr<sub>5</sub>(PO<sub>4</sub>)<sub>3</sub>OH phosphor powders for photodynamic therapy</i>
9:20-9:40	Oral 22: <b>Ashwini Kumar</b> <i>p. 33: Co-operative energy transfer in Yb<sup>3+</sup> -Tb<sup>3+</sup> co-doped SrGd<sub>4</sub>O<sub>7</sub> upconverting phosphor</i>
9:40-10:20	Invited Talk 9: <b>Lucas C. V. Rodrigues</b> (p. ix) <i>p. 34: Designing infrared persistent luminescence materials</i>
10:20-10:40	Tea (Conference Hall)
10:40-12:40	POSTER SESSION B: posters 39 – 74 (p. 81 – 116) (Conference Hall upstairs)
	
12:40-13:00	CONFERENCE PHOTO
13:00-14:00	Lunch (Conference Hall)
<b>ORAL SESSION 7: Chairperson – Hendrik Swart</b>	
14:00-14:40	Invited Talk 10: <b>Philippe F. Smet</b> (p. ix) <i>p. 35: Enhancing the performance of persistent phosphors: focus on the trapping defects and detrapping processes</i>
14:40-15:00	Oral 23: <b>Vishal Sharma</b> <i>p. 36: Combustion synthesis of blue long lasting phosphor CaAl<sub>4</sub>O<sub>7</sub>: Eu<sup>2+</sup>, Dy<sup>3+</sup> and its novel application in fingerprint and lip mark detection</i>
15:00-15:20	Oral 24: <b>Jorma Hölsä</b> <i>p. 37: Defects and impurities: from Bologna Stone to gem stones</i>
15:20-15:40	Oral 25: <b>Iorkyaa Ahemen</b> <i>p. 38: Spectroscopic investigation of Ce<sup>3+</sup>/Eu<sup>3+</sup> co-doped Li<sub>2</sub>BaZrO<sub>4</sub> nanophosphors</i>
16:00-18:00	Free time
18:00-20:30	CONFERENCE DINNER (Mountain Lodge)

# Luminescence behaviour of lanthanide ions in different host lattices and their application in LED for lighting

**S. J. Dhoble<sup>1\*</sup>**

<sup>1</sup>Department of Physics, R.T.M. Nagpur University, Nagpur, India- 440033

\*Corresponding author e-mail address: [sjdhoble@rediffmail.com](mailto:sjdhoble@rediffmail.com)

## 1. Introduction

Light-emitting diodes (LED) have been in the higher demands for the solid-state lighting technology in recent years [1, 2]. The technological advancements in the LED industry are rapidly growing with improvement in the quality and reliability of phosphors. Most of the times, the key to efficient solid state lighting lies in the proper selection of high efficiency phosphors capable of giving good visible light emission. The route of synthesis plays an important role for the development of good phosphors with proper morphology and desired characteristics. The lanthanide ions have a distinct ability to produce visible light emission by absorbing in the UV or near-UV region. Most of the lanthanides are capable of producing emission by virtue of f-f transition that are considered to be forbidden by selection rules. However, their introduction in some suitable host lattice can remarkably relax these forbidden transitions. If the lanthanide ion occupies a site with non-inversion symmetry, the probability of achieving intense electric dipole transitions increases. The  $\text{Eu}^{2+}$  and  $\text{Ce}^{3+}$  ions show their emissions by virtue of  $5d \rightarrow 4f$  transitions and are spectroscopically allowed transitions. These ions vary their emission bands depending on the host in which they are incorporated.

## 2. Results

The objective of the present abstract is to summarize the trends in the synthesis, characterization and potential areas of application of lanthanide activated phosphor in the field of luminescence. This is supposed to be a step forward towards the next generation lamp phosphor. Non-absorbing hosts, doped with impurities to act as absorption and emission centers, provide useful phosphors. Here, I am discussing some selective results of LED phosphors which were prepared in our laboratory. Our approach is to describe the possible classes of rare earth activated phosphors, which are characteristically associated with its luminescence study. Different low cost synthesis routes were considered for preparation of phosphors for lamp industry. Synthesis and luminescence characterization of some of the phosphors are discussed in this abstract, such as:  $\text{Eu}^{2+}$  doped  $\text{Sr}_5(\text{PO}_4)_3\text{Cl}$ ;  $\text{Ce}^{3+}$  doped  $\text{Na}_5(\text{PO}_4)\text{SO}_4$ ; Dy and Ce doped  $\text{M}_6\text{BP}_5\text{O}_{20}$  (Where M=Sr and Ca),  $\text{Na}_3\text{Al}_2(\text{PO}_4)_3:\text{RE}$  (RE= $\text{Ce}^{3+}$ ,  $\text{Eu}^{3+}$  and  $\text{Mn}^{2+}$ ),  $\text{Na}_2\text{Sr}(\text{PO}_4)\text{F}:\text{Dy}^{3+}$ ,  $\text{Ca}_3(\text{PO}_4)_2:\text{Eu}$ ,  $\text{Ca}_3(\text{PO}_4)_2:\text{Dy}$  phosphors.

## 3. References

- [1] A. Zukauskas, M.S. Shur, R. Gaska, *Introduction to SSL*, (Wiley, New York, 2002).
- [2] J.S. Kim, Y.H. Park, J.C. Choi, H.L. Park, G.C. Kim, J.H. Yoo, *Solid State Comm.* **137** (2006) 187.

# Potential of $\text{Sm}^{3+}$ doped $\text{LiSrVO}_4$ nanophosphor to fill amber gap in LEDs

Vinay Kumar<sup>1,2\*</sup>, P. Biswas<sup>1</sup>, A. K. Bedyal<sup>2</sup>, Vishal Sharma<sup>3</sup>, H. C. Swart<sup>2</sup>

<sup>1</sup>Department of Physics, Shri Mata Vaishno Devi University, Katra-182320 (J&K) India

<sup>2</sup>Department of Physics, University of the Free State, P.O. Box 339, Bloemfontein, ZA9300, South Africa

<sup>3</sup>Institute of Forensic Science and Criminology, Panjab University, Chandigarh-160014 India

\*Corresponding author e-mail address: vinaykumar@smvdu.ac.in, vinaykdhiman@yahoo.com

## 1. Introduction

Currently, the increasing demands of low cost, energy saving, high efficiency and durable lighting devices have attracted the attention of researchers to develop new phosphor converted LEDs that can effectively be excited in the blue, near ultraviolet and ultraviolet range [1-2]. In particular, white light-emitting diodes (w-LEDs) are now rapidly replacing the traditional incandescent, fluorescent and discharge lamps because of their highly desirable characteristics [3]. A lot of attention has been given to alkali-alkaline doped with the trivalent rare-earth (RE) orthovanadate due to their unique luminescence properties under near-UV excitation for different potential applications in lighting devices. In this communication, we report the structural and optical properties of nanocrystalline  $\text{LiSrVO}_4$  doped with varying concentrations of  $\text{Sm}^{3+}$  synthesized by combustion method. These properties of this phosphor are considered to explore their importance to fill yellow amber gap in solid state lighting and LED displays based on near-UV (300–400 nm) LED chips.

## 2. Results

The optimized  $\text{LiSr}_{0.9775}\text{VO}_4:0.015\text{Sm}^{3+}$  phosphor displayed orange-red emission in the range of 500–750 nm with a maximum peak at 601 nm upon excitation with 317 nm. Figure 1 shows the emission spectra with four sharp peaks attributed to the  ${}^4\text{G}_{5/2} \rightarrow {}^6\text{H}_J$  ( $J = 5/2, 7/2, 9/2, 11/2$ ) transitions of  $\text{Sm}^{3+}$ . The emission has CIE chromaticity coordinates at (0.59, 0.41). The band gap and Urbach energy of a typical  $\text{LiSr}_{0.9775}\text{VO}_4:0.015:\text{Sm}^{3+}$  phosphor sample, using DRS studies, were estimated to be 3.65 eV and 165.5 meV. The results indicated that the  $\text{LiSrVO}_4:\text{Sm}^{3+}$  phosphor is a potential orange-red phosphor candidate for near-Ultra violet light emitting diode chips reliant white light emitting diodes. The emission has CIE chromaticity coordinates at (0.59, 0.41) as shown in figure 2. The band gap and Urbach energy of a typical  $\text{LiSr}_{0.9775}\text{VO}_4:0.015:\text{Sm}^{3+}$  phosphor sample, using DRS studies, were estimated to be 3.65 eV and 165.5 meV. The results indicated that the  $\text{LiSrVO}_4:\text{Sm}^{3+}$  phosphor is a potential orange-red phosphor candidate for near-Ultra violet light emitting diode chips reliant white light emitting diodes.

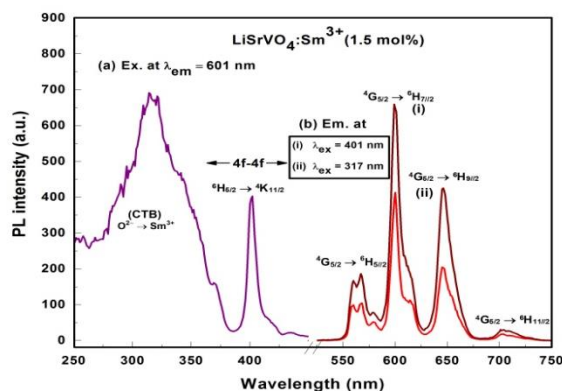


Fig. 1: PL excitation and emission spectra of  $\text{LiSrVO}_4:\text{Sm}^{3+}$  (1.5 mol%).

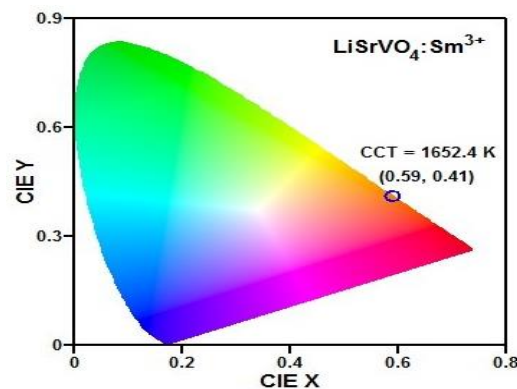


Fig. 2: CIE chromaticity diagram for  $\text{LiSrVO}_4:\text{Sm}^{3+}$  (1.5 mol%) nanophosphor under 401 nm excitation.

## 3. References

- [1] A. K. Bedyal, Vinay Kumar, R Prakash, OM Ntweaborwa, Swart H C *Appl. Surf. Sci.* **329** (2015) 40.
- [2] J. Huang, Q Li, D Chen, *Mater Sci Eng B* **172** (2010) 108.
- [3] S Ye, F Xiao, YX Pan, YY Ma, QY Zhang, *Mater Sci Eng R Rep* **71**(1) (2010) 1.

# Up-conversion luminescence of Er<sup>3+</sup>/Yb<sup>3+</sup> doped Sr<sub>5</sub>(PO<sub>4</sub>)<sub>3</sub>OH phosphor powders for photodynamic therapy

P. P. Mokoena<sup>1\*</sup>, H. C. Swart<sup>1</sup>, O. M. Ntwaeaborwa<sup>2</sup>

<sup>1</sup>Department of Physics, University of the Free State, Bloemfontein, ZA9300, South Africa

<sup>2</sup>School of Physics, University of Witwatersrand, Private Bag 3, Wits, 2050, South Africa

\*Corresponding author e-mail address: puse8814@gmail.com

## 1. Introduction

Strontium phosphate is considered as a promising host for efficient upconversion due to its short distance between positions that can be occupied by the dopants, high solubility of ytterbium ions and it exhibit close ionic size to lanthanides [1]. For upconversion luminescence, the ionic radius of lanthanides needs to match with the host [2]. Intense visible upconversion luminescence can be obtained from lanthanides such as Yb<sup>3+</sup>/Er<sup>3+</sup>, Yb<sup>3+</sup>/Ho<sup>3+</sup> and Yb<sup>3+</sup>/Tm<sup>3+</sup> by excitation of near infrared (NIR) light [3]. Yb<sup>3+</sup> has a high and broad absorption band (ranging from 850-1050 nm), which makes it an excellent sensitizer. In this study, strontium phosphate co-doped with Er<sup>3+</sup>/Yb<sup>3+</sup> was successfully synthesized by urea combustion method. Phase structure analysis was carried out using x-ray diffraction (XRD) Bruker AXS D8 ADVANCE X-ray diffractometer. Particle morphology was analysed using Jeol JSM 7800F thermal field emission scanning electron microscope (FE-SEM). The chemical composition analysis was carried out using an Oxford Instruments AzTEC energy dispersive spectrometer (EDS), with X-Max80 silicon drift detector (SDD) system, attached to the FE-SEM. Upconversion emissions were measured by using a FLS980 Spectrometer consisting of 980 nm NIR laser as the excitation source, photomultiplier (PMT) detector.

## 2. Results

The XRD data of Sr<sub>5</sub>(PO<sub>4</sub>)<sub>3</sub>OH powder exhibited characteristic diffraction patterns of hexagonal structure referenced in standard JCPDS card number 00-033-1348. The sharp peaks revealed formation of Sr<sub>5</sub>(PO<sub>4</sub>)<sub>3</sub>OH with fine crystallinity. Rods and spherical shapes were formed. The enhanced red emission due to the <sup>4</sup>F<sub>9/2</sub>→<sup>4</sup>I<sub>15/2</sub> transitions of Er<sup>3+</sup> was observed and attributed to energy transfer from Yb<sup>3+</sup>. Upon addition of Yb<sup>3+</sup>, the green emission is suppressed and red emission is enhanced, this is due to energy transfer process between Er<sup>3+</sup> and Yb<sup>3+</sup>. Figure 1 shows the luminescence spectra of Sr<sub>5</sub>(PO<sub>4</sub>)<sub>3</sub>OH:Er<sup>3+</sup> and Sr<sub>5</sub>(PO<sub>4</sub>)<sub>3</sub>OH:Er<sup>3+</sup>,Yb<sup>3+</sup> phosphor powders .

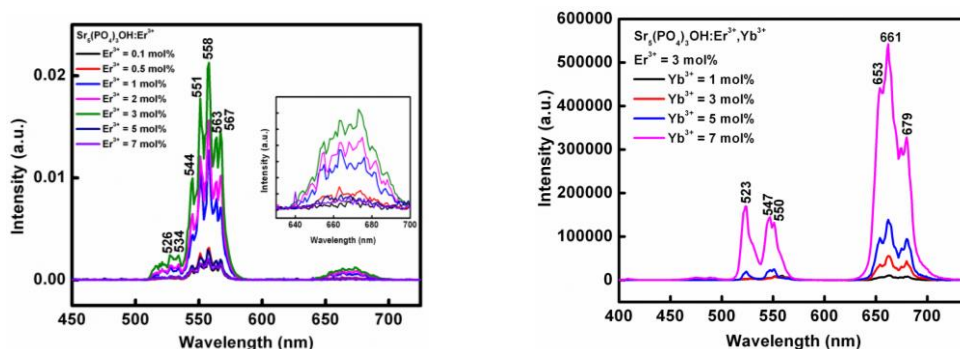


Fig. 1: Up-conversion luminescence spectra of (a) Sr<sub>5</sub>(PO<sub>4</sub>)<sub>3</sub>OH:Er<sup>3+</sup> and (b) Sr<sub>5</sub>(PO<sub>4</sub>)<sub>3</sub>OH:Er<sup>3+</sup>,Yb<sup>3+</sup> phosphor powders

## 3. References

- [1] A. Stefan, O. Toma, S. Georgescu, *Journal of Luminescence*, **180** (2016) 376.
- [2] J. Fu, R. Pang, Y. Jia, W. Sun, L. Jiang, S. Zhang, *Journal of Luminescence*, **181** (2017) 240.
- [3] Z. Liang, S. Zhao, Z. Xu, B. Qiao, Y. Yang, W. Zhu, X. Xu, *Optical Materials*, **62** (2016) 255.

# Co-operative energy transfer in Yb<sup>3+</sup> -Tb<sup>3+</sup> co-doped SrGd<sub>4</sub>O<sub>7</sub> upconverting phosphor

Ashwini Kumar<sup>1\*</sup>, Trilok K. Pathak<sup>1</sup>, S. J. Dhoble<sup>2</sup>, J. J. Terblans<sup>1</sup>, H. C. Swart<sup>1\*</sup>

<sup>1</sup>Department of Physics, University of the Free State, PO Box 339, Bloemfontein 9300, South Africa

<sup>2</sup>Department of Physics, RTM Nagpur University, Nagpur 440033, India

\*Corresponding author e-mail address: Ashwini Kumar (ashwinikumar.vnit@gmail.com); H. C. Swart (swarthc@ufs.ac.za)

## 1. Introduction

Upconversion nanoparticles (UCNPs) have shown considerable anticipation in many fields; however, low upconversion efficiency of UCNPs is still the most severe limitation of their applications. Herein, we report for the first time, Yb<sup>3+</sup> and Tb<sup>3+</sup> co-doped SrGd<sub>4</sub>O<sub>7</sub> (Strontium Gadolinium Oxide) upconversion (UC) phosphors synthesized by a modified co-precipitation process [1].

## 2. Results

The upconversion properties were investigated by direct excitation with a 980 nm laser, Figure 1, it was observed that the as prepared materials show relatively weak green emission, whereas after calcination, there is an increase in the upconversion luminescence intensity and the intensity of the red component found to decrease relatively. The effect of different calcination temperatures on the emission spectra and X-ray diffraction patterns of the heat treated upconversion materials have also been studied. Thermal analysis (TG-DTA) was later used further for the optimization of suitable temperature for heat treatment. The luminescence lifetimes and International Commission on Illumination (CIE) coordinates for these as prepared and heat treated samples were also determined to understand the energy transfer (ET) mechanisms occurring between Yb<sup>3+</sup> and Tb<sup>3+</sup> in SrGd<sub>4</sub>O<sub>7</sub> host matrix. Also, the upconversion luminescence intensity as a function of laser pump power was monitored and it was confirmed that the upconversion process in SrGd<sub>4</sub>O<sub>7</sub>: Yb<sup>3+</sup>/Tb<sup>3+</sup> is a two-photon absorption mechanism. The findings reported here are expected to provide a better approach for understanding of ET mechanisms in oxide based Yb<sup>3+</sup>/Tb<sup>3+</sup> co-doped UC phosphors. This study might be helpful in precisely defined applications where optical transitions are essential criterion and this can be easily achieved by smart tuning of the emission properties of Yb<sup>3+</sup>/Tb<sup>3+</sup> co-doped UC phosphors.

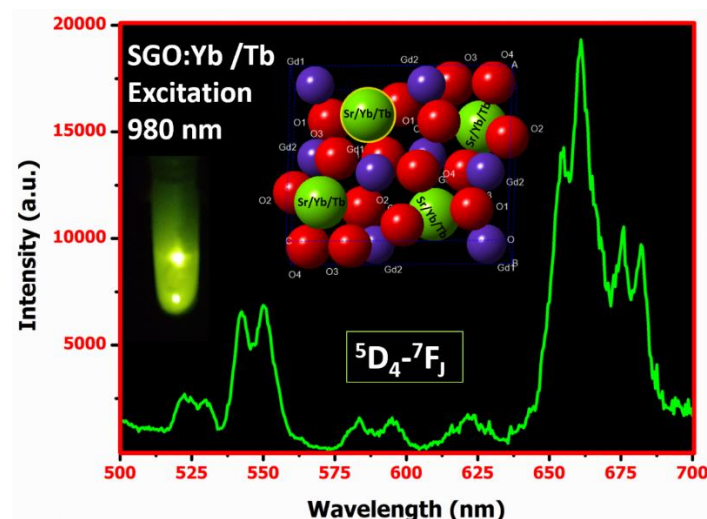


Fig. 1: SrGd<sub>4</sub>O<sub>7</sub>: Yb<sup>3+</sup>/Tb<sup>3+</sup> crystal structure, UC emission spectrum and colour image of the excited phosphor.

## 3. Reference

[1] Xiao H, Li P, Jia F, Zhang L, *J. Phys. Chem. C* **113** (2009) 21034.

# Designing infrared persistent luminescence materials

Lucas C. V. Rodrigues<sup>1\*</sup>, José M. Carvalho<sup>1,2</sup>, Cássio Pedroso<sup>1</sup>, Veronica C. Teixeira<sup>3</sup>, Hermi Brito<sup>1</sup>, Ian P. Machado<sup>1</sup>

<sup>1</sup>Institute of Chemistry, University of São Paulo, São Paulo-SP, Brazil.

<sup>2</sup>Department of Chemistry, University of Turku, Turku FI-20014, Finland.

<sup>3</sup>National Laboratory of Synchrotron Light (LNS-CNPEM), Campinas-SP, 13083-970, Brazil

\*Corresponding author e-mail address: lucascvr@iq.usp.br

## 1. Introduction

Despite the huge amount of publications about persistent luminescence, there is a lack of materials with emission in the near infrared (NIR) region of the electromagnetic spectrum. NIR persistent luminescence materials can be potentially applied as *in vivo* nanoprobe and as solar cells sensitizers by reducing the spectral mismatch losses [1–3]. Among many activator ions for NIR persistent luminescence, the Yb<sup>3+</sup>-activated materials are good candidates due to their unique 980 nm emission [4].

According to the lanthanide ions (Ln<sup>2+</sup> and Ln<sup>3+</sup>) ground level diagram, the energy levels of trivalent Eu<sup>3+</sup> and Yb<sup>3+</sup> are similar [5]. We expect that the substitution of Eu<sup>3+</sup> for Yb<sup>3+</sup> ion should not change the persistent luminescence mechanism, creating persistent luminescence material activated by the NIR emission of Yb<sup>3+</sup>. In this work, the R<sub>2</sub>O<sub>2</sub>S:Yb<sup>3+</sup>,Mg<sup>2+</sup>,Ti<sup>3+/IV</sup> materials (R<sup>3+</sup>: La, Gd, Y) are presented as an efficient NIR persistent luminescence phosphor.

## 2. Results

After irradiation at the O<sup>2</sup>(2p)→Yb<sup>3+</sup>(4f<sup>13</sup>) and S<sup>2</sup>(3p)→Yb<sup>3+</sup>(4f<sup>13</sup>) charge transfer bands (310 nm), the R<sub>2</sub>O<sub>2</sub>S:Yb<sup>3+</sup>,Mg<sup>2+</sup>,Ti<sup>3+/IV</sup> materials exhibit NIR photoluminescence arising from the Yb<sup>3+</sup> <sup>2</sup>F<sub>5/2</sub>→<sup>2</sup>F<sub>7/2</sub> transitions. The NIR emission of La<sub>2</sub>O<sub>2</sub>S:Yb<sup>3+</sup>,Mg<sup>2+</sup>,Ti<sup>3+/IV</sup> material could be visualized from fluorescence micrographs essays (Fig. 1). When ceasing the irradiation on the materials, both Ti<sup>3+</sup> and Yb<sup>3+</sup> persistent luminescence can be observed, ranging from the red (600) to the NIR (980 nm) region of the spectrum, respectively (Fig. 2). The persistent luminescence mechanism of Yb<sup>3+</sup> probably involves a hole trapping process as the proposed to Eu<sup>3+</sup> materials, followed by the hole feeding to the Yb<sup>3+</sup>-e<sup>-</sup> pair. The infrared persistent luminescence involving the Yb<sup>3+</sup> <sup>2</sup>F<sub>5/2</sub>→<sup>2</sup>F<sub>7/2</sub> transition makes this new material suitable for future applications.

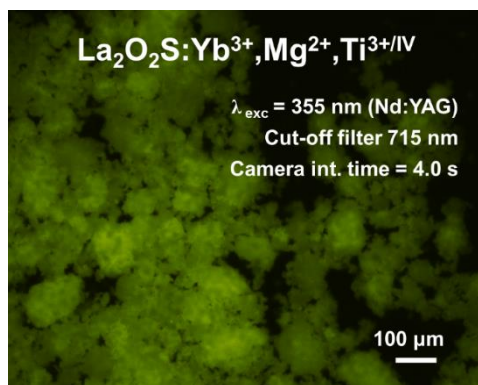


Fig. 1 Fluorescence micrograph of Y<sub>2</sub>O<sub>2</sub>S:Yb<sup>3+</sup>,Mg<sup>2+</sup>,Ti<sup>3+/IV</sup> material, showing the NIR emission from Yb<sup>3+</sup> ion.

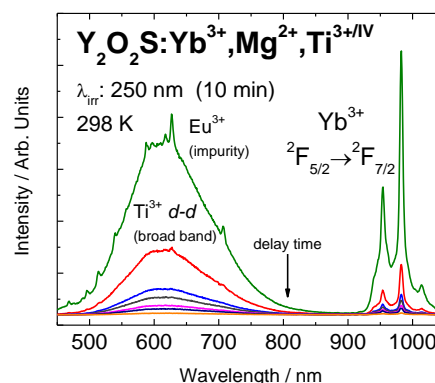


Fig. 2 Persistent luminescence emission spectra of Y<sub>2</sub>O<sub>2</sub>S:Yb<sup>3+</sup>,Mg<sup>2+</sup>,Ti<sup>3+/IV</sup> material, registered immediately from ceasing the excitation.

## 3. References

- [1] Q. le Masne de Chermont, C. Chanéac, J. Seguin, F. Pellé, S. Maîtrejean, J-P. Jolivet, D. Gourier, M. Bessodes, D. Scherman. *Proc. Natl. Acad. Sci. U.S.A.*, **104** (2007) 9266.
- [2] T. Maldiney, C. Richard, J. Seguin, N. Wattier, M. Bessodes, D. Scherman. *ACS Nano*, **5** (2011) 854.
- [3] D.-C. Yu, R. Martín-Rodríguez, Q.-Y. Zhang, A. Meijerink, F.T. Rabouw. *Light Sci. Appl.*, **4** (2015) 344.
- [4] Liang Y-J, Liu F, Chen Y-F, Wang X-J, Sun K-N, Pan Z. *Light Sci Appl* **5** (2016) e16124.
- [5] Dorenboos P. *Phys Rev B - Condens Matter Mater Phys* **85** (2012) 1.

# Enhancing the performance of persistent phosphors: focus on the trapping defects and detrapping processes

**Philippe F. Smet<sup>1</sup>, Katleen Korthout<sup>1</sup>, Claude Tydtgat<sup>1</sup>, David Vander Heggen<sup>1</sup>, Simon Michels<sup>1</sup>, Dirk Poelman<sup>1</sup>, Ives Debaere<sup>2</sup>, Mathias Kersemans<sup>2</sup>**

<sup>1</sup>LumiLab, Department of Solid State Sciences, Ghent University, Krijgslaan 281-S1, 9000 Gent (Belgium)

<sup>2</sup>Mechanics of Materials and Structures MMS, Department of Materials Science and Engineering, Ghent University, Technologiepark 903, 9052 Zwijnaarde (Belgium)

\*Corresponding author e-mail address: philippe.smet@ugent.be

## 1. Introduction

Persistent phosphors, also called glow-in-the-dark materials, are a specific type of luminescent materials. They can emit light long after the excitation ended, which is realized by temporarily storing energy in the crystal lattice [1,2]. Ambient heat can release the trapped charge carriers, after which recombination and light emission can occur. Several materials are known to emit light for tens of hours after the end of the excitation, not only in the visible part of the electromagnetic spectrum, but also in the infrared, opening novel applications in the field of bio imaging.

## 2. Optically stimulated detrapping

For many applications, such as in emergency signage, the storage capacity of persistent phosphors should further be increased, which would open new application areas, such as glowing road marks [3]. We show that the excitation of the europium center in the blue emitting  $\text{Sr}_2\text{MgSi}_2\text{O}_7:\text{Eu,Dy}$  by near-UV light not only leads to charge trapping – essential to the persistent luminescence - but also to optically stimulated release of previously trapped charges and subsequent luminescence (OSL) [4]. Furthermore, the optical detrapping is observed to be significantly more important when a larger fraction of the traps is already filled, suggesting OSL is the limiting factor in the storage capacity of persistent phosphors. The impact of this OSL process on the quantum efficiency of the persistent phosphor is demonstrated, which has implications for phosphors used in high brightness applications (e.g. laser based illumination).

## 3. Mechanical detrapping

Also mechanical pressure can in certain (mechanoluminescent (ML)) phosphors lead to light emission, allowing their use as pressure gauges or stress indicators [5]. Here we focus on the use of ML phosphors as a visualisation tool for ultrasound pressure fields [6]. In the case of  $\text{BaSi}_2\text{O}_2\text{N}_2:\text{Eu}$ , a bluish green ML signal is observed proportional to the ultrasound intensity which can be used to build a three dimensional representation of the ultrasound pressure field. The obtained results are validated by comparison to numerical simulations, showing an excellent match [6].

## 4. Nature of the trapping defects

Based on the insights from the temperature dependency of trapping and detrapping processes, in combination with the chemical nature of the defects, an empirical model is constructed to understand the trapping and detrapping mechanisms in persistent phosphors. A key element is the careful use of x-ray absorption spectroscopy to proof and evaluate the extent of valence state changes for the rare earth (co)dopants in persistent phosphors [7].

## 5. References

- [1] K. Van den Eeckhout, P.F. Smet, D. Poelman, *Materials* **3** (2010), 2536.
- [2] K. Van den Eeckhout, D. Poelman, P.F. Smet, *Materials* **6** (2013), 2789.
- [3] J. Botterman and P. F. Smet, *Opt. Express* **23** (2015) A868.
- [4] C. Tydtgat, K.W. Meert, D. Poelman, P.F. Smet, *Opt. Mater. Express* **6** (2016) 844.
- [5] C.N. Xu et al., *Appl. Phys. Lett.* **74** (1999) 2414.
- [6] M. Kersemans, P.F. Smet, N. Lammens, J. Degrieck, W. Van Paepegem, *Appl. Phys. Lett.* **107** (2015) 234102.
- [7] K. Korthout, K. Van den Eeckhout, J. Botterman, S. Nikitenko, D. Poelman and P.F. Smet, *Phys. Rev. B* **84** (2011) 085140



# Combustion synthesis of blue long lasting phosphor $\text{CaAl}_4\text{O}_7: \text{Eu}^{2+}, \text{Dy}^{3+}$ and its novel application in fingerprint and lip mark detection

Amrita Das<sup>1</sup>, Vishal Sharma<sup>1\*</sup>, Vijay Kumar<sup>2</sup>, Vinay Kumar<sup>3</sup>, H. C. Swart<sup>4</sup>

<sup>1</sup>Institute of Forensic Science & Criminology, Panjab University, Chandigarh, India

<sup>2</sup>Department of Applied Physics, Chandigarh University, Gharuan, Mohali (Punjab), India

<sup>3</sup>Department of Physics, Shri Mata Vaishno Devi University, Katra 182320, J&K, India

<sup>4</sup>Department of Physics, University of the Free State, Bloemfontein, South Africa

\*Corresponding author e-mail address:sharmavishal05@gmail.com

## 1. Introduction

The drive of luminescent materials with superior optical and photoluminescent properties in a wide range of areas have shared the research efforts in this sector aimed in the direction of achieving better material features. Rare earth ions are considered as primary activators luminescent centres in large numbers of host materials and expressed by a partially filled 4f shell that is covered by  $5s^2$  and  $5p^6$  electrons therefore, generally combined to synthesize luminescent materials with better properties. RE ions doped phosphor materials have been the subject of scientific interest due to their significant applications in a variety of fields such as, display devices, temperature sensors, solar cell, bio-imaging, optoelectronics devices, etc. The  $\text{RE}^{2+}$  doped calcium aluminates are prospective persistent luminescence candidates [1-2]. The aluminates exhibit strong luminescence at the blue/green region which is categorized by a fast decay of  $\text{Eu}^{2+}$  ion followed by very long after glow [1-3]. The afterglow can be further improved by co-doping the aluminates with some  $\text{RE}^{3+}$  ions [3-4]. In this work, long persistent  $\text{Eu}^{2+}, \text{Dy}^{3+}$  doped  $\text{CaAl}_4\text{O}_7$  was prepared using a solution combustion method with urea as organic fuel. The objectives of this study were (1) to prepare  $\text{Eu}^{2+}, \text{Dy}^{3+}$  doped  $\text{CaAl}_4\text{O}_7$  phosphors and to characterize them with different techniques such as X-ray diffraction for phase identification, morphology was studied using Field Emission Scanning Electron Microscope and the optical study was carried out using Photo luminescence Spectrophotometer; and (2) to study the effect of co-dopants on the optical and luminescence properties. Probable mechanisms of long persistent in the synthesized phosphors were discussed in the light of the existing literature. The obtained results point out that  $\text{Eu}^{2+}, \text{Dy}^{3+}$  doped  $\text{CaAl}_4\text{O}_7$  phosphor has the potential to be used for real applications in the area of long-lasting phosphors for the uses in fingerprint and lip mark detection. An effort has been made to compare the results with the earlier existed literature on the synthesis, characterization and applications of long-lasting phosphors based on rare earth doped inorganic materials in turn to make this work more enlightening.

## 2. Results

The emission spectrum was recorded with an excitation wavelength of 326 nm (figure 1) and the major bands were recorded at 447 nm corresponding to the blue color and two minor bands were recorded at 577 nm and 616 nm. Using the prepared phosphor, different latent fingerprints were developed, where the present nano-powders have successfully developed the finger marks on various surfaces. For the first time in the present research work, the use of nanophosphor in developing latent lip print was performed successfully. Cheilosophy is the science which deals with identification of humans based on lips traces, and aids in forensic investigation (figure 2). The aim of this study is to develop the lipmarks to establish the uniqueness of lip prints which aids in personal identification. The results showed that the developed fingerprints and lip prints are quite good in contrast.

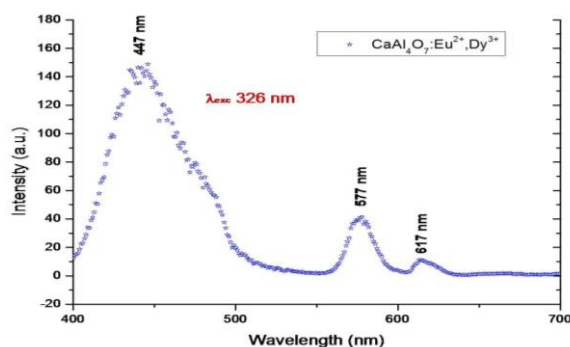


Fig. 1: PL emission spectra of  $\text{CaAl}_4\text{O}_7: \text{Eu}^{2+}, \text{Dy}^{3+}$  at 326 nm



Fig. 2: Fingerprint and lip print developed using the synthesized nanophosphor excited under UV light.

## 3. References

- [1] T. Aitasalo, J. Holsa, H. Jungner, M. Lastusaari, J. Niittykoski. *Mater. Sci.* **20** (2002) 15.
- [2] A. N. Yerpude, S. J. Dhoble. *Lumin.* **27** (2012) 450.
- [3] V. Sharma, A. Das, V. Kumar, O. M. Ntwaeaborwa, H. C. Swart. *J. Mater. Sci.* **49** (2014) 2225.
- [4] W. Jia, H. Yuan, L. Lu, H. Liu, W. M. Yen. *J. Lumin.* **76-77** (1998) 424.

# Defects and impurities: from Bologna Stone to gem stones

Jorma Hölsä<sup>1\*</sup>, Lucas C.V. Rodrigues<sup>2</sup>, Hendrik C. Swart<sup>1</sup>, Mika Lastusaari<sup>3,4</sup>

<sup>1</sup>University of the Free State, Department of Physics, Bloemfontein ZA-9300, Republic of South Africa

<sup>2</sup>Universidade de São Paulo, Instituto de Química, Departamento de Química Fundamental, São Paulo-SP, Brasil

<sup>3</sup>University of Turku, Department of Chemistry, FI-20014 Turku, Finland

<sup>4</sup>Turku University Centre for Materials and Surfaces (MatSurf), Turku, Finland

\*Corresponding author e-mail address: jholsa@utu.fi

## 1. Introduction

The defects and impurities are as old phenomena as luminescence. In fact, the dopants are nothing else than impurities. The famous luminescence material, the Bologna Stone, is obtained by chemical reduction of barite ( $\text{BaSO}_4$  to  $\text{BaS}$ ) while retaining a copper ( $\text{Cu}^+$ ) impurity intact [1]. The valence impurities, *i.e.* the same element but with a different valence, are found in materials when the dopant can be easily reduced or oxidized. Such a common dopant as  $\text{Eu}^{3+}$  may thus show  $\text{Eu}^{2+}$  luminescence [2], too, albeit with different features and decay times which makes the identification challenging. The band emission of  $\text{Eu}^{2+}$  is easily taken as a “host” or “lattice” or “defect” emission; strictly speaking the last one is true though only unwittingly. The blue-green emission due to  $\text{Ti}^{3+}$  from oxidic Zr/Hf materials [3] is frequently ascribed incorrectly to “defect” emission. The almost constant color irrespective of the actual oxide host is yet posing a theoretical challenge. Other elemental impurities frequently encountered include  $\text{Cr}^{3+}$  in aluminates and  $\text{Er}^{3+}$  (or  $\text{Tm}^{3+}$ ) in the  $\text{Yb}^{3+}$  ( $\text{Er}^{3+}$ ) up-conversion phosphors. The role of  $\text{Er}^{3+}$  in the build-up of other  $\text{Yb}^{3+}$ ,  $\text{R}^{3+}$  (*e.g.*  $\text{Tb}^{3+}$ ) up-conversion needs further elaboration.

## 2. Results

Genuine defect emission due to charge compensation can be observed from *e.g.* the  $\text{R}^{3+}$  doped  $\text{CdSiO}_3$  [4] though the defect emission is usually obtained only at low temperatures with short lifetime. Due to the specific crystal structure of  $\text{CdSiO}_3$ , the  $\text{R}^{3+}$  doping promotes dopant pair formation due to aliovalent (*i.e.* charge mismatch,  $\text{R}^{3+}$  vs  $\text{Cd}^{2+}$ ) substitution, also involving unstable oxide intermediate between the two  $\text{R}^{3+}$  ions. This kind of pair (or cluster) may result in the quenching of luminescence from higher excited levels offering a possibility to tune the emission color as observed for *e.g.* the  $\text{Tb}^{3+}$  or  $\text{Pr}^{3+}$  doped  $\text{CdSiO}_3$  where the blue and green emissions from the  $^5\text{D}_3$  and  $^3\text{P}_{0-1}$  levels, respectively, are quenched. Unintentional pair formation due to imperfect materials preparation can, as well, result in unexpected quenching despite very low (below 1 mol-%) doping levels of  $\text{Pr}^{3+}$ ,  $\text{Eu}^{3+}$ , or  $\text{Tb}^{3+}$  in  $\text{Lu}_2\text{O}_3$  [5]. One thus needs to master not only the amount but also the distribution of the different types of defects, *i.e.* dopants, co-dopants and defects, with *a priori* hostile effects on luminescence. Another blunder (oxygen in gas phase) in materials preparation lead to a cheerful result: weak  $\text{Tb}^{3+}$  emission in MS ( $\text{CaS}$ ,  $\text{ZnS}$ ) was enhanced due to the presence of  $\text{Tb}_2\text{O}_2\text{S}$  [6]. Due to low  $\text{Tb}^{3+}$  concentration, no quenching is observed.

The bright sides of the defects and impurities include the persistent luminescence. Some highly priced materials, *i.e.* artificial gemstones, may benefit from impurities, as well. Let alone the banal colored diamonds, the colorless YAG ( $\text{Y}_3\text{Al}_5\text{O}_{12}$ ) crystals can be given a bluish hue using the isovalent  $\text{Eu}^{3+}$  and aliovalent  $\text{Hf}^{\text{IV}}$  doping [7]. Both dopants occupy the  $\text{Y}^{3+}$  site in YAG though due to charge compensation, part (or all) of  $\text{Eu}^{3+}$  is reduced to  $\text{Eu}^{2+}$  the amount of which depends on the relative concentrations of the dopants. The charge compensation scheme (using the Kröger-Fink notation) can be written:  $\text{Hf}_\text{Y}^\cdot + \text{Eu}_\text{Y}^\cdot$  suggesting that these two sites act as electron and hole traps, respectively. Although absorption of light by  $\text{Eu}^{2+}$  may yield the bluish hue to  $\text{Y}_3\text{Al}_5\text{O}_{12}:\text{Hf},\text{Eu}$ , persistent luminescence from the  $\text{Hf}^{\text{IV}}$  stabilized  $\text{Eu}^{2+}$  may be a more appropriate explanation. In the end,  $\text{Eu}^{2+}$  is by far the most efficient persistent luminescence center and the electron and hole traps furnish the components for energy storage. Since the  $\text{Ce}^{3+}$  doped YAG is an efficient persistent phosphor [8], the  $\text{Eu}^{2+}$  doped YAG should be similar as well.  $\text{Y}_3\text{Al}_5\text{O}_{12}:\text{Eu}^{3+},\text{Hf}^{\text{IV}}$  is thus the first persistent gemstone reported so far. Eventually, a detailed time-resolved and VUV excimer laser excited luminescence study revealed, in addition to the ostensible  $\text{Eu}^{2+}$  and  $\text{Eu}^{3+}$  species, the UV and red  $\text{Gd}^{3+}$  impurity emission. Their spectral properties should be elaborated in the future.

## 3. References

- [1] M. Lastusaari, T. Laamanen, M. Malkamäki, K.O. Eskola, A. Kotlov, S. Carlson, E. Welter, H.F. Brito, M. Bettinelli, H. Jungner, and J. Hölsä, *Eur. J. Miner.* **24** (2012) 885.
- [2] P. Gluchowski, W. Stręk, M. Lastusaari, and J. Hölsä, *Phys. Chem. Chem. Phys.* **17** (2015) 17246.
- [3] V. Kumar, O.M. Ntwaeaborwa, J. Hölsä, and H.C. Swart, *Opt. Mater.* **46** (2015) 510.
- [4] L.C.V. Rodrigues, J. Hölsä, M. Lastusaari, M.C.F.C. Felinto, and H.F. Brito, *J. Mater. Chem. C* **2** (2014) 1612.
- [5] Y. Charreire, A. Marbeuf, G. Tourillon, M. Leskelä, L. Niinistö, E. Nykänen, P. Soininen, and O. Tolonen, *J. Electrochem. Soc.* **139** (1992) 619.
- [6] L.I. Kazakova, G.M. Kuz'micheva, and E.M. Suchkova, *Inorg. Mater.* **39** (2003) 959.
- [7] L.I. Kazakova, J. Lindblom, H. Häkkinen, M. Lastusaari, and J. Hölsä, (unpublished).
- [8] Y. Li, M. Gecevicius, and J. Qiu, *Chem. Soc. Rev.* **45** (2016) 2090.

# Spectroscopic investigation of Ce<sup>3+</sup>/Eu<sup>3+</sup> co-doped Li<sub>2</sub>BaZrO<sub>4</sub> nanophosphors

Iorkvaa Ahemen<sup>1\*</sup>, Francis Dejene<sup>1</sup>

<sup>1</sup>Department of Physics, University of the Free State-QwaQwa Campus, Private Bag X13, Phuthaditjhaba, 9866 South Africa  
\*Corresponding author e-mail address: anemior@gmail.com

## 1. Introduction

In a world suffering from energy crisis and the environmental impact occasioned by high energy consumption from conventional lighting technologies, significant reduction in energy wastage through efficient lighting technologies is crucial for human development and health. Solid state lighting technology using white light emitting diodes (WLEDs) holds this promise. The common WLED phosphor is the YAG: Ce<sup>3+</sup> and it produces white light with poor colour rendition index (CRI) due to the absence of the red spectrum. Multi-phase phosphors provide poor/diminished luminous efficiency because of the different decay time of the constituent phases. To overcome these challenges, rare-earth ions such as Tb<sup>3+</sup>, Eu<sup>3+</sup>, Ce<sup>3+</sup> and Dy<sup>3+</sup> have been incorporated into different hosts in various configurations in order to achieve single-phase white-light phosphors with CRI greater than 90. Some examples include; sodium germanate co-doped Tb<sup>3+</sup> and Eu<sup>3+</sup>[1], zinc-sodium-aluminosilicate glass doped with Tb<sup>3+</sup> and Eu<sup>3+</sup>[2] and Tb<sup>3+</sup>/Eu<sup>3+</sup> co-doped oxyfluoride glass[3] and zirconium oxide films co-doped with Tb<sup>3+</sup> and Eu<sup>3+</sup> [4].

In this work, we investigate the spectroscopic properties of Li<sub>2</sub>BaZrO<sub>4</sub> nanoparticles, a novel phosphor host matrix for application in white light emitting diodes. The host matrix was singly- and co-doped with Ce<sup>3+</sup> and Eu<sup>3+</sup> at varying activator ions concentration in order to achieve white light.

## 2. Results

Excitation of the singly doped phosphors with UV and blue light emitting sources show the characteristic red (Figure 1a & 1b) and blue-green luminescence of Eu<sup>3+</sup> (Figure 1a) and Ce<sup>3+</sup> ions, respectively. A broad photoluminescence (PL) emission spectrum comprising of emission bands from the host and the dopant ions obtained from Ce<sup>3+</sup>/Eu<sup>3+</sup> co-doped systems of these host gave white light. Concentration quenching phenomenon is discussed in the light of energy transfer, electron-phonon coupling and ion-ion interactions. The influence of ligands on the luminescence intensity of the dopant ions is discussed on the bases of Judd-Ofelt parameters using PL emission spectra. Photometric characterization such as colour temperature and CIE coordinates show the suitability of these phosphors for both red and blue-green emissions in LEDs and their potentials as complementary colours for white LED application.

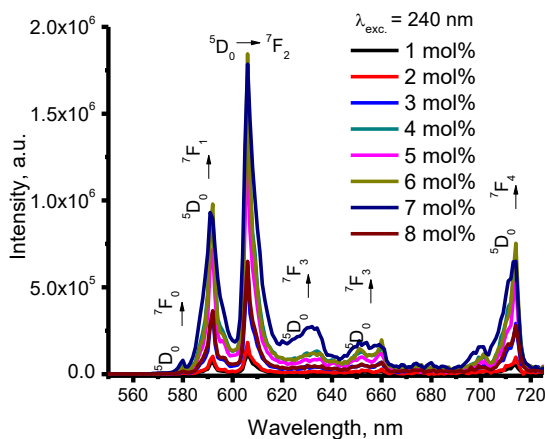


Fig. 1a: PL of Eu<sup>3+</sup> singly doped Li<sub>2</sub>BaZrO<sub>4</sub>



Fig. 2: Red light emitted from Eu<sup>3+</sup> singly doped Li<sub>2</sub>BaZrO<sub>4</sub>

## 3. References

- [1] E. Álvarez, M. E. Zayas, J. Alvarado-rivera, and F. Félix-domínguez. *J. Lumin.* **153** (2014) 198.
- [2] U. Caldiño, A. Speghini, S. Berneschi, M. Bettinelli, M. Brenci, and E. Pasquini. *J. Lumin.* **147** (2014) 336.
- [3] R. Wang, D. Zhou, J. Qiu, Y. Yang, and C. Wang. *J. Alloys Compd.* **629** (2015) 310.
- [4] C. F. A.I. Ramos-Guerra, J. Guzmán-Mendoza, M. García-Hipólito, n, O. Alvarez-Fregosob. *Ceram. Int'l.* **41** (2015) 11279.

## Poster Abstracts – Session A (posters 1-38)

Poster	Presenter	Title
1 (p. 43)	Edwin Mapasha	Electronic properties of B and Al doped <i>graphane</i> : A hybrid density functional study
2 (p. 44)	Emmanuel Igumbor	First principle studies of electronic properties of single and bilayer mixed dichalcogenide
3 (p. 45)	Emmanuel Igumbor	Hybrid functional study of P, As, Sb and Bi defect levels in Ge
4 (p. 46)	Felana Andriambelaza	First principles studies of Te line ordered alloys in a MoS <sub>2</sub> monolayer
5 (p. 47)	Helga T. Danga	Electrically active defects in epitaxial <i>p</i> -type silicon after alpha-particle irradiation
6 (p. 48)	Helga Danga	Electrical characterization of alpha-particle induced defects in Pd/ZnO Schottky barrier diodes
7 (p. 49)	Benard S. Mwankemwa	Effects of surface morphology on the optical and electrical properties of Schottky diodes of CBD deposited ZnO nanostructures
8 (p. 50)	Alexander T. Paradzah	Ultrafast electron and hole dynamics of photo-excited hematite thin films: An intensity dependency study
9 (p. 51)	Abraham Barnard	Activation energy and mechanism of the annealing of Sb-vacancy and E' complex's in n-type germanium
10 (p. 52)	Kelebogile Maabong	Optical and photoelectrochemical properties of hematite photoanode: influence of thickness and growth temperature
11 (p. 53)	Ezekiel Omotoso	The influence of thermal annealing on the characteristics of Au/Ni Schottky contacts on <i>n</i> -type 4H-SiC
12 (p. 54)	Shandirai M. Tunhuma	Doping dependence of the electrical characteristics of nitrogen-doped n-type 4H-silicon carbide
13 (p. 55)	Fatemeh Taghizadeh	Laplace DLTS characterization of the fine structure associated with the radiation induced E3 defect in GaAs
14 (p. 56)	Kian Ostvar	Electric field dependence study of the E <sub>c</sub> -0.58 eV centre in bulk grown n-type gallium arsenide using Laplace DLTS
15 (p. 57)	P. N. M. Ngoepe	Characterisation of ion implanted GaN by DLTS
16 (p. 58)	Walter Meyer	In-system monitoring of MOSFET threshold voltage due to radiation degradation
17 (p. 59)	V. E. Gora	Determination of the optimum annealing temperature to erase alpha induced defects on Co-4H-SiC Schottky contacts
18 (p. 60)	V. E. Gora	Comparison of the properties of nickel, cobalt, palladium and tungsten Schottky contacts on 4H-silicon carbide
19 (p. 61)	SJ Dhoble	Energy Transfer from Pr <sup>3+</sup> to Gd <sup>3+</sup> in BaB <sub>8</sub> O <sub>13</sub> phosphor and its application in phototherapy lamp

20 (p. 62)	Winfred Mueni Mulwa	DFT+U and experimental studies of Ce <sup>3+</sup> Cu <sup>2+</sup> : $\gamma$ -Al <sub>2</sub> O <sub>3</sub>
21 (p. 63)	Sudhakar Reddy Busireddy	Preparation and characterization of Eu <sup>3+</sup> & Tb <sup>3+</sup> ions doped alkali oxide (Li <sub>2</sub> O/Na <sub>2</sub> O/K <sub>2</sub> O) modified borophosphate glasses for red and green laser and display device applications
22 (p. 64)	E. Coetsee	Energy transfer study between Ce <sup>3+</sup> and Tb <sup>3+</sup> ions in a calcium fluoride crystal
23 (p. 65)	D. I. Shahare	Luminescence properties of Na <sub>2</sub> Sr <sub>2</sub> Al <sub>2</sub> PO <sub>4</sub> Cl <sub>9</sub> :Sm <sup>3+</sup> phosphor
24 (p. 66)	George Tshabalala	Synthesis and characterization of MV <sub>0.5</sub> P <sub>0.5</sub> O <sub>4</sub> :Sm <sup>3+</sup> , Tm <sup>3+</sup> (Ln = Gd, La, Y) for solar cells application
25 (p. 67)	Jorma Holsa	Paramagnetism of rare earth ions with the same 4f <sup>7</sup> electron configuration: Eu <sup>2+</sup> , Gd <sup>3+</sup> and Tb <sup>IV</sup> in EuAl <sub>2</sub> O <sub>4</sub> , Gd <sub>2</sub> O <sub>3</sub> , and TbO <sub>2</sub>
26 (p. 68)	Jorma Holsa	Microstructural and spectroscopic properties of the CaTiO <sub>3</sub> :Pr <sup>3+</sup> ,Zn <sup>2+</sup> red emitting persistent phosphor
27 (p. 69)	D. D. Ramteke	Physical and optical properties of lithium borosilicate glasses doped with Dy <sup>3+</sup> ions
28 (p. 70)	Simon N. Ogugua	Photoluminescent dynamics of Pr <sup>3+</sup> and Dy <sup>3+</sup> in R <sub>2</sub> SiO <sub>5</sub> (R = La, Y) host
29 (p. 71)	Kishore Kumar Nair	Synthesis of Ag-SnO <sub>2</sub> nanocomposites and evaluation of optical, photoluminescence and antimicrobial properties
30 (p. 72)	L. Mathevula	Structural and optical properties of rare-earth doped $\alpha$ -Fe <sub>2</sub> O <sub>3</sub> nanoparticles
31 (p. 73)	R.E. Kroon	Reflection measurements for luminescent powders
32 (p. 74)	R.E. Kroon	Investigating the capability of ToF-SIMS to determine the oxidation state of Ce ions
33 (p. 75)	L. J. B. Erasmus	Characterisation of the optical thermometry properties of La <sub>2</sub> O <sub>2</sub> S:Eu phosphor material
34 (p. 76)	Trilok K. Pathak	Effect of annealing temperature on structural and luminescence properties of Eu doped NaYF <sub>4</sub> phosphor
35 (p. 77)	LF Koao	Influence of citric acid solution on LiMn <sub>2</sub> O <sub>4</sub> nanostructures prepared by chemical bath deposition method
36 (p. 78)	LF Koao	Structural and luminescence properties of self-yellow emitting undoped Zn <sub>2</sub> V <sub>2</sub> O <sub>7</sub> and (Ca, Ba, Sr)-doped Zn <sub>2</sub> V <sub>2</sub> O <sub>7</sub> phosphors synthesised by combustion method
37 (p. 79)	A. Balakrishna	Host sensitized near-infrared emission in Nd <sup>3+</sup> doped different alkaline earth-sodium-phosphors
38 (p. 80)	M.M. Duvenhage	Role of target and Ga particulates on the surface and optical properties of Y <sub>3</sub> (Al,Ga) <sub>5</sub> O <sub>12</sub> :Tb thin films prepared by PLD

## Poster Abstracts – Session B (posters 39-74)

Poster	Presenter	Title
39 (p. 81)	Danielle Venter	Capacitance spectroscopy on GaNAs/GaAs quantum structure embedded solar cells
40 (p. 82)	Sebastian Mienie	Hall effect electrical characterization of solar cell materials
41 (p. 83)	A. J. Fourie	Deposition of CZT-precursor layers for CZTS solar cell
42 (p. 84)	Peter C. Korir	Effect of selenization time on the structural and morphological properties of Cu(In,Ga)Se <sub>2</sub> thin film absorber layer using a two-step growth process
43 (p. 85)	JR Botha	Effect of dopant density on contact potential difference across n-type GaAs homojunctions using Kelvin probe force microscopy
44 (p. 86)	J. R. Botha	Patterned growth of ZnO nanorods for organic/inorganic hybrid solar cell
45 (p. 87)	Francis Dejene	Effect of growth temperature on structural and luminescence properties of ZnO nanoparticles
46 (p. 88)	Francis Dejene	Effects of precursor concentration on morphological and structure properties of TiO <sub>2</sub> synthesized via sol-gel method
47 (p. 89)	A. K. Bedyal	A potential green emitting citrate gel synthesized NaSrBO <sub>3</sub> :Tb <sup>3+</sup> phosphor for display application
48 (p. 90)	LL Noto	Photoluminescence and thermoluminescence properties of BaGa <sub>2</sub> O <sub>4</sub>
49 (p. 91)	Vinod Kumar	Tailoring and optimization of optical properties of CdO thin films for optoelectronic applications
50 (p. 92)	Vinod Kumar	Photons and electron beam pumped luminescence characteristics of holmium activated CaMoO <sub>4</sub> phosphor
51 (p. 93)	Chinedu C. Ahia	Photoluminescence and structural properties of single and double MOVPE-grown InGaSb/GaSb quantum wells
52 (p. 94)	Ngcali Tile	Atmospheric pressure-MOVPE growth of GaSb/GaAs quantum dots
53 (p. 95)	S. R. Dobson	Photoluminescence measurements of InAs <sub>(1-x)</sub> Sb <sub>(x)</sub> lattice matched to GaSb
54 (p. 96)	V. Craciun	Optical and structural properties of Type-II quantum dots
55 (p. 97)	Vijay Kumar	Recent advances in rare earth doped alkali-alkaline earth borates for solid state lighting applications: a mini review
56 (p. 98)	Vladimir Kolkovsky	Hydrogen-related defects in Al <sub>2</sub> O <sub>3</sub> layers grown on <i>n</i> -type Si by the atomic layer deposition technique
57 (p. 99)	Mustafa Ahmed	Effect of Sm doping on the structural and optical properties of ZnO nanorods grown by chemical bath deposition
58 (p. 100)	S. R. Tankio Djiokap	Influence of NiO as intermediate layer on the properties of ZnO grown on Si by chemical bath deposition
59 (p. 101)	E. Hasabeldaim	Effect of substrate temperature and post annealing temperature on ZnO:Zn PLD thin film properties
60 (p. 102)	Jatani Ungula	Effect of pH on the structural, optical and morphological properties of Ga-doped ZnO nanoparticles prepared by reflux method
61 (p. 103)	A. Talla	Block copolymer templates for zinc oxide nanorods

62 (p. 104)	T. L. Lotha	Sol-gel synthesis and characterization of doped barium titanate nanophosphors
63 (p. 105)	Dickson Andala	Magnetic and optical properties of un-doped and Co-doped TiO <sub>2</sub> nanotubes from electrospun carbon fiber templates
64 (p. 106)	Dickson Andala	Photochemical and photophysical properties gold nanoparticles supported on electrospun TiO <sub>2</sub> nanofibers
65 (p. 107)	G. L. Kabongo	Investigation of ZnO:RE <sup>3+</sup> nanostructures for efficient charge transfer in hybrid based P3HT heterostructures
66 (p. 108)	G. L. Kabongo	Enhanced room temperature ferromagnetism in sol-gel derived ZnO:Ho <sup>3+</sup> nanostructures
67 (p. 109)	BS Mwankemwa	Thickness determination of interfacial SiO <sub>2</sub> ultra-thin films between ZnO based materials and the Si substrate
68 (p. 110)	Mantwa A. Lephoto	Study on photoluminescence and energy transfer of Eu <sup>3+</sup> /Sm <sup>3+</sup> single-doped and co-doped BaB <sub>8</sub> O <sub>13</sub> phosphors
69 (p. 111)	Sharon Kiprotich	A comparison investigation of optical, structural and luminescence properties of CdO <sub>x</sub> Te <sub>1-x</sub> and CdTe <sub>x</sub> Se <sub>1-x</sub> nanoparticles prepared by a simple one pot method
70 (p. 112)	Sharon Kiprotich	High luminescent L-cystine capped CdTe quantum dots prepared at different reaction times
71 (p. 113)	Fekadu Gashaw Hone	Roles of cationic concentration and pH on the structural, morphological and optical band gap of chemically synthesized lead sulphide thin films
72 (p. 114)	Promod Kumar	Plasmonic metamaterial-based graphene/TiO <sub>2</sub> /Ag thin film by a simple spray pyrolysis technique
73 (p. 115)	Shadrach Akinkuade	Synthesis, structural, optical and electrical characteristics of nickel oxide thin films by chemical processing methods
74 (p. 116)	Zamaswazi Tshabalala	Structural transformation and enhanced gas sensing characteristics of TiO <sub>2</sub> nanostructures induced by annealing

# Electronic properties of B and Al doped *graphane*: A hybrid density functional study

**Edwin Mapasha<sup>1\*</sup>, Emmanuel Igumbor<sup>1</sup>, Felana Andriambelaza<sup>1</sup>, Nithaya Chetty<sup>1,2</sup>**

<sup>1</sup>Department of Physics, University of Pretoria, Private bag X 20, Hatfield 0002, Pretoria, South Africa

<sup>2</sup>National Institute for Theoretical Physics, Johannesburg 2000, South Africa

\*Corresponding author e-mail address: edwin.mapasha@up.ac.za

## 1. Introduction

Recently, the two-dimensional (2D) materials such as graphene, *graphane*, hexagonal boron nitride and various transition metal dichalcogenides monolayers have attracted great research interests owing to their special properties. These materials have a potential of being used in a wide range of nanotechnological devices such as optoelectronic, photovoltaic and spintronic. *Graphane*, a fully hydrogenated graphene, firstly synthesized by Elias *et al.*[1], is a wide band gap semiconductor with a large exciton binding energy according to density functional theory (DFT) predictions[2]. The magnitude of the band gap greatly depend on the method employed, for example the 3.5 eV and 4.4 eV values were obtained from the standard DFT and hybrid functional respectively[2], as such, the later has been employed in our calculations. Just like in any material, controlling the electronic behaviour of *graphane* should be necessary for technological devices. Doping is the most successful way to engineer the electronic properties of nanomaterials. The B and N atoms substituting the C atoms in a *graphane* material create the p-type and n-type hybrid systems [3]. The other possible defect that has not yet reported is the B atom replacing a CH pair B<sub>CH</sub>. Removal of a CH pair from *graphane* leaves the three C atoms surrounding the vacancy (V<sub>CH</sub>), and each have a dangling bond. The substitution of B or Al having three valence electrons should saturate the C dangling bonds through pairing. In this work, the electronic properties of B<sub>CH</sub> and Al<sub>CH</sub> defects involving their multiple charge states were investigated using the hybrid DFT.

## 2. Results

The density of states (DOS) plot reveals that the band gap of *graphane* is slightly tuned down due to the B<sub>CH</sub> doping. The dramatic change is noted on the Al<sub>CH</sub> DOS plot shown on Fig.1, where the metallic character has been revealed. An addition of the electrons into a Al<sub>CH</sub> defect yield the n-type systems, while the positive charges re-open the band gap of *graphane*, although with a small values. Our findings suggests possibility of fine tuning the band gap of *graphane* through the defects and charge dopings, for suitable in nanoelectronic applications.

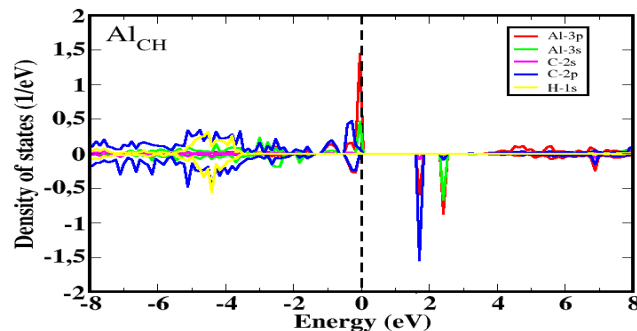


Fig. 1: The density of states (DOS) of Al<sub>CH</sub> in graphane monolayer.

## 3. References

- [1] Elias *et al. Sci.*, **323** (2009) 610.
- [2] H. Sahin, O. Leenaerts, S. K. Singh and F. M. Peeters, *WIREs Comput Mol Sci.* **5** (2015).
- [3] Y. Wang, Y. Ding, S. Shi and W. Tang, *Appl. Phys. Lett.*, **98** (2011) 163104.



# First principle studies of electronic properties of single and bilayer mixed dichalcogenide

**Emmanuel Igumbor<sup>1,2\*</sup>, Edwin R. Mapasha<sup>1</sup>, Walter E. Meyer<sup>1</sup>**

<sup>1</sup>Department of Physics, University of Pretoria, Pretoria 0002, South Africa

<sup>2</sup>Department of Mathematical and Physical Sciences, Samuel Adegboyega, University, Ogori Edo State Nigeria

\*Corresponding author e-mail address: elgumuk@gmail.com

## 1. Introduction

Two-dimensional (2D) material such as transition metal dichalcogenides (TMDs) are attracting interest due to their applications in nano electronic devices [1]. Two-dimensional material have advantage over one-dimensional material, because it is easy to fabricate complex structures such as quantum wells, multilayer superlattices, and heterostructures.  $\text{MoS}_2$ ,  $\text{MoSe}_2$ ,  $\text{MoTe}_2$ ,  $\text{WS}_2$ ,  $\text{WTe}_2$  and  $\text{WSe}_2$  are good examples of TMDs that have been attracting attention in recent years. The Te is expensive, less abundance in the earth crust and has high concentration than Se [2, 3], to obtain a TMD with less Te atom(s), we change the TMD of the  $\text{WTe}_2$  for single layer to  $\text{WTeSe}$  and  $\text{WTeS}$ , and for bilayer to  $(\text{WSeSe})_2$ ,  $(\text{WSeTe})_2$  and  $(\text{WSTe})_2$ . Further more, we calculated the new structural and electronic properties of mixed dichalcogenide using the PBE and HSE hybrid functional [4].

## 2. Results

Fig. 1 shows the relaxed geometric structure of the mixed TMDs. The bond distant between a W and Se atom is the the bond distant between a Te and W atom. Fig. 2 displays the plot of the electronic band structure showing the indirect gap of the mixed TMD of  $\text{WTeSe}$ . Fig. 3 shows the plot of the partial density of states for the  $\text{WTeSe}$ .

The band gap and density of states of the  $\text{WTe}_2$ ,  $\text{WSe}_2$  and  $\text{WS}_2$  with their various combinations exhibit properties of indirect gap. While the band gap of the  $\text{WSeS}$  is 1.14 eV that of the  $\text{WSeTe}$  is 1.45 eV, as predicted by the PBE. The energy of the band gap show that replacing one Se atom with Te in  $\text{WSe}_2$  does not change the band gap contrary to the  $\text{WTe}_2$ , where we observed a decrease in the band gap. The orbital ground state of the  $\text{WSeTe}$ ,  $\text{WSeS}$  and  $\text{WSTe}$ , show evidence of orbital hybridization. Further more, the density of states plots show that the single and double layer of the  $\text{WTe}_2$ ,  $\text{WSe}_2$  and  $\text{WS}_2$  are not spin dependent.

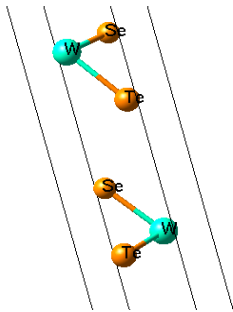


Fig. 1: Relaxed geometric structure of the mixed TMDs

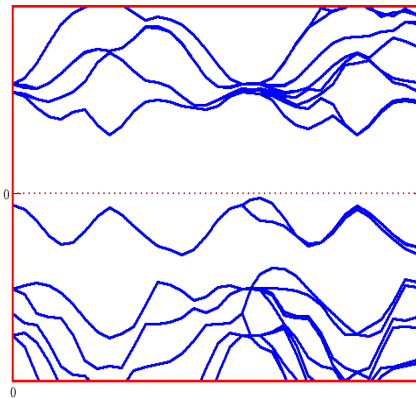


Fig. 2: Plot of band structure of mixed TMDs

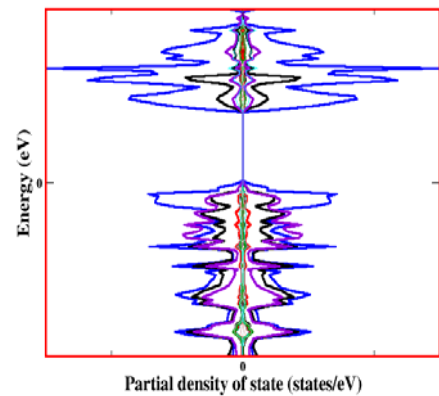


Fig. 3: Plot of partial density of states of mixed TMDs

## 3. References

- [1] M. S. Xu, T. Liang, M. M. Shi and H. Z. Chen, *Chem. Rev.* **113** (2013) 3766.
- [2] N.L. Heda, A. Dashora, A. Marwal, Y. Sharma, S.K. Srivastava, G. Ahmed, R. Jain, B.L. Ahuja. *J. Phys. Chem. Solids* **71** (2010) 187.
- [3] Y. Ma, Y. Dai, M. Guo, C. Niu, J. Lu, B. Huang, *Phys. Chem. Chem. Phys.* **13** (2011) 15546–15553.
- [4] J. Heyd and E. G. Scuseria. *J. Chem Phys* **121** (2004) 3.

# Hybrid functional study of P, As, Sb and Bi defect levels in Ge

**Emmanuel Igumbor<sup>1,2\*</sup>, Helga T. Danga<sup>1</sup>, Shandirai M. Tunhuma<sup>1</sup>, Ezekiel Omotoso<sup>1</sup>, Walter E. Meyer<sup>1</sup>**

<sup>1</sup>Department of Physics, University of Pretoria, Pretoria 0002, South Africa

<sup>2</sup>Department of Mathematical and Physical Sciences, Samuel Adegboyege University, Ogwa Edo State Nigeria

\*Corresponding author e-mail address: elgumuk@gmail.com

## 1. Introduction

Intrinsic and extrinsic diffusion of P, As, and Sb in Ge results reveal evidence of interactions between the dopants and the vacancies leading to the formation of dopant–vacancy pairs [1]. The diffusion activation enthalpy of P, As, and Sb, respectively, show a decreasing activation enthalpy and increasing binding energies with increasing size of the dopant element [1, 2]. The formation energy and the charge state transition levels created in the band gap are important parameters that determine how defect influences a semiconductor material. In this report, we present an ab initio study results of the X (P, As, Sb and Bi) substitutional ( $X_{Ge}$ ) and interstitials ( $X_I$ ) in Ge. We used the hybrid functional of Heyd, Scuseria, and Ernzerhof (HSE) [3, 4] under the framework of density functional theory to calculate the structural and electronic properties of the  $X_{Ge}$  and the  $X_I$ . We calculated the formation energies of both the  $X_{Ge}$  and the  $X_I$  with a view to finding the most energetically favourable defect. The charge state transition levels induced by the  $X_{Ge}$  and the  $X_I$  within the band gap of Ge were obtained and compared with available experimental data.

## 2. Results

Fig. 1 shows the relaxed geometric structure of the  $As_{Ge}$ . The results of the structural properties of  $X_{Ge}$  show that the bond distance between the X and Ge atoms after structural relaxation is within 0.24 Å, while for the  $X_I$  the bond length of the X and G atoms is within 0.15 Å. The formation energies of the P, As Sb and Bi substitutions in Ge varied from 0.61 to 1.90 eV, and for the interstitial, the formation energies varied from 3.53 to 6.69 eV. The double substitution in Ge ( $X_{2Ge}$ ) was not stable for all X. The charge state transition levels induced by the P, As, Sb and Bi in Ge for both the  $X_{Ge}$  and  $X_I$  were not stable in the band gap of Ge. The +2 (as shown in Fig.2) and the neutral charge states are stable for all Fermi energies for the  $X_{Ge}$  and  $X_I$ , respectively.

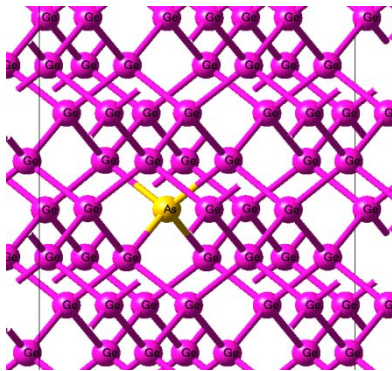


Fig. 1: Relaxed geometric structure of the  $As_{Ge}$

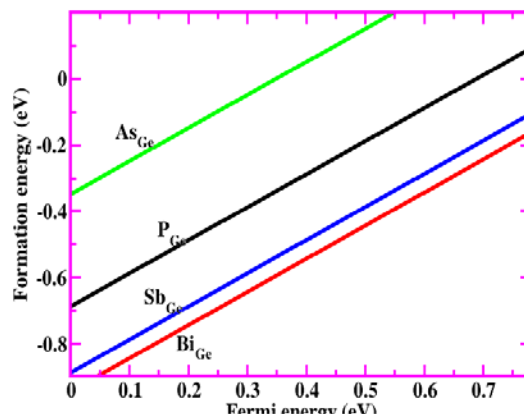


Fig. 2: Plot of formation energies as a function of the Fermi energy for the  $X_{Ge}$

## 3. References

- [1] S. Brotzmann, H. Bracht. *Journal of Applied Physics* **103** (3) (2008) 033508.
- [2] E. Igumbor, C. Ouma, G. Webb, W. Meyer. *Physica B: Condensed Matter* **480** (2016) 191-195.
- [3] J. Heyd and E. G. Scuseria. *J. Chem Phys* **121** (2004) 3.
- [4] P. Deak, B. Aradi, T. Frauenheim, E. Janzen, A. Gali, *Phys. Rev. B* **81**, (2010) 153203.

# First principles studies of Te line ordered alloys in a MoS<sub>2</sub> monolayer

Felana Andriambelaza<sup>1\*</sup>, Edwin Mapasha<sup>1</sup>, Nithaya Chetty<sup>1,2</sup>

<sup>1</sup> Department of Physics, University of Pretoria, Pretoria 0002, South Africa

<sup>2</sup> National Institute for Theoretical Physics, Johannesburg, 2000, South Africa

\*Corresponding author e-mail address: arinala.f@gmail.com

## 1. Introduction

The discovery of graphene, a single sheet of graphite, in 2004 [1], transpired the studies of other two dimensional (2D) materials. Since then, 2D materials have become the focus of many researches in materials science due to their unique properties. The 2D transition metal dichalcogenides (TMDs) have particularly attracted a lot of attention due to their high mechanical strength, direct band gap and optical transparency [2]. TMDs monolayer vary from metal to semiconductor materials. A molybdenum disulfide (MoS<sub>2</sub>) monolayer is an example of TMDs semiconductor that is widely studied. Compared to other TMDs monolayer, a MoS<sub>2</sub> monolayer has a large direct band gap. The electronic and optical properties of a 2D semiconductor material are usually controllable by tuning the band gap. Thus, engineering the band gap of a 2D material is essential for designing nanoelectronic devices. The band gap of a MoS<sub>2</sub> monolayer can be tuned by creating alloys either at the molybdenum (Mo) sites or sulfur (S) sites. Computing all the possible alloy configurations in a large supercell is impossible. Different alloy isomers such as clusters (in the shape of triangle-like, square, circular, etc.), lines and randomly scattered away from each other, can be formed at each concentration. The most popular studied alloys are the random and cluster alloys which successfully fine tuned the band gap of a MoS<sub>2</sub> monolayer. The line ordered alloy can appear in different configurations and can affect the properties of a MoS<sub>2</sub> monolayer. In this work, a theoretical study based on density functional theory (DFT) methods as implemented in the Vienna *ab-initio* package (VASP) [3] has been performed to study the effect of Tellurium (Te) line ordered alloys in a MoS<sub>2</sub> monolayer. Different configurations of the Te line ordered alloys at the S sites are identified and characterized. The thermodynamic stability, structural and electronic properties of the system are investigated. Based on the formation energies analysis, we predict the most thermodynamically stable line configuration at each concentration, and further characterize their electronic properties.

## 2. Results

In order to understand the effect of the Te line ordered alloys in a MoS<sub>2</sub> monolayer, the physical properties of the pristine MoS<sub>2</sub> and MoTe<sub>2</sub> monolayers need to be known first. Both MoS<sub>2</sub> and MoTe<sub>2</sub> monolayers are semiconductor materials with the band gaps of 1.65 eV and 1.06 eV, respectively. All the possible Te line ordered alloy configurations at each concentration are explored. Calculated formation energies suggest that these alloys are thermodynamically stable at room temperature (see Fig. 1). The increase in Te concentration rises the lattice constants of the systems linearly (see inset of Fig. 2), since the S atoms have small atomic radii compared to the Te atoms. The density of states (DOS) analysis show that the electronic properties of the MoS<sub>2</sub> monolayer are greatly affected by the Te line ordered alloys. The band gap of a MoS<sub>2</sub> monolayer is tuned and the magnitude decreases with the increase of the Te concentration (see Fig. 2). Our results show that the driving forces of the band gap tuning are the Te concentration and configurations. Note that the band gap magnitudes of the Te line ordered alloys are suitable for the application in electronic and optoelectronic devices.

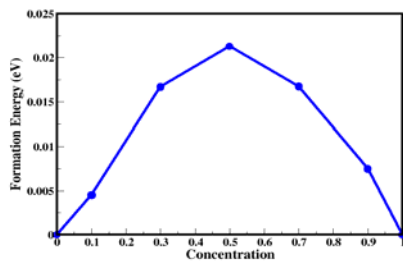


Fig. 1: The formation energies of the Te line ordered alloys at different concentration.

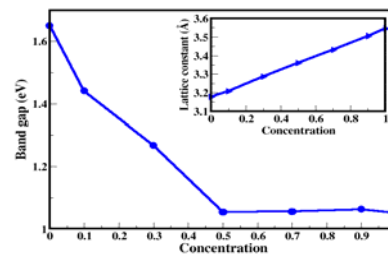


Fig. 2: The band gap of the Te line ordered alloys at different concentration.

## 3. References

- [1] A. K. Geim, K. S. Novoselov, *Nat. Mater.* **6** (2007) 183.
- [2] A. Kuc, T. Heine, A. Kis, *MRS BULL.* **40** (2015) 577.
- [3] G. Kresse, J. Hafner, *Phys. Rev. B* **47** (1993) 558.

# Electrically active defects in epitaxial *p*-type silicon after alpha-particle irradiation

Helga T. Danga<sup>1\*</sup>, Francois D. Auret<sup>1</sup>, Shandirai M. Tunhuma<sup>1</sup>, Ezekiel Omotoso<sup>1,2</sup>, Emmanuel Igumbor<sup>1</sup>  
Valentine E. Gora<sup>3</sup>, Walter E. Meyer<sup>1</sup>

<sup>1</sup>Department of Physics, University of Pretoria, Private Bag X20, Hatfield 0028, South Africa

<sup>2</sup>Departments of Physics, Obafemi Awolowo University, Ile-Ife, 220005, Nigeria

<sup>3</sup>Department of Applied Physics Midlands State University, Private Bag 9055, Gweru, Zimbabwe

\*Corresponding author e-mail address: helga.danga@up.ac.za

## 1. Introduction

Silicon(Si) is one of the most important semiconductor materials and it has been studied extensively [1]. This is mainly due to its low cost, thermal stability and good durability [2]. These properties have enabled researchers to make major advances towards reliable and cost-effective silicon-based photonic–electronic integration [3]. The study of radiation-induced defects in semiconductors comprises a significant area of research on semiconductors for essential reasons as well as from the point of view of device applications [4]. Alpha-particle-induced defects are a cause of principal concern for the in-use failure of electronic applications of Si devices. Not many studies on alpha-particle radiation induced defects exist in literature to the best of our knowledge [5].

In this paper, we report on defects introduced in epitaxially grown boron-doped *p*-type Si after irradiation by alpha-particles at room temperature. We identified the carbon interstitial and a boron-related defect using deep level transient spectroscopy technique (DLTS) and Laplace-DLTS. DLTS has been considered to be one of the most sensitive and reliable tools to measure the variety of electrically active defects in semiconductors [6-8].

## 2. Results

After exposure to alpha-particles with a fluence of  $5.1 \times 10^{10} \text{ cm}^{-2}$ , the energy levels of the hole traps measured are shown in Fig 1. : H(0.16), H(0.33) and H(0.52). The trap H(0.33) was identified as the interstitial carbon ( $C_i$ ) related defect. It was a result of irradiation damage and could only be explained by the presence of donor-like traps [9]. H(0.52) was a boron-related defect [10]. The identity of (0.16) was not clear.

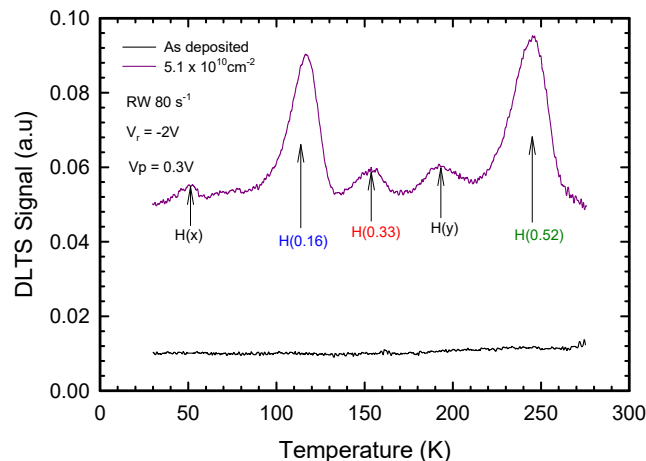


Fig. 1: DLTS spectra illustrating the as-deposited sample and defects obtained after alpha-particle irradiation at a fluence of  $5.1 \times 10^{10} \text{ cm}^{-2}$  Al/*p*-Si.

## 3. References

- [1] S.M. Sze, K.K. NG, Physics of semiconductors, 3 ed., A John Wiley & Sons, Inc, New Jersey, (2007).
- [2] H.T. Danga, F.D. Auret, S.M. Coelho, M. Diale, *Physica B: Condensed Matter*, **480** (2016) 206.
- [3] S. Chen, W. Li, J. Wu, Q. Jiang, M. Tang, S. Shutts, S.N. Elliott, A. Sobiesierski, A.J. Seeds, I. Ross, *Nature Photonics*, (2016).
- [4] N. Zafar, M.Z. Iqbal, *J. Appl. Phys.* **68** (1990).
- [5] M. Asghar, M.Z. Iqbal, N. Zafar, *J. Appl. Phys.* **73** (1993).
- [6] D.V. Lang, *J. Appl. Phys.* **45** (1974).
- [7] F.D. Auret, P.N.K. Deenapanray, *Critical Reviews in Solid State and Materials Sciences*, **29** (2004) 1.
- [8] J. Senawiratne, J.S. Cites, J.G. Couillard, J. Moll, C.A.K. Williams, P.G. Whiting, *Solid State Phenomena* 156-158 (2010) 313.
- [9] O. Paz, F.D. Auret, *MRS Proceedings*, **25** (1983).
- [10] C. Nyamhere, A.G.M. Das, F.D. Auret, M.H. C, *Journal of Physics: Conference Series*, **100** (2008) 042004.

# Electrical characterization of alpha-particle induced defects in Pd/ZnO Schottky barrier diodes

Meehleketo Advice Mayimele<sup>1\*</sup>, Helga T. Danga<sup>1</sup>, F. Danie Auret<sup>1</sup>, Mmantsae Diale<sup>1</sup>

<sup>1</sup>Department of Physics, University of Pretoria, Pretoria 0002, South Africa  
\*Corresponding author e-mail address: meehleketo@gmail.com

## 1. Introduction

The influence of alpha-particle irradiation from Am-241 radio-nuclide on Pd/ZnO samples has been investigated over the temperature range of 80-350 K. Current-voltage (IV), capacitance-voltage and deep level transient spectroscopy (DLTS) were used to characterize the devices before and after irradiation. For both devices, the IV characteristics were well described by thermionic emission (TE) in the high temperatures but deviated from TE theory at low temperatures [1]. The current flowing through the interface at a bias of 2.0 V from pure TE to thermionic field emission within the depletion region with the free carrier concentration of the devices decreases after alpha-particle irradiation. The modified Richardson constants were determined from the Gaussian distribution of the barrier height across the contacts. New defects appeared after alpha-particle irradiation.

## 2. Results

Figure 1 shows DLTS spectra of as deposited and alpha-particle irradiated Pd/ZnO Schottky barrier diodes. The spectra show three prominent (E1, E3 & E4) defects which are common defects in ZnO regardless of the growth, processing and contact fabrication techniques [2]. The E2 defect (have been found to) be introduced with further irradiation. Temperature dependent current voltage measurements were performed to analyse the diode parameters with increasing radiation dosage.

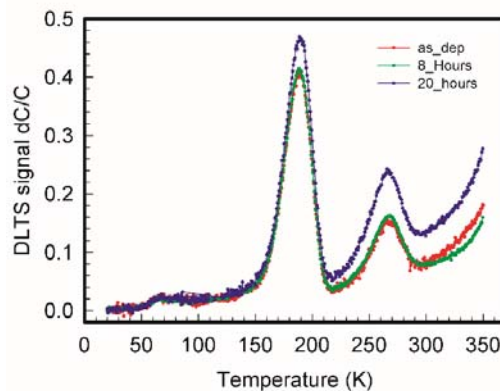


Fig. 1: DLTS spectra of as deposited and after alpha-particle irradiation on Pd/ZnO Schottky barrier diodes.

## 3. References

- [1] A.B. Djurišić, A.M.C. Ng, X.Y. Chen. *Progress in Quantum Electronics* **34** (2010) 191.
- [2] W. Mtangi, F.D. Auret, P. J. Janse van Rensburg, S. Coelho, M.J. Legodi, J. Nel, W. Meyer, A. Chawanda. *Journal of Applied Physics* **110** (2011) 094504.

# Effects of surface morphology on the optical and electrical properties of Schottky diodes of CBD deposited ZnO nanostructures

**Benard S. Mwankemwa<sup>1,2\*</sup>, Jacqueline Nel<sup>1</sup>, Mmantsae Diale<sup>1</sup>**

<sup>1</sup>Physics Department, University of Pretoria, Private bag X20, Hatfield, Republic of South Africa

<sup>2</sup>College of Natural and Mathematical Sciences, School of Physical Sciences, Physics Department, University of Dodoma, P. O. Box 338, Dodoma, Tanzania

Corresponding author e-mail address: ul5315836@tuks.co.za

## 1. Introduction

ZnO has been identified as a novel material for numerous opto-electronic, ferromagnetic and piezoelectric applications. Recent advances in ZnO nanostructures presented added advantages in ferromagnetic and piezoelectric properties, with specific applications for sprintonics and piezoelectric nanogenerators [1]. Furthermore, it is characterized by having multi-colour emissions [2,3] adding substantial advantages to its uses. Recently, Schottky diodes based on ZnO thin films/nanostructures have been reported [4]. However, further studies on the effects of surface morphology of ZnO nanostructure Schottky diodes need to be conducted. In this study we have synthesized ZnO nanostructures using chemical bath deposition. The effects of surface morphology on the optical and electrical properties of Schottky diodes based on ZnO nanostructures were demonstrated.

## 2. Results

In this study, three samples having different morphologies were used. It was found that the shape, size, density and orientations of the nanostructures are crucial for the optical and electrical properties of ZnO nanostructures. Fig. 1 shows high magnification FESEM image of ZnO nanorods with hexagonal flat tops originating from a single point and Fig. 2 show its corresponding room temperature Raman spectrum with strong characteristic peaks for a wurzite structure of ZnO crystal. Other physical properties like electrical and optical properties including PL, UV-Vis transmittance and absorbance will be discussed.

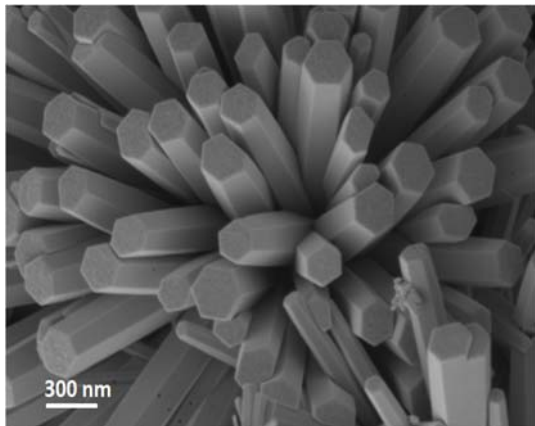


Fig. 1: High resolution FESEM image of ZnO nanorods.

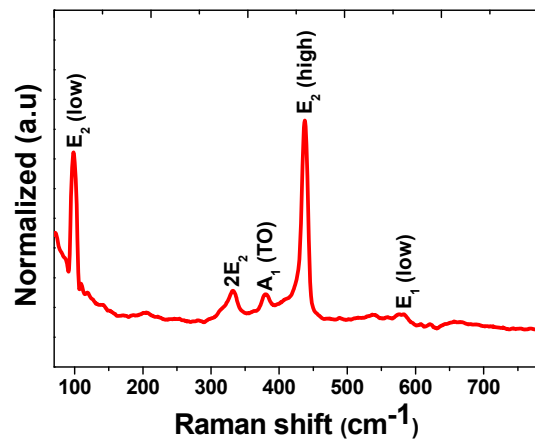


Fig. 2: Room temperature Raman spectrum taken with excitation wavelength of 514.5 nm

## References

- [1] Y. Köseoğlu, *Ceram. Int.* **40** (2014) 4673.
- [2] W. Liu, S.L. Gu, J.D. Ye, S.M. Zhu, S.M. Liu, X. Zhou, et al., *Appl. Phys. Lett.* **88** (2006). doi:10.1063/1.2169908.
- [3] C.H. Ahn, Y.Y. Kim, D.C. Kim, S.K. Mohanta, H.K. Cho, *J. Appl. Phys.* **105** (2009) 1.
- [4] Q. Feng, J. Liu, J. Lu, Y. Mei, Z. Song, P. Tao, et al., *Mater. Sci. Semicond. Process.* **40** (2015) 436.

# Ultrafast electron and hole dynamics of photo-excited hematite thin films: An intensity dependency study

Alexander T. Paradzah<sup>1\*</sup>, Kelebogile Maabong<sup>1</sup>, Mmantsae Diale<sup>1</sup>, Tjaart P. J. Krüger<sup>1</sup>

<sup>1</sup>University of Pretoria, Private Bag X20, Pretoria

\*Corresponding author e-mail address: Alexander.Paradzah@up.ac.za

## 1. Introduction

The drive towards cleaner renewable energy has become inevitable due to fast depletion and the carbon footprint associated with fossil fuels. This has led to extensive research on semiconductor materials that can be used in solar technologies. Although several materials are already in use for solar energy technologies, the materials being used as yet have low energy conversion efficiency. Hematite, best known as  $\alpha\text{-Fe}_2\text{O}_3$ , has a relatively small bandgap of 2.14–2.2 eV and can thus absorb substantially in the visible spectrum of the solar radiation reaching the earth's surface [1]. Hematite also has some desirable properties, which include low toxicity, easy synthesis as well as being a naturally abundant material.  $\alpha\text{-Fe}_2\text{O}_3$  nonetheless also comes with its deficits, most notably being ultrafast electron-hole recombination rates, short hole diffusion lengths, and low conductivity. These shortfalls consequently lead to low photocurrent. It is without doubt that the rate of electron-hole recombination following photo-illumination of a semiconducting material is an important indicator of whether a material can be sustainably used in solar technology, either in photovoltaics or in solar water oxidation. Hematite has been shown to undergo rapid electron-hole recombination rates in the order of a few hundred femtoseconds to a few microseconds. These measurements were performed on nanostructures of different geometries, such as nanowires, nanorice, spheroidal nanoparticles, and also with different dopants to prolong the carrier lifetimes. Sufficiently high pump intensities lead to the creation of multiple excitons, leading to processes such as Auger recombination and exciton-exciton annihilation (EEA).

Not much work has as yet been done to determine the effect of excitation intensity variations on the decay lifetimes in hematite nanostructures. Cherepy et al. carried out a power-dependent study up to a total fluence of 1.2 mJ/(pulse·cm<sup>2</sup>) and did not observe any intensity-dependent decay, owing to the high density of trap states [2]. In this work, we carried out femtosecond pump-probe spectroscopy on  $\alpha\text{-Fe}_2\text{O}_3$  nanostructures grown on thin films. We show that using higher fluences than previously reported (i.e. from 1.40 to 4.19 mJ/(pulse·cm<sup>2</sup>)), results in a significant amount of EEA, which noticeably affects the spectral decay lifetimes. A kinetic model was applied to determine exact electron-hole recombination channels and associated rate constants.

## 2. Results

Fig. 1 shows a typical 3D graph of data obtained from a pump probe measurement of hematite nanostructured thin films. We observed the occurrence of EEA in  $\alpha\text{-Fe}_2\text{O}_3$  nanostructures after high pump intensities from annihilation calculations. Using target analysis, we developed a model that shows the electron-hole recombination channels that likely dominate following a pump pulse.

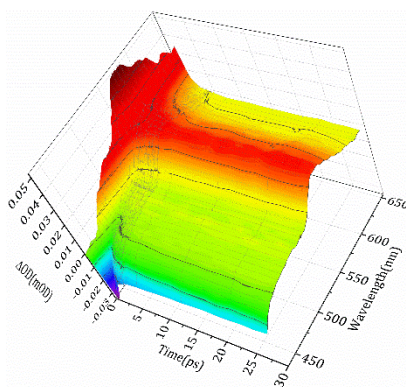


Fig. 1: Transient absorption difference spectra obtained after a pump intensity of 4.19 mJ/(pulse·cm<sup>2</sup>) centered at 387.5 nm.

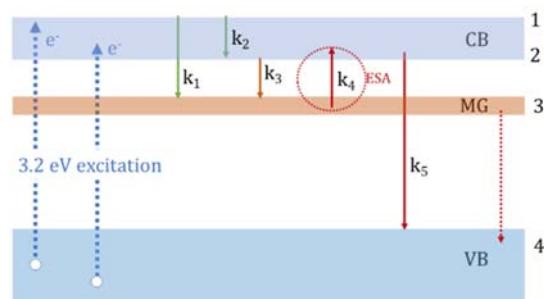


Fig. 2: Model for the decay dynamics following a 3.2 eV pump excitation with a fluence of 1.40 mJ/(pulse·cm<sup>2</sup>). The excitation is taken to populate the excited state bands within the conduction band (CB). The decay compartments include mid-gap (MG) states at low energies and the valence band (VB).  $k_1 - k_5$  denote rate constants.

## 3. References

- [1] B. G. C. Frandsen, E.R. Maxey, D.M. Sherman. *Phys. Rev. B* **79** (2009) 035108.
- [2] N.J. Cherepy, D.B. Liston, J.A. Lovejoy, H. Deng, J.Z. Zhang., *J. Phys. Chem. B* **102**(1998) 770.

# Activation energy and mechanism of the annealing of Sb-vacancy and E' complex's in n-type germanium

Abraham Barnard<sup>1\*</sup>, Danie Auret<sup>1</sup>, Walter Meyer<sup>1</sup>

<sup>1</sup>University of Pretoria, Private Bag X20, Hatfield Pretoria,

\*Corresponding author e-mail address: Abrahamwillembarnard@gmail.com

## 1. Introduction

Deep-level transient spectroscopy was used to study the defects induced n-type germanium by alpha-particle irradiation from an Am<sup>241</sup> source. Previous investigations of the well know Sb-vacancy defect has led to the discovery of a second defect, known as the E', with only slightly different emission rates, but different annealing properties. In this study we investigated further properties of this E' defect. The annealing activation energy was determined through isothermal annealing profiles for both the Sb-Vacancy and the E'. The Sb doped samples were irradiated at 270 K with an Am<sup>241</sup> source, while Laplace deep level transient spectroscopy was used to determine the concentration of each defect. An isothermal annealing study of the E' was carried out in the temperature range 300 K to 325 K in 5 K increments, while the Sb-vacancy was annealed out at 390 K onwards, long after the E' was completely annealed out

## 2. Results

Isothermal annealing of the E-centre and E' concentrations follow a first order annealing rate described as:

$$N_T(t) = N_T(t)e^{-c(T)t} \quad (1)$$

However the emission rates of the two defects are very similar making the concentration indistinguishable. Since the E' anneals at a lower temperature than the E-centre, the isothermal annealing concentration of the E' can be described as:

$$N_T(t) = A + N_T(t)e^{-c(T)t} \quad (2)$$

where A is the concentration of the E-centre. In this case A is assumed to be a constant as the temperature difference is too great to affect each other. Figure 1 shows some of the isothermal annealing profiles of the E' after these conditions are taken into consideration. The implications of these results will be discussed in the paper.

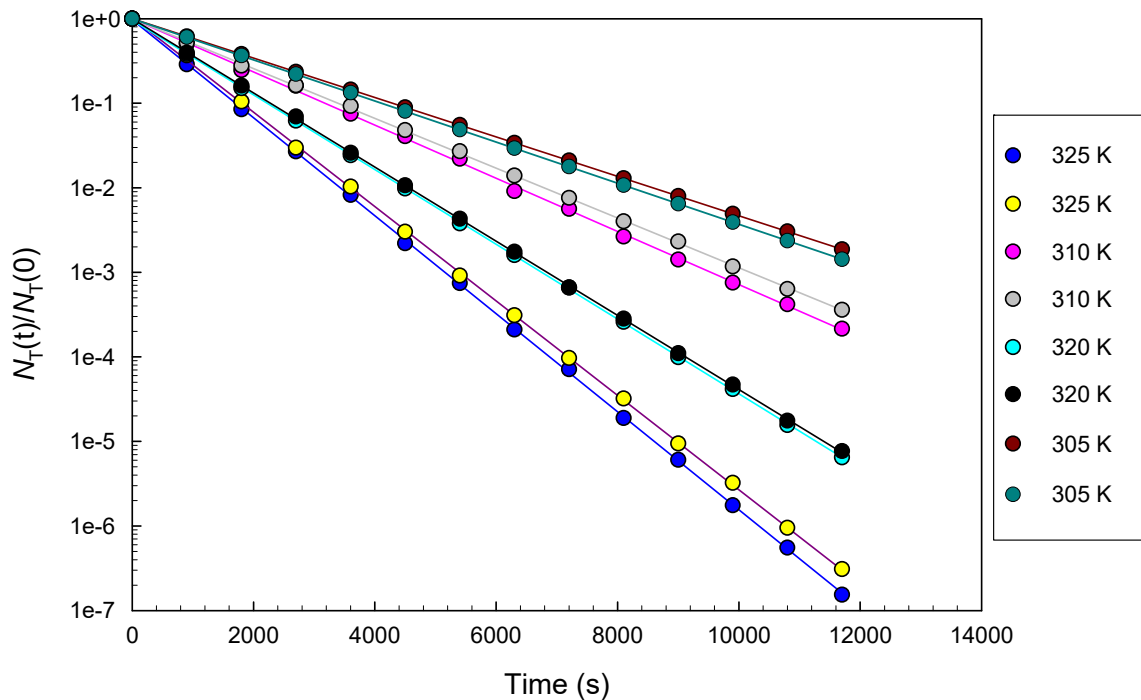


Fig. 1: Isothermal annealing of E' at different temperatures

## 3. Reference

[1] J. Fage-Pederson and A. Nylandsted Larsen. *Physical Review B*. **62** 15 (2000) 10116.



# Optical and photoelectrochemical properties of hematite photoanode: influence of thickness and growth temperature

**Kelebogile Maabong<sup>1,2\*</sup>, Augusto G.J. Machatine<sup>1</sup>, Artur Braun<sup>3</sup>, Mmantsae M. Diale<sup>1</sup>**

<sup>1</sup>University of Pretoria, Pretoria 0028, South Africa

<sup>2</sup>University of Botswana, Department of Physics, UB 0022 Gaborone, Botswana

<sup>3</sup>Empa, Swiss Federal Laboratories for Materials Science and Technology, CH – 8600 Dübendorf, Switzerland

\*Corresponding author e-mail address: Kele.Maabong@up.ac.za

## 1. Introduction

In the search for a stable and affordable semiconductor photoelectrode for hydrogen production from photoelectrochemical water splitting, hematite ( $\alpha\text{-Fe}_2\text{O}_3$ ) has emerged as one of the promising materials for solar-fuel applications [1, 2]. The absorption band of hematite allows absorption of photons from near infra-red region into the UV region. Nevertheless, its maximum capacity in photoelectrochemical (PEC) water splitting systems is limited by the low absorption coefficient due to indirect (phonon assisted) transitions. Optical properties of the photoanode play an important role in a PEC system. Hematite films were prepared by a simple and economic dip coating on fluorine doped tin oxide (FTO) substrate, followed by sintering at 450 to 600 °C. The influence of film thickness and treatment temperature on optical and photoelectrochemical properties was investigated. UV-vis spectrophotometer and Raman scattering spectroscopy are used to probe the optical and vibrational properties of the thin films.

## 2. Results

X-ray diffraction revealed increased crystallinity with both increasing treatment temperature and film thickness. The XRD diffraction in Fig. 1 shows increased peak intensity with film thickness. Optical absorption of the films reveals a shift on the fundamental band gap edge to higher wavelength region with increasing thickness. The measured photocurrent density (Fig. 2) increased from 0.094 to 0.36 mA cm<sup>-2</sup> versus RHE, for films annealed at 450 and 550 °C respectively, after which it decreased.

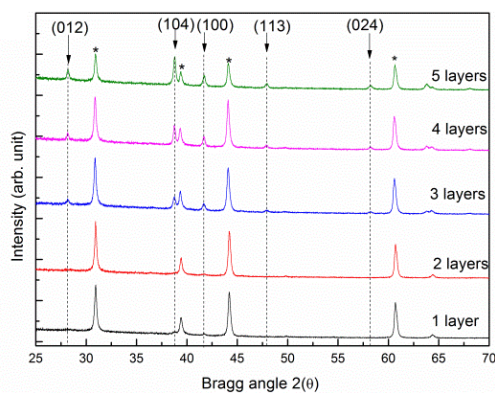


Fig. 1: XRD diffractions of hematite films of different thicknesses prepared on FTO substrate, showing increasing peak intensity with film thickness.

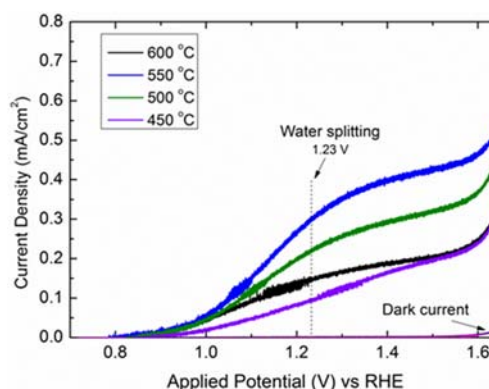


Fig. 2: Current density as a function of external bias from a hematite photoelectrode annealed at different temperatures, measured under dark and illumination (1.5 AM).

## 3. References

- [1] K. Sivula, F. Le Formal, M. Gratzel, *ChemSusChem*, **4** (2011) 432.
- [2] M.J. Katz, S.C. Riha, N.C. Jeong, A.B.F. Martinson, O.K. Farha, J.T. Hupp, *Coordination Chemistry Reviews* **256** (2012) 2521.

# The influence of thermal annealing on the characteristics of Au/Ni Schottky contacts on *n*-type 4H-SiC

Ezekiel Omotoso<sup>1,2\*</sup>, F. Danie Auret<sup>1</sup>, Emmanuel Igumbor<sup>1</sup>, Shandirai M. Tunhuma<sup>1</sup>, Helga T. Danga<sup>1</sup>, Phuti N. M. Ngoepe<sup>1</sup>, Mmantsae Diale<sup>1</sup>, Matshisa J. Legodi<sup>1</sup>, Bidini A. Taleatu<sup>2</sup>, Walter E. Meyer<sup>1</sup>

<sup>1</sup>Department of Physics, University of Pretoria, Private Bag X20, Hatfield 0028, South Africa

<sup>2</sup>Department of Physics, Obafemi Awolowo University, Ile-Ife, 220005, Nigeria

\*Corresponding author e-mail address: ezekiel.omotoso@up.ac.za

## 1. Introduction

The 4H-SiC, a wide band gap semiconductor material of 3.26 eV [1], is a promising polytype for vertical type high-voltage devices due to its higher bulk and small anisotropy. SiC has drawn attention of many researchers because of its outstanding properties such as high thermal conductivity, high breakdown field and high saturated drift velocity [2]. It has offered economically substantial benefits to aircraft, power, communications and energy production industries because of the aforementioned characteristics.

We have successfully studied the effect of annealing temperature on the electrical and structural characteristics of Au/Ni/4H-SiC Schottky barrier diodes (SBDs).

The Ni ohmic and Au/Ni Schottky contacts of thicknesses 3000 Å and 200 Å/800 Å, respectively, have been thermally evaporated on highly doped ( $1.9 \times 10^{16} \text{ cm}^{-3}$ ) *n*-type 4H-SiC. The SBDs were isochronally annealed under Ar ambient in 100 – 600 °C in steps of 50 °C. In this study, current-voltage (*I-V*), capacitance-voltage (*C-V*), scanning electron microscopy (SEM), X-ray diffractometer (XRD) and deep level transient spectroscopy (DLTS) were employed to determine the thermal dynamics of deep level defects present in as-deposited Au/Ni/4H-SiC SBDs.

## 2. Results

Prior to the thermal annealing of Schottky contacts, the *I-V* measurements results confirmed the good rectification of SBDs with ideality factor, Schottky barrier height and series resistance of 1.07, 1.20 eV and 7 Ω, respectively. A decrease in contact's quality with increasing annealing temperature was observed from the *I-V* and *C-V* results showed in Figs 1 and 2. The SBDs maintained their high rectification quality up to the annealing temperature of 500 °C before the contacts started deteriorating with increase in annealing temperature. The Schottky barrier height of as-deposited contacts was less than after annealing at 500 °C which was due to the metallurgical reactions taking place at the interface and probably reduced the interfacial oxide layer. We observed four defects with energies 0.10, 0.12, 0.16 and 0.65 eV below the conduction band before the isochronal annealing. There was no difference in the number of deep level defects present after annealing at 600 °C but the DLTS signal was reduced in height.

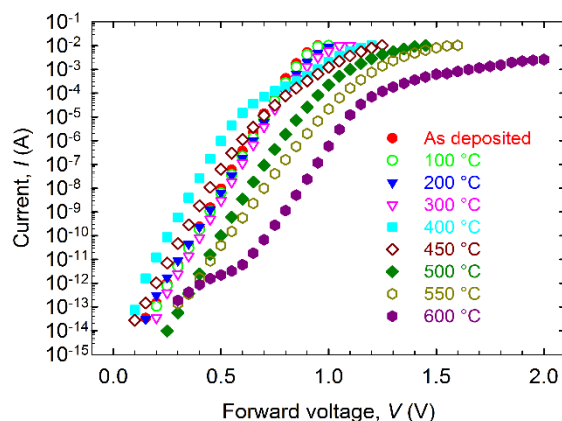


Fig. 1: Logarithmic forward *I-V* characteristics of Au/Ni/4H-SiC Schottky barrier diodes before and after isochronal annealing from 100 to 600 °C.

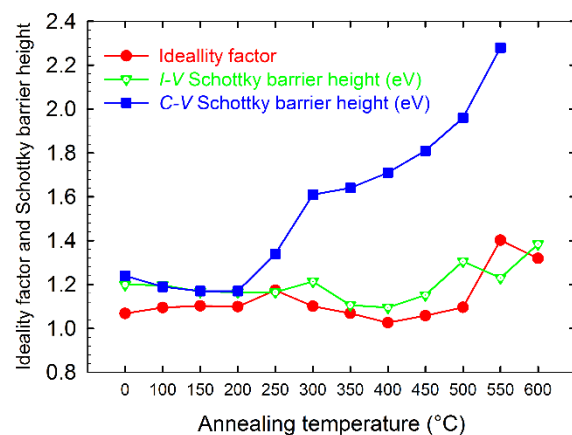


Fig. 2: The variation of ideality factor and Schottky barrier height as a function of annealing temperature for Au/Ni/4H-SiC Schottky barrier diodes.

## 3. References

- [1] L.M. Tolbert, B. Ozpineci, S.K. Islam and M.S. Chinthavali. *Power and Energy Systems, Proceedings* 1 (2003) 317.
- [2] M. Siad, M. Abdesslam and A.C. Chami. *Appl. Surf. Sci.* 258(18) (2012) 6819.

# Doping dependence of the electrical characteristics of nitrogen-doped *n*-type 4*H*-silicon carbide

**Shandirai M. Tunhuma<sup>1\*</sup>, F. Danie Auret<sup>1</sup>, Jackie Nel<sup>1</sup>, Helga T. Danga<sup>1</sup>, Emmanuel Igumbor<sup>1</sup>, Ezekiel Omotoso<sup>1</sup>, Mmantsae Diale<sup>1</sup>**

<sup>1</sup>University of Pretoria, Private Bag X20, Hatfield, Pretoria, South Africa

\*Corresponding author e-mail address: malven.tunhuma@up.ac.za

## 1. Introduction

Recent observations point at silicon carbide as the ideal material for use to build electrically driven single photon emitting devices [1]. These are promising in the fields of quantum computing and cryptography. Quantum computing requires that all devices be made on the same material [2]. The selection of the right substrate for device fabrication demands a thorough understanding of how the material properties vary during operation.

We investigated how the current-voltage (*I-V*) characteristics of Schottky diodes on 4*H*-SiC are affected by the degree of nitrogen doping in the  $10^{14}$  to  $10^{16}$  cm<sup>-3</sup> range. The measurements were carried out in the 300 – 600 K temperature range.

## 2. Results

The forward *I-V* characteristics were strongly dependent on the doping concentration. The zero-bias barrier height decreased and the ideality factor increased with decreasing temperature and increasing doping concentration; the changes are quite significant at low temperatures. The significant decrease in barrier height and increase in ideality factor at low temperatures and high doping concentrations can be explained by thermionic field-emission theory. According to Tung's approach of lateral inhomogeneities, the homogeneous barrier height and the effective barrier heights are closely matched, which demonstrates the good quality of the 4*H*-SiC films. The barrier height inhomogeneities at the interface also explain the results of barrier height and ideality factor change at low temperatures at all doping concentrations.

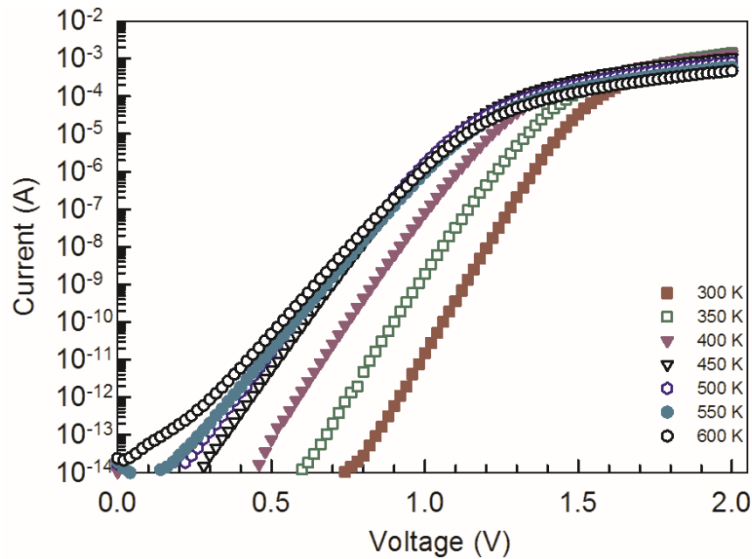


Fig.1: Semi-logarithmic forward *I-V* curves as a function of temperature for Ni/*n*-4*H*-SiC Schottky barrier diodes for a doping density  $7 \times 10^{15}$  cm<sup>-3</sup>.

## 3. References

- [1] S. Castelletto, B. Johnson, V. Ivády, N. Stavrias, T. Umeda, A. Gali, T. Ohshima. *Nature materials*, **13** (2014) 151.
- [2] S. Castelletto, L. Rosa, B.C. Johnson. *Silicon carbide for novel quantum technologies* (Intech) Chap. 8.

# Laplace DLTS characterization of the fine structure associated with the radiation induced E3 defect in GaAs

**Fateme Taghizadeh<sup>1\*</sup>, F. Danie Auret<sup>1</sup>, Walter E. Meyer<sup>1</sup>**

<sup>1</sup>Department of Physics, University of Pretoria, Private Bag X20, Hatfield 0028, Pretoria

\*Corresponding author e-mail address: fatemehtaghizadeh86@gmail.com

## 1. Introduction

Deep Level Transient Spectroscopy (DLTS) developed by Lang in 1974 [1], is a high frequency technique based on metal semiconductor junction capacitance that is used to study the electrical properties of defects in semiconductors [2]. In this study we used high resolution Laplace DLTS, introduced by Dobaczewski [3], to study the thermal emission of carriers from E3 defect in GaAs. We irradiated four different carrier densities of Si-doped GaAs with electrons from a <sup>90</sup>Sr source.

## 2. Results

From Laplace DLTS results we found that the well-known E3 defect consists of three different components which we labeled E3a, E3b and E3c. From the Arrhenius plots we calculated the energy levels and apparent capture cross sections of these defects. The introduction rates of the E3 defects were identical for all four carrier densities used, indicating the E3 defect structures do not include the dopant, Si. Electric field dependent measurements revealed that the field enhanced emission that was observed was caused by phonon assisted tunneling.

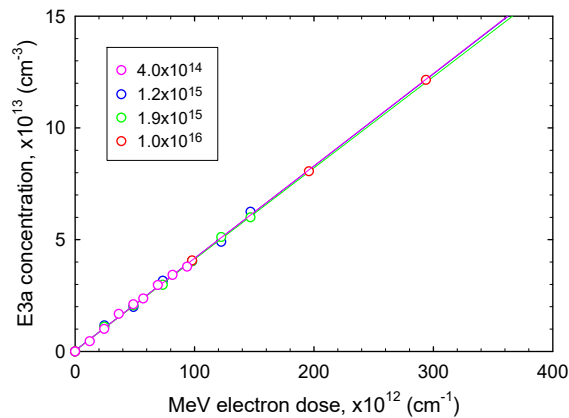


Fig. 1: Introduction rate of E3a for electrons from a <sup>90</sup>Sr radionuclide

## 3. References

- [1] D. V. Lang. *J. Appl. Phys.* **45** (1974) 3023.
- [2] F. D. Auret, S. A. Goodman, G. Myburg, and W. E. Meyer. *Appl. Phys. A Solids Surfaces* **56** (1993) 547.
- [3] L. Dobaczewski, A. R. Peaker, and K. Bonde Nielsen. *J. Appl. Phys.* **96** (2004) 4689.

# Electric field dependence study of the $E_C$ -0.58 eV centre in bulk grown n-type gallium arsenide using Laplace DLTS

**Kian Ostvar<sup>1\*</sup>, F. D. Auret<sup>1</sup>, W. E. Meyer<sup>1</sup>**

<sup>1</sup>Department of Physics, University of Pretoria, Private Bag X20, Hatfield 0028, Pretoria  
\*Corresponding author e-mail address: kn.ostvar@gmail.com

## 1. Introduction

In this work, the  $E_C$ -0.58 defect in bulk grown n-type gallium arsenide was studied using highly sensitive Laplace DLTS technique. The presence of the defect was observed by series of conventional DLTS scans, carried out within the temperature range of 20K to 300K. The samples were chosen from three bulk wafers, each having free carrier concentrations between  $2 \times 10^{16}$  and  $4 \times 10^{16} \text{ cm}^{-3}$ .

Field enhanced emission study is a Laplace DLTS based technique that can provide information regarding the charge state of deep levels [1]. Through this type of measurement, it is possible to obtain necessary information to determine the dominant emission mechanism of a deep level when it is subjected to an electric field. This is achieved through observation of the level of enhancement to the emission rate as a function of applied field. Two dominant mechanisms are the phonon assisted tunneling, also known as Ganichev-Prettl emission [1], and Poole-Frenkel emission [2]. Eq. 1, describes the phonon assisted tunneling while Eq. 2 corresponds to Poole-Frenkel emission. Depending on how the acquired data fit to each model (equation), the dominant mechanism can be determined.

$$\log(e) = \log(e_0) + \frac{\tau_2^3 q^2 E^2}{3m^* h} \quad (1)$$

$$\log(e) = \log(e_0) + \left[ \frac{1}{kT} \left( \frac{qE}{\pi\epsilon} \right) \right]^2 \quad (2)$$

## 2. Results

Fig.1 demonstrates the position of the  $E_C$ -0.58 peak in the conventional DLTS signal and also the shift in the emission rate as a result of increasing electric field. After the data is fitted to both the Ganichev-Prettl and Poole-Frenkel models, as is shown in Fig.2, the results indicate that the dominant emission mechanism in the case of  $E_C$ -0.58 is phonon assisted tunnelling.

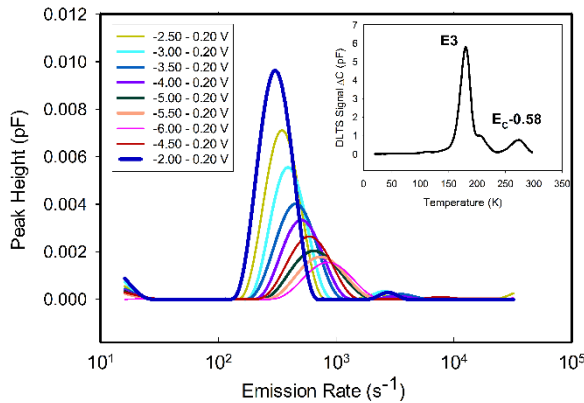


Fig. 1: The position of the  $E_C$ -0.58 and the shift in emission rate as a function of electric field.

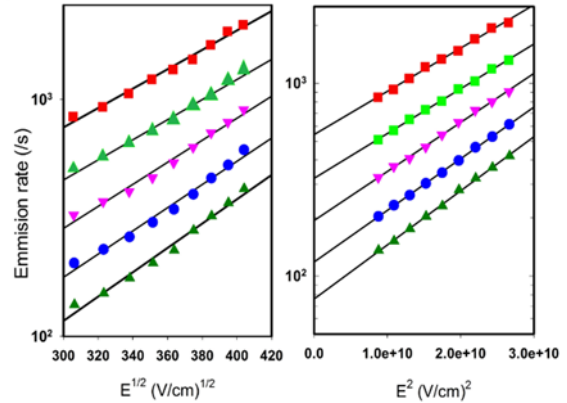


Fig. 2: Data fitted to both the Poole-Frenkel and Ganichev-Prettl models.

## 3. References

- [1] S. D. Ganichev, E. Ziemann, W. Prettl, I. N. Yassievich, A. A. Istratov, and E. R. Weber. *Phys. Rev. B* **61** (2000) 10361.
- [2] O. Mitrofanov. *J. Appl. Phys.* **95** (2004) 6414.

# Characterisation of ion implanted GaN by DLTS

P. N. M. Ngoepe<sup>1\*</sup>, W. E. Meyer<sup>1</sup>, F. D. Auret<sup>1</sup>, E. Omotoso<sup>1</sup>, T. T. Hlatshwayo<sup>1</sup>, M. Diale<sup>1</sup>

<sup>1</sup>Department of Physics, University of Pretoria, Private bag X20, Hatfield, 0028

\*Corresponding author e-mail address: phuti.ngoepe@up.ac.za

## 1. Introduction

GaN is a wide direct bandgap semiconductor with a wurzite crystal structure. GaN based material systems have been studied for various optoelectronic applications including detectors [1]. The bandgap of GaN based materials can be varied from 1.9 eV (InN) to 6.3 eV (AlN) whereby GaN has a bandgap of 3.4 eV. This property makes them good candidates for fabrication of devices in a wide spectral range. GaN is also a radiation hard material. The implantation of protons, electrons and ions has been performed on it with the aim of understanding the defects induced in it [2-4]. In this study, Schottky contacts of Ni (200 Å)/ Au (600 Å) were fabricated onto a GaN sample by using a resistive evaporation system. The sample was then implanted with Cs ions with energy of 360 keV. The ions were implanted at room temperature at a fluence of  $10^{11}$  cm<sup>-2</sup>. We report on the electrical characterization of this Cs ion implanted GaN using deep level transient spectroscopy (DLTS).

## 2. Results

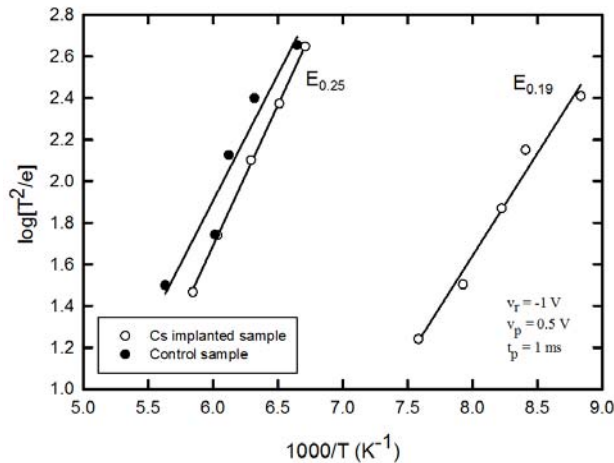


Fig. 1: Arrhenius plots of Ni/Au Schottky diodes fabricated on GaN. One sample was implanted with Cs while the other was used as a control sample..

Arrhenius plots of the defects obtained from DLTS measurements are shown in Fig. 1. The intrinsic defect has an energy level of 0.26 eV below the conduction band while the apparent capture cross section is  $9.39 \times 10^{-16}$  cm<sup>2</sup>. Cs irradiation induced a defect which has energy of 0.19 eV below the conduction band and a capture cross section of  $1.11 \times 10^{-15}$  cm<sup>2</sup>. The induced defect is similar to the electron beam deposition induced defect reported by Auret et al. [5].

## 3. References

- [1] P.N.M. Ngoepe, W.E. Meyer, M. Diale, F.D. Auret, and L. van Schalkwyk, *Physica B* **439** (2014) 119.
- [2] M. Schmidt, H. de Meyer, P.J. Janse van Rensburg, W.E. Meyer, and F.D. Auret, *Phys. Status Solidi B*, **251**(1) (2014) 211.
- [3] Z-Q. Fang, J.W. Hemsley D.C. Look and M. P. Mack, *Appl. Phys. Lett.* **72** (1998) 448.
- [4] M. Senthil Kumar, G. Sonia, D. Kanjilal, R. Dhanasekaran, and J. Kumar, *Nucl. Instrum. Meth. B*, **207** (2003) 308.
- [5] F.D. Auret, S.A. Goodman, G. Myburg, F.K. Koschnick, J.-M. Spaeth, B. Beaumont, and P. Gibart, *Physica B* **273-274** (2003) 84.

# In-system monitoring of MOSFET threshold voltage due to radiation degradation

Hendrik Weideman<sup>1\*</sup>, Walter Meyer<sup>1</sup>, Tinus Stander<sup>1</sup>

<sup>1</sup>University of Pretoria, Private Bag X 20, Hatfield, Pretoria, 0028, South Africa  
\*Corresponding author e-mail address: u10539362@tuks.co.za

## 1. Introduction

Total dose ionizing radiation is known to alter the threshold voltage in MOSFET devices. We present a technique which can be used to monitor the degradation of threshold voltage by means of independent voltage output readings. The output voltage of the threshold reference circuit is shown to be only sensitive to variation in threshold voltage. Using  $I$ - $V$  characterization it can be determined if the proposed circuit does measure the change in threshold voltage correctly. Using  $C$ - $V$  combined with deep level transient spectroscopy (DLTS) the damage due to irradiation caused due to irradiation may be measured and correlated with the change in threshold voltage. We have implemented and tested this circuit using silicon MOSFETs.

## 2. Results

From Fig. 1, the gate source voltage of M5 is given by

$$V_a = V_{th} + \sqrt{\frac{2I}{\mu_n C_{ox} \left(\frac{W}{L}\right)_1}} \quad (1)$$

Similarly, the gate source voltage M6 is

$$V_b = V_{th} + \frac{1}{\sqrt{K}} \sqrt{\frac{2I}{\mu_n C_{ox} \left(\frac{W}{L}\right)_1}} \quad (2)$$

With  $K$  the ratio between the gate widths of M6 and M5,  $K = W_{M6}/W_{M5}$  while equal  $V_{th}$  is assumed for M5 and M6. Thus the current through  $R_1$  can be described by

$$I = \frac{V_a - V_b}{R} = \frac{1}{\sqrt{K}} \sqrt{\frac{2I}{\mu_n C_{ox} \left(\frac{W}{L}\right)_1}} (\sqrt{K} - 1) \quad (3)$$

This enables the independent extraction of  $V_{th}$  as the output if the resistor relationship condition  $R_2 = \frac{1}{\sqrt{K}-1} R$  is met, then

$$V_{out} = V_b - IR_2 \quad (4)$$

$$V_{out} = V_{th} \quad (5)$$

The circuit in Fig. 1 can, therefore, be used to monitor the simultaneous change in  $V_{th}$  in M5 and M6. As expected, the results shown in Fig. 2 indicate near-perfect representation of  $V_{th}$  at  $V_o$ , and below 0.06% variation in  $V_{th}$  for a sweep in  $\mu_n$  from  $8.389 \times 10^{-5}$  to  $8 \times 10^{-4} \text{ m}^2/\text{Vs}$

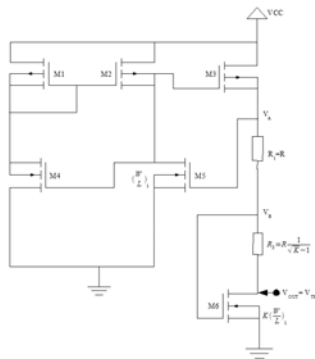


Fig. 1: Schematic of the threshold reference circuit used to measure the change in threshold voltage during irradiation

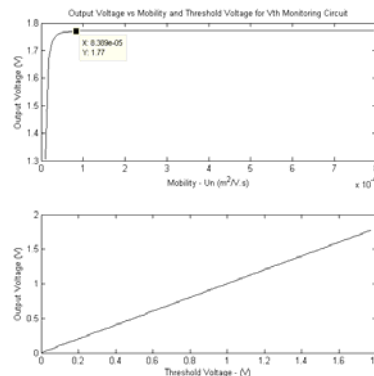


Fig. 2: Simulation showing the measured output voltage to a variation in threshold voltage and mobility

## References

- [1] L. E. Toledo, P. A. Petrashin, W. J. Lancioni, F. C. Dualibe, and L. R. Canali, *2013 IEEE Fourth Latin American Symposium on Circuits and Systems (LASCAS)*, (2013) 1.

# Determination of the optimum annealing temperature to erase alpha induced defects on Co-4H-SiC Schottky contacts

V. E. Gora<sup>1</sup>, A. Chawanda<sup>1</sup>, F. Mazunga<sup>1</sup>, C. Nyamhere<sup>1</sup>, B. Chibaya<sup>1</sup>, F. D. Auret<sup>2</sup>, M. S. Tunhuma<sup>2</sup>, E. Omotoso<sup>2</sup>, H. Danga<sup>2</sup>

<sup>1</sup>Department of Applied Physics and Telecommunications, Midlands State University, Private Bag 9055, Gweru, Zimbabwe

<sup>2</sup>Department of Physics, University of Pretoria, Private Bag X20, Hatfield 0028, Pretoria, South Africa

Corresponding author e-mail address: goraelifas@gmail.com

## 1. Introduction

Cobalt-SiC Schottky contacts have been fabricated on  $5 \times 10^{15} \text{ cm}^{-3}$  nitrogen doped 4H-SiC. *IV* and *CV* characteristics were carried out on the diodes. A Deep Level Transient Spectroscopy (DLTS) was used to characterize the devices. Defects were identified at 0,10 eV; 0,12 eV; 0,17 eV and 0,67 eV below the conduction band. The diodes were irradiated by alpha radiation from a 5,4MeV, AM-24I radioactive source at time intervals up to 18 hours. DLTS measurements were carried out for each exposure time to identify any new defects. New defects were identified at 0,40 eV and 0,65 eV below the conduction band. The diodes were annealed for 20 minutes at temperatures starting from 200 °C in steps of 100 °C until the defects vanished. The carrier concentration of the defects decreased with annealing temperature until they completely vanished at 400 °C. The optimum temperature to erase induced defects is 400 °C.

## 2. Results

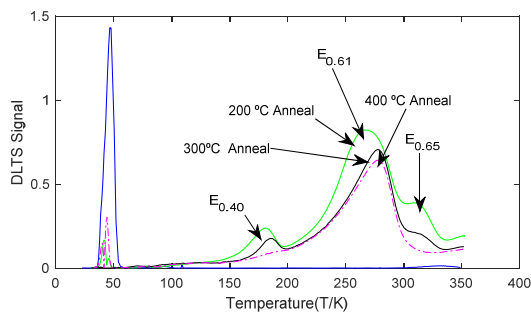


Fig. 1: DLTS spectra for the annealed Co-SiC Schottky contact.

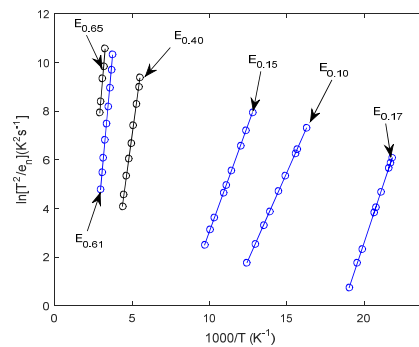


Fig. 2: Defects after 18 hours alpha irradiation.

## 3. References

- [1] S.M.Size. *Physics of semiconductor devices*, (New York, 1981) 245.
- [2] D.K.Schroder, *Semiconductor material and device characterization*, (IEEE PRESS. 2006) 158.



# Comparison of the properties of nickel, cobalt, palladium and tungsten Schottky contacts on 4H-silicon carbide

V. E. Gora<sup>1</sup>, A. Chawanda<sup>1</sup>, F. Mazunga<sup>1</sup>, C. Nyamhere<sup>1</sup>, T. Jaure<sup>1</sup>, F. D. Auret<sup>2</sup>, M. S. Tunhuma<sup>2</sup>, E. Omotoso<sup>2</sup>, H. Danga<sup>2</sup>

<sup>1</sup>Department of Applied Physics and Telecommunications, Midlands State University, Private Bag 9055, Gweru, Zimbabwe

<sup>2</sup>Department of Physics, University of Pretoria, Private Bag X20, Hatfield 0028, Pretoria, South Africa

Corresponding author e-mail address: goraelifas@gmail.com

## 1. Introduction

Nickel, cobalt, palladium and tungsten Schottky contacts have been fabricated on  $5 \times 10^{15} \text{ cm}^{-3}$  nitrogen doped 4H-SiC. The current voltage ( $IV$ ) and capacitance voltage ( $CV$ ) measurements were carried out to investigate the characteristics of each of the diodes in the 300-800 K temperature range. Results derived from the  $IV$  measurements showed that barrier height, ideality factor, reverse leakage current and series resistance were all temperature dependant. Schottky barrier height increased with temperature with tungsten maintaining the highest level throughout the whole temperature range. Series resistance generally decreased with increasing temperature with tungsten deviating from this behavior after 600 K. Ideality factor decreased with increase in temperature with tungsten maintaining low values for most of the 300-800 K temperature range while reverse leakage current increased with increasing temperature. Tungsten had the highest values of reverse leakage current while nickel registered the lowest values.

## 2. Results

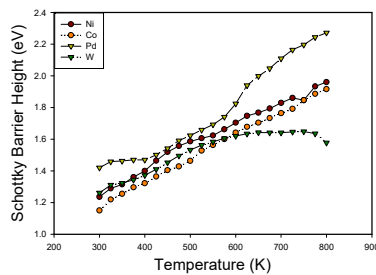


Fig. 1: Schottky barrier height ( $\Phi_B$ ) as a function of absolute temperature for Ni, Co, Pd and W Schottky contacts on 4H-SiC. levels.

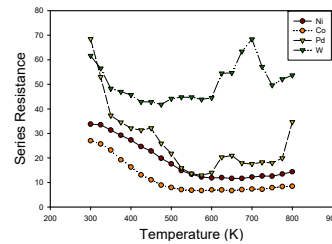


Fig. 2: Series resistance as a function of absolute temperature for Ni, Co, Pd and W Schottky contacts on 4H-SiC.

## 3. References

- [1] C D.K.Schroder, *Semiconductor material and device characterization*, (IEEE PRESS.2006) 158.
- [2] S.M.Size. *Physics of semiconductor devices*, (New York. 1981) 245.

# Energy transfer from Pr<sup>3+</sup> to Gd<sup>3+</sup> in BaB<sub>8</sub>O<sub>13</sub> phosphor and its application in phototherapy lamp

Sumedha Tamboli<sup>1</sup>, Govind B. Nair<sup>1\*</sup>, S. J. Dhoble<sup>1</sup>

<sup>1</sup>Department of Physics, R.T.M. Nagpur University, Nagpur, India- 440033

\*Corresponding author e-mail address: govind1291@yahoo.com

## 1. Introduction

BaB<sub>8</sub>O<sub>13</sub> compound is reported to be excellent host for rare earth ion doping due to its suitable structural properties. BaB<sub>8</sub>O<sub>13</sub> is made up of two separate interlocking three-dimensional networks as triborate and pentaborate groups and forms BO<sub>3</sub> and BO<sub>4</sub> tetrahedral units. It consists of tetragonal BO<sub>4</sub> and trigonal BO<sub>3</sub> group. In such big anion rare earth ions has sufficient place for substitution. Rare earth ions get isolate from one another and the energy loss due to ion-ion interaction is becomes less. BaB<sub>8</sub>O<sub>13</sub>: Sm<sup>2+</sup>, Yb<sup>2+</sup>, Eu<sup>2+</sup>, Tb<sup>3+</sup>, Tm<sup>3+</sup>. [1-3] A series BaB<sub>8</sub>O<sub>13</sub> compound doped with different concentrations of Gd<sup>3+</sup> ions and co-doped with Pr<sup>3+</sup> ions was synthesized by solid state synthesis method. The photoluminescence excitation spectra of the phosphor show excitation peaks at 246 nm, 252 nm and 274 nm. The prominent emission peak was observed at 313 nm which is near UVB range. Energy transfer was done by co-doping Pr<sup>3+</sup> with Gd<sup>3+</sup>. Photoluminescence decay time was measured for BaB<sub>8</sub>O<sub>13</sub>: Gd<sup>3+</sup>, Pr<sup>3+</sup> phosphor. The intense emissions can be used to produce phototherapy lamps to use in the treatment of skin diseases.

## 2. Results

Fig.1 shows photoluminescence excitation spectra of BaB<sub>8</sub>O<sub>13</sub>: Pr, Gd phosphor obtained by monitoring emission wavelength at 313 nm. Broad excitation peak centred at 220 nm can be assigned to 4f-4f5d transition. Sharp peak at 274 nm corresponds to <sup>8</sup>S<sub>7/2</sub> - <sup>6</sup>I<sub>1</sub> transition of Gd<sup>3+</sup> ions. Emission spectra were recorded by monitoring excitation wavelength at 220 nm shown in Fig. 2. A single emission peak is obtained at 313 nm corresponds to <sup>8</sup>P<sub>7/2</sub> - <sup>8</sup>S<sub>7/2</sub> transition of Gd<sup>3+</sup> ions. Emission peak is very intense and intensity enhances with increase in concentration of dopant. This emission is useful for phototherapy applications.

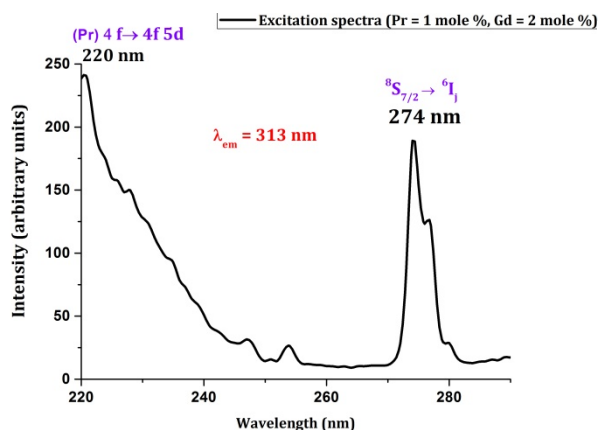


Fig. 1 PL excitation spectra of BaB<sub>8</sub>O<sub>13</sub>:Pr<sup>3+</sup>, Gd<sup>3+</sup> at  $\lambda_{em}$  = 313 nm

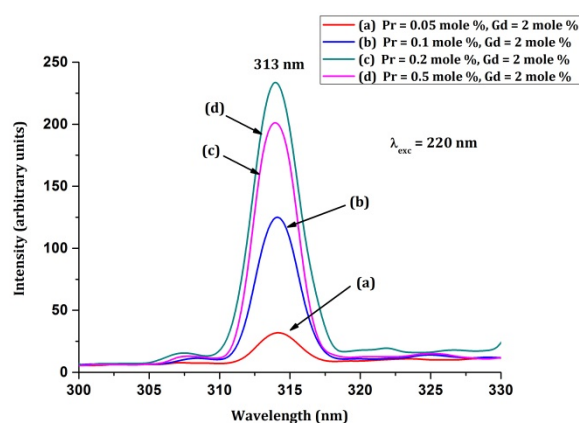


Fig. 2 PL emission spectra of BaB<sub>8</sub>O<sub>13</sub>:Pr<sup>3+</sup>, Gd<sup>3+</sup> at  $\lambda_{exc}$  = 220 nm

## 3. References

- [1] T Koskentalo, L Niisto, M. J. Leskela, *Less-Common Met.*, **67** (1985) 112
- [2] J Krogh-Moe, M. Ihara, *Acta Crystallogr. B*, **25** (1969) 2153
- [3] H. Ling, W. Yuhua, S. Weimin, *J. Rare Earths* **27** (2009) 385-389

# DFT+U and experimental studies of $\text{Ce}^{3+}\text{Cu}^{2+}:\gamma\text{-Al}_2\text{O}_3$

Winfred Mueni Mulwa<sup>1\*</sup>, Francis Birhanu Dejene<sup>1</sup>, Martin Onani<sup>2</sup>, Cecil Moro Ouma<sup>3</sup>

<sup>1</sup>Department of physics, University of the Free State-Qwaqwa Campus, Private Bag x13, Phuthaditjhaba, 9866, South Africa

<sup>2</sup>Chemistry Department, University of the Western Cape, Private Bag X17, Bellville, Cape Town, South Africa

<sup>3</sup>Natural Resources and Environment, Council for Scientific and Industrial Research, P.O. Box 395, Pretoria, 0001, South Africa

\*Corresponding author e-mail address: moronaphaty84@gmail.com

## 1. Introduction

In this work, we report a cheap sol-gel technique used to prepare  $\text{Al}_2\text{O}_3$  and  $\text{Ce}^{3+}\text{Cu}^{2+}:\text{Al}_2\text{O}_3$  nanoparticles. Powder X-ray diffraction (XRD), scanning electron microscopy (SEM), high resolution transmission electron microscopy (HR-TEM) and ultraviolet visible spectroscopy (UV-vis) measurements were used to characterize the powders. The chemical composition of the powders was measured using energy dispersive spectroscopy (EDS). *Ab initio* calculations were carried out to confirm the experimental findings. The structural, electronic and optical properties of a 80 atom supercell were investigated by use of density functional theory (DFT) with the Hubbard correction term U and plane wave pseudopotentials as implemented in quantum ESPRESSO code. Computationally, the photoluminescence (PL) levels were calculated from the thermodynamic transition levels corresponding to defect levels [1]. Where, each of thermodynamic transition levels usually has an associated optical transition. An optical transition was arrived at using the Frank-Condon principle [1]

$$E_{PL} = E_g - \varepsilon^{therm}(+1/+2) - E_{rel} \quad (1)$$

where  $E_{PL}$  is the optical transition,  $E_g$  is the band gap energy,  $\varepsilon^{therm} + 1/+2$  is the thermodynamic transition level between +1 and +2 charges.  $E_{rel}$  is the Frank-Condon shift. Experimentally the PL peaks under excitation 236 nm were found at 430 nm and 458 nm. The electronic structure calculations showed that the valence band maximum consists of filled O 2p orbitals while the conduction band has empty Al 3p and Al 3s orbitals. Structural strain was realized computationally on doping due to reduced bond lengths which was revealed by the use of the XCRYSDEN program and confirmed experimentally by the XRD results.

## 2. Results

XRD findings showed the presence of  $\gamma\text{-Al}_2\text{O}_3$  phase with peaks located at  $2\theta = 31.99, 37.71, 39.45, 45.88, 60.84, 66.89$  degrees. From the SEM micrographs, it was realized that the powder particles grew into sheet forms while nano regime and high crystallinity could be realized from HR-TEM results as well as an average particle size of approximately 20 nm. EDS analysis indicated that the synthesized powders had 60% oxygen and 40% aluminium in the presence of  $\text{Ce}^{3+}\text{Cu}^{2+}$  as dopants which indicates a stoichiometry close to the expected one for alumina. From computational point of view, DFT is known to underestimate the band gap [2]. This was the case in our findings that the experimental band gap of 5.25 eV reduced to 4.0 eV as shown in Fig. 1 and 2 below.

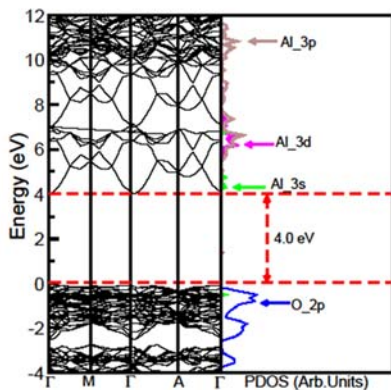


Fig. 1: Calculated band structure and projected density of states.

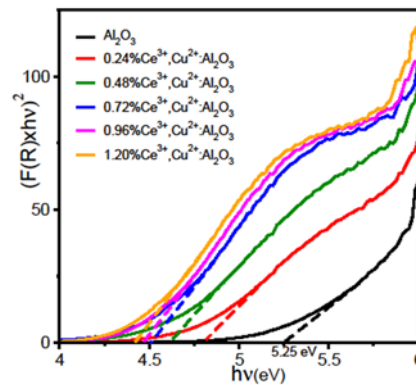


Fig. 2: The Kubelka-Munk structure.

## 3. References

- [1] C.G. Van de Walle. *J. Appl. Phys.* **95** (2004) 3851
- [2] A. Walsh, J.L.F Da Silva, S.H. Wei, C. Korber, A. Klein. *PRL* **100** (2008) 167402.

# Preparation and characterization of $\text{Eu}^{3+}$ & $\text{Tb}^{3+}$ ions doped alkali oxide ( $\text{Li}_2\text{O}/\text{Na}_2\text{O}/\text{K}_2\text{O}$ ) modified borophosphate glasses for red and green laser and display device applications

B. Sudhakar Reddy<sup>1\*</sup>, G. Moulika<sup>1</sup>, R. Ramanaiyah<sup>1</sup>, B. Naveen Kumar Reddy<sup>1</sup>, S. J. Dhoble<sup>2</sup>

<sup>1</sup>Department of Physics, S.V. Degree College, Kadapa-516003, Andhra Pradesh, India

<sup>2</sup>Department of Physics, RTM Nagpur University, Nagpur-India

\*Corresponding author e-mail address: drbsreddyphd@gmail.com

## 1. Introduction

Alkali oxide modified borophosphate glasses doped with  $\text{Eu}^{3+}$ ,  $\text{Tb}^{3+}$  ions with the chemical composition of  $69.5 \text{ B}_2\text{O}_3 + 10 \text{ P}_2\text{O}_5 + 10 \text{ CaF}_2 + 5 \text{ Li}_2\text{O} + 5 \text{ ZnO} + \text{R} + 0.5 \text{ Eu}_2\text{O}_3$  [where  $\text{R} = 5 (\text{Li}_2\text{O}/\text{Na}_2\text{O}/\text{K}_2\text{O})$ ] have been prepared by conventional melt quenching technique and the spectroscopic properties of the prepared glasses have been studied by XRD, FTIR, DSC, absorption, excitation and emission spectral analysis. XRD pattern shows amorphous nature of the glasses has been observed. From the DSC profile, the glass transition temperature ( $T_g$ ), melting temperature ( $T_m$ ) and crystallization temperature ( $T_c$ ) have been evaluated. From the measurements of FTIR spectra, the functional groups of  $\text{Eu}^{3+}$ ,  $\text{Tb}^{3+}$  ions doped boro phosphate glasses have been identified.

## 2. Results

The red emission corresponding to  ${}^5\text{D}_0 \rightarrow {}^7\text{F}_2$  (614 nm) transition is measured at excitation of 396 nm of the  $\text{Eu}^{3+}$  ions doped glasses. In the case of  $\text{Tb}^{3+}$  ions doped glasses four emission transitions such as  ${}^5\text{D}_4 \rightarrow ({}^7\text{F}_6, {}^7\text{F}_5, {}^7\text{F}_4 \& {}^7\text{F}_3)$  that are located at 489, 545, 584 and 622 nm respectively have been measured with  $\lambda_{\text{exci}} = 374 \text{ nm}$  ( ${}^7\text{F}_6 \rightarrow {}^5\text{G}_6$ ). Based on the excitation and emission spectral properties such as fluorescence intensity ratio, J-O Intensity parameter peak emission wavelength peak emission wavelength, effective linewidth, radiative transition probabilities, stimulated emission cross-section, experimental branching ratios and gain bandwidth parameters were calculated. Based on the spectral results, Eu and Tb glasses were potential candidates for the red and green color centers in display devices as well as red and green emission lasers at 614 nm and 545 nm.

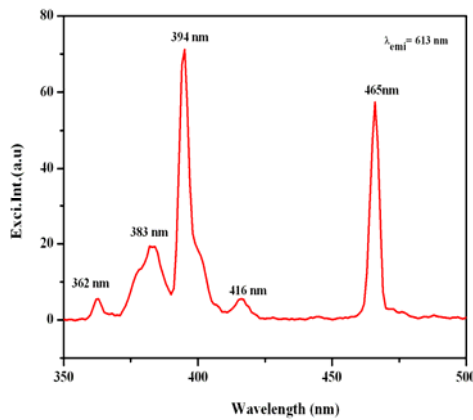


Fig 1: Emission spectra of 0.5 mol%  $\text{Eu}^{3+}$  doped glass

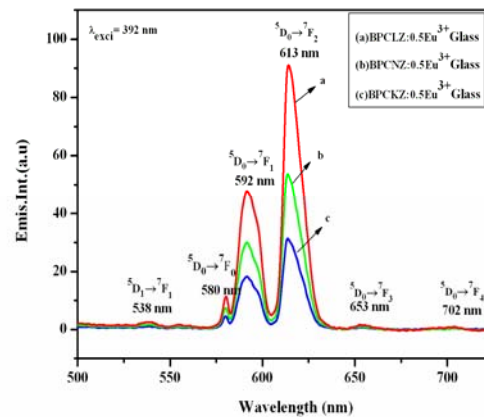


Fig 2: Emission spectra of 0.5 mol%  $\text{Eu}^{3+}$  doped glasses

## 3. Reference

[1] P. Kaur, D. Singh, T. Singh *J. Non-Cryst. Solids* **452** (2016) 87

# Energy transfer study between Ce<sup>3+</sup> and Tb<sup>3+</sup> ions in a calcium fluoride crystal

E. Coetsee<sup>1\*</sup>, H. C. Swart<sup>1</sup>, M. Y. A. Yagoub<sup>1,2</sup>

<sup>1</sup>Department of Physics, University of the Free State, P.O. Box 339, Bloemfontein, ZA9300, South Africa

<sup>2</sup>Department of Physics, Sudan University of Science and Technology, Khartoum, Sudan

\*Corresponding author e-mail address: coetsee@ufs.ac.za

## 1. Introduction

Energy transfer from Ce<sup>3+</sup> to Tb<sup>3+</sup> ions in a single crystal of CaF<sub>2</sub> has been analyzed for down-conversion application in Si solar cells. Inorganic hosts doped with the Tb<sup>3+</sup>-Yb<sup>3+</sup> couple have been extensively investigated for solar cell application [1]. The Tb<sup>3+</sup> ion absorbs a UV photon and feeds the Yb<sup>3+</sup> ions with two photons. This gives rise to the emission of two near infrared photons that can be used to generate electron-hole pairs. However, the weak absorption cross-section of the 4f-4f transition of the Tb<sup>3+</sup> ion limits the application of such promising materials. A suggestion to this limitation is to add a third sensitizer with dipole-allowed 4f-5d transitions, such as Ce<sup>3+</sup>, Eu<sup>2+</sup> and Yb<sup>2+</sup> [2, 3]. This transition strongly depends on the crystal field of the matrix. Efficient energy transfer between a sensitizer and a donor can only occur when the emission band of the sensitizer overlap with the excitation band of the donor. CaF<sub>2</sub> is one of the fluoride compounds that is widely used as a phosphor material because of its stability, non-hygroscopic and transparency behavior. In this investigation, the possibility of using the Ce<sup>3+</sup> ion as a sensitizer for the Tb<sup>3+</sup> ion in the CaF<sub>2</sub> single crystal, for solar cell application, are discussed.

## 2. Results

The CaF<sub>2</sub>:Ce,Tb nanophosphor samples were successfully synthesized by the co-precipitation method. Results obtained with x-ray diffraction indicated that the crystallite size were in the range of 30-40 nm. The patterns crystallized in cubic structures of CaF<sub>2</sub> (file number ICSD 00-075-0363), and no impurity peaks are observed. This indicate that the Ce and Tb ions did not change the structure of the CaF<sub>2</sub> lattice. X-ray photoelectron spectroscopy confirmed the formation of the matrix and the presence of the dopants. The luminescence data obtained clearly indicate that energy transfer between Ce<sup>3+</sup> and Tb<sup>3+</sup> takes place inside the crystalline matrix. The emission of Ce<sup>3+</sup> in the co-doped sample was quenched and an enhancement of the Tb emission was observed, Fig. 1a). The Tb<sup>3+</sup> emissions were enhanced steadily with an increase Tb<sup>3+</sup> concentration, see fig. 1b). The calculated energy transfer efficiency is relatively efficient at a high Tb<sup>3+</sup> concentration. This process can occur because the emission of Ce<sup>3+</sup> overlaps the excitation spectra of Tb<sup>3+</sup>. The energy transfer from the Ce<sup>3+</sup> to Tb<sup>3+</sup> ions feeds the <sup>4</sup>D<sub>4</sub> level of the Tb<sup>3+</sup> ion where the quantum cutting process towards the Yb<sup>3+</sup> is likely to occur. The results suggested that Ce<sup>3+</sup> may therefore be used as an efficient sensitizer to feed the Tb<sup>3+</sup> ions in a CaF<sub>2</sub> crystal.

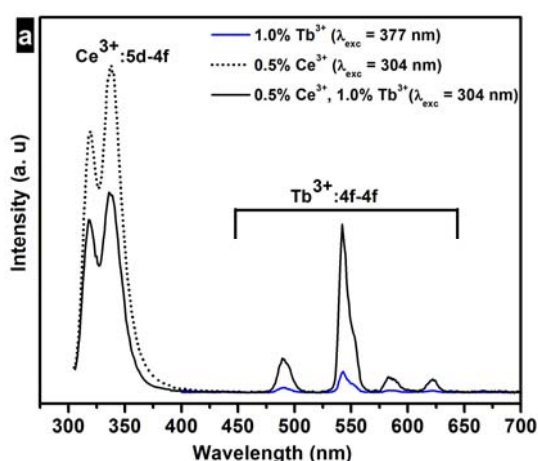


Fig. 1a): Variation of Ce<sup>3+</sup> (0.5 mol%) emission intensity as a function of the Tb<sup>3+</sup> concentration for CaF<sub>2</sub>.

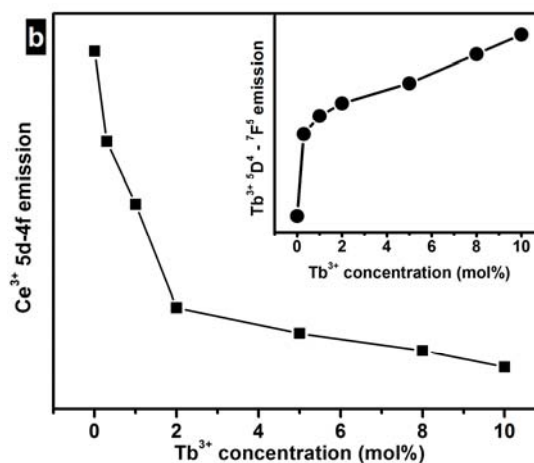


Fig. 1b): Variation of Tb<sup>3+</sup> emission intensity as a function of the Tb<sup>3+</sup> concentration for CaF<sub>2</sub> containing 0.5 mol% Ce<sup>3+</sup>.

## 3. References

- [1] L. A. Florêncio, L. A. Gómez-Malagón, B. C. Lima, A. S.L. Gomes, J.A.M. Garcia, L. R.P. Kassab, Sol. Energy Mater. Sol. Cells **157** (2016) 468-475.
- [2] A. Guille, A. Pereira, G. Breton, A. Bensalah-ledoux, B. Moine, J. Appl. Phys. **111** (2012) 043104-043108.
- [3] Q. Yan, J. Ren, Y. Tong, G. Chen, J. Am. Ceram. Soc. **96** (2013) 1349-1351.

# Luminescence properties of $\text{Na}_2\text{Sr}_2\text{Al}_2\text{PO}_4\text{Cl}_9:\text{Sm}^{3+}$ phosphor

Sumedha Tamboli<sup>1</sup>, D. I. Shahare<sup>2\*</sup>, S. J. Dhoble<sup>1\*</sup>

<sup>1</sup>Department of Physics, R. T. M. Nagpur University, Nagpur -440033, India

<sup>2</sup>Department of Physics, J.M.Patel College, Bhandara, India

\*Corresponding author e-mail address: dishahare@yahoo.com; sjdhoble@rediffmail.com

## 1. Introduction

Trivalent-lanthanide ions doped phosphor materials have gained massive attention owing to their wide application in the field of fluorescent lighting, white light emitting diodes (W-LED), display devices, bio-imaging, phototherapy, radiation dosimetry etc. [1–4] Red emitting phosphor can be used along with green and blue emitting phosphor to enhance the colour rendering index of the W-LED.  $\text{Sm}^{3+}$  ions show different type of behaviour in different hosts since the ratio of intensities of magnetic dipole transition to electric dipole transition varies from host to host. In some host it gives red emission and in some host it gives orange-red emission. [5]  $\text{Na}_2\text{Sr}_2\text{Al}_2\text{PO}_4\text{Cl}_9:\text{Sm}^{3+}$  has not been studied yet for its photoluminescence and thermoluminescence properties. This compound belongs to the orthophosphate family which is a broadly studied system. Bonding of tetrahedral  $\text{PO}_4^{3-}$  group to other structural units provides diversity to this class of materials. These are well tolerant host lattices for the substitution of activator ions. In this paper we report photoluminescence and thermoluminescence properties of  $\text{Na}_2\text{Sr}_2\text{Al}_2\text{PO}_4\text{Cl}_9:\text{Sm}^{3+}$  phosphor synthesized by solid state synthesis.

## 2. Results

Fig. 1 shows an excitation spectrum of  $\text{Na}_2\text{Sr}_2\text{Al}_2\text{PO}_4\text{Cl}_9:\text{Sm}^{3+}$  ( $\text{Sm}^{3+} = 1$  mole %) obtained by monitoring its emission wavelength at 595 nm. Excitation spectra consist of several peaks at 365 nm, 379 nm, 398 nm, 406 nm, 419 nm and 443 nm. These peaks can be attributed to interconfiguration f-f transition of  $\text{Sm}^{3+}$  rare earth ions. Emission spectra obtained by monitoring excitation at 406 nm for different mole % of  $\text{Sm}^{3+}$  ions as shown in Fig 2.

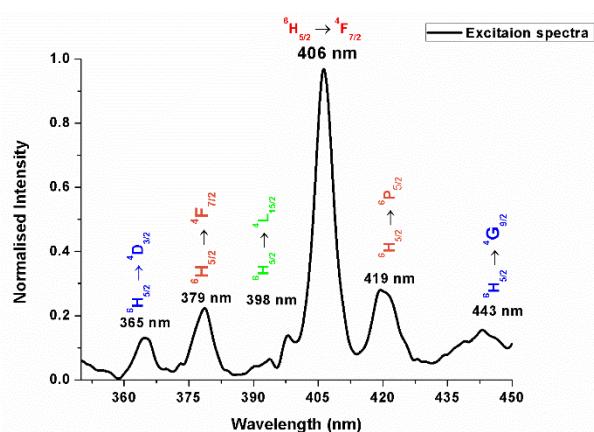


Fig. 1: PL excitation spectra of  $\text{Na}_2\text{Sr}_2\text{Al}_2(\text{PO}_4)\text{Cl}_9:\text{Sm}^{3+}$  at  $\lambda_{\text{em}} = 595$  nm

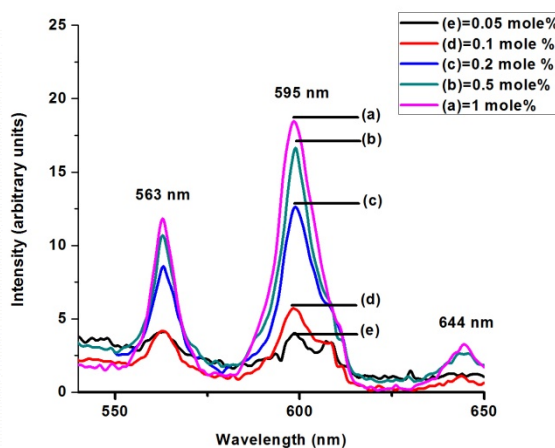


Fig. 2: PL emission spectra of  $\text{Na}_2\text{Sr}_2\text{Al}_2(\text{PO}_4)\text{Cl}_9:\text{Sm}^{3+}$  at  $\lambda_{\text{exc}} = 406$  nm

## 3. References

- [1] S. R. Anishia, M. T. Jose, O Annalakshmi, V Ramasamy, *J. Lumin.* **131** (2011) 2492.
- [2] A. A. Setlur, *Electrochem. Soc. Interface* **18** (2009) 32.
- [3] J. Wang, F. Zhang, J. Zhang, W. Tang, A. Tang, H. Peng, Z. Xu, F. Teng, Y. Wang, *J. Photochem. Photobiol. C Photochem. Rev.* **17** (2013) 69.
- [4] R. Liang, M. Wei, D. G. Evans, X. Duan, *Chem. Commun.* **50** (2014) 14071.
- [5] G. B. Nair, S. J. Dhoble, *J. Fluoresc.* **26** (2016) 1865.

# Synthesis and characterization of $MV_{0.5}P_{0.5}O_4:Sm^{3+},Tm^{3+}$ ( $Ln = Gd, La, Y$ ) for solar cells application

Selepe J. Motloulung<sup>1</sup>, Mantwa A. Lephoto<sup>1</sup>, Kamohelo G. Tshabalala<sup>1\*</sup>, Odireleng M. Ntwaeaborwa<sup>2</sup>

<sup>1</sup>Department of Physics, University of the Free State, QwaQwa campus, Private Bag X13, Phuthaditjhaba, 9866, South Africa

<sup>2</sup>School of Physics, University of the Witwatersrand, Private Bag 3, Wits, 2050, South Africa

\*Corresponding author e-mail address: tshabalakg@ufs.ac.za

## 1. Introduction

Lanthanide orthovanadates ( $LnVO_4$ ) have been extensively studied and applied as promising inorganic materials due to their potential uses in different fields such as catalyst, laser host materials, magnetic materials, and phosphors. They have two crystalline polymorphs, one is monoclinic monazite type ( $m-LnVO_4$ ), and the other is tetragonal zircon type ( $t-LnVO_4$ ) [1]. On the other hand, lanthanide phosphates ( $LnPO_4$ ) have attracted much attention due to their novel promising applications in several fields of science and technology like lanthanide orthovanadates,  $LnPO_4$  compounds have either a monoclinic structure (monazite-type, space group  $P2_1/n$ ) for the lighter Rare Earth Elements (REE) (from La to Gd) or a tetragonal one (xenotime-type, space group  $I4_1/amd$ ) for the heavier REE (from Tb to Lu) [2]. Lanthanide orthovanadates and orthophosphates can be combined together to form a multicomponent structure of lanthanide phosphovanadate. This is achieved by partial replacement of  $[VO_4]^{3-}$  by  $[PO_4]^{3-}$  in  $LaVO_4$  ( $[PO_4]^{3-}$  by  $[VO_4]^{3-}$  in  $LnPO_4$ ). Several synthesis methods have been used before to prepare  $LnV/PO_4$ . For this work, a simple, straightforward, cost effective and time saving solution combustion process was used for the preparation of samarium and thulium co-activated  $MV_{0.5}P_{0.5}O_4$  ( $M = Gd, La, Y$ ) for possible application in dye sensitized solar cells (DSSC).

## 2. Results

Samarium and thulium co-activated  $MV_{0.5}P_{0.5}O_4$  phosphors were synthesized by solution combustion method using urea as a fuel. The preparation temperature was set at  $600 \pm 10^\circ C$ . The samples were then annealed at  $900^\circ C$  for 2 hours. Fig 1. Shows XRD pattern of  $YV_{0.5}P_{0.5}O_4:Sm^{3+},Tm^{3+}$  together with JCPDS file of  $YVO_4$  (17-0341) and  $YPO_4$  (11-0254). The results indicate that the peaks for  $YV_{0.5}P_{0.5}O_4:Sm^{3+},Tm^{3+}$  are intermediate between that of  $YPO_4$  and  $YVO_4$ . Fig. 2 shows the emission spectra of  $GdV_{0.5}P_{0.5}O_4:Sm^{3+},Tm^{3+}$ , and  $LaV_{0.5}P_{0.5}O_4:Sm^{3+},Tm^{3+}$  and  $YV_{0.5}P_{0.5}O_4:Sm^{3+},Tm^{3+}$  respectively. In all cases, five emission peaks are observed. The broad band extending from 400 to 650 nm originates from the host while the sharp peak at wavelength 477 nm is due to ( $^1G_4 - ^3H_6$ ) transition of  $Tm^{3+}$  ions. The other three emission peaks observed at 566 nm ( $^4G_{5/2} - ^6H_{5/2}$ ), 603 nm ( $^4G_{5/2} - ^6H_{7/2}$ ) and 648 nm ( $^4G_{5/2} - ^6H_{9/2}$ ) are due to transitions of  $Sm^{3+}$  ions.

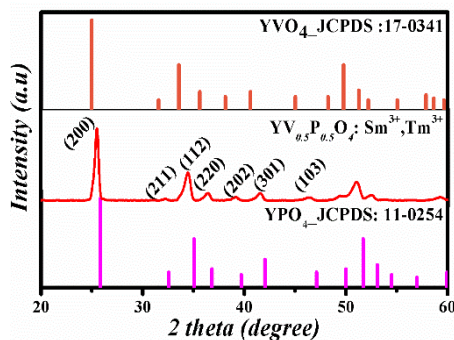


Fig. 1: XRD pattern of  $YV_{0.5}P_{0.5}O_4:Sm^{3+},Tm^{3+}$  powder and JCPDS files of  $YVO_4$  and  $YPO_4$ .

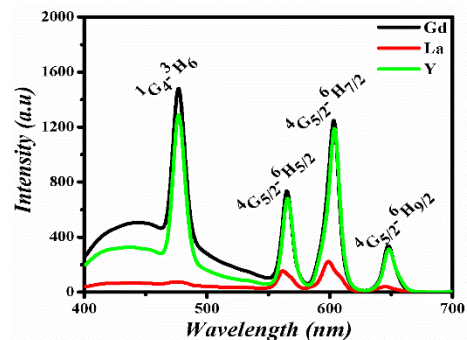


Fig. 2: Emission spectra of  $MV_{0.5}P_{0.5}O_4:Sm^{3+},Tm^{3+}$  ( $M=Gd, La, Y$ )

## 3. References

- [1] Nuria O. Nunez, Sonia R. Liviano, Manuel Ocana, *J. Colloid Interface Sci.* **349** (2010) 484.
- [2] Pengfei Chen, Qiang Wu, Li Zhang, Weifeng Yao, *Catal. Commun.* **66** (2015) 6.

# Paramagnetism of rare earth ions with the same $4f^7$ electron configuration: $\text{Eu}^{2+}$ , $\text{Gd}^{3+}$ and $\text{Tb}^{\text{IV}}$ in $\text{EuAl}_2\text{O}_4$ , $\text{Gd}_2\text{O}_3$ , and $\text{TbO}_2$

Mika Lastusaari<sup>1,2</sup>, Dariusz Hreniak<sup>3</sup>, Edward Lee<sup>4</sup>, André M. Strydom<sup>5,6</sup>,  
Hendrik C. Swart<sup>4</sup>, Jorma Hölsä<sup>3,4\*</sup>

<sup>1</sup>University of Turku, Department of Chemistry, FI-20014 Turku, Finland

<sup>2</sup>Turku University Centre for Materials and Surfaces (MatSurf), Turku, Finland

<sup>3</sup>Polish Academy of Sciences, Institute of Low Temperature and Structure Research, PL-50-422 Wroclaw, Poland

<sup>4</sup>University of the Free State, Department of Physics, Bloemfontein ZA-9300, South Africa

<sup>5</sup>Max Planck Institute for Chemical Physics of Solids, D-01187 Dresden, Germany

<sup>6</sup>University of Johannesburg, Physics Department, Highly Correlated Matter Research Group, Auckland Park ZA-2006, South Africa

\*Corresponding author e-mail address: jholsa@utu.fi

This contribution is dedicated to the memory of Dr Paul Caro (1934-2016), Membre Correspondant de l'Académie des Sciences, France

## 1. Introduction

Most luminescent materials (*i.e.* phosphors) consist of a host with a deliberately added dopant. The latter is a defect (or impurity) albeit a beneficial one - until proven otherwise. Awkwardly, the two most common rare earth dopants, Eu and Tb, exist at two oxidation states,  $\text{Eu}^{2+/3+}$  and  $\text{Tb}^{3+/IV}$ . Their detection is difficult with optical methods and most chemical ones are helpless with valence impurities, *i.e.* the same element but with an unlike valence. A small amount of  $\text{Eu}^{2+}$  can be detected in a quantitative manner in a material containing predominantly  $\text{Eu}^{3+}$  by measuring the temperature dependent paramagnetic susceptibility of the material [1]. The opposite  $\text{Eu}^{3+}$  in  $\text{Eu}^{2+}$  case is much more difficult, however. The analysis of a  $\text{Tb}^{\text{IV}}$  content in a  $\text{Tb}^{3+}$  material is also possible. In both cases the paramagnetic susceptibility of both  $\text{Eu}^{2+}$  and  $\text{Tb}^{\text{IV}}$  was assumed to evolve identically to  $\text{Gd}^{3+}$ . In the end, all three have the same  $4f^7$  electron configuration. The present contribution verifies this hypothesis, using both theoretical and experimental studies of the paramagnetic susceptibility of the  $\text{EuAl}_2\text{O}_4$ ,  $\text{Gd}_2\text{O}_3$  and  $\text{TbO}_2$  materials. Moreover, no systematic and meticulous studies for  $\text{Eu}^{2+}$  and  $\text{Tb}^{\text{IV}}$  magnetism exist to facilitate a comparison to  $\text{Gd}^{3+}$ .

## 2. Results

The main challenge with  $\text{Eu}^{2+}$  and  $\text{Tb}^{\text{IV}}$  systems is the preparation of pure materials.  $\text{Gd}_2\text{O}_3$  was, in contrast, got by heating a high-purity oxide for 2 h @ *ca.* 1000 °C to chase off  $\text{H}_2\text{O}$  and  $\text{CO}_2$  absorbed from air.  $\text{EuAl}_2\text{O}_4$  was prepared as described earlier [2]. The HTHP methods failed to produce pure  $\text{TbO}_2$ , so the ingenious soft chemistry method by dissolving  $\text{Tb}^{3+}$  from  $\text{Tb}_4\text{O}_7$  with acetic acid @ <100 °C was used. The sonochemical treatment may be more effective though [3]. The temperature evolution of the paramagnetic susceptibility of  $\text{EuAl}_2\text{O}_4$  (white body color),  $\text{Gd}_2\text{O}_3$  (white) and authentic  $\text{TbO}_2$  (bright red) powders was measured from 1 to 350 K. The  $4f^7$  energy levels and paramagnetic susceptibilities were calculated with a parametric model using a program REEL [4]. The calculated paramagnetic susceptibilities of  $\text{EuAl}_2\text{O}_4$  and  $\text{TbO}_2$  gave a Curie type temperature behaviour indistinguishable from that of  $\text{Gd}_2\text{O}_3$  (Fig. 1). The  $4f^7$  level scheme has an isolated  $^8\text{S}_{7/2}$  ground multiplet with a energy difference of *ca.* 27 000  $\text{cm}^{-1}$  ( $\text{Eu}^{2+}$ ) but larger for  $\text{Gd}^{3+}$  and  $\text{Tb}^{\text{IV}}$  (Fig. 2). Due to this large difference and the restrictions of the crystal field, the mixing of wave functions is decimated, and the susceptibility depends only on the  $^8\text{S}_{7/2}$  multiplet (splitting <2  $\text{cm}^{-1}$ ). The identical Curie type curves are thus no wonder, though, if not found experimentally, mixing of  $^8\text{S}_{7/2}$  with the low-energy  $4f^65d^1$  and charge transfer states (CTS) should be blamed.

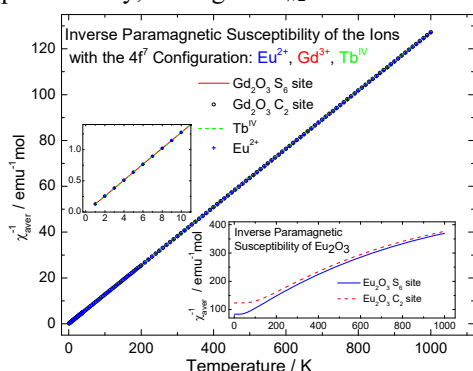


Fig. 1: Inverse paramagnetic susceptibilities of  $\text{Eu}^{2+}$ ,  $\text{Gd}^{3+}$  and  $\text{Tb}^{\text{IV}}$ .

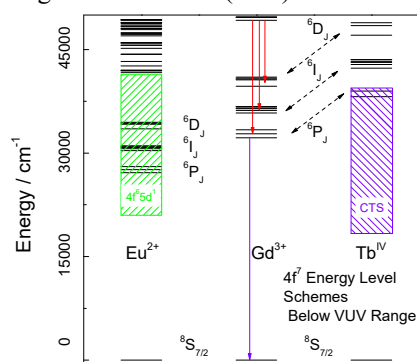


Fig. 2: Energy level schemes for  $\text{Eu}^{2+}$ ,  $\text{Gd}^{3+}$  and  $\text{Tb}^{\text{IV}}$ .

## 3. References

- [1] L.C.V. Rodrigues, J. Hölsä, H.F. Brito, M. Maryško, J.R. Matos, P. Paturi, R.V. Rodrigues, and M. Lastusaari, *J. Lumin.* **170** (2016) 701.
- [2] G. Schierming, M. Batentschuk, A. Osvet, A. Stiegelschmitt, and A. Winnacker, *Phys. Status Solidi C* **2** (2005) 109.
- [3] M. Gasgnier, L. Albert, J. Derouet, L. Beaury, P. Maestro, T. Chopin, and P. Caro, *J. Solid State Chem.* **112** (1994) 367.
- [4] P. Porcher, *Computer Program REEL for the Simulation of  $d^n$  and  $f^n$  Configurations Involving the Real Crystal Field Parameters*, Ecole Nationale Supérieure de Chimie de Paris - Chimie Paristech, Institut de Recherche de Chimie Paris - UMR 8247, Paris France 2005.



# Microstructural and spectroscopic properties of the $\text{CaTiO}_3:\text{Pr}^{3+},\text{Zn}^{2+}$ red emitting persistent phosphor

Dariusz Hreniak<sup>1</sup>, Wiesław Stręk<sup>1</sup>, Łukasz Marciniak<sup>1</sup>, Paweł Gluchowski<sup>1</sup>, Jakub Cichos<sup>2</sup>,  
Mirosław Karbowski<sup>2</sup>, Marco Pedroni<sup>3</sup>, Fabio Piccinelli<sup>3</sup>, Marco Bettinelli<sup>3</sup>,  
Adolfo Speghini<sup>3</sup>, Hendrik C. Swart<sup>4</sup>, Jorma Hölsä<sup>1,4\*</sup>

<sup>1</sup>Polish Academy of Sciences, Institute of Low Temperature and Structure Research, PL-50-422 Wrocław, Poland

<sup>2</sup>University of Wrocław, Faculty of Chemistry, PL-50-383 Wrocław, Poland

<sup>3</sup>University of Verona, Department of Biotechnology, I-17134 Verona, Italy

<sup>4</sup>University of the Free State, Department of Physics, Bloemfontein ZA-9300, Republic of South Africa

\*Corresponding author e-mail address: jholsa@utu.fi

## 1. Introduction

Persistent luminescence has several important applications such as lighting, photocatalysis, biological markers, sensors and detectors, harvesting solar energy as well as security markers [1]. At present, these materials should show their true potential in practice. The  $\text{Pr}^{3+}$  doped  $\text{CaTiO}_3$  materials are among the most studied persistent phosphors [1] especially due to quenching of the characteristic blue-green emission of  $\text{Pr}^{3+}$  and subsequent feeding of the red emission instead (Fig. 1). The  $\text{Pr}^{3+}$  dopant is also much cheaper than the traditional  $\text{Eu}^{2+}$  dopant though its performance leaves a lot to hope for. The  $\text{Zn}^{2+}$  co-dopant should introduce special features into the persistent luminescence behaviour because of, for example, the high volatility of zinc. This work focuses on how to improve the performance and chemical stability as well as to disclose the effects of the phosphor particle size and selective excitation with blue diodes.

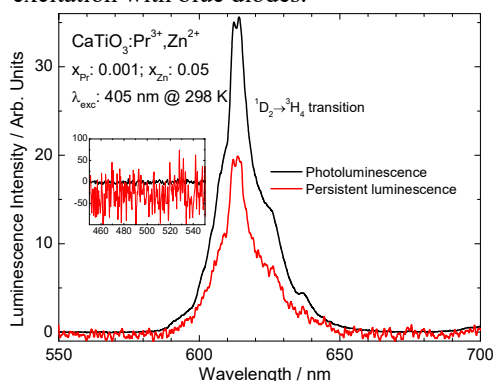


Fig. 1: Emission spectra of  $\text{CaTiO}_3:\text{Pr}^{3+},\text{Zn}^{2+}$ .

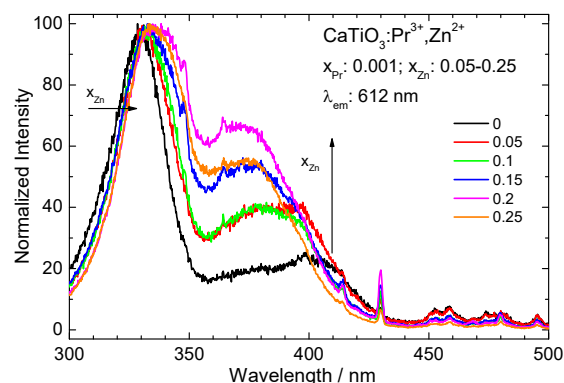


Fig. 2: Excitation spectra of  $\text{CaTiO}_3:\text{Pr}^{3+},\text{Zn}^{2+}$ .

## 2. Results

The  $\text{CaTiO}_3:\text{Pr}^{3+}(\text{Zn}^{2+} \text{ or } \text{Sr}^{2+})$  materials were prepared with the sol-gel, solid state reaction, and co-precipitation methods and their properties characterized with the usual methods (EDS mapping, SEM imaging, X-ray powder diffraction as well as luminescence emission and excitation spectroscopies).  $\text{CaTiO}_3:\text{Pr}^{3+}$  has interesting features such as the low host absorption threshold energy and the Inter-Valence Charge Transfer (IVCT) region at *ca.* 3.76 and 3.26-3.49 eV [2,3], respectively (see also Fig. 2). These should have an important role in its persistent luminescence properties.

The  $\text{Sr}^{2+}$  co-dopant weakens the persistent luminescence and, at all times, decreases the average crystallite size of  $\text{CaTiO}_3:\text{Pr}^{3+}$  as well. This suggests that incorporation of  $\text{Sr}^{2+}$  causes structural disorder and imperfections resulting in a trap structure not favouring persistent luminescence. As to  $\text{Zn}^{2+}$  co-doping, despite isovalent ( $\text{Zn}^{2+} \rightarrow \text{Ca}^{2+}$ ) substitution the solid solubility of  $\text{Zn}^{2+}$  in  $\text{CaTiO}_3$  is limited as evidenced at higher ( $\geq 0.15$ ) Zn concentrations by the appearance of a  $\text{Zn}_2\text{Ti}_3\text{O}_8$  impurity phase. This may be due to the size difference between  $\text{Ca}^{2+}$  and  $\text{Zn}^{2+}$ , clearly larger (*ca.* 20) than the one (*ca.* 15 %) proposed by the Vegard's rules as a prerequisite for complete solid solubility.  $\text{ZnO}$  is the worst Zn source;  $\text{Zn}^{2+}$  was not incorporated into the  $\text{CaTiO}_3$  lattice when the solid state method was used. Instead, zinc acetate yielded better results. A zinc source freshly prepared may evidently be better than an aged one. The most homogeneous materials (particle size, dopant distribution) were obtained by using the co-precipitation. The persistent luminescence can thus be enhanced with a  $\text{Zn}^{2+}$  co-dopant though the effect is difficult to predict, at least partially due to the volatility of zinc. This factor brings a new dimension to the present studies.

## 3. References

- [1] Y. Li, M. Gecevicius, and J. Qiu, *Chem. Soc. Rev.* **45** (2016) 2090.
- [2] P. Boutinaud, L. Sarakha, E. Cavalli, M. Bettinelli, P. Dorenbos, and R. Mahiou, *J. Phys. D: Appl. Phys.* **42** (2009) 045106.
- [3] W. Jia, D. Jia, T. Rodriguez, D.R. Evans, R.S. Meltzer, and W.M. Yen, *J. Lumin.* **119-120** (2006) 13.

# Physical and optical properties of lithium borosilicate glasses doped with Dy<sup>3+</sup> ions

V. Y. Ganvir<sup>1,2</sup>, D. D. Ramteke<sup>3\*</sup>, H. C. Swart<sup>3</sup>, R. S. Gedam<sup>2\*</sup>

<sup>1</sup>Department of Applied Physics, Rajiv Gandhi College of Engineering & Research, Nagpur -441110, (India)

<sup>2</sup>Department of Applied Physics, Visvesvaraya National Institute of Technology, Nagpur-440 010, (India)

<sup>3</sup>Department of Physics, University of the Free State, P.O. Box 339, Bloemfontein 9300, South Africa

\*Corresponding author e-mail address: ddphyvniit@gmail.com; rupesh\_gedam@rediffmail.com

## 1. Introduction

In the recent years, the luminescence properties of materials has been widely investigated for the applications in light emitting diode (LED), scintillators, medical application and in the laser industry. Glasses are excellent host for the rare earth ions because of its easy preparation method and excellent solubility of rare earth ions in it. Glasses also offer the wide range of composition which allow one to tune the physical and optical properties according to specific application. Rare earth ions are known for their emission due to 4f-4f and 4f-5d electronic transitions. Also one can use specific rare earth or co-doped rare earth ion containing materials with specific application [1]. By keeping in mind the advantage of rare earth ion and glasses we prepared the glass series with general formula 30 Li<sub>2</sub>O-70[1/7 SiO<sub>2</sub>:6/7B<sub>2</sub>O<sub>3</sub>] by conventional melt quench technique. The prepared lithium borosilicate glasses were doped with Dy<sub>2</sub>O<sub>3</sub>. We analyzed the density of glasses by Archimedes principle. Thermal study was performed by using Differential Thermal Analysis (DTA). We also analyzed the optical absorption spectra and luminescence properties of the prepared glasses. Finally we tried to correlate physical and optical properties of the prepared glasses for LED application.

## 2. Results

Figure 1 shows the excitation spectra of 0.5 mol % Dy<sub>2</sub>O<sub>3</sub> containing glass measured at excitation wavelength of 573.5 nm as representative. The excitation spectra show seven prominent peaks due to transition from the ground state to excited state. These peaks are <sup>6</sup>H<sub>15/2</sub>→<sup>4</sup>M<sub>17/2</sub> (324 nm), <sup>6</sup>H<sub>15/2</sub>→<sup>6</sup>P<sub>7/2</sub> (349 nm), <sup>6</sup>H<sub>15/2</sub>→<sup>6</sup>P<sub>5/2</sub> (365 nm), <sup>6</sup>H<sub>15/2</sub>→<sup>4</sup>I<sub>13/2</sub> (387 nm), <sup>6</sup>H<sub>15/2</sub>→<sup>4</sup>G<sub>11/2</sub> (426 nm), <sup>6</sup>H<sub>15/2</sub>→<sup>4</sup>I<sub>15/2</sub> (452nm) and <sup>6</sup>H<sub>15/2</sub>→<sup>4</sup>F<sub>9/2</sub> (470 nm) [2]. Out of these the transition <sup>6</sup>H<sub>15/2</sub>→<sup>6</sup>P<sub>7/2</sub> (349 nm) is the most prominent and was used to study the emission properties of the glasses.

Figure 2 shows the emission spectra of all Dy<sub>2</sub>O<sub>3</sub> doped glasses under excitation at 349 nm. Emission spectra of glasses show two sharp bands centred at 482 nm (blue) and 573 nm (yellow). These bands are assigned to <sup>4</sup>F<sub>9/2</sub>→<sup>6</sup>H<sub>15/2</sub> and <sup>4</sup>F<sub>9/2</sub>→<sup>6</sup>H<sub>13/2</sub> transitions, respectively. The glass with 0.5 mol % Dy<sub>2</sub>O<sub>3</sub> shows the maximum emission and the emission intensity decreased with further addition of Dy<sub>2</sub>O<sub>3</sub> in the glass matrix. This effect can be termed as luminescence quenching and an increased number of Dy<sup>3+</sup> ions in the glass matrix is responsible for this behaviour. From the excitation and emission properties it is clear that the glasses can be excited by near UV-light and they are further useful for LED applications [1,2].

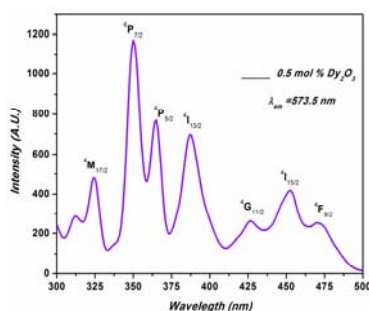


Fig. 1: Excitation spectra of 0.5 mol % Dy<sub>2</sub>O<sub>3</sub> doped lithium borosilicate glasses.

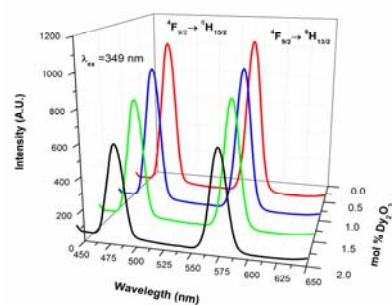


Fig. 2: Luminescence spectra of different concentration Dy<sub>2</sub>O<sub>3</sub> doped lithium borosilicate glasses.

## 3. References

- [1] X.Y. Sun, S. Wu a, X. Liu, P. Gao and S. Huang, J. Non-Cryst. Solids, **368** (2013) 51–54.
- [2] W. T. Carnall, P. R. Fields and K. Rajnak, J. Chem. Phys. **49** (1968) 4424.

# Photoluminescent dynamics of Pr<sup>3+</sup> and Dy<sup>3+</sup> in R<sub>2</sub>SiO<sub>5</sub> (R = La, Y) host

Simon N. Ogugua<sup>1</sup>, Hendrik C. Swart<sup>1</sup>, Martin O. Ntwaeaborwa<sup>2\*</sup>

<sup>1</sup>Department of Physics, University of the Free State, Bloemfontein, ZA9300, South Africa.

<sup>2</sup>School of Physics, University of the Witwatersrand, Private Bag 3, Wits, 2050, South Africa.

\*Corresponding author e-mail address: ntwaeab@gmail.com

## 1. Introduction

Pr<sup>3+</sup> doped matrices have shown two prominent emission lines in the visible region emanating from the <sup>3</sup>P<sub>0</sub> (green) and the <sup>1</sup>D<sub>2</sub> (red) energy levels. Depending on the crystal field strength of the host material, Pr<sup>3+</sup> can show either the <sup>3</sup>P<sub>0</sub> or the <sup>1</sup>D<sub>2</sub> or the two emission lines [1-3]. Furthermore, the branching ratio of the <sup>3</sup>P<sub>0</sub> to <sup>1</sup>D<sub>2</sub> emission lines of Pr<sup>3+</sup> can vary when doped into different host materials [3, 4]. Unlike Pr<sup>3+</sup>, Dy<sup>3+</sup> doped matrices have two dominant emission bands usually observe around 484 nm (<sup>4</sup>F<sub>9/2</sub>→<sup>6</sup>H<sub>15/2</sub>) and 573 nm (<sup>4</sup>F<sub>9/2</sub>→<sup>6</sup>H<sub>13/2</sub>). These two emission lines are observed in every Dy<sup>3+</sup> doped matrices. However, the branching ratios of the two emission lines can vary depending on where Dy<sup>3+</sup> ions are located in the symmetry of the host [5-8].

## 2. Results

We have prepared two sets of powder phosphors, La<sub>2-x</sub>Y<sub>x</sub>SiO<sub>5</sub>:P<sup>3+</sup> (x = 0, 0.5, 1.0, 1.5 and 2.0) and La<sub>2-x</sub>Y<sub>x</sub>SiO<sub>5</sub>:P<sup>3+</sup>, Dy<sup>3+</sup> (x = 0, 0.5, 1.0, 1.5 and 2.0) using solution combustion method. The structure, morphology and the elemental compositions of the phosphors were studied using X-ray diffractometer (XRD), field emission scanning electron spectroscopy (FE-SEM) and energy dispersive X-ray spectroscopy (EDS), respectively. Time-of-flight secondary ion mass spectroscopy (ToF-SIMS) was used to study the distribution of the atomic and molecular ionic species on the surface of the samples. The photoluminescence emission spectra of La<sub>2-x</sub>Y<sub>x</sub>SiO<sub>5</sub>:P<sup>3+</sup>, Dy<sup>3+</sup> (x = 0, 0.5, 1.0, 1.5 and 2.0), shown in Fig. 1, were recorded by exciting the phosphors using a 325 nm He-Cd laser. The colour purity of the phosphors calculated using the CIE co-ordinates (Fig. 2) showed tunable emission as the ratio of L:Y were varied in the matrix.

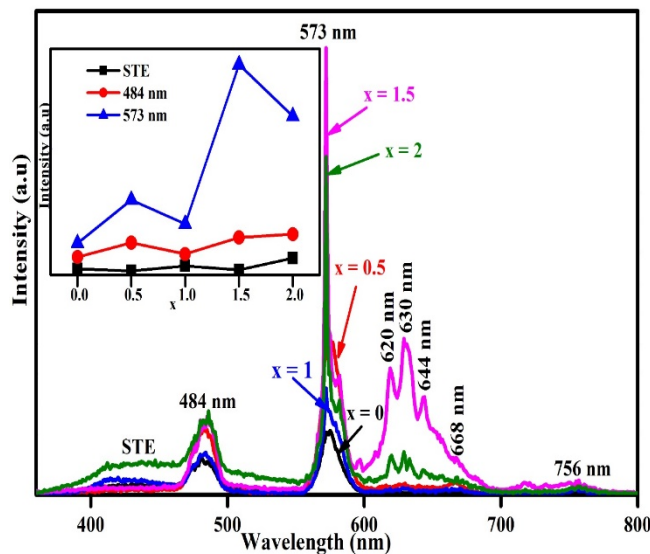


Fig. 1: PL emission spectra of La<sub>2-x</sub>Y<sub>x</sub>SiO<sub>5</sub>:P<sup>3+</sup>, Dy<sup>3+</sup> (x = 0, 0.5, 1.0, 1.5 and 2.0) phosphors excited with a 325 nm He-Cd laser.

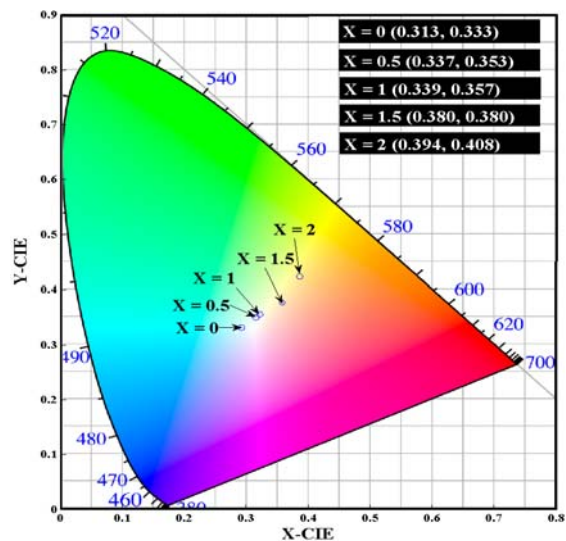


Fig. 2: The CIE co-ordinates of La<sub>2-x</sub>Y<sub>x</sub>SiO<sub>5</sub>:P<sup>3+</sup>, Dy<sup>3+</sup> (x = 0, 0.5, 1.0, 1.5 and 2.0) phosphors.

## 3. References

- [1] H.E. Hoefdraad and G. Blasse. Phys. Stat. Sol. (a). **29** (1975) K95.
- [2] G.C. Aumuller, W. Kostler, B.C. Grabmair and R. Frey. J. Phys. Chem. Solids **55** (1994) 767.
- [3] C. De Mello Donegá, A. Meijerink and G. Blasse. J. Phys. Chem. Solids. **56** (1995) 673.
- [4] L.L. Noto, M.L. Chithambo, O.M. Ntwaeaborwa and H.C. Swart. J. Alloys Compd. **589** (2014) 88.
- [5] J. Kuang, Y. Liu and J. Zhang. J. Solid State Chem. **179** (2006) 266.
- [6] A.N. Yerpude and S. J. Dhoble. J. Lumin. **132** (2012) 2975.
- [7] C.R. Kesavulu and C.K. Jayasankar. Mat. Chem. Phys. **130** (2011) 1078.
- [8] P. Babu, K.H. Jang, E.S. Kim, L. Shi, H.J. Seo, F.R. López, U.R.R. Mendoza, V. Lavín, R. Vijaya, C.K. Jayasankar and L.R. Moorthy. J. Appl. Phys. **105** (2009) 013516.

# Synthesis of Ag-SnO<sub>2</sub> nanocomposites and evaluation of optical, photoluminescence and antimicrobial properties

**Kishore Kumar Nair<sup>1\*</sup>, Jai Prakash<sup>2</sup>, Vinod Kumar<sup>3</sup>, Promod Kumar<sup>1</sup>, R.A. Harris<sup>1\*</sup>, R. E. Kroon<sup>1</sup>, H. C. Swart<sup>1</sup>**

<sup>1</sup>Department of Physics, University of the Free State, (UFS), Bloemfontein, ZA 9300, South Africa

<sup>2</sup>Department of Chemical Engineering, Indian Institute of Technology, Kanpur, Uttar Pradesh, India 208016

<sup>3</sup>Centre for Energy Studies, Indian Institute of Technology, Delhi, India 110 016

\*Corresponding author e-mail address: kknair9@gmail.com; HarrisRA@ufs.ac.za

## 1. Introduction

The synthesis of functional nanocomposites for various applications has been a subject of great interest in recent years. One such nanocomposite material is Ag doped with SnO<sub>2</sub>. Where SnO<sub>2</sub> has a range of different functionalities like sensor, photocatalysis, and solar cell applications [1], silver, on the other hand, is known for its antimicrobial properties. Therefore, when doped with a metal oxide such as tin oxide, this nanocomposite has a range of different synergistic properties. For example, silver doped tin oxide has been used for contact welding and gas sensing due to its low contact resistance [2]. Materials based on silver doped tin oxide are generally used in air contractors of low voltage, high current equipment, within a switching current range of 100 - 3 000 A [2]. The present study evaluates another important property of this nanocomposite: the photoluminescence (PL) and antimicrobial properties. It is envisaged that the synergistic effect of silver and tin oxide may be exploited to develop effective and efficient bacterial sensors as well as to employ biorational management of *E.Coli* for treatment of waste water. Therefore, a proper, systematic and thorough investigation into the synergistic properties of this nanocomposite is invaluable.

## 2. Results

Silver doped and undoped nanocomposites were synthesized *via* a sol-gel technique [3]. It was annealed at 1000 °C and further characterized by transmission electron microscopy, x-ray diffraction, photoluminescence and UV-visible spectroscopy. Figure 1 shows the UV spectra of undoped and silver doped tin oxide. The absorbance increases when pure tin oxide is doped with silver. The band gap was calculated from Tauc's formula and it decreases after silver doping from 3.4 eV to 3.2 eV. Figure 2 shows the PL spectra which shows the two bands when silver was doped in tin oxide.

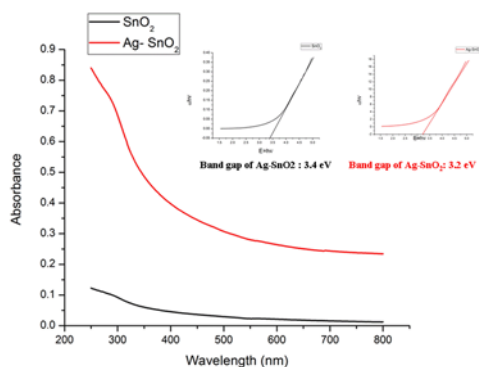


Fig. 1: UV spectra of doped and undoped SnO<sub>2</sub>

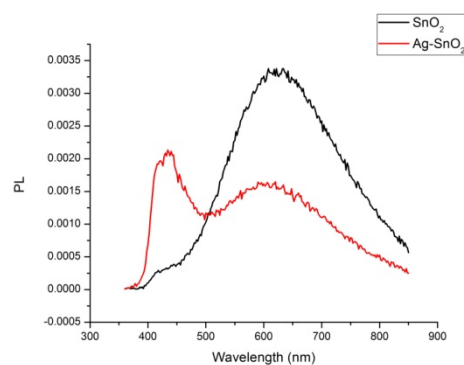


Fig. 2: PL spectra of doped and undoped SnO<sub>2</sub>

To investigate the antibacterial activity of the prepared nanocomposites, the microbial count of *escherichia coli* was recorded on an hourly basis. The antimicrobial assay against *E.Coli* shows the synergistic effect of silver with tin oxide: the microbial count decreased more in silver doped nanocomposites compared to pure tin oxide nanomaterial. The colony forming unit decreased in both doped and undoped tin oxide after every hour. Thus, silver doped tin oxide may possibly be used for the biorational management of *E.Coli* for treatment of waste water before discharge, when all other related factors are thoroughly considered.

## 3. References

- [1] M. Batzill, U. Diebold. *Progress in Surface Science* **79** (2005) 47.
- [2] Y. Tian-zu, DU Zuo-juan, GU Ying-ying, QIU Xiao-yong, J. Ming-xi, CHU Guang. *Trans. Nonferrous Met. SOC. China* **17** (2007) 434.
- [3] F. Gu, S. F. Wang, M. K. Lu1, G. J. Zhou, D. Xu, and D. R. Yuan. *J. Phys. Chem. B* **108** (2004) 8119.

# Structural and optical properties of rare-earth doped $\alpha$ -Fe<sub>2</sub>O<sub>3</sub> nanoparticles

L. Mathevu<sup>1\*</sup>, B. K. Mothudi<sup>1</sup>, M. S Dhlamini<sup>1</sup>

<sup>1</sup>Department of Physics, University of South Africa, P. O. Box 392, 0003, south Africa

\*Corresponding author e-mail address: mathele@unisa.ac.za

## 1. Introduction

$\alpha$ -Fe<sub>2</sub>O<sub>3</sub> is an environmentally friendly n-type semiconductor with the band gap of ~2.1 eV. It is the most stable iron oxide under ambient conditions. It is widely used in gas sensing, high density magnetic recording media, clinical therapy, Magnetic resonance imaging and diagnosis [1-3]. Rare earth atoms recently have been introduced into the iron oxide matrix which leads to a material that shows multiple interesting effects.

Rare-earth doped  $\alpha$ -Fe<sub>2</sub>O<sub>3</sub> nanoparticles were successfully synthesized by sol-gel method using PVA as polymerizing agent. The main advantage of PVA is to provide long stability for nanoparticles and by preventing the particles agglomeration. The powders were doped with different concentrations of the rare-earth. The structural, size, purity and luminescence studies of the synthesized powder were characterized by XRD, FT-IR, UV-Vis and PL spectral techniques. The doped  $\alpha$ -Fe<sub>2</sub>O<sub>3</sub> samples were subjected to radiation from the 980 nm laser beam source to investigate anti-stokes luminescence.

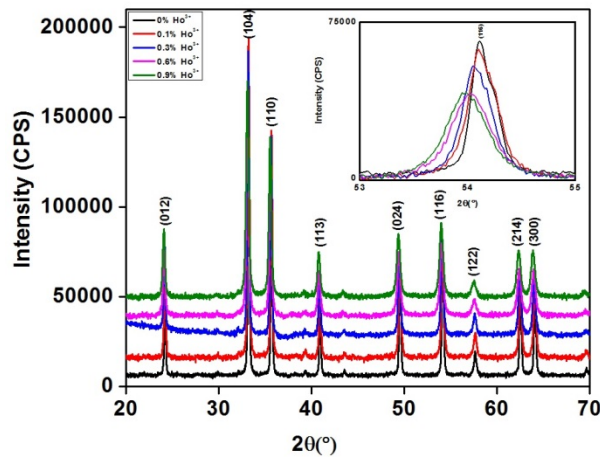


Fig. 1: XRD pattern of un-doped and Fe<sub>2</sub>O<sub>3</sub>:Ho<sup>3+</sup> nanoparticles at different doping concentration annealed at 600°C. The insert is the magnified region of (116) peak

## 2. References

- [1] M. N Batin and V. Popesca, *optoelectronics and advanced materials-rapid communications*, **6** (2012) 727.
- [2] Libor Machala, Radek Zboril, and Aharon Gedanken, *J. Phys. Chem.*, **111** (2007) 4003.
- [3] Maryam Mohammadikish, *Ceramics international* **40** (2014) 1351.

# Reflection measurements for luminescent powders

R. E. Kroon<sup>1\*</sup>

<sup>1</sup>Department of Physics, University of the Free State, Bloemfontein, South Africa

\*Corresponding author e-mail address: KroonRE@ufs.ac.za

## 1. Introduction

Fluorescent materials are useful in applications varying from lighting and display technologies to document security features and medical research, amongst many others. While the emission wavelength (colour) of a phosphor is critical, it is also vital to consider its excitation range: for example a red emitting phosphor to be used as a component in a white light emitting diode may need to be effectively excited in the near ultraviolet (360-400 nm), but for use in a fluorescent light bulb it must absorb the 254 nm emission of mercury, and for use in a plasma display panel effective excitation is required from the emission of xenon between 140-180 nm [1]. For liquids the absorbance may be determined by transmission measurements using an ultraviolet-visible (UV-vis) spectrophotometer, but for powders this is not possible and instead the absorption bands are revealed by a decrease in the measured reflectance of the material and may be interpreted using the Kubelka-Munk theory [2]. For this purpose UV-vis spectrophotometer may be upgraded with an integrating sphere to allow measurement of the diffuse reflectance of powders. Although such data is useful and often reported in the literature, it may be problematic for luminescent materials which do not merely reflect or absorb the incident light but also emit light at a different wavelength.

## 2. Results

Fig. 1 shows the reflectance of a 1 mol% Tb doped silica powder measured with a PerkinElmer Lambda 950 UV-vis spectrophotometer fitted with a 150 mm Spectralon™ integrating sphere, which appeared to exceed 100% at short wavelengths below 250 nm. In fact the Tb<sup>3+</sup> ions absorb strongly in this region due to an allowed *f-d* transition and therefore may be effectively excited for green luminescence (Fig. 2, top panel). To obtain a more reliable measurement of the reflectance, only the light from the sample having the original incident wavelength must be measured, which can be achieved by means of a synchronous scan with a zero wavelength offset using a fluorescence spectrometer. The key difference is that the additional emission monochromator of the fluorescence spectrometer prevents the luminescent light from reaching the detector. Fig. 2 (bottom panel) shows the reflectance of the same sample measured with an Edinburgh Instruments FLS980 fluorescence spectrometer fitted with a 120 mm Benflect™ integrating sphere, obtained by taking the ratio of the steady state Xe lamp light signal reflected from the sample relative to a Benflect™ standard. The reflectance values remained physically reasonable and the *f-d* absorption band below 250 nm corresponding to a strong excitation of green emission from the Tb doped silica sample was revealed. This alternative method of measuring powder reflectance may therefore be used to eliminate artefacts which may occur due to the luminescence of phosphor samples when measured using a UV-vis spectrophotometer with integrating sphere but having no emission monochromator.

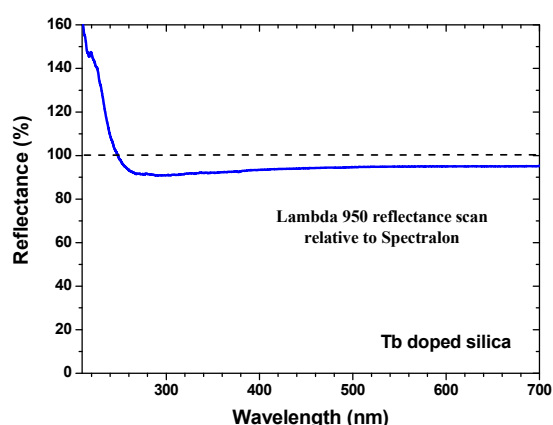


Fig. 1: Reflectance of Tb-doped silica measured using UV-vis spectrophotometer.

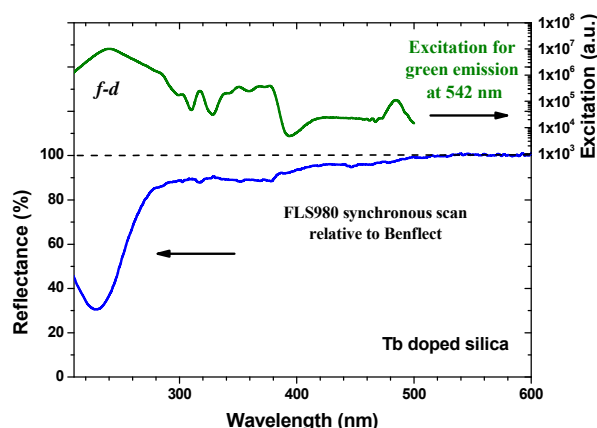


Fig. 2: Reflectance of Tb-doped silica measured using fluorescence spectrometer. The top panel shows the excitation spectrum for the green Tb emission at 542 nm.

## 3. References

- [1] A. Lakshmanan. *Luminescence and Display Phosphors: Phenomena and Applications* (Nova Science, 2007).
- [2] H. G. Hecht. *Journal of Research of the National Bureau of Standards* **80A** (1976) 567.

# Investigating the capability of ToF-SIMS to determine the oxidation state of Ce ions

H. A. A. Seed Ahmed<sup>1\*</sup>, H. C. Swart<sup>2</sup>, R. E. Kroon<sup>2</sup>

<sup>1</sup>Department of Physics, Faculty of Education, University of Khartoum, Omdurman, Sudan

<sup>2</sup>Department of Physics, University of the Free State, Bloemfontein, South Africa

\*Corresponding author e-mail address: welydoon@uofk.edu

## 1. Introduction

Lanthanide ions are widely used in luminescent materials. In particular, Ce<sup>3+</sup> ions have many applications due to the unique properties of their emissions [1], which make Ce<sup>3+</sup> ions good activators as well as useful sensitizers [2]. On the other hand side, the possibility of Ce ions to be found in the tetravalent Ce<sup>4+</sup> oxidation state, which is non-luminescent, creates some difficulties to use these ions as luminescent centres in phosphors. X-ray photoelectron spectroscopy (XPS) is a suitable technique to investigate the oxidation state [3] and we have previously made use of it to investigate the ratio of Ce<sup>3+</sup>/Ce<sup>4+</sup> in two different samples of SiO<sub>2</sub>:Ce, one annealed in air and the other in a hydrogen containing reducing atmosphere [4]. Similar to Ce, the lanthanide Eu can also occur in two different oxidation states (Eu<sup>2+</sup>/Eu<sup>3+</sup>), and although both of these are luminescent, their emission properties are very different. Eu<sup>2+</sup> has emission from an allowed *d-f* transition which is host dependent, whereas Eu<sup>3+</sup> has emission from forbidden *f-f* transitions at wavelengths that do not vary with the host material. The success of Swart *et al.* to successfully differentiate between the oxidation states of Eu<sup>2+</sup> and Eu<sup>3+</sup> in Sr<sub>5</sub>(PO<sub>4</sub>)<sub>3</sub>F:Eu phosphor material using time of flight secondary ion mass spectrometry (ToF-SIMS) [5] led us to investigate in this study whether this technique could also be applied to differentiate the oxidation state of Ce ions, which would be of great importance in the study of Ce-based phosphors as well as other industries, such as catalysis, where Ce is employed.

## 2. Results

ToF-SIMS spectra were collected from two samples of 4 mol% Ce doped silica, one sample annealed in air and the other one annealed in (H<sub>2</sub>/Ar) reducing atmosphere in order to investigate the capability of ToF-SIMS to determine the oxidation state of Ce ions in these two different samples. The obtained spectra shown in Fig. 1 are very similar; hence no significant difference was observed that could lead to differentiate between the oxidation states of Ce ions in the two samples, despite previous results from XPS, diffuse reflectance and PL measurements revealing that annealing in a reducing atmosphere favours the formation of trivalent Ce<sup>3+</sup> ions. Since we could not readily distinguish the Ce ion oxidation state in the Ce doped silica samples, possibly due to the relatively low Ce concentration (4 mol%), the results of ToF-SIMS analysis on CeF<sub>3</sub> and CeF<sub>4</sub> will also be presented to assess the possibility of distinguishing the Ce ion oxidation state using ToF-SIMS further.

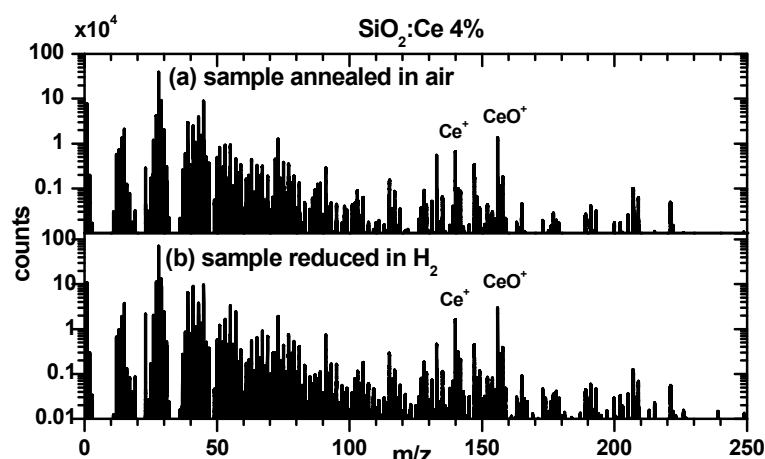


Fig. 1: The positive ToF-SIMS mass spectra of SiO<sub>2</sub>:Ce(4 mol%) for the full mass range: (a) sample annealed in air (b) sample reduced in H<sub>2</sub>/Ar.

## 3. References

- [1] R. Reisfeld, A. Pantra, G. Panczer and M. Gaft. *Opt. Mat.* **13** (1999) 81.
- [2] R.S. Meltzer and S.P. Feofilov. *J. Lumin.* **102–103** (2003) 151.
- [3] F. Larachi, J. Pierre, A. Adnot and A. Bernis. *App. Surf. Sci.* **195** (2002) 236.
- [4] H.A.A. Seed Ahmed, W.D. Roos, O.M. Ntwaeaborwa, H.C. Swart and R.E. Kroon. 2011 in Proceedings of SAIP2011, the 56th Annual Conference of the South African Institute of Physics, edited by I. Basson and A.E. Botha (University of South Africa, Pretoria, 2011), p. 280. ISBN: 978-1-86888-688-3. Available online at <http://www.saip.org.za>.
- [5] H.C. Swart, I.M. Nagpure, O.M. Ntwaeaborwa, G.L. Fische and J.J. Terblans. *Opt. Express* **20** (2012) 17119.

# Characterisation of the optical thermometry properties of La<sub>2</sub>O<sub>2</sub>S:Eu phosphor material

L. J. B. Erasmus<sup>1\*</sup>, J. J. Terblans<sup>1</sup>, H. C. Swart<sup>1</sup>

<sup>1</sup>Department of Physics, University of the Free State, Bloemfontein, South Africa

\*Corresponding author e-mail address: ErasmusLB@ufs.ac.za

## 1. Introduction

This study was focused on the measurements of the optical thermometry properties of Lanthanum Oxysulphide doped with Europium (La<sub>2</sub>O<sub>2</sub>S:Eu) commercial phosphor material by utilising an in-house modified photoluminescence (PL) system. La<sub>2</sub>O<sub>2</sub>S:Eu is a well-known thermographic phosphor. The outermost shell of the Eu<sup>3+</sup> ions is a closed shell and therefore absorption and emission of photons occur via electronic transitions within the 4f shell that is partially filled and is contained within the completed external 5s and 5d shells. These outermost close shells are important because they shield the emitting 4f shell from effects of the La<sub>2</sub>O<sub>2</sub>S host that tend to influence the emission and absorption. However, there still exist interactions between the La<sub>2</sub>O<sub>2</sub>S and the states of the Eu<sup>3+</sup> ion which render this phosphor's emission temperature-sensitivity and give it thermometry properties. Optical thermometry properties of thermographic phosphor materials can be measured by several techniques, however the techniques focused on in this study are the fluorescence intensity and intensity ratio techniques.

## 2. Results

For this study the emission spectra of La<sub>2</sub>O<sub>2</sub>S:Eu were obtained from 30 to 200 °C (Fig. 1) and the intensity ratio between two thermally coupled levels was monitored (Fig. 2). This was done by studying the peak intensities of the different PL peaks due to the different transitions from Eu<sup>3+</sup> in La<sub>2</sub>O<sub>2</sub>S:Eu at different temperatures. The inset in Fig. 1 also shows the ln of the different peaks as function of 1/temperature (1/T). It was clear that La<sub>2</sub>O<sub>2</sub>S:Eu can be used as a temperature sensor by using the calibration data. The viability of this phosphor as a stable and accurate temperature sensor was also evaluated by investigating its structural and chemical properties by utilising the modified PL system, X-ray Diffraction and X-Ray Photo-electron Spectroscopy systems.

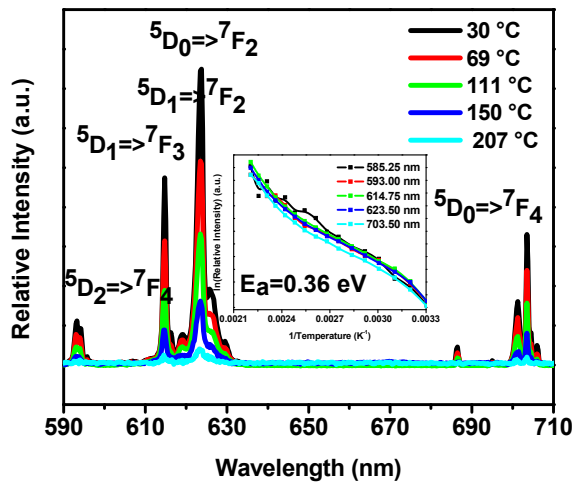


Fig. 1 Emission spectra of La<sub>2</sub>O<sub>2</sub>S:Eu. Inset shows the ln(intensity) of the different peaks as function of 1/T..

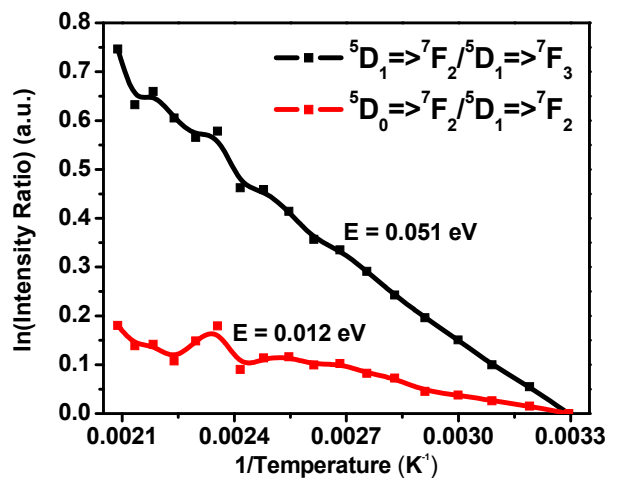


Fig. 2: Arrhenius intensity ratios between peaks as a function of temperature.

## 3. References

- [1] S. W. Allison and G.T. Gillies *Remote thermometry with thermographic phosphors: instrumentation and applications* (Rev. Sci. Instrum, 1997)
- [2] – K. Binnemans *Interpretation of europium(III) spectra* *Coordination Chemistry Reviews* **295** (2015) 6.



# Effect of annealing temperature on structural and luminescence properties of Eu doped NaYF<sub>4</sub> phosphor

Trilok K. Pathak<sup>1\*</sup>, Ashwini Kumar<sup>1</sup>, H. C. Swart<sup>1</sup>, R. E. Kroon<sup>1\*</sup>

<sup>1</sup>Department of Physics, University of the Free State, Bloemfontein, South Africa  
\*Corresponding author e-mail address: tpathak01@gmail.com, KroonRE@ufs.ac.za

## 1. Introduction

Rare earth fluorides normally possess a high refractive index and low phonon energy. Furthermore, they exhibit adequate thermal and environmental stability and therefore are regarded as excellent host lattices for down-conversion (DC) and up-conversion (UC) luminescence of lanthanide ions [1]. Among the investigated fluorides, NaYF<sub>4</sub>, as one of the most efficient DC and UC host lattices, has attracted more and more attention in the field of materials science over the past two decades [2]. The crystal structure of NaYF<sub>4</sub> exhibits two polymorphic forms, namely, cubic ( $\alpha$ ) and hexagonal ( $\beta$ ) phases, depending on the synthesis conditions and methods. Eu<sup>3+</sup> ions are excellent red emitters and famous structural probes under UV light excitation. Thus, it is attractive to explore the impact of annealing on the structure and on the spectra of Eu<sup>3+</sup> ions in a NaYF<sub>4</sub> matrix. In this work, Eu<sup>3+</sup> was doped in nanocrystalline NaYF<sub>4</sub> to investigate the structure, morphology and luminescence properties.

## 2. Results

Analytical grade yttrium nitrate hexahydrate, europium nitrate hexahydrate, ammonium fluoride, sodium nitrate, urea, 1-octadecene and oleic acid were obtained from Sigma Aldrich. The yttrium nitrate, ammonium fluoride and urea were dissolved in double distilled water with an appropriate amount of europium nitrate replacing yttrium nitrate for the doped samples. Sodium nitrate solution was added drop-wise and the solution then stirred thoroughly to obtain a homogeneous solution. When placed inside a pre-heated muffle furnace at 600 °C the mixture ignited with a flame and the rapid evolution of enormous amounts of gases produced a voluminous foamy black ash which turned white after about 15 min. This was ground to produce the final powder. Scanning electron microscopy showed that this as-synthesized sample consisted of a large quantity of hexagonal micro prisms with great uniformity. However, x-ray diffraction patterns (Fig. 1) showed mixed cubic (JCPDS 01-77-2042) and hexagonal (JCPDS 16-0334) phases of NaYF<sub>4</sub>. No other impurity peaks were detected. Annealing the samples at 600°C for 3 h favoured the hexagonal phase. Red photoluminescence from the samples excited at 394 nm is associated with transitions of Eu<sup>3+</sup> ions from the excited <sup>5</sup>D<sub>0-3</sub> levels to the <sup>7</sup>F<sub>J</sub> levels [3, 4]. The luminescence intensity increased with increasing Eu concentration up to the maximum (9%) used in this study, and also increased significantly for all samples after annealing (Fig. 2). Lifetime measurements were also made for the <sup>5</sup>D<sub>0</sub>–<sup>7</sup>F<sub>J</sub> emission at 616 nm. The excitation wavelength of these samples (394 nm) makes them suitable for red phosphors in UV-pumped white LED devices.

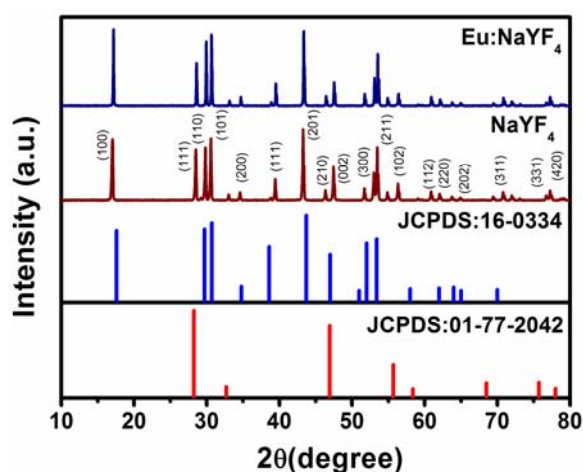


Fig.1: X-ray diffraction patterns of NaYF<sub>4</sub> and Eu doped NaYF<sub>4</sub>.

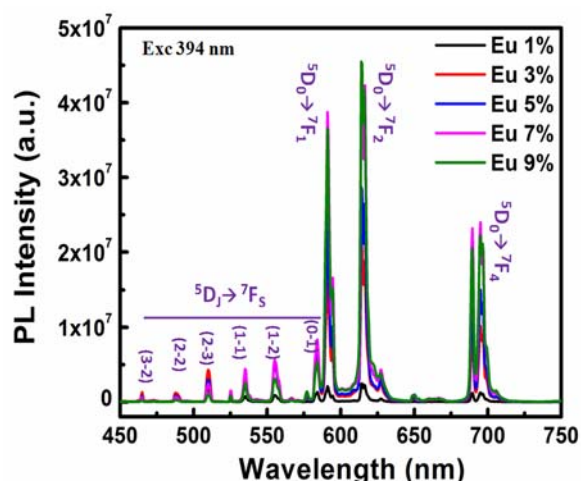


Fig.2: Luminescence spectra of Eu doped NaYF<sub>4</sub> excited at 394 nm.

## 3. References

- [1] J. W. Stouwdam and F. C. J. M. van Veggel. *Nano Lett.* **2** (2002) 733.
- [2] C. Li, Z. Quan, J. Yang, P. Yang and J. Lin. *Inorg. Chem.* **46** (2007) 6329.
- [3] L. Wang, Z. Liu, Z. Chen, D. Zhao, G. Qin and W. Qin. *J. Lum.in.* **1-2** (1970) 106.
- [4] C. Li, Z. Quan, J. Yang, P. Yang and J. Lin. *Inorg. Chem.* **46** (2007) 6329.

# Influence of citric acid solution on $\text{LiMn}_2\text{O}_4$ nanostructures prepared by chemical bath deposition method

Thamsanqa L. Majola<sup>1</sup>, Lehlohonolo F. Koao<sup>1\*</sup>, Setumo V. Motlounge<sup>2</sup>, Tshwafo E. Motaung<sup>3</sup>

<sup>1</sup>Department of Physics, University of the Free State (Qwaqwa campus), Private Bag X13, Phuthaditjhaba, 9866, South Africa

<sup>2</sup>Department of Physics, Sefako Makgatho Health Science University, P. O. Box 94, Medunsa, 0204, South Africa

<sup>3</sup>Department of Chemistry, University of Zululand, Private Bag X1001, KwaDlangezwa 3886, South Africa

\*Corresponding author e-mail address: koaolf@ufs.ac.za

## 1. Introduction

Lithium secondary batteries have been considered as an attractive source for a wide variety of applications, such as cellular phones, notebook computers and electric vehicles, etc. The  $\text{LiMn}_2\text{O}_4$  materials are environmentally friendly and thermally stable, and shows very good electrochemical performance. It is well known that the electrochemical performance of lithium ions materials is strongly affected by particle sizes, morphology, specific surface area, crystallinity, and composition [1]. In order to increase the charge capacity and to improve the conductivity of  $\text{LiMn}_2\text{O}_4$ , many works on its preparation method were performed. However, to the best of our knowledge, there is no report on syntheses of  $\text{LiMn}_2\text{O}_4$  nanoparticles synthesized by chemical bath deposition method (CBD). The CBD is a large area production process, simple in instrumental operation [2], cheap and convenient process to prepare semiconducting materials. The more recent interest in all things 'nano' has provided a boost for CBD, since it is a low temperature, solution (almost always aqueous) technique, crystal size is often very small and it gives better homogeneity. The CBD process has been used extensively to synthesize semiconductor powders and thin films.

## 2. Results

$\text{LiMn}_2\text{O}_4$  powders were prepared by chemical bath method using citric acid solution (CAS) as a catalyst. The effect of CAS on the thermal analysis, structure and morphology of  $\text{LiMn}_2\text{O}_4$  nanostructures were investigated. The CAS were varied from 20 up to 90 mL. The X-ray diffraction (XRD) patterns of the  $\text{LiMn}_2\text{O}_4$  nanostructures correspond to the various planes of a spinel  $\text{LiMn}_2\text{O}_4$  phase as shown in Fig. 1. From Fig. 2, it was observed that the diffraction peaks increase in intensity with an increase in CAS. The estimated average grain sizes calculated using the XRD spectra were found to be in the order of  $48 \pm 1$  nm. Scanning electron microscopy (SEM) observations showed the presence of the irregular nanoparticle. The irregular nanoparticle increased in size with an increase in CAS. The thermogravimetric analyses (TGA) and differential scanning calorimeter (DSC) showed that the final yield decreases with an increase in the CAS.

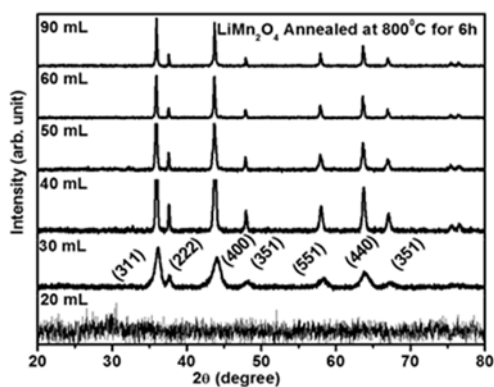


Fig. 1: X-ray powder diffraction patterns for  $\text{LiMn}_2\text{O}_4$  nanostructures prepared by CBD method.

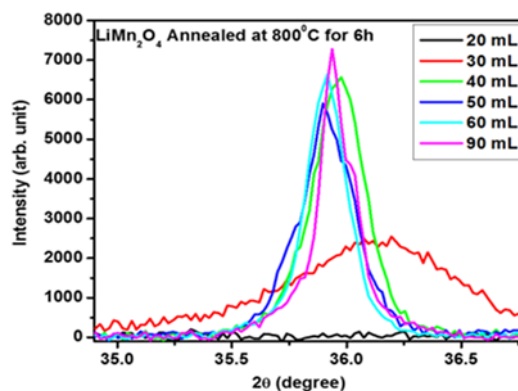


Fig. 2: X-ray powder diffraction patterns at (311) for  $\text{LiMn}_2\text{O}_4$  prepared by CBD method.

## 3. References

- [1] S. H. Choi, J. H. Kim, Y. N. Ko, Y. C. Kang, *Int. J. Electrochem. Sci.* **8** (2013) 1162.
- [2] L. F. Koao, F. B. Dejene, M. Tsega, H. C. Swart. *Physica B.* **480** (2016) 57.

# Structural and luminescence properties of self-yellow emitting undoped $\text{Zn}_2\text{V}_2\text{O}_7$ and (Ca, Ba, Sr)-doped $\text{Zn}_2\text{V}_2\text{O}_7$ phosphors synthesised by combustion method

Kewele E. Foka<sup>1</sup>, Lehonolonolo F. Koao<sup>1\*</sup>, Francis B. Dejene<sup>1</sup>, Setumo V. Motloung<sup>2</sup>, Hendrik C. Swart<sup>3</sup>

<sup>1</sup>Department of Physics, University of the Free State (QwaQwa Campus), Private Bag X13, Phuthaditjhaba, 9866, South Africa

<sup>2</sup>Department of Physics, Sefako Makgatho Health Science University, P. O. Box 94, Medunsa, 0204, South Africa

<sup>3</sup>Department of Physics, University of the Free State, P.O Box 339, Bloemfontein 9300

\*Corresponding author e-mail address: koaolf@ufs.ac.za

## 1. Introduction

Development of phosphor materials has been accelerated with the expansion of lighting and display applications as well as the progress on material science [1]. Lately light emitting device (LED) has attracted many attentions because of its success as a new light source to the incandescent lamp and fluorescent [2]. Vanadates (vanadium oxide) base materials such as  $\text{Zn}_3\text{V}_2\text{O}_8$ ,  $\text{CsVO}_3$  have attracted special attention due to their unique structural and optical properties which might render a possible substitute in near future. These vanadates show an efficient and broad emission from 400 to 700 nm which are due to the charge transfer (CT) of an electron from the oxygen 2p orbital to the vacant 3d orbital of  $\text{V}^{5+}$  in tetrahedral  $\text{VO}_4$  with  $T_d$  symmetry [3]. In this study  $\text{Zn}_2\text{V}_2\text{O}_7$  nano phosphor doped with the different dopants were synthesized by combustion method and material properties investigated. In contrast to previous studies it was found that the XRD structure obtained was single phase at low and higher synthesis temperature and the best luminescent intensity was obtained for samples synthesized at 600°C.

## 2. Results

A self activated yellow emitting  $\text{Zn}_2\text{V}_2\text{O}_7$  was synthesized by combustion method. The influence of the processing parameters such as synthesis temperature and dopants concentration on the structure, morphology and luminescence properties was investigated. The X-ray diffraction analysis shown in Fig. 1 confirmed that the samples have a tetragonal structure and no significant structural change was observed in varying both the synthesis temperature and the dopants concentration. The estimated average grain size was 78 nm for the samples synthesized at different temperatures and 77 nm for the doped samples. Scanning electron microscope images show agglomerated hexagonal-like shape particles with straight edges at low temperatures and the shape of the particles changed to cylindrical-like structures at moderate temperatures but were destroyed at higher temperatures. The microstructure retained its original structure when the phosphor was doped with Ba, Ca and Sr. The photoluminescence of the product (Fig. 2) exhibited broad emission bands ranging from 400 to 800 nm. The best luminescence intensity was observed for the undoped  $\text{Zn}_2\text{V}_2\text{O}_7$  samples and those synthesized at 600 °C. Any further increase in synthesis temperature, type and concentration of dopants led to a decrease in the luminescence intensity. The broad band emission peak of  $\text{Zn}_2\text{V}_2\text{O}_7$  consist of two broad band's corresponding to emission from the  $\text{Em}_1$  ( ${}^3\text{T}_2 \rightarrow {}^1\text{A}_1$ ) and  $\text{Em}_2$  ( ${}^3\text{T}_1 \rightarrow {}^1\text{A}_1$ ) transitions.

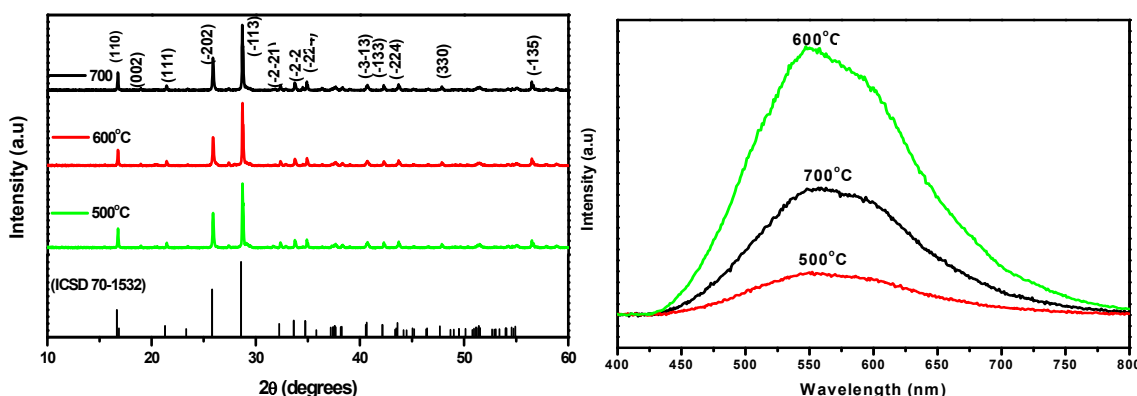


Fig. 1: XRD patterns of  $\text{Zn}_2\text{V}_2\text{O}_7$  phosphor prepared at different synthesis combustion

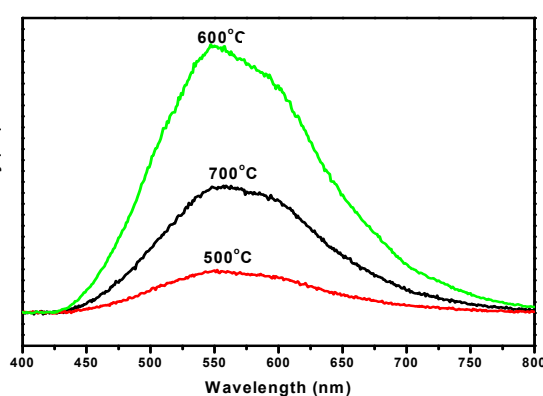


Fig. 2: Effect of synthesis temperature on the PL emission spectra of  $\text{Zn}_2\text{V}_2\text{O}_7$  nanophosphors

## 3. References

- [1] S. Shionoya and W. M. Yen, "Phosphor Handbook," CRC Press, Boca Raton, 1999.
- [2] L. Chen, K. Chen, C. Lin, S. Hu, M. Lee and R. Liu, *J. Comb. Chem.*, **12**, (2010) 587.
- [3] Y. Huang, Y. M. Yu, T. Tsoboi and H. J. Seo, *Optics express*, **20**, (2012) 4360.

# Host sensitized near-infrared emission in Nd<sup>3+</sup> doped different alkaline earth-sodium-phosphors

A. Balakrishna<sup>1\*</sup>, H. C. Swart<sup>1</sup>, O. M. Ntwaeaborwa<sup>2</sup>

<sup>1</sup>Department of Physics, University of the Free State, P.O. Box 339, Bloemfontein, ZA9300, South Africa

<sup>2</sup>School of Physics, University of the Witwatersrand, Private Bag 3, Wits, 2050, South Africa.

\*Corresponding author: ntwaeab@gmail.com; balakrishna.veera@gmail.com

## 1. Introduction

Ln-doped near-infrared (NIR) emitting phosphors are particularly interesting for their applications as active material in telecommunication components, lasers and polymer displays. In particular, NIR luminescence is used as a fluorescent label in bioassays due to the possibility of achieving high sensitivity of detection as a result of absence of interfering with background fluorescence. Nd<sup>3+</sup> is one of the most popular and efficient ions for obtaining NIR emission at 1.06 μm which is useful for high peak power laser applications, in addition to the possibility of lasing at other wavelengths such as 1350 and 880 nm at room temperature (RT) [1]. Also, its absorption in the UV–VIS–NIR regions allows efficient pumping either with a broad band sources (Xenon lamp) or with sources of selected wavelength using diode lasers. As an important family of luminescent materials, orthophosphates are generating interest because of their excellent fundamental properties such as large band gap and the high absorption of PO<sub>4</sub><sup>3-</sup> in the VUV region, moderate phonon energy, the high thermal and chemical stability, and the exceptional optical damage threshold [2]. In the present work, the effects of different alkaline (Mg, Ca, Sr and Ba) ions on morphology, luminescence and absorption spectra as well as decay kinetics of MNa[PO<sub>4</sub>]-Nd<sup>3+</sup> phosphors have been investigated, showing that they could explore their potential applications in NIR light amplification.

## 2. Results

The X-ray powder diffraction peaks of the studied samples are consistent with the standard CGPS data, which is a α-monoclinic phase with space group **pn21a** for MgNa[PO<sub>4</sub>] and SrNa[PO<sub>4</sub>] and orthorhombic phase with space group **P-3m1**(164) for CaNa[PO<sub>4</sub>] and BaNa[PO<sub>4</sub>]. As shown in Fig. 1 the wider FWHMs of excited state absorption bands of Nd<sup>3+</sup> in MNa[PO<sub>4</sub>]-Nd<sup>3+</sup> are helpful to tolerate the excitation wavelength shift of blue LED chips. Fig. 2 displays that the emission peak intensity of NIR emission has been varied with the variation of matrix composition in the order of: CaNa[PO<sub>4</sub>] > SrNa[PO<sub>4</sub>] > BaNa[PO<sub>4</sub>] > MgNa[PO<sub>4</sub>]. The substitution of Nd<sup>3+</sup> at a Ca<sup>2+</sup> site in CaNa[PO<sub>4</sub>] will comparatively lead to less distortion and induced more oxygen vacancies in the host. These oxygen vacancies (crystal defects) will produce and result in the different luminescent properties and splitting of different peaks. However, among all the prepared samples the CaNa[PO<sub>4</sub>]-Nd<sup>3+</sup> phosphors emit the highest PL brightness, therefore the Nd<sup>3+</sup> doped calcium phosphate phosphors can be regarded as promising candidates for the potential applications in near-infrared light amplification. The values of average lifetime ( $\tau_{avg}$ ) were 2285, 257, 316 and 384 μs for MNa[PO<sub>4</sub>]-Nd<sup>3+</sup> where M= Mg, Ca, Sr and Ba phosphors (Inset Fig. 2), respectively, as calculated from the non-exponential fitted curves. The life time value of the <sup>4</sup>F<sub>3/2</sub> level measured for the MgNa[PO<sub>4</sub>]-Nd<sup>3+</sup> phosphor was higher than the rest, suggesting that the magnesium phosphate host is suitable for the Nd<sup>3+</sup> doping with low non-radiative energy.

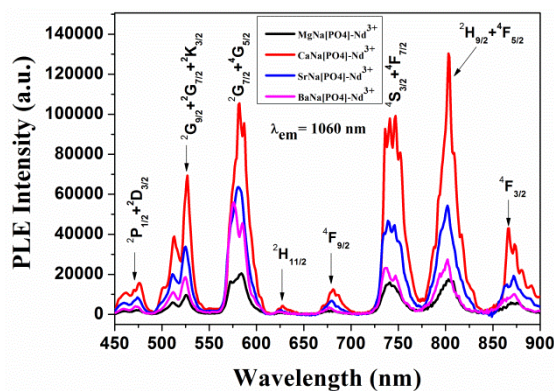


Fig. 1: Excitation spectra of MNa[PO<sub>4</sub>]-Nd<sup>3+</sup> (M= Mg, Ca, Sr and Ba).

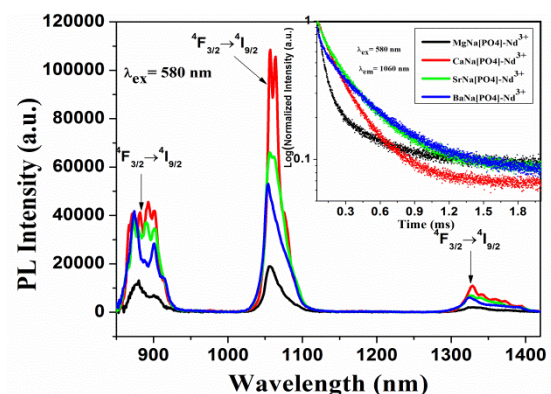


Fig. 2: Emission spectra of MNa[PO<sub>4</sub>]-Nd<sup>3+</sup>. Inset Shows the decay curves of the <sup>4</sup>F<sub>3/2</sub> levels.

## 3. References

- [1] M. Puchalska, A. Watras, *J. Alloys Compds.*, **688** (2016) 253.
- [2] J. Sun, X. Zhang, Z. Xi, H. Du, *Mater. Res. Bull.*, **46** (2011) 2179.

# Role of target and Ga particulates on the surface and optical properties of $Y_3(Al,Ga)_5O_{12}:Tb$ thin films prepared by PLD

A. Yousif<sup>1,2</sup>, M. M. Duvenhage<sup>1\*</sup>, J. J. Terblans, O. M. Ntwaeaborwa<sup>1</sup>, H. C. Swart<sup>1</sup>

<sup>1</sup>Department of Physics, University of the Free State, P.O. Box 339, Bloemfontein, ZA 9300, South Africa.

<sup>2</sup>Department of Physics, Faculty of Education, University of Khartoum, P.O. Box 321, Postal Code 11115, Omdurman, Sudan.

\*Corresponding author e-mail address: duvenhagem@ufs.ac.za

## 1. Introduction

Growing of thin films by the Pulsed laser deposition (PLD) technique has become a widely used method in many areas of scientific and technological applications. The dominant application has become film deposition of metallic, insulating, ferroelectric, magnetic properties as well as inorganic materials. Since this method has turned out to reproduce the chemical composition of the target very well [1]. In addition, PLD revealed particular features such as preferential sputtering of more volatile element, molecular emission, and existence of a fluence threshold separating the domain of defect-initiated sputtering from the regime of true ablation [2]. In the case of compound or multi-component targets for example, the stoichiometry of the target surface will differ from that of the bulk [3]. This modified stoichiometry will then be reflected in the plume generated in any subsequent ablation events and, conceivably, in the composition of the deposited film [3].

$Y_3(Al,Ga)_5O_{12}:Tb$  thin films (70 nm) have been prepared by PLD on a Si (100) substrate at the substrate temperature of 300°C. The effect of annealing time on the structural, morphological and luminescence properties of  $Y_3(Al,Ga)_5O_{12}:Tb$  thin films at 800 °C were studied. The crystal structure of the samples was studied by X-ray diffraction (XRD) and showed shifts in the peak positions to lower diffraction angles for the annealed film compared to the XRD peak positions of the commercial  $Y_3(Al,Ga)_5O_{12}:Tb$  powder. The peak positions of the XRD peaks for the annealed thin films have shifted to lower diffraction angles with respect to the commercial powder of  $Y_3(Al,Ga)_5O_{12}:Tb$  (Fig.1). A new excitation band different from the original  $Y_3(Al,Ga)_5O_{12}:Tb$  powder was also observed for the annealed films (Fig. 2). The shift in the XRD pattern and the new excitation band for the annealed film suggested that the films were enriched with Ga after annealing. The Atomic Force Microscope images showed the presence of a smooth ultra-thin film in some regions on the surface of the  $Y_3(Al,Ga)_5O_{12}:Tb$  thin films.

## 2. Results

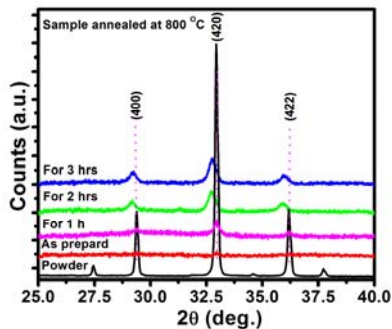


Fig. 1: XRD patterns of as prepared and annealed  $Y_3(Al,Ga)_5O_{12}:Tb$  film. The pattern for the annealed films for 2 and 3 hrs shows a shift to lower diffraction angles compared with the powder.

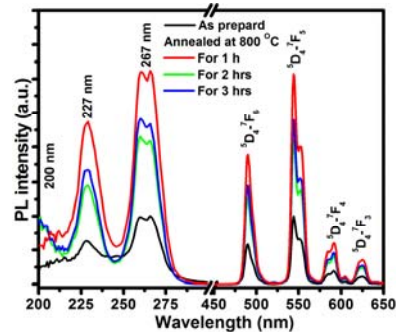


Fig. 2: PL excitation and emission of as prepared and annealed  $Y_3(Al,Ga)_5O_{12}:Tb$  films.

## 3. References

- [1] W. Svendsen, J. Schou, B. Thestrup, O. Ellegaard, *Applied Surface Science* **96-98** (1996) 518.
- [2] L. Vivet, B. Dubreuil, T. Gibert-Legrand, M. F. Barthe, *Journal Applied Physics* **79** (1996) 1099.
- [3] M.N.R. Ashfold, F. Claeysens, G.M. Fuge and S.J. Henley, *Chemical Society Reviews* **33** (2004) 23.

# Capacitance spectroscopy on GaNAs/GaAs quantum structure embedded solar cells

Danielle Venter<sup>1\*</sup>, Joachim Bollmann<sup>2</sup>, Martin Elborg<sup>3</sup>, J. R. Botha<sup>1</sup>, André Venter<sup>1</sup>

<sup>1</sup>Nelson Mandela Metropolitan University, University Way Port Elizabeth, South Africa

<sup>2</sup>Technische Universität Bergakademie Freiberg, 50937 Freiberg, Germany

<sup>3</sup>National Institute for Materials Science, 305-0047 Tsukuba, Japan

\*Corresponding author e-mail address: s212244450@nmmu.ac.za

## 1. Introduction

Quantum structures for low dimensional electron confinement in semiconductors offer significant potential for the development of unique optoelectronic devices. In particular, nitrogen containing alloys such as, amongst others, GaNAs and GaInNAs are interesting for fundamental research as well for the potential development of long wavelength optoelectronics, vertical-cavity surface-emitting laser diodes and intermediate-band solar cells. It is well known that the bandgap of GaNAs is inversely correlated with the nitrogen concentration through the lowering of the conduction band minimum. This results in strong confinement of electrons in GaNAs/GaAs quantum well structures (QWs) and consequently in reduced electron-hole recombination rates. Moreover, carrier generation-recombination mechanisms are strongly influenced by defects. A thorough understanding of the electronic behavior of defects is therefore a vital requirement for the enhancement of solar cell efficiency [1-4].

In this study, deep level transient spectroscopy (DLTS) and admittance spectroscopy (AS) have been used to study the properties of electrically active deep level centers present in GaNAs/GaAs quantum well (QW) embedded *p-i-n* solar cells. The structures were grown by molecular beam epitaxy (MBE). In particular, the effect of Si (*n*-type) and Be (*p*-type) doping of the QWs on the electrical properties were investigated. For this purpose, four samples: a) no embedded QWs (reference), b) un-doped QWs, c) Be-doped QWs and d) Si doped QWs, were prepared and characterized.

## 2. Results

Current-voltage (IV) measurements, performed on all the *p-i-n* diodes, show rectification of around 3 orders of magnitude (at  $\pm 1V$ ) with a reverse current below 10nA at -4V. Capacitance-voltage (CV) measurements were used to obtain doping profiles. Admittance spectroscopy (Fig. 1) revealed two traps in the *p*-doped samples with activation energies (Fig. 2) of 127 meV and 243 meV. A comparison of the electronic properties of these samples (a-d), as obtained by DLTS and AS respectively, will be presented.

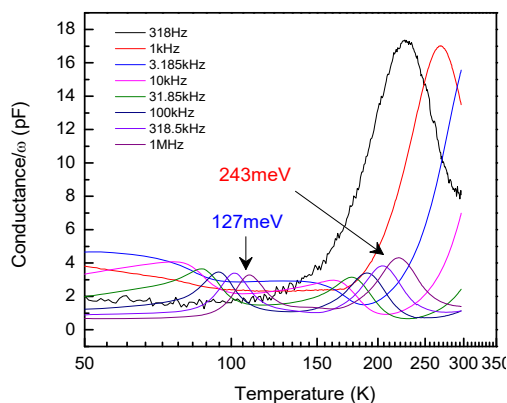


Fig. 1: Admittance spectra obtained at a reverse bias of 1V in the temperature range 20K-300K for Be doped GaNAs QWs in GaAs.

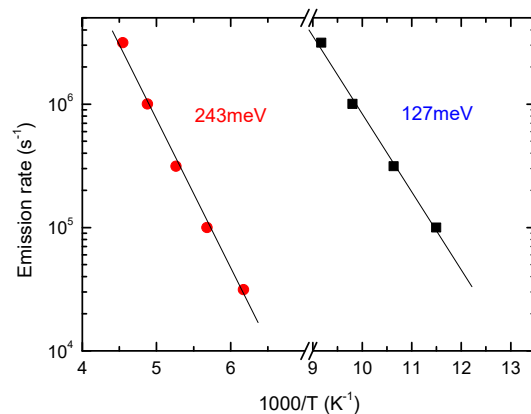


Fig. 2: Arrhenius plots for defects detected in Be doped GaNAs QWs in GaAs.

## 3. References

- [1] P. Krispin, S. G. Spruytte, J. S. Harris, and K. H. Ploog, *Journal of Applied Physics* **90**, 2405 (2001) 1391218.
- [2] I. A. Buyanova, W. M. Chen, G. Pozina, J. P. Bergman, B. Monemar, H. P. Xin, and C. W. Tu, *Applied Physics Letters* **75**, 501 (1999) 124429.
- [3] T. Mano, M. Jo, K. Mitsuishi, M. Elborg, Y. Sugimoto, T. Noda, Y. Sakuma, and K. Sakoda, *Applied Physics Express* **4**, (2011) 125001.
- [4] M. Elborg, M. Jo, Y. Ding, T. Noda, T. Mano, and K. Sakoda, *Japanese Journal of Applied Physics* **51**, (2012) 06FF15.

# Hall effect electrical characterization of solar cell materials

Sebastian Mienie<sup>1</sup>, Johan Janse van Rensburg<sup>1</sup>, Mmantsae Diale<sup>1\*</sup>

<sup>1</sup>University of Pretoria, Corner of Lynnwood and Roper street Hatfield South Africa  
\*Corresponding author e-mail address: Mmantsae.diale@up.ac.za

## 1. Introduction

First discovered by E.T. Hall in 1879 [1], the Hall Effect is a phenomena where if a material is placed in a magnetic field and a current is flowing through the material, an electric field is produced. Measuring the electric field a transverse potential is recorded, known as the Hall voltage and in turn used to calculate the Hall coefficient. The Hall coefficient is then used to calculate the mobility, carrier density and resistivity of the material. The Hall mobility describes the effectiveness of how these charge carriers move through the material and is given by equation (1)

$$\mu_H = R_H \sigma \quad (1)$$

where  $R_H$  is the Hall coefficient given by equation (2) and  $\sigma$  is the conductivity, the inverse of the resistivity  $\rho$ .

$$R_H = \left(\frac{d}{8B}\right) (R_{31,42}^+ - R_{13,42}^+ + R_{42,13}^+ - R_{24,13}^+ + R_{13,42}^- - R_{31,42}^- + R_{24,13}^- - R_{42,13}^-) \quad (2)$$

where  $d$  is the thickness of the studied sample and  $R_{\alpha\beta,\gamma\delta}$  indicates the resistance measurement for the different configurations. In this project we have used n- and p-type GaAs, PEDOT:PSS,  $Al_2O_3$  and n-type Si. All these materials with GaAs are material widely used in photovoltaic technology to produce highly durable and efficient solar cells [2].

Using the Van Der Pauw method a LabVIEW program was designed to automate the temperature dependent hall measurement (TDH) system. Environment temperatures from 25K to 300K were measured and the effect of the temperature on the semiconductor properties was measured. A constant magnetic field of 0.5T and current of 1mA was supplied to ensure accurate measurements.

## 2. Results

The Hall mobility for p-type and n-type GaAs are very different and seen from figures 1 and 2. One factor for this difference is the dependence on the effective mass of the mobility. The peak shape of the mobility is a result of impurity scattering and optical-phonon scattering. Impurity scattering is typically only seen at lower temperatures. From the experiment a difference of  $10^2$  was measured between the n-type and p-type GaAs. P-type and n-type GaAs measured a carrier density at 300K of  $10^{16}$  and  $10^{15}$  and a freeze out region below 30K and 25K respectively. Resistivity of 1.2  $\Omega$ m.cm and 0.2  $\Omega$ .cm was measured for p and n-type GaAs respectively. Samples also studied in this project include PEDOT:PSS, n-type Si and  $Al_2O_3$ .

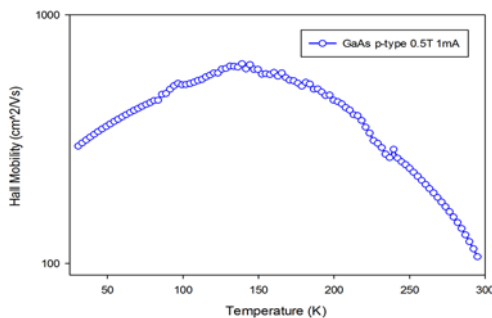


Fig. 1: Hall mobility as a function of temperature for p-type GaAs.

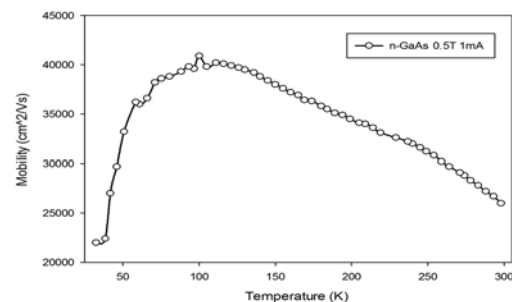


Fig. 2: Hall mobility as a function of temperature for n-type GaAs.

The TDH method is an effective and resourceful technique to measure electrical properties of materials and the effect of temperature on these properties.

## 3. References

- [1] S.A. Goodman, The characterization of GAs and AlGAs by the Hall effect, University of Port Elizabeth, 1989
- [2] M. Zeman, Introduction to Photovoltaic solar energy, Delft University of Technology, 2005

# Deposition of CZT-precursor layers for CZTS solar cell

A. J. Fourie<sup>1\*</sup>, J. J. Terblans<sup>1\*</sup>, H. C. Swart<sup>1</sup>

<sup>1</sup>Department of Physics, University of the Free State, Bloemfontein, South Africa

\*Corresponding authors: fouriea1@ufs.ac.za; terblansjj@ufs.ac.za

## 1. Introduction

Building on the development done on Copper indium gallium (di)selenide (CIGS) and CdTe solar cells, Copper zinc tin sulfide (CZTS) might provide a solution for sustainable solar cell production. They are made from common, non-toxic materials that are already produced on a large scale.[1] However, to really make this an environmentally friendly solar cell, the production methods also need to be developed with that aim in mind. The first and most important part of the photovoltaic cell that is being made is the CZTS ( $\text{Cu}_2\text{ZnSnS}_4$ ) photo absorber layer. In this study the first step was the deposition of Mo on glass using electron beam evaporation (EB). Then Cu, Zn and Sn were deposited in three different ways, pulsed laser deposition (PLD), electron beam evaporation (EB), and electroplating (EP). The EP was done in an environmentally friendly and inexpensive deep eutectic solvent called Reline. Reline is easily made using choline chloride and urea, and is well suited for use as an electrolyte. [2] The CZT (Cu-Zn-Sn) precursor layer then underwent sulfurization to form the desired CZTS crystalline structure.

## 2. Results

Characterisation of the thin films were done using several techniques, such as Auger electron spectroscopy (AES) and time of flight secondary ion mass spectrometry (TOF-SIMS). A depth profile of the CZT precursor layer before annealing was done with AES using an argon ion gun for sputtering, see figure 1. The CZT precursor layers deposited on Mo covered microscope glass were annealed in a vacuum at different temperatures. Some of the TOF-SIMS results after the annealing is shown in figure 2. It is clear that diffusion occurred during annealing.

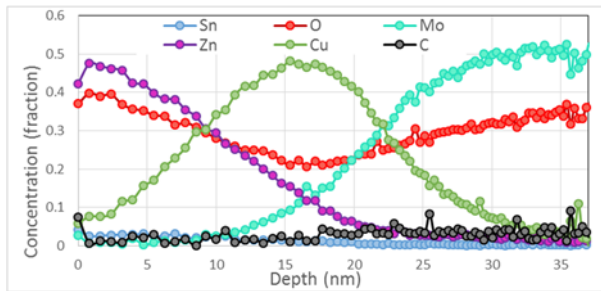


Fig. 1: Depth profile of the CZT layer deposited by PLD.

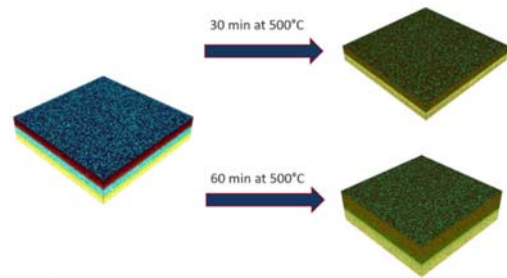


Fig. 2: TOF-SIMS analysis of the CZT precursor layer deposited using electron beam evaporation, before and after annealing.

## 3. References

- [1] Hongxia W, Progress in thin film solar cells based on  $\text{Cu}_2\text{ZnSnS}_4$ , *International Journal of Photoenergy*, **2011** (2011) 801292.
- [2] Chen H, Ye Q, He X, Ding J, Zhang Y, Han J, Liu J, Liao C, Mei J and Lau W, *Electrodeposited CZTS solar cell from Reline electrolyte*, *Green Chem.* **16** (2014) 3841.



# Effect of selenization time on the structural and morphological properties of Cu(In,Ga)Se<sub>2</sub> thin film absorber layer using a two-step growth process

Peter C. Korir<sup>1</sup>, Francis B. Dejene<sup>1\*</sup>

Department of Physics, University of the Free State (QwaQwa Campus), Private Bag X13, Phuthaditjhaba, 9866, South Africa  
Corresponding author e-mail address: dejenebf@qwa.ufs.ac.za

## 1. Introduction

Cu(InGa)Se<sub>2</sub>-based solar cells have often been touted as being among the most promising of solar cell technologies for cost-effective power generation [1, 2]. This is partly due to the advantages of thin films for low-cost, high-rate semiconductor deposition over large areas using layers only a few microns thick and for fabrication of monolithically interconnected modules. In classical two-step growth processes, Cu-In-Ga metallic precursors deposited by sputtering are selenized in elemental Se vapor or a H<sub>2</sub>Se/Ar gas mixture to form Cu(In,Ga)Se<sub>2</sub>. A seemingly insurmountable disadvantage of these processes is that the resultant semiconductor absorber films are heterogeneous. Due to the difference in the reaction rates between the binary selenides, the bulk of the material contains discrete CuInSe<sub>2</sub> and CuGaSe<sub>2</sub> phases. Alternatively, graded film structures are obtained with most of the gallium located at the back of the film [3]. In this study Cu(InGa)Se<sub>2</sub> thin films were prepared on soda lime glass substrates by selenization of sputtered Cu-In-Ga metallic precursors. Selenization was performed at three different selenization times of 45 minutes, 60 minutes and 90 minutes for a fixed selenization temperature of 515 °C. The effects of selenization time (Fig. 1) on the surface morphology of the grown films were analysed using scanning electron microscopy (SEM). The structures of precursor and selenized thin film were investigated by X-ray diffraction and the PL spectroscopy using a photoluminescence spectrophotometer.

## 2. Results

The surface morphology revealed the plate like particles grown uniformly over the substrate surface. The X-ray diffraction pattern as shown in Fig 2 indicated that the films grown for 60 minutes delivers single-phase Cu(In, Ga)Se<sub>2</sub> films with a high degree of surface compositional uniformity. This was nicely highlighted by the PL spectrum showing CIGS peaks, with largest shifts, indicating films with higher gallium incorporations. These results were supported by Electron profile microprobe analysis (EPMA), revealing a uniform distribution of the elements (Cu, In, Ga and Se) through the entire depth of the alloy. All the films showed an intense peak at  $2\theta=26.7^\circ$  which corresponds to the (112) plane. The crystallite size is calculated using the (112) peak of the XRD pattern and varies with the selenization time.

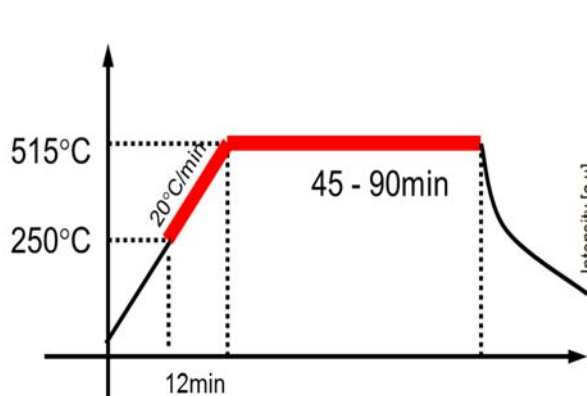


Fig. 1: Selenization profile

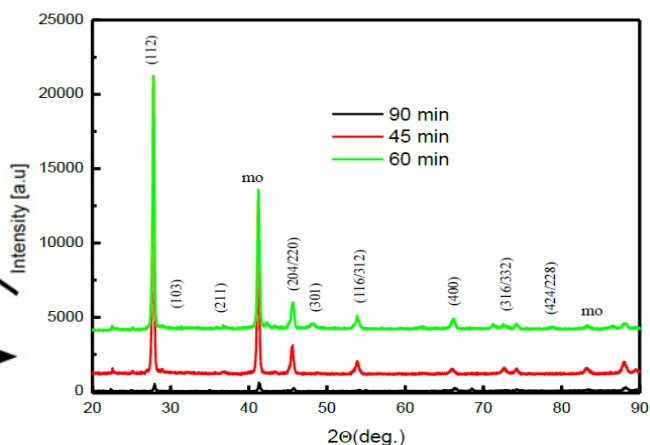


Fig. 2: XRD spectra of the selenized Cu(In-Ga)Se<sub>2</sub> absorber thin films

## 3. References

- [1] Junfeng Han, Cheng Liao, Tao Jiang, Huamu Xie, Kui Zhao and M.-P. Besland. *Journal of Crystal Growth* **382** (2013) 56.
- [2] F.B. Dejene, *Solar Energy Materials and Solar Cells* **93** (2009) 577.
- [3] F.B. Dejene, *Current Applied Physics* **10** (2010) 36.

# Effect of dopant density on contact potential difference across n-type GaAs homojunctions using Kelvin probe force microscopy

C. Kameni Boumenou<sup>1\*</sup>, Z. N. Urgessa<sup>1</sup>, S. R. Tankio Djiokap<sup>1</sup>, J. Nel<sup>2</sup>, J. R. Botha<sup>1</sup>

<sup>1</sup>Department of Physics, P.O Box 77000, Nelson Mandela Metropolitan University, Port Elizabeth 6031, South Africa

<sup>2</sup>Department of Physic, University of Pretoria, Private bag X20, Hatfield 0028, South Africa

\*Corresponding author-email address: Christian.kameniboumenou@nmmu.ac.za

## 1. Introduction

Potential profiling of semiconductor devices and semiconductor heterostructures on a nanometer scale has long been an important challenge for material and device engineers [1]. Several measurement techniques have been developed for these purposes. Among these, Kelvin Probe Force Microscopy (KPFM) proposed in 1991 by Nonnenmacher et al. [2] appears as the most powerful. It extracts simultaneously the 3D topographic information (with 1 nm in the x-y plane and 0.1 nm in the z direction resolution) [3] as well as the surface electrical properties of materials on the nanometer scale [4]. In principle, KPFM measures the sample surface potential, by minimizing the interaction force between a sharp conducting tip and the sample surface. The measurement is usually carried out in one of two different modes: Frequency Modulation (FM) or Amplitude Modulation (AM) KPFM. In FM-KPFM mode, the electrostatic force gradient is minimized, while in AM-KPFM mode the electrostatic force itself is minimized. In this study, AM-KPFM is used to study the contact potential difference (CPD) across the interface between semi-insulating GaAs and GaAs epilayers with different dopant densities. Four samples with electron densities (room temperature) as obtained from Hall measurements, of  $\sim 4.9 \times 10^{18} \text{cm}^{-3}$ ,  $\sim 6 \times 10^{18} \text{cm}^{-3}$ ,  $\sim 6.5 \times 10^{18} \text{cm}^{-3}$  and  $\sim 6.8 \times 10^{18} \text{cm}^{-3}$  have been considered for investigation. The samples were grown by metalorganic chemical vapour deposition.

## 2. Results

Figure 1 shows the CPD between the semi-insulating GaAs substrate and n-type GaAs epilayers with different dopant densities. It is clear that the CPD changes with electron density. The variation in CPD as a function of dopant density is summarized in figure 2. A detailed discussion of these results and the underlying theory will be presented in this paper.

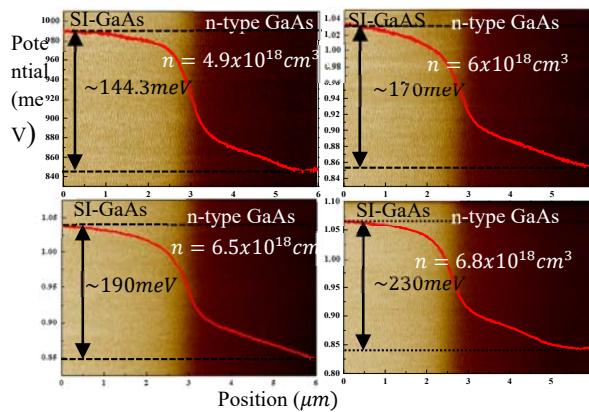


Figure 1: Cross-sectional potential imaging of  $3 \mu\text{m}$  n-type GaAs/SI-GaAs. Four samples with same the layer thicknesses, grown on the same substrate, but with difference in electron density have been considered for the studies.  $n$  is the electron density

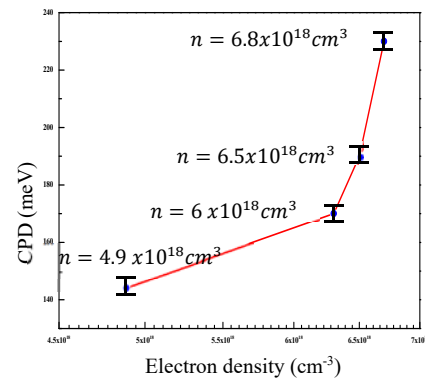


Figure 2: Evolution of the CPD across n-type GaAs/SI-GaAs versus electron density. Vertical bars indicate the fluctuation of the measured CPD values.

## 3. References

- [1] T. Muzutani, T. Usunami, S. Kishimoto and K. Maezawa. *Jpn. J. Appl. Phys.* **37** (1999) 767.
- [2] M. Nonnenmacher, M. P. O'Boyle and H. K. Wickramasinghe. *Appl. Phys. Lett.* **58** (1991) 2921.
- [3] R. Bozek. *Acta Phys. Pol., A.* **108** (2005) 541.
- [4] W. Melitz, J. Shen, A. Kummel and S. Lee. *Surf. Sci. Rep.* **66** (2011) 1.

# Patterned growth of ZnO nanorods for organic/inorganic hybrid solar cell

Z. N. Urgessa<sup>1\*</sup>, J. R. Botha<sup>1</sup>, C. Coleman<sup>2</sup>, S. Bhattacharyya<sup>2</sup>

<sup>1</sup>Department of Physics, Nelson Mandela Metropolitan University, P.O. Box 77000, Port Elizabeth 6031, South Africa

<sup>2</sup> Nano-Scale Transport Physics Laboratory, School of Physics, and DST/NRF Centre of Excellence in Strong Materials, University of Witwatersrand, South Africa

\*Corresponding author e-mail address: zelalem.urgessa@nmmu.ac.za

## 1. Introduction

Vertically aligned ZnO nanorods have a variety of applications in optoelectronics as well as nano-scale devices, such as solar cells, UV lasers and light emitting diodes [1-3]. In conventional solar cells, sol-gel synthesized nanoparticles of TiO<sub>2</sub> or ZnO are often used as electron collecting layer in different organic/inorganic hybrid solar cells, such as dye sensitized solar cells (DSSCs) [2], bulk heterojunction [3] and perovskite [4] cells. However, the grain boundaries between nanoparticles that result in electron-hole recombination, low charge collection efficiency and hence a low solar to electrical conversion efficiency become an issue. Therefore, one dimensional nanostructures such as nanorods have drawn attention because of their geometry that guide carriers during conduction [2-3]. Also, densely packed nanorods provide limited area for loading the active materials (dyes/polymers) for solar absorbance. In this study, the growth of ordered ZnO nanorods using chemical bath deposition on a patterned seed layer is demonstrated. Electron beam lithography (EBL) was employed to generate a patterned mask made of poly(methyl methacrylate) (PMMA), over the ZnO seed layer[1]. The pit diameter and pitch were set at 300 nm and 1 μm, respectively.

## 2. Results

Fig.1 shows a scanning probe microscopy (SPM) topography image of EBL-patterned PMMA on silicon coated with a ZnO seed layer. The patterning is clearly illustrated. Fig.2 (a) shows a low magnification scanning electron micrograph (SEM) of ZnO nanorods subsequently grown on the PMMA-patterned surface, whereas Fig. 2(b) shows a higher magnification of a region in (a). As the diameters of the openings to the ZnO seed layer in this preliminary study were all greater than 300 nm, thus exposing a number of ZnO grains in the seed layer, it is clear that multiple nanorods grow from a single pit (see red circles). Detailed results showing the effect of the patterning parameters on the subsequent growth of ZnO nanorods for application as ECL in organic/inorganic hybrid solar cells, will be presented in the paper.

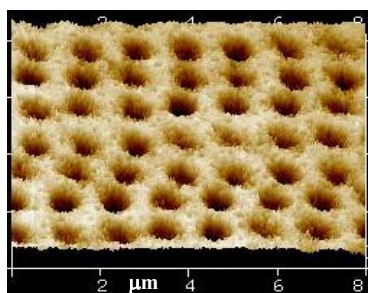


Fig. 1: scanning probe microscopy (SPM) topography image of EBL patterned PMMA on a ZnO seed layer

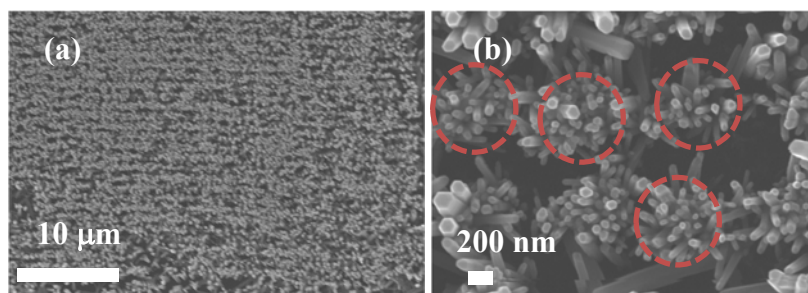


Fig. 2: SEM micrograph of ZnO nanorods grown on EBL-patterned ZnO seed layer at (a) low magnification and (b) higher magnification.

## 3. References

- [1] S. Xu, Y. Wei, M. Kirkham, J. Liu, W. Mai, D. Davidovic, R. L. Snyder and Z. Lin Wang, *J. AM. CHEM. SOC.* **130**, (2008) 14958.
- [2] Fang-I Lai, Jui-Fu Yang, and Shou-Yi Kuo *Materials*, **8**, (2015) 8860.
- [3] S. Shao, K. Zheng, T. Pullerits, and F. Zhang *ACS Appl. Mater. Interfaces*, **5**, (2013) 380.
- [4] D.Y. Son, K.H Bae, H.S Kim, and N.G Park *J. Phys. Chem. C*, **119**, (2015) 10321.

# Effect of growth temperature on structural and luminescence properties of ZnO nanoparticles

Francis Dejene<sup>1\*</sup>, Jatani Ungula<sup>1</sup>, Dickson Andala<sup>2</sup>, Martin Onani<sup>3</sup>

<sup>1</sup>Department of Physics, University of the Free State (Qwa Qwa Campus), Private Bag X 13, Phuthaditjhaba 9866, South Africa

<sup>2</sup>Multimedia University of Kenya, PO Box 15653-00503, Nairobi-Kenya

<sup>3</sup>Department of Chemistry, University of the Western Cape, Private Bag X17, Bellville, Cape Town, South Africa

\*Corresponding author e-mail address: dejenebf@qwa.ufs.ac.za

## 1. Introduction

ZnO is one of the few semiconductors which exhibit quantum confinement effect. As such the nanoparticles have a unique characteristic of size dependent electrical and optical properties. It is well documented that the shape and size of materials strongly affect their properties and the applications. Hence much effort is dedicated on controlling the size and shape of the particles by varying different growth parameters such as time, temperature, concentration, precursors, capping molecule, solvents, and others [1, 2]. Growth temperature is a key factor in controlling the morphology, optical and electrical properties of nanostructures. Optimization of growth temperature is therefore a key procedure to obtain high quality ZnO nanostructures.

## 2. Results

ZnO nanoparticles (ZnO NPs) were synthesized by the sol-gel method at different temperatures. The effects of growth temperature on the structure and optical properties of ZnO NPs were investigated in detail. Temperature is an important thermodynamic factor that plays a key role in controlling the growth rate of a crystal, the morphology and aspect ratio of ZnO nanostructures. The characterization of the nanoparticles with scanning electron microscopy (SEM) showed that at low temperatures (35 and 45 °C) needle like particles were observed. As the growth temperature increased to 75 °C, spherical particles were formed. SEM results also showed increased ZnO NPs sizes with increase in growth temperatures. The particle size, lattice parameters and crystal structures of the nanoparticles were characterized by X-ray diffraction (XRD). The average crystallite sizes have been found to increase from 28 to 35 nm with the increase in growth temperatures. Results of XRD (Fig. 1) showed a systematic shift in peak positions towards lower  $2\theta$  values with the increase in growth temperatures caused by change in lattice parameters. The intensity of the DLE band, as observed from photoluminescence spectra (Fig. 2) decreased with the increase in growth temperature. FTIR measurement illustrated the highest % transmittance at all wave numbers to be at room temperature. The trend of % transmittance of ZnO NPs, generally declined with the increase in growth temperature. The estimated band gap reduced from 3.31 to 3.24 eV with the increase in the growth temperature due to tensile strain while compressive strain results into an increase of the band gap. The band gap from reflectance curve; however, was observed to be lower than that of the bulk ZnO (3.37 eV). This band gap reduction may be due to surface defects density of undoped ZnO.

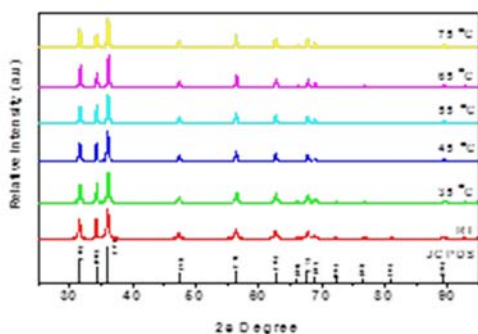


Fig. 1: X-ray powder diffraction pattern for ZnO nanoparticles prepared at different growth temperature.

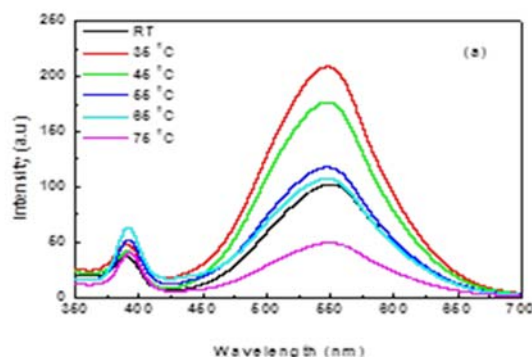


Fig. 2: PL emission spectrum for ZnO nanoparticles prepared at different growth temperatures.

## 3. References

- [1] Jun Y. W.; Choi J. S.; Cheon J.; *Angewandte Chemie-International Edition* **45** (2006) 3414.
- [2] Guo M.; Diao P.; Wang X.; Cai S.; *Journal of Solid State Chemistry* **178** (2005) 3210.

# Effects of precursor concentration on morphological and structure properties of TiO<sub>2</sub> synthesized via sol-gel method

Francis Dejene<sup>1\*</sup>, Moses Sithole<sup>1</sup>, Lehlohonolo Koao<sup>1</sup>, Setumo Motloulung<sup>2</sup>, Dickson Andala<sup>3</sup>, Martin Onani<sup>4</sup>

<sup>1</sup>Department of Physics, University of the Free State (Qwa Qwa Campus), Private Bag X 13, Phuthaditjhaba 9866, South Africa

<sup>2</sup>Department of Physics, Sefako Makgatho Health Science University, P. O. Box 94, Medunsa, 0204, South Africa

<sup>3</sup>Multimedia University of Kenya, PO Box 15653-00503, Nairobi-Kenya

<sup>4</sup>Department of Chemistry, University of the Western Cape, Private Bag X17, Bellville, Cape Town, South Africa

\*Corresponding author e-mail address: dejenebf@qwa.ufs.ac.za

## 1. Introduction

Nano-crystalline TiO<sub>2</sub> have been intensively investigated in recent years, because of their different potential applications including water purification [1] and solar cell devices [2]. Heterogeneous solar photocatalysts effectively utilize the ultraviolet (UV) energy from the sunlight, a renewable energy, for the photocatalytic reactions that can potentially reduce the water treatment costs. Normally, TiO<sub>2</sub> exhibits polymorphs with three phases; anatase, rutile as tetragonal whereas brookite is orthorhombic. While rutile phase is optically active and the most stable of these three; anatase phase has attracted much attention because of its higher photocatalytic activity. Sol-gel process is one of the most common methods used for producing photocatalytic TiO<sub>2</sub> material in the form of powder or coatings. In this study the effect of tetra-n-butyl-orthotitanate on the structure, morphology and optical properties of the synthesized TiO<sub>2</sub> nanoparticles was investigated. The primary aim of the investigation was to evaluate the effect of tetra-n-butyl-orthotitanate on the stability of TiO<sub>2</sub> nanoparticles.

## 2. Results

Figure 1 shows the XRD patterns of TiO<sub>2</sub> powder prepared using the sol-gel solution. It is proven that all TiO<sub>2</sub> powder exhibit anatase phase (JCPD file No. 84-1286). The crystallite sizes were estimated using (101) diffraction peaks according to the Scherrer equation and was found to be 16, 17, 25 and 41 nm when grown using 3, 5, 9 and 17 ml of tetra-n-butyl-orthotitanate, respectively. Scanning electron microscopy (Fig. 2) studies depicts small spherical shapes that become agglomerated, as the concentrations of precursors increases. Whenever the concentration of precursor was low, the samples were less agglomerated with small voids between nanoparticles. The observed voids were due to degassing during the annealing process. The diffuse reflectance spectra of pure TiO<sub>2</sub> prepared at different concentrations of tetra-n-butyl-orthotitanate was found to decrease in the visible region and absorption band edge red shifts to the longer wavelengths. The TiO<sub>2</sub> sample revealed a broad intensity band centered at 460 nm with a weak band at higher wavelength of 560 nm. These two emissions were assigned to photon incident lines and oxygen defect trap, respectively. The synthesized TiO<sub>2</sub> nanomaterials band gap energy (3.7, 3.6, 3.3, 3.3 eV) are larger than the value of 3.2 eV for the bulk TiO<sub>2</sub> nanomaterials. This is due to quantum confinement as the particle sizes decrease.

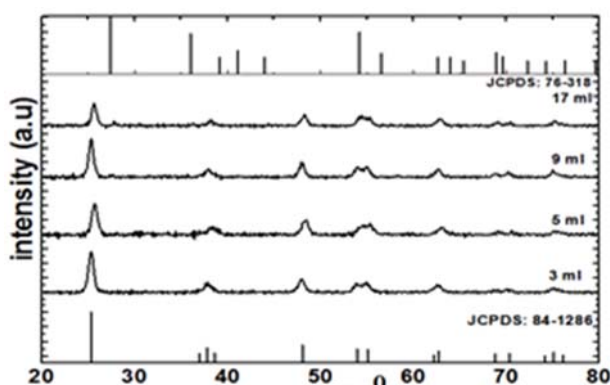


Fig. 1: XRD patterns of TiO<sub>2</sub> nanoparticles prepared at different concentrations of tetra-n-butyl-orthotitanate.

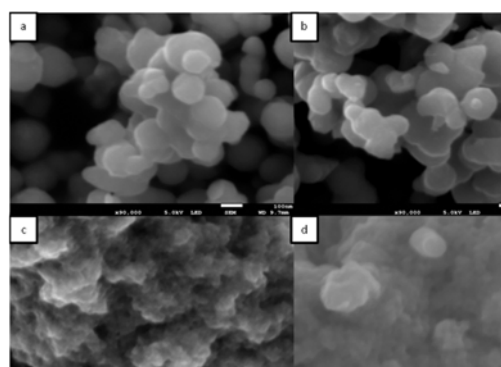


Fig. 2: SEM micrograph of TiO<sub>2</sub> nanoparticles prepared at different concentrations of tetra-n-butyl-orthotitanate

## 3. References

- [1] Jun Y. W.; Choi J. S.; Cheon J.; *Angewandte Chemie-International Edition* **45** (2006) 3414.
- [2] Guo M.; Diao P.; Wang X.; Cai S.; *Journal of Solid State Chemistry* **178** (2005) 3210.

# A potential green emitting citrate gel synthesized NaSrBO<sub>3</sub>:Tb<sup>3+</sup> phosphor for display application

A. K. Bedyal<sup>1,2\*</sup>, Vinay Kumar<sup>1,2</sup>, H. C. Swart<sup>1\*</sup>

<sup>1</sup>Department of Physics, University of the Free State, P.O. Box 339, Bloemfontein, ZA9300, South Africa

<sup>2</sup>Department of Physics, Shri Mata Vaishno Devi University, Katra-182320 (J&K), India

\*Corresponding author e-mail address: ankushbediyal@gmail.com; swarthc@ufs.ac.za

## 1. Introduction

White light production, using light emitting diodes (LED) with high efficiency, high color rendering index and low cost is the current challenge for scientific community, as the demand of energy is growing day by day. In this respect currently, tri-color (Red, Green, Blue) phosphor plus ultraviolet LED based strategy had been followed by the researchers because of the advent of InGaN based LEDs, in which there is a possibility to vary the emission wavelength of the GaN-based blue LEDs between 370 nm (band gap of pure GaN) and 470 nm by increasing the In (Indium) content in the InGaN devices [1]. Tb<sup>3+</sup> is a suitable choice among rare earth ions for green emission as it has relatively large absorption and bright green emission. Recently, alkali-alkaline borate based phosphor captured the scientific interest because of high melting point, low thermal conductivity, high thermal expansion coefficient, high thermal and chemical stability and strong absorption in the near-ultraviolet region and hence investigated for diverse application such as solid state lightning, display applications, photoinduced nonlinear optics etc [2]. A potential green emitting NaSrBO<sub>3</sub>:Tb<sup>3+</sup> (1-9 mol%) phosphor was synthesized by citrate gel combustion method and had been investigated for its potential applications. X-ray diffraction patterns confirmed the monoclinic phase of the phosphor. The phosphor emits intense green emission under near-UV and electron excitation. X-ray photoelectron spectroscopy was carried out to analyze the chemical states of the elements.

## 2. Results

Figure 1 presents the excitation and emission spectrum of the NaSrBO<sub>3</sub>:Tb<sup>3+</sup> phosphor. The phosphor emits intense green emission under 375 nm excitation due to the characteristics transitions <sup>5</sup>D<sub>4</sub>→<sup>7</sup>F<sub>6</sub> (488 nm), <sup>5</sup>D<sub>4</sub>→<sup>7</sup>F<sub>5</sub> (544 nm), <sup>5</sup>D<sub>4</sub>→<sup>7</sup>F<sub>4</sub> (586 nm) and <sup>5</sup>D<sub>4</sub>→<sup>7</sup>F<sub>3</sub> (622 nm) of Tb<sup>3+</sup> ions. The optimal molar concentration of Tb<sup>3+</sup> ions was found to be 7 mol%, after that concentration quenching occurs. The dipole-dipole interaction was found to be accountable for energy transfer between the Tb<sup>3+</sup> ions [3]. Figure 2 presents the cathodoluminescence (CL) spectra for different emission current and accelerating voltage by keeping the one constant at a time. The spectra shows the same characteristic emission peaks as found in the PL spectrum. Instead of that we also observed some weak emission peaks at 382 nm, 415 nm and 437 nm that correspond to the transitions from higher excited state of Tb<sup>3+</sup> (<sup>5</sup>D<sub>3</sub>) which were attributed to the low vibration energy of the BO<sub>3</sub><sup>3-</sup> groups. These weak emission peaks from the <sup>5</sup>D<sub>3</sub> level arose because of the inability of the BO<sub>3</sub><sup>3-</sup> groups to bridge the gaps between the higher levels of the Tb<sup>3+</sup> ion. The increase in the CL intensity with accelerating voltages is a good indication that this phosphor may also be used in field emission displays in addition to its possible application in LEDs. X-ray photoelectron spectroscopy results demonstrated that terbium was mostly presented in the (+3) valance state in the phosphor. The approximated Commission Internationale de l'Eclairage coordinates for the PL (0.31, 0.61) and CL (0.33, 0.57) were found to be very close to the well known green emitting phosphors. The obtained results suggest that the studied phosphor could be an ultimate choice for green emission in display applications.

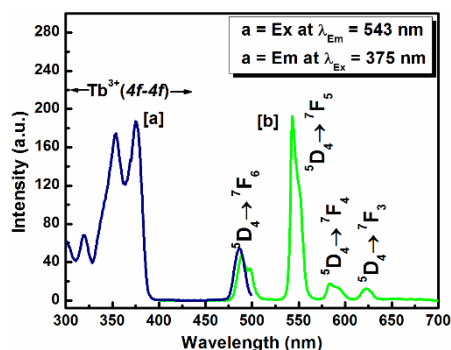


Fig. 1: PL excitation (a) and emission (b) spectrum of NaSrBO<sub>3</sub>:Tb<sup>3+</sup>

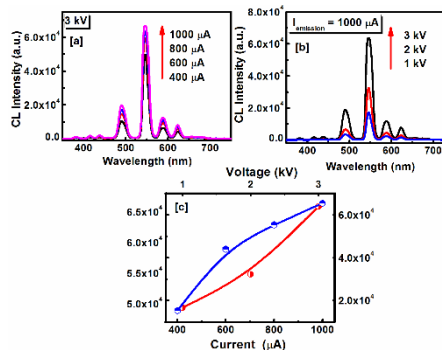


Fig. 2: CL emission spectra of NaSrBO<sub>3</sub>:Tb<sup>3+</sup> phosphor for (a) different beam currents and (b) voltages and (c) the maximum intensity as function of voltage and current.

## 3. References

- [1] Z. Xia, Z. Xu, M. Chen and Q. Liu, *Dalt Trans.*, **45**(2016)11214.
- [2] K. Bedyal, V. Kumar, V. K. Singh et al, *Nucl. Inst. Meth. B* **351**(2015) 27.
- [3] P. A. Nagpure, S. K. Omanwar, *J. Rare Earths*, **30** (2012) 856.

# Photoluminescence and thermoluminescence properties of BaGa<sub>2</sub>O<sub>4</sub>

L. L. Noto<sup>1\*</sup>, D. Poelman<sup>2</sup>, V. R. Orante-Barron<sup>3</sup>, R. Nyenge<sup>4</sup>, H. C. Swarf<sup>5</sup>, M. Chithambo<sup>6</sup>, B. M. Mothudi<sup>1</sup>, M. S. Dhlamini<sup>1\*</sup>

<sup>1</sup>Department of Physics, University of South Africa, P.O. Box 392, Pretoria ZA0003, South Africa

<sup>2</sup>Department of Solid State Sciences, University of Gent, Krijgslaan 281, S1, B-9000 Gent, Belgium

<sup>3</sup>Departamento de investigacion en Polimeros y Materiales de la Universidad de Sonora, Apartado Postal 130, Hermosillo, Sonora 83000, Mexico

<sup>4</sup>Kenyatta University, Nairobi, Kenya, P.O Box 43844-00100, Nairobi, Kenya

<sup>5</sup>Physics Department, University of the Free State, P. O. Box 339, Bloemfontein, 9300, South Africa

<sup>6</sup>Physics and Electronics department, Rhodes University, P.O. Box 94, Grahamstown 614 South Africa

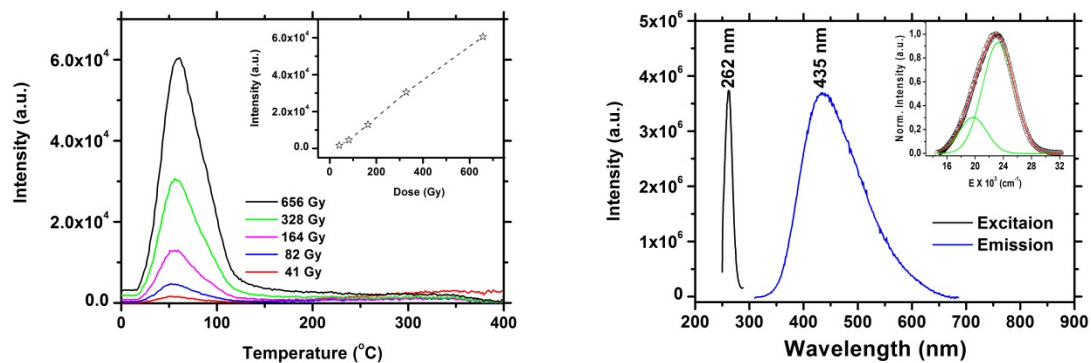
\*Corresponding Author: Dhlamms@unisa.ac.za, luyanda.noto@gmail.com

## 1. Introduction

Photoluminescence has found several applications in the industry, ranging from Light emitting diodes, Display devices, biological mapping and dosimetry, to mention a few. Luminescence can either be spontaneous or stimulated, where the earlier emerges from extrinsic defects or intrinsic defects with an activation energy that is equal or smaller than the thermal energy of the ambient temperature [1]. The latter, emerges from intrinsic defects with an activation energy that is greater than the thermal energy of the ambient temperature. In this case we are referring to these defect centers as F-centers, which have the capacity to trap and hold electrons. This phenomenon is important in dosimetry devices, and its characteristics are investigated through a thermoluminescence spectroscopy. Different models have been put to place to investigate the kinetics of the trapped electrons and to compute for the activation energy of the electrons. Such models include Chen's peak geometry, Initial Rise and Variable heating rate model, just to mention a few [2].

## 2. Results

A rare-earth free luminescent material was fabricated via solid state reaction method at 1200 °C for 5 Hrs. The starting reagents were Ga<sub>2</sub>O<sub>3</sub> and BaO, which were mixed together into a slurry using ethanol, then fired inside a furnace. A single phased compound was obtained, which matched with the BaGa<sub>2</sub>O<sub>4</sub> standard with a JCSPDS – 000 card numbers. The surface morphology and the distribution of the corresponding ions were probed using a Scanning Electron Microscopy (SEM) and an Energy Dispersive X-Ray Spectroscopy (EDX). The spontaneous and stimulated luminescence was measured using the Photoluminescence and Thermoluminescence Spectroscopy. Furthermore, the electron kinetics involved under stimulated luminescence were determined and the corresponding activation energy was approximated using the initial rise and the variable heating rate model.



## 3. References

- [1] L.L. Noto, PhD Thesis, University of the Free State, 2014.
- [2] McKeever SWS, *Thermoluminescence of Solids*, 1985, Cambridge University Press, New York

# Tailoring and optimization of optical properties of CdO thin films for optoelectronic applications

L. P. Purohit<sup>1\*</sup>, Trilok K. Pathak<sup>1,2</sup>, Vinod Kumar<sup>2,3</sup>, H. C. Swart<sup>2</sup>; Jeevitesh K. Rajput<sup>1\*</sup>

<sup>1</sup>Semiconductor Research Lab, Department of Physics, Gurukula Kangri University, Haridwar, India

<sup>2</sup>Department of Physics, University of the Free State, Bloemfontein, South Africa

<sup>3</sup>Photovoltaic Laboratory, Centre for Energy Studies, Indian Institute of Technology Delhi, New Delhi, India.

\*Corresponding author e-mail address: profppurohitphys@gmail.com; jeevitesh.phys@gmail.com

## 1. Introduction

CdO is an n-type II–VI semiconductor with a direct band gap (~2.3 eV) which is characterized by a high transmission, a wide band gap [1] and high conductivity due to moderate electron mobility and high carrier concentration contributed by shallow donors resulting from an inherent non-stoichiometry [2-3]. Structural and optical properties of highly oriented transparent CdO thin films of different molarity, synthesized by the sol-gel spin coating on glass were studied at room temperature. X-ray diffraction (XRD) patterns indicated that the CdO films from 0.2 M to 0.8 M solutions (with 0.2 M = M<sub>1</sub>, 0.5 M = M<sub>2</sub> and 0.8 M = M<sub>3</sub>) have a stable cubic structure with a (111) preferred orientation. Scanning electron microscopy images revealed that the films adopted a rectangular to cauliflower like morphology. The optical transmittance of the thin films was observed in the range 200-800 nm and it was found that the 0.2 M CdO (M<sub>1</sub>) thin films showed about 83% transmission in the visible region. The optical band gap energy of the thin films was found to be a direct allowed transition that varied from 2.10 to 3.30 eV with the increase in concentration. The photoluminescence spectra of the samples have violet to blue emission peaks centred at 435 nm. High conductivity CdO thin film may be used in solar cell and gas sensing applications.

## 2. Results

XRD analysis was performed to investigate the crystal phase as well as the average particle size of the CdO thin films. Fig. 1 displayed all the diffraction peaks of M<sub>1</sub>, M<sub>2</sub> and M<sub>3</sub> films. XRD spectra can be indexed as the face-centred cubic (FCC) CdO, which is well consistent with the JCPDS [Card No. 05-0640]. Intense peaks were observed at 2θ values of 33.54°, 38.76° and 55.65° corresponding to the (111), (200) and (220) crystal planes. Fig. 2 shows that the transmittance was the lowest in the visible region - about 50 to 60% for the M<sub>2</sub> film. This may be due to the largest grain size. The transmittance of the M<sub>1</sub> films was the highest (85%) in the visible region with respect to air due the smallest particles size. The average transmittance of the M<sub>3</sub> sample was 60% in the visible region with respect to air.

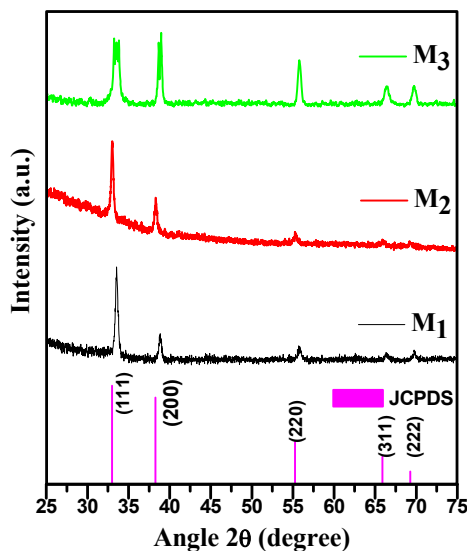


Fig 1: X-ray diffraction pattern of CdO thin film.

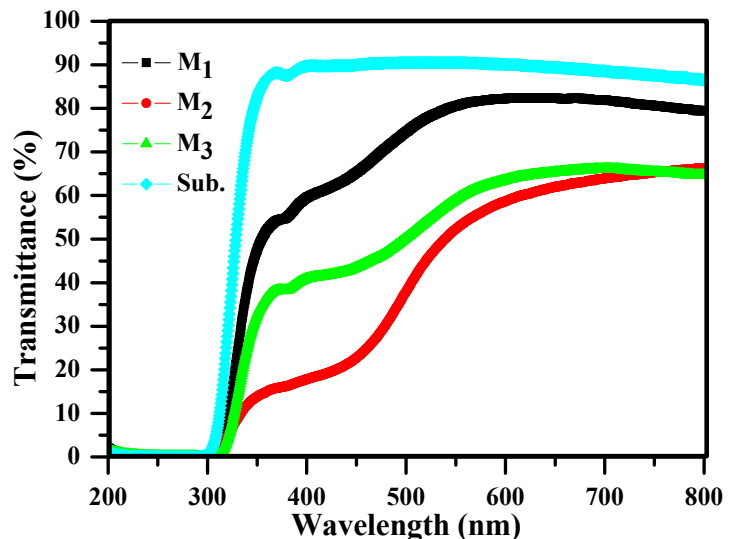


Fig. 2: Transmittance of CdO thin film with respect to air.

## 3. References

- [1] K. Karthik, S. Dhanuskodi, C. Gobinath, S. Sivaramakrishnan, *Spectrochimica Acta Part A: Mol. Bio. Spect.* **139** (2015) 7.
- [2] A. Zaouia, M. Zaouia, S. Kacimia, A. Boukourt, B. Bouhafsa, *Materials Che. and Phy.* **120** (2010) 98.
- [3] Trilok K. Pathak, Jeevitesh K. Rajput, Vinod Kumar, L.P. Purohit, H.C. Swart, R.E. Kroon, *J. Coll. Intf. Sci.* **487** (2017) 378.



# Photons and electron beam pumped luminescence characteristics of holmium activated $\text{CaMoO}_4$ phosphor

Anurag Pandey<sup>1\*</sup>, Vinod Kumar<sup>1</sup>, A. Yousif<sup>1</sup>, R. E. Kroon<sup>1</sup>, E. Coetsee<sup>1</sup>, H. C. Swart<sup>\*</sup>

<sup>1</sup>Department of Physics, University of the Free State, P. O. Box 339, Bloemfontein 9300, South Africa  
\*Corresponding authors e-mail address: anuragpandey439@gmail.com; swarhc@ufs.ac.za

## 1. Introduction

Luminescent materials are in continuous demand owing to their broad area of application fields [1]. Several studies reported on luminescence characteristics via changing the materials components, preparation methods, pumping source, etc. Among them molybdate based materials are very attractive due to broad absorption band of Mo-O bond near ultraviolet region. In this contest, we have selected  $\text{CaMoO}_4$  as host matrix because of its versatile features [2]. On the other hand holmium is chosen as activator because of its strong emission transition in visible region. Various studies are available on lanthanides activated  $\text{CaMoO}_4$  phosphors but no reports were available on holmium activated  $\text{CaMoO}_4$  phosphors pumped by electron beam. Facile auto combustion route is adopted to prepare the phosphor sample by using the  $(\text{NH}_4)_6\text{Mo}_7\text{O}_{24}\cdot 4\text{H}_2\text{O}$ ,  $\text{Ca}(\text{NO}_3)_2\cdot 4\text{H}_2\text{O}$  and  $\text{Ho}(\text{NO}_3)_3\cdot 5\text{H}_2\text{O}$  of highly pure (99.90-99.99%) analytical grade (Sigma Aldrich) as raw materials while urea was used as the organic fuel.

## 2. Results

We have prepared a well known and efficient  $\text{CaMoO}_4:\text{Ho}^{3+}$  phosphor by solution combustion method. The structural morphology of the present phosphor material is detailed on the basis of X-ray diffraction and Scanning electron microscopy studies (Fig. 1). Diffuse reflectance spectrum exhibits several transitions of dopant holmium ions whereas the band gap calculated was in well agreement of actual one of the host matrix. The photoluminescence investigations were done by recording excitation and emission spectra display strong green emission from the phosphor while cathodoluminescence spectra and decay profile (Fig. 2) shows degradation in observed luminescence intensity. The results were explained on the basis of X-ray photo electron spectroscopy observations before and after irradiation of sample.

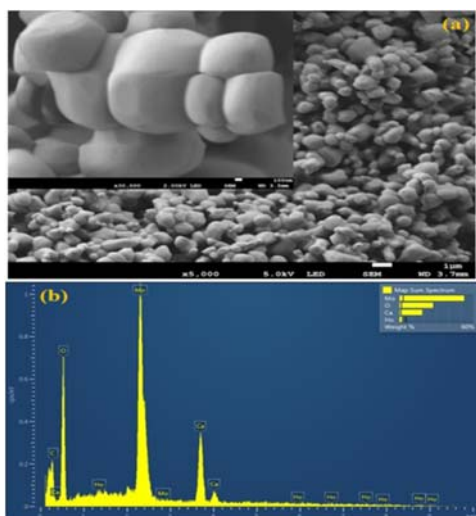


Fig. 1: SEM and EDS images of the  $\text{CaMoO}_4:\text{Ho}^{3+}$  phosphor.

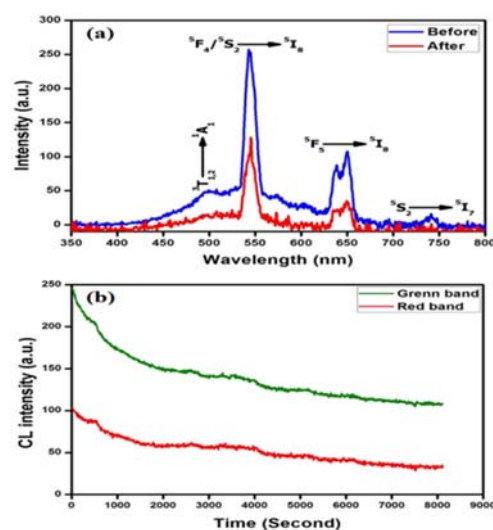


Fig. 2: CL spectra and corresponding decay profile of  $\text{CaMoO}_4:\text{Ho}^{3+}$  phosphor.

## 3. References

- [1] A. Pandey, V. K. Rai, V. Kumar, V. Kumar and H. C. Swart. *Sensor Actuat. B-Chem.* **209** (2015) 352.
- [2] B. P. Singh, A. K. Parchur, R. S. Ningthoujam, A. A. Ansari, P. Singh and S. B. Rai. *Dalton Trans.* **43** (2004) 4779.

# Photoluminescence and structural properties of single and double MOVPE-grown InGaSb/GaSb quantum wells

**Chinedu C. Ahia<sup>1\*</sup>, Johannes R. Botha<sup>1</sup>, E. J. Olivier<sup>2</sup>**

<sup>1</sup>Department of Physics, PO Box 77000 Nelson Mandela Metropolitan University, Port Elizabeth, South Africa

<sup>2</sup>Centre for High Resolution Transmission Electron Microscopy, Nelson Mandela Metropolitan University, South Africa

\*Corresponding author e-mail address: chinedu@aims.ac.za

## 1. Introduction

The structural and photoluminescence (PL) characterization of InGaSb quantum well (QW) structures grown on GaSb substrate (100) using atmospheric pressure Metalorganic Vapor Phase Epitaxy (MOVPE) is presented in this work. Both structures (single and double-InGaSb QWs) were inadvertently formed during an attempt to grow capped InSb/GaSb quantum dots (QDs). This study is inspired by the significant interest and controversy over the years concerning the emission wavelength of InSb/GaSb QDs, with some groups [1-3] having reported emission in the near-infrared (0.70 – 0.75 eV) region, and others [4] in the mid-infrared (0.3 – 0.5 eV) region. The quenching of the PL from the QWs at  $\sim 0.74$  eV (see Figure 1) with increasing temperature, which can be described by a thermal activation energy (see Arrhenius plots of the 0.74 eV-lines for the two samples in Figure 2) will be discussed in detail in this paper. Bright field cross-sectional TEM of the sample containing two QWs revealed the presence of threading dislocations in contrast with the single QW sample for which no evidence of structural defects was found. The effect of spacer thickness on the optical properties of the double QWs will also be demonstrated in this work via simulation, by applying a model which makes use of the self-consistent Schrodinger-Poisson-current calculation to simulate a 1D band alignment representation of the energy levels and wave functions of the samples using the information (composition and thickness) obtained from TEM.

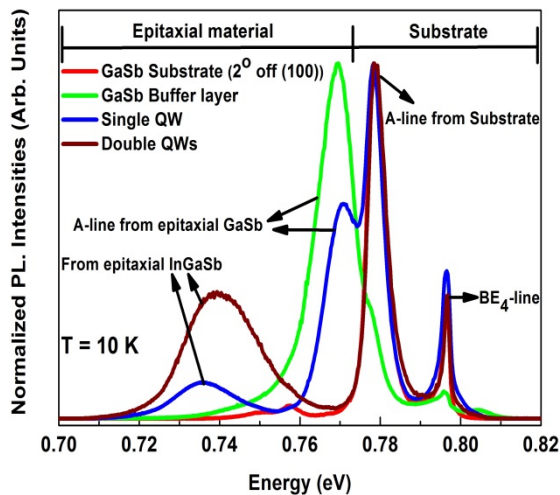


Fig. 1: PL spectra of both single and double InGaSb/GaSb QWs, GaSb substrate and substrate with buffer layer.

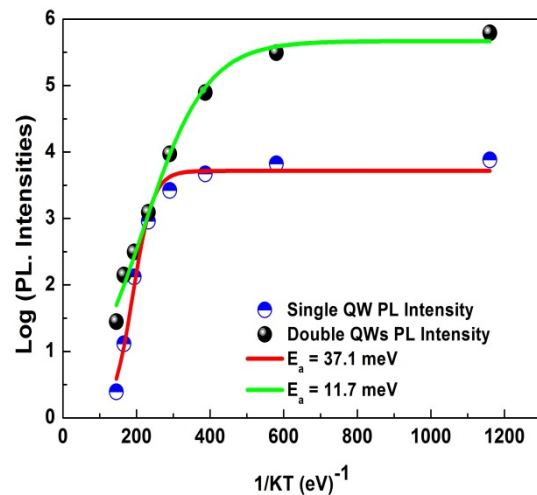


Fig. 2: Arrhenius plot of the integrated PL intensity of the low energy PL for both samples.

## 2. References

- [1] E. Alphandery, R. J. Nicholas, N. J. Mason, B. Zhang, P. Mock and G. R. Booker, *Applied Physics Letters* **74** (1999) 2041.
- [2] R. J. Nicholas, P. A. Shields, R. A. Child, L. J. Li, E. Alphandery, N. J. Mason, C. Bumby, *Physica E* **20** (2004) 204.
- [3] S. Shusterman, Y. Paltiel, A. Sher, V. Ezersky, Y. Rosenwaks, *Journal of Crystal Growth* **291** (2006) 363.
- [4] V. Tasco, N. Deguffroy, A. N. Baranov, E. Tournie, B. Satpati, A. Trampet, M. S. Dunaevskii and A. Titkov, *Applied Physics Letters* **89** (2006) 263118.

# Atmospheric pressure-MOVPE growth of GaSb/GaAs quantum dots

**Ngcali Tile<sup>1\*</sup>, Christian Chinedu Ahia<sup>1</sup>, Johannes Reinhardt Botha<sup>1</sup>**

<sup>1</sup>Physics department, Nelson Mandela Metropolitan University, Port Elizabeth, South Africa

\*Corresponding author e-mail address: s213506696@nmmu.ac.za

## 1. Introduction

Quantum dots (QDs) formed through the creation of GaSb nanostructures in a GaAs matrix have some unique and appealing properties that are being continually exploited. This system has a type-II band alignment, providing strong spatial confinement for holes, and only binding electrons via Coulomb interaction [1, 2]. This leads to optical properties different from type-I QDs, such as a long radiative lifetime, a dot-shape dependent oscillator strength, and large tunability of emitted/absorbed photons. It has been shown recently that GaAs based p-i-n solar cells containing layers of GaSb quantum dots/rings fabricated by molecular beam epitaxy (MBE) have improved efficiency at longer wavelengths of up to 1.5  $\mu\text{m}$  [3]. In order to improve this device functionality there is a need to understand the formation of these dot structures in order to control/tune their structural properties and therefore improve their optical and electrical properties.

Just like MBE, metalorganic vapor phase epitaxy (MOVPE) in principle also provides the control over the deposition conditions required to systematically study QD formation. In this work we show the fabrication of GaSb QDs in a GaAs matrix using an atmospheric pressure (AP) MOVPE system. Tertiarybutylarsine, triethylgallium (TEG), and trimethylantimony (TMSb) are used as arsenic, gallium, and antimony sources, respectively. The influence of TMSb/TEG ratio and growth temperature on the size, morphology and density of uncapped QD structures, as well as on the optical properties of capped QD structures, will be presented in this paper.

## 2. Results

For the best uncapped dots (Fig. 1), the average dot height, base diameter and density are 5 nm, 45 nm and  $4.5 \times 10^{10} \text{ cm}^{-2}$ , respectively. Photoluminescence (PL) measurements of a capped QD sample (Fig. 2) showed peaks for the QDs at 1.13 eV and for the wetting layer (WL) at 1.26 eV, proving the successful fabrication of GaSb/GaAs quantum dot structures [4]. Variable temperature PL measurements of the QD sample showed the decrease in the intensity of the WL peak to be faster than that of the QD peak. The WL peak also shifted more strongly to lower energies compared to the QD peak. An increase in excitation power caused the QD and WL peaks to shift to higher energies. This is attributed to the electrostatic band bending leading to triangular potential wells, typical of type II alignment between GaAs and strained GaSb.

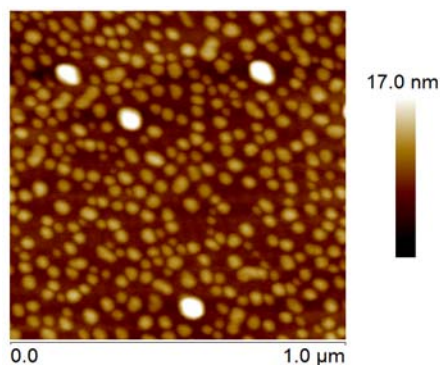


Fig. 1: AFM image of GaSb self-assembled QDs on a GaAs buffer grown on GaAs substrate.

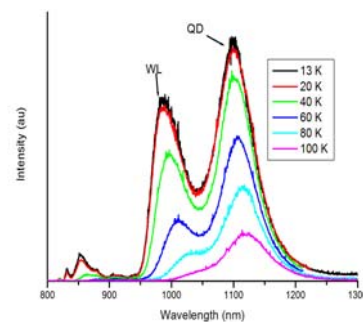


Fig. 2: Temperature dependent PL of AP-MOVPE grown capped GaSb/GaAs QD structure.

## 3. References

- [1] R.A Hogg, K. Suzuki, K. Tachibana, L. Finger, K. Hirakawa and Y. Arakawa, *Appl. Phys. Lett.* **72** (1998) 2856.
- [2] L. Muller-Kirsch, R. Heitz, U.W. Pohl, D. Bimberg, I. Hausler, H. Kirmse and W. Neumann, *Appl. Phys. Lett.* **79** (2001) 1027.
- [3] P.J. Carrington, A.S. Mahajumi, M.C. Wagener, J.R. Botha, Q. Zhuang, and A. Krier, *Physica B* **407** (2012) 1493.
- [4] K. Suzuki, R. A. Hogg, and Y. Arakawa, *J. Appl. Phys.* **85** (1999) 8349.

# Photoluminescence measurements of $\text{InAs}_{(1-x)}\text{Sb}_x$ lattice matched to GaSb

S. R. Dobson<sup>1\*</sup>, V. Wagener<sup>1</sup>, M. C. Wagener<sup>1</sup>, J. R. Botha<sup>1</sup>

<sup>1</sup>Physics Department, PO Box 77000, NMMU, Port Elizabeth, 6031

\*Corresponding author e-mail address: Stephen.Dobson@nmmu.ac.za

## 1. Introduction

The alloy  $\text{InAsSb}$  has the lowest band gap energy among all III-V semiconductors and therefore has received a great deal of attention as an important material for infrared optoelectronic devices.  $\text{InAsSb}$  photodetectors have the potential to reach wavelengths of up to  $8.5 \mu\text{m}$  (bandgap energy of  $146\text{meV}$ , with a bowing parameter of  $670\text{meV}$ ) [1]; however, to reach these wavelengths requires high quality thin films with few defects and impurities. A key issue is the lack of substrates available that provide lattice matching to the various compositions of  $\text{InAsSb}$  that will operate at these longer wavelengths. To date, the best performing  $\text{InAsSb}$  devices are lattice matched to GaSb substrates. This requires a composition of  $\text{InAs}_{0.911}\text{Sb}_{0.089}$ , allowing for device operation between  $3 \mu\text{m}$  and  $4 \mu\text{m}$  [2]. The purpose of this study is to produce high quality thin films, between  $2 \mu\text{m}$  and  $4 \mu\text{m}$  in thickness, of  $\text{InAs}_{0.911}\text{Sb}_{0.089}$  on 2-inch diameter GaSb and GaAs substrates. Growth is conducted via metal organic chemical vapour deposition (MOCVD). An initial buffer layer of GaSb or InAs is grown (in the nanometer thickness range) in order to ensure strain free  $\text{InAsSb}$  thin films. High resolution X-ray diffraction (HRXRD) is used to precisely determine the composition of the thin films and also investigate uniformity across the wafer. Photoluminescence (PL), using a Fourier-transform infrared (FTIR) spectrometer, is employed to further explore the quality and purity of the  $\text{InAsSb}$  thin films.

## 2. Results

Photoluminescence spectra (PL) of  $\text{InAsSb}$  grown on GaAs substrate with an InAs buffer, are shown in figures 1 and 2. The composition obtained from HRXRD (insert to figure 1) is  $\text{InAs}_{0.914}\text{Sb}_{0.086}$ , which gives the same lattice parameter as GaSb. The PL spectra contain two clear peaks, the lower energy peak being ascribed to donor-acceptor pair (DAP) recombination and the higher energy peak to band-to-band (B-B) recombination.

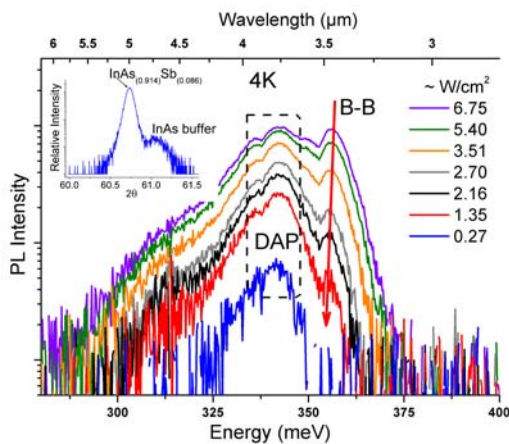


Fig. 1: Power dependent PL spectra of  $\text{InAsSb}$  matched to GaSb, taken at 4K. Top left includes an XRD image showing an  $\text{InAs}_{(1-x)}\text{Sb}_x$  composition of  $x \sim 0.086$ .

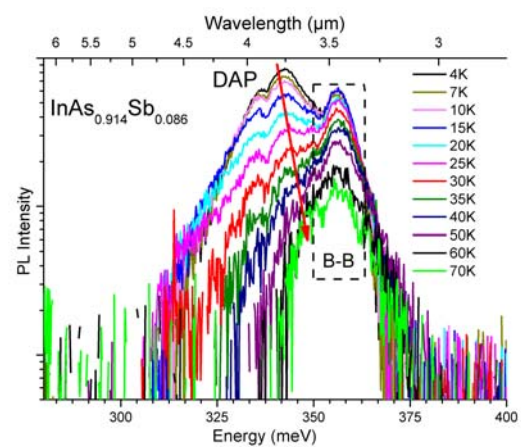


Fig. 2: Temperature dependent PL spectra of  $\text{InAsSb}$  matched to GaSb. PL shows two peaks, related to B-B recombination and another related to DAP.

## 3. References

- [1] P.T. Webster, N.A. Riordan, S. Liu, E.H. Steenberg. *et al. J. Appl. Phys.* **118(24)** (2015) 245706.
- [2] Z.M.Fang, K.Y. Ma, D.H. Jaw, *et al. J. Appl. Phys.* **67(11)** (1990) 7037.

# Optical and structural properties of Type-II quantum dots

A. Ben Daly<sup>1,2</sup>, V. Craciun<sup>3\*</sup>, I. Alexandru<sup>4</sup>, S. Lazar<sup>4</sup>, B. S. Vasile<sup>5</sup>, E-Laura Ursu<sup>6</sup>, A. Lemaitre<sup>7</sup>, F. Iacomi<sup>2</sup>

<sup>1</sup>Laboratoire Matériaux, Molécules et Applications, Institut Préparatoire aux Études Scientifiques et Techniques, BP 51, 2070 La Marsa, Université de Carthage, Tunis, Tunisia

<sup>2</sup>Faculty of Physics, Alexandru Ioan Cuza University of Iasi, Iasi, Romania

<sup>3</sup>National Institute for Laser, Plasma and Radiation Physics, Magurele, Romania

<sup>4</sup>Nanotechnology, FEI Company, Eindhoven, The Netherlands

<sup>5</sup>Faculty of Applied Chemistry and Material Science, Polytechnic University of Bucharest, Bucharest, Romania

<sup>6</sup>Centre of Advanced Research in Bionanoconjugates and Biopolymers "Petru Poni", Institute of Macromolecular Chemistry, Iasi, Romania

<sup>7</sup>Laboratoire de Photonique et Nanostructures, CNRS, UPR 20, Route de Nozay, F-91460 Marcoussis, France

\*Corresponding author e-mail address: valentin.craciun@inflpr.ro

## 1. Introduction

Photoluminescence (PL) and Raman spectroscopy are powerful tools to study the optical properties in self-assembled type-II quantum dot (QD) structures, which are potentially attractive for device applications such as memories [1] and spin-qubit [2] because of characteristics arising from their specific band alignment [3, 4]. One of the type-II QDs obtained through the Stranski-Krastanov growth mode with conduction states localized in the band-gap, is  $\text{Al}_x\text{In}_{1-x}\text{As}$  deposited on another material with different lattice parameter, e.g.,  $\text{Al}_y\text{Ga}_{1-y}\text{As}$ .  $\text{AlInAs}$  is a III-V semiconductor, having the zinc blende crystal structure. The lattice parameter of  $\text{Al}_x\text{Ga}_{1-x}\text{As}$  can be written  $a_0(x) = 5.656 + 0.00809x$  in units of  $\text{Å}$  at 300K [5]. However,  $\text{AlAs}$  has a larger lattice parameter than  $\text{GaAs}$ , thus thin  $\text{AlAs}$  films deposited on  $\text{GaAs}$  substrates are compressively strained.  $\text{GaAs}$  and  $\text{InAs}$  are direct-gap semiconductors, while  $\text{Al}_x\text{Ga}_{1-x}\text{As}$  has a direct bandgap for  $x < 0.46$ , and an indirect one at higher aluminium composition [6]. The maxima of the uppermost (heavy and light holes) valence bands of all III-V semiconductors are situated at the  $\Gamma$  point; however, there are three conduction band minima (at the  $\Gamma$ , L and X points). The relative arrangement of these minima determines the nature of the bandgap. The bottom of the conduction band is located at the  $\Gamma$  point, the semiconductor has a direct bandgap.

## 2. Results

High resolution X-ray diffraction investigations showed that the multilayer structure is epitaxial, having the in-plane lattice parameters equal to those of the substrate. High resolution transmission electron microscopy confirmed that the multilayer structure was epitaxial. The PL spectra of the samples obtained at low temperature ( $T=6\text{K}$ ) are shown in Fig. 1. The broad PL signal comes from optical transitions within the  $\text{Al}_{0.55}\text{In}_{0.45}\text{As}$  QDs. We clearly showed the existence of the two indirect type-II transitions:  $X\text{-S}_h$  and  $X\text{-P}_h$  [7]. The  $X\text{-S}_h$  transition was observed at lower energies, around 1.926eV. We have also analyzed the Raman shift of the QD with different aluminum concentrations (see Fig. 2). The narrow line systematically measured at  $382\text{-}397\text{ cm}^{-1}$ , is attributed to the LO  $\text{AlGaAs}$  ( $\text{AlAs}$ -like) phonon of the upper  $\text{AlGaAs}$  layer [8]. The LO phonon shifts toward lower frequency with the increase of the Al content.

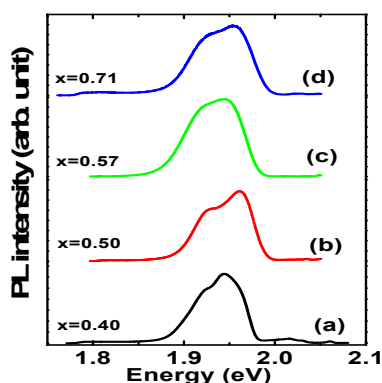


Fig. 1: Low-temperature (6 K) PL spectra of the studied samples.

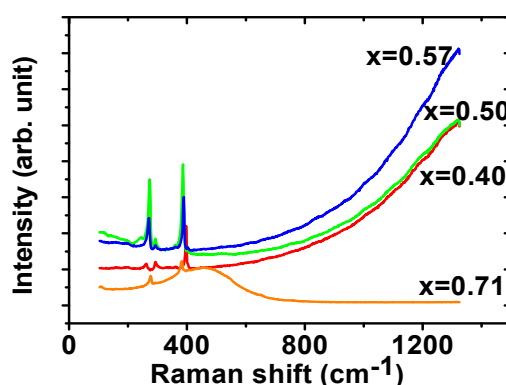


Fig. 2: Raman spectra of the studied samples obtained at low temperature ( $T=6\text{K}$ ).

## 3. References

- [1] M. C. Bodefeld, R. J. Warburton, K. Karrai, J. P. Kotthaus, G. Medeiros-Ribeiro and P. M. Petroff, *Appl. Phys. Lett.* **74** (1999) 1839.
- [2] D. Loss, and D. P. DiVincenzo, *Phys. Rev. A* **57** (1998) 120.
- [3] F. Hatami, N.N. Ledentsov, M. Grundmann, J. Bohrer, F. Heinrichsdorff, M. Beer, D. Bimberg, et al. *Appl. Phys. Lett.* **67** (1995) 656.
- [4] M. Geller, C. Kapteyn, L. Muller-Kirsch, R. Heitz, and D. Bimberg, *Appl. Phys. Lett.* **82** (2003) 2706.
- [5] S. Adachi, *GaAs and related materials, bulk semiconducting and superlattice properties* (World Scientific, Singapore, 1994).
- [6] K. Ohdaira, H. Murata, S. Koh, M. Baba, H. Akiyama, R. Ito and Y. Shiraki, *J. of the Physical Society of Japan*, **72** (2003) 3271-3275.
- [7] R. Neffati, I. Saidi, S. Ben Radhia, A. Ben Daly, M. A. Maaref, K. Boujdaria, et al. *Superlattices and Microstructures* **97** (2016) 529-535.
- [8] O.F. Kilonys, V.V. Strelchuk, T.S. Shamirzaev. A. S. Romanyuk, P. Tronc, *Appl. Surface Science*, **260** (2012) 47-50.

# Recent advances in rare earth doped alkali-alkaline earth borates for solid state lighting applications: a mini review

Shefali Verma<sup>1</sup>, Kartikey Verma<sup>1</sup>, Deepak Kumar<sup>1</sup>, Sudipta Som<sup>2</sup>, Vishal Sharma<sup>3</sup>, Vijay Kumar<sup>1,2\*</sup>, Hendrik C. Swart<sup>2\*</sup>

<sup>1</sup>Department of Applied Physics, Chandigarh University, Gharuan, Mohali (Punjab), India

<sup>2</sup>Department of Physics, University of the Free State, Bloemfontein, South Africa

<sup>3</sup>Institute of Forensic Science & Criminology, Panjab University, Chandigarh, India

\*Corresponding author e-mail address: vj.physics@gmail.com; swarthc@ufs.ac.za

## 1. Introduction

The scientific society acknowledged 2015 as the International Year of Light and Light-based Technologies owing to the significance of lighting and display devices in every part of the mankind evolution [1]. The light-based technologies have changed different phases of science and technology to a greater extent. Noteworthy research endeavours have been aimed to discover for eco-friendly, better performance, cost and energy efficient phosphor materials for the application in the solid-state lighting devices [1-2]. The drive of luminescent materials with superior optical and photoluminescence properties in a wide range of areas has shared the research efforts in this sector aimed in the direction of achieving better material features.

Recently, the alkali-alkaline earth borates have gained profound interest due to their low phonon energy, unique spectroscopic behaviour, chemical durability, high thermal stability, cost effective synthesis procedure and high absorption in the UV region, etc. These properties make them better candidates to be utilized in specific technological applications such as in display devices, temperature sensors, solar cell, bio-imaging, optoelectronics devices, etc. This review will cover the broad aspects of rare earth (RE) doped mixed borates for tuneable colour emissions, and will be beneficial to the researchers involved in this area. Much of the material is drawn from the personal experience in synthesizing, characterizing, and applying luminescent solids since the twentieth century to the modern development of the practical devices. In addition, this review will be of huge interest to researchers who are working towards their doctorate degrees in these areas. A platform for all researchers is also made available as it will cover considerable background from past to current literature, together with acronyms used. This article envelops the fundamental knowledge and latest innovations of the research and development in the areas of RE doped mixed borates for light-based technologies.

## 2. Results

Till date, a large number of methods have been used for obtaining RE doped mixed borate phosphors that are used for making devices for different applications [2-4]. Because of the large number of crystal structures, alkali-alkaline earth borates are potential host to investigate phosphors with better luminescence properties [3]. In this regard, a group from China investigated that Dy<sup>3+</sup>, Tm<sup>3+</sup> and Eu<sup>3+</sup> codoped showed a great potential for use as single-component phosphors for warm ultraviolet white light-emitting diodes [3]. Later, the same group has synthesized Sm<sup>3+</sup> doped K<sub>2</sub>Sr<sub>4</sub>(BO<sub>3</sub>)<sub>3</sub> phosphors by using a solid state reaction method [4]. They have proposed an energy transfer from one Sm<sup>3+</sup> ion to another Sm<sup>3+</sup> ion by a simple energy level diagram as shown in Fig. 1 [4].

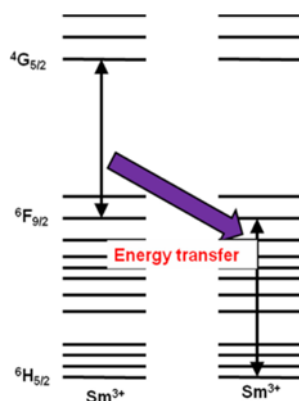


Fig. 1. Schematic diagram of cross relaxation process in the self-concentration quenching of Sm<sup>3+</sup> ions in K<sub>2</sub>Sr<sub>4</sub>(BO<sub>3</sub>)<sub>3</sub>:Sm<sup>3+</sup>.

## 3. References

- [1] V. Kumar, S. Som, S. Dutta, S. Das, H. C. Swart, *Mater. Design* 93 (2016) 203.
- [2] S. Chun-Yi, W. Xin-Long, Z. Xiao, Q. Chao, L. Peng, S. Zhong-Min, Z. Dong-Xia, S. Guo-Gang, S. Kui-Zhan, W. Han, L. Jing, *Nat. Commun.* 4 (2013) 2717.
- [3] Y. Zhang, W. Liu, M. Ji, B. Wang, Y. Kong, and J. Xu, *Opt. Mater. Express* 2(1), 92–101 (2012).
- [4] L. Wu, M. Ji, H. Wang, Y. Kong, Y. Zhang, *Opt. Mater. Express* 4(8) (2014) 1535.

# Hydrogen-related defects in Al<sub>2</sub>O<sub>3</sub> layers grown on *n*-type Si by the atomic layer deposition technique

Vladimir Kolkovsky<sup>1\*</sup>, Ronald Stübner<sup>1</sup>

<sup>1</sup>IPMS Fraunhofer, Dresden Maria-Reiche Str. 2 01109 Dresden Germany  
\*Corresponding author e-mail address: uladimir.kalkouski@ipms.fraunhofer.de

## 1. Introduction

Aluminum oxide thin films, which provide excellent surface passivation of *n*- and *p*-type Si, can be used in different applications of modern microelectronics and photovoltaics. The atomic layer deposition (ALD) technique allows to grow the alumina layers on large wafers with a high degree of homogeneity, reproducibility and a considerably lower defect concentration in comparison to the sputtering techniques. However, the growth of Al<sub>2</sub>O<sub>3</sub> films by the ALD technique is inseparably linked with the unintentional introduction of hydrogen into these layers since di-ionized water is used as a precursor. The presence of hydrogen can modify the electrical properties of alumina layers and lead to undesirable effects in microelectronic and photovoltaic devices. Until now no experimental data about the influence of H on the electrical properties of Al<sub>2</sub>O<sub>3</sub> grown on *n*-type Si exists in the literature. In the present study we analyze the electrical properties of Al<sub>2</sub>O<sub>3</sub> films grown with different thicknesses by the ALD technique before and after annealing in Ar and H atmospheres at different temperatures. We show that the introduction of H results in the formation of a negative charge in alumina layers.

## 2. Results

The electrical and structural properties of alumina films grown by the atomic layer deposition technique on *n*-type Si with different thicknesses varying from 15 nm to 150 nm are analyzed. We show that alumina layers with a thickness of more than 60 nm indeed provide an excellent surface passivation with a density of interface states below  $1 \times 10^{10} \text{ cm}^{-2} \text{ eV}^{-1}$ . The role of a post-deposition annealing in hydrogen and argon atmosphere and the influence of a dc H plasma treatment performed at different temperatures on these layers is investigated. The heat treatments in H atmosphere result in the introduction of negatively charged defects in the alumina films (see Fig. 1) while these defects are not observed after annealing at low temperatures (around 320 K-370 K) in Ar atmosphere. The concentration of these defects increases with a higher H content in the alumina films. The origin of these traps is discussed. The presence of the additional negative charges in the Al<sub>2</sub>O<sub>3</sub> films can be beneficial for photovoltaic applications. However, it can be undesirable for the microelectronic devices such as capacitive micromachined ultrasonic transducers or bimorph actuators.

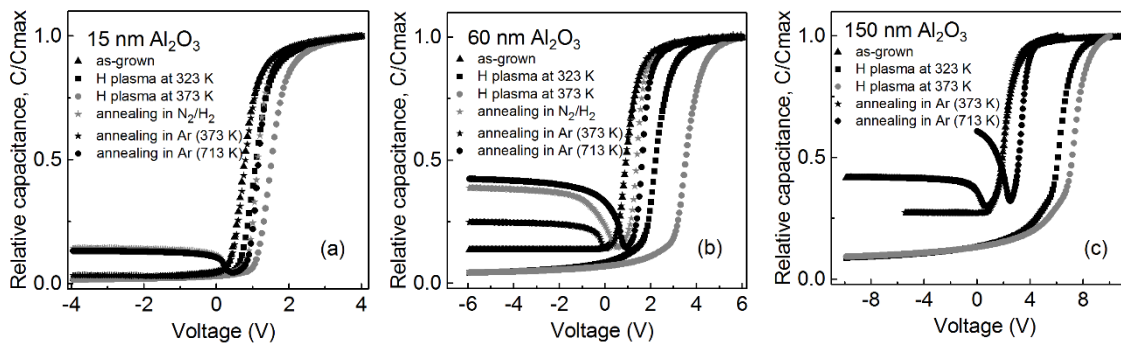


Fig. 1: C-V characteristics recorded at 100 kHz for the structures with 15 nm (a), 60 nm (b), and 150 nm (c) Al<sub>2</sub>O<sub>3</sub> before and after various heat treatments in Ar and H atmosphere.

# Effect of Sm doping on the structural and optical properties of ZnO nanorods grown by chemical bath deposition

**Mustafa Ahmed<sup>1,2\*</sup>, Walter Meyer<sup>1</sup>, Jackie Nel<sup>1</sup>**

<sup>1</sup>Department of Physics, University of Pretoria, Private bag X 20, Hatfield 0028, South Africa

<sup>2</sup>Departments of Physics, University of Khartoum, Faculty of Education, P O Box 406, Sudan

\*Corresponding author e-mail address: Mustafa.ahmed@up.ac.za

## 1. Introduction

Recently, one-dimensional (1D) semiconductor nanomaterials such as nanowires, nanorods, nanotubes and nanobelts have attracted much interest due to their unique properties and potential use in a wide range of device such as photodiodes [1], single electron transistors [2] and sensing applications [3]. 1D structures of ZnO having a wide band gap (3.37 eV) and large exciton binding energy (60 meV) at room temperature have been studied intensively [4]. One of the most effective ways to enhance the electrical and optical properties of ZnO is the doping with some cations. For example, rare-earth (RE) elements are usually used as cations in some of the host materials, because of their high fluorescence efficiencies and very sharp fluorescence bands [5]. In this work, we report on the synthesis and characterization of RE samarium (Sm) doped ZnO nanorods with doping concentrations ranging from 0 to 5 at. %. These nanorods were synthesised and deposited on an indium tin oxide (ITO) substrate using a simple two step chemical bath deposition method at 85 – 90°C. The effects of doping on the structural and optical properties were investigated.

## 2. Results

The room temperature X-ray diffraction spectroscopy (XRD) pattern of as-prepared ZnO and Sm doped ZnO nanorods are shown in Figure 1. The XRD pattern shown in Figure 1 revealed that the ZnO nanorods have the wurtzite crystal structure. Figure 2 shows the morphology of as-prepared samples obtained using scanning electron microscopy (SEM). Furthermore, results from photoluminescence spectroscopy (PL), UV-visible spectroscopy (UV-vis), and Raman spectroscopy as well as X-ray photoelectron spectroscopy (XPS) will be described in more detail.

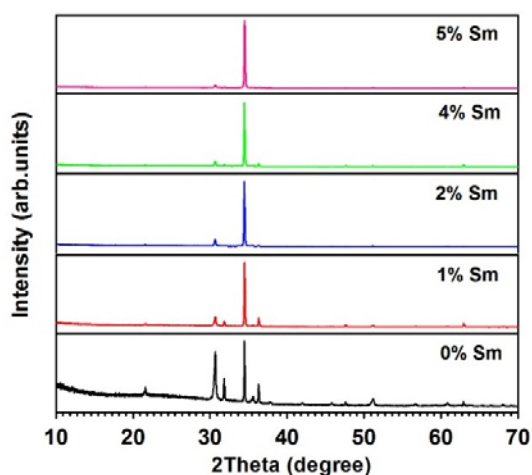


Fig. 1: XRD spectra of pure and Sm doped ZnO nanorods with different concentrations doping.

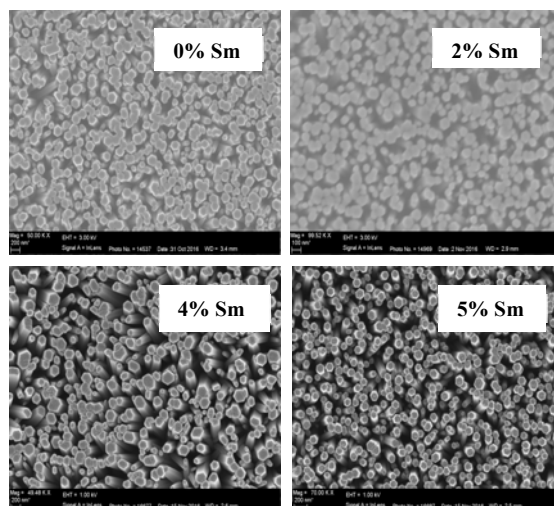


Fig. 2: SEM images of pure (top left) and Sm doped ZnO nanorods (top right, bottom left and bottom right) with concentrations doping.

## 3. References

- [1] L. Wang, R.X. Yan, Z.Y. Hao, L. Wang, J.H. Bao, X. Wang, Q. Peng and Y.D. Li. *Angew. Chem. Int. Ed.* **44** (2005) 6054.
- [2] F. Vetrone, J.C. Boyer and J.A. Capobianco. *Adv. Mater.* **16** (2005) 23.
- [3] L.F. Dong, Z.L. Cui and Z.K. Zhang. *Nano. Struct. Mater.* **8** (1997) 815.
- [4] G.C. Yi, C. Wang and W.I.I. Park. *Semicond. Sci. Technol.* **20** (2005) 22.
- [5] D. K. Sharma, K.K. Sharma and V. Kumar. *J. Mater. Sci: Mater Electron.* **27** (2016) 10330.



# Influence of NiO as intermediate layer on the properties of ZnO grown on Si by chemical bath deposition

S. R. Tankio Djiokap<sup>1\*</sup>, Z. N. Urgessa<sup>1</sup>, C. M. Mbulanga<sup>1</sup>, C. Kameni Boumenou<sup>1</sup>, A. Venter<sup>1</sup>, J. R. Botha<sup>1</sup>

<sup>1</sup>Department of Physics, Nelson Mandela Metropolitan University, P.O. Box 77000, Port Elizabeth 6031, South Africa  
\*Corresponding author e-mail address: stive.tankiodjiokap@nmmu.ac.za

## 1. Introduction

ZnO is a direct wide band gap (3.37 eV) semiconductor and has a large exciton binding energy of 60 meV. These unique properties provide a solid platform for optoelectronic applications such as light emitting diodes (LEDs) [1]. However, stable p-type doping still remains challenging and therefore ZnO homojunction devices are still not commercially available. Different p-type substrates (GaN, SiC,...) have been combined with n-type ZnO to build heterojunctions[2-3]. Due to its availability and cheaper price, Si substrate is an attractive alternative for ZnO-based devices. However, the large difference between its band gap (1.12 eV) and that of ZnO leads to a large valence band offset and a small conduction band offset. This leads to the injection of electrons into the silicon substrate, and minimize emission on the ZnO side of the heterojunction. Some wide band gap materials (MgO, AlN) have been investigated as electron-blocking layer between silicon and ZnO [4-5]. In the present study, NiO is used as intermediate layer. In addition to acting as an electron-blocking layer, NiO is native p-type and may also supply holes to the ZnO. This paper focuses on the structural and optical properties of ZnO/NiO/Si.

## 2. Results

Ni was resistively evaporated onto p-type Si substrate and subsequently annealed in oxygen, which produced NiO films. Chemical bath deposition was then employed to prepare ZnO nanorods. Fig. 1 shows the XRD patterns of ZnO/Si and ZnO/NiO/Si. Peaks resulting from diffraction in both ZnO and NiO can be seen. The (002) ZnO peak is found to be the most dominant, which indicates that the ZnO grows preferentially with its c-axis perpendicular to the substrate. The (111) and (200) peaks observed for NiO is ascribed to its polycrystalline nature. Fig. 2 displays the room temperature photoluminescence of ZnO/Si and ZnO/NiO/Si. Both spectra exhibit two distinct peaks. The UV emission at around 3.29 eV is associated with free exciton recombination, whereas the broad visible emission band around 2.25 eV is usually ascribed to defect-related emission [6]. The intensity ratios  $I_{UV}/I_{vis}$  were found to be  $\sim 9$  for both samples, which indicate that the concentrations of native defects are almost the same. The electrical properties (current-voltage) have also been investigated and will be presented in this paper.

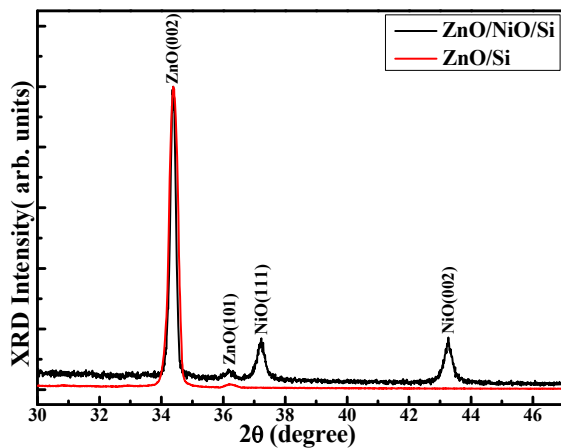


Fig. 1: Normalized XRD patterns of ZnO/Si and ZnO/NiO/Si

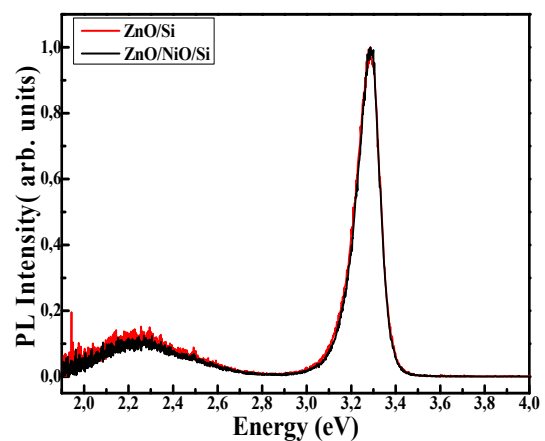


Fig. 2: PL spectra of ZnO/Si and ZnO/NiO/Si

## 3. References

- [1] D.M. Bagnall, Y.F. Chen, Z. Zhu, T. Yao, S. Koyama, M.Y. Shen and T. Goto, *Appl. Phys. Lett.* **70** (1997) 2230.
- [2] S.P. Chang, R.W. Chuang, S.J. Chang, Y.Z. Chiou and C.Y. Lu, *Thin Solid Films* **517** (2009) 5054.
- [3] S. Li, M.E. Ware, J. Wu, V.P. Kunets, M. Hawkrige, P. Minor, Z. Wang, Z. Wu, Y. Jiang, G.J. Salamo, *J. Appl. Phys.* **112** (2012) 053711
- [4] B.O. Jung, J.H. Lee, J.Y. Lee, J. H. Kim and H. K. Cho, *Journal of The Electrochemical Society*, **159** (2012) 102.
- [5] W. Wang, C. Chen, G. Zhang, T. Wang, H Wu, Y. Liu and C. Liu, *Nanoscale Research Letters* **10** (2015) 91.
- [6] W.Z. Liu, H.Y. Xu, J.G. Ma, C.Y. Liu and Y.X. Liu, *Appl. Phys. Lett.* **100** (2012) 203101.

# Effect of substrate temperature and post annealing temperature on ZnO:Zn PLD thin film properties

E. Hasabeldaim<sup>1\*</sup>, O. M. Ntwaeaborwa<sup>1</sup>, R. E. Kroon<sup>1</sup>, E. Coetsee<sup>1</sup>, H. C. Swart<sup>1\*</sup>

<sup>1</sup>Department of Physics, University of the Free State, Bloemfontein ZA-9300, South Africa

\*Corresponding author e-mail address: hasabeldaimehh@ufs.ac.za; SwartHC@ufs.ac.za

## 1. Introduction

ZnO is a promising material for emissive semiconductor and piezoelectric applications [1, 2]. It is stable at or above room temperature because of its large exciton binding energy [3]. ZnO has a direct and wide band gap near the UV region [4]. Pulsed laser deposition (PLD) technique is a popular technique that has been used for thin films deposition. ZnO:Zn thin film were deposited on Si substrates at different substrate temperatures, and then post annealed in air at different temperatures. The structure, surface morphology and optical properties of the deposited and post-annealed films were investigated.

## 2. Results

ZnO:Zn PLD thin films were deposited at different substrate temperatures of 50 °C, 200 °C and 400 °C. The films deposited at the substrate temperature of 50 °C and 200 °C were post-annealed in air at 400 °C and 600 °C for two hours. The films all have a preferred orientation with the c-axis perpendicular to the substrate surface. The nature of stress was found to be compressive with values -3.289 GPa, -4.864 GPa and -4.425 GPa for the film deposited at 50 °C, 200 °C and 400 °C, respectively. After post-annealing treatments, the stress of the films was almost completely released and free-stress films were obtained. The crystallite sizes were 19 nm, 25 nm and 39 nm, while the average particles sizes were 95 nm, 85 nm and 129 nm for the film deposited at 50 °C, 200 °C and 400 °C respectively. The crystallite sizes and particles sizes seemed to increase with the increase in the substrate temperature. Contrary to this, the change in crystallite sizes were inversely proportional to the particles size when increasing the post-annealing temperatures. Deconvoluted X-ray photo electron spectroscopy peaks of the O1s showed that the films deposited at different substrate temperatures contained oxygen-related defects. Photoluminescence studies revealed that the films all emitted ultra-violet luminescence around 379 nm. The film deposited at 50 °C emitted a broad green emission centred at ~ 524 nm. By increasing the substrate temperature up to 200 °C and 400 °C a new orange emission around 621 nm and 634 nm as well as weak emissions around 416 nm and 500 nm were observed, respectively. After post-annealing treatments, new bands over the visible region (blue, green and orange-red) were observed. The orange-red emissions at ~ 626 nm to 681 nm were dominant for the annealed samples. The mechanism of defect-related visible emission was discussed in detail and it was in good agreement with previous studies.

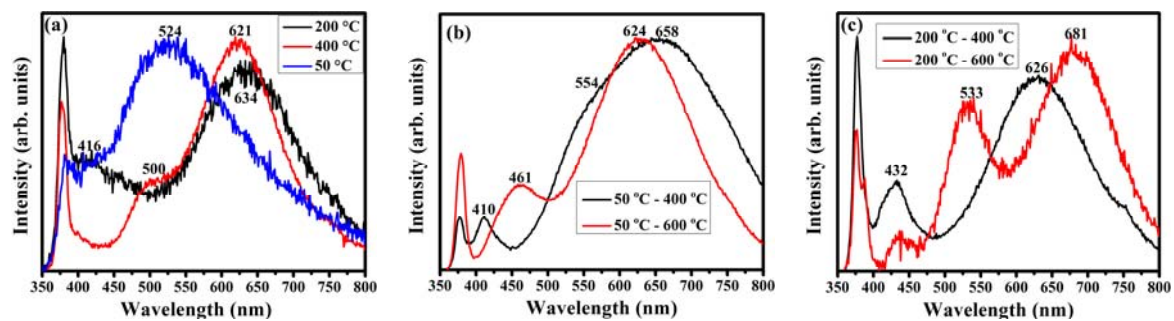


Fig. 1: PL emissions of ZnO:Zn films deposited at (a) different substrate temperatures, (b) deposited at 50 °C and annealed, (c) 200 °C and annealed.

## 3. References

- [1] O. Ümit, D. Hofstetter and H. Morkoc. *Proc. IEEE* **98** (2010) 1255.
- [2] H. J. Fan, W. Lee, R. Hauschild, M. Alexe, G. Le Rhun, R. Scholz, A. Dadgar, K. Nielsch, H. Kalt, A. Krost, and M. Zacharias. *small* **4** (2006) 561.
- [3] D. C. Look. *Mater. Sci. Eng. B* **80** (2001) 383.
- [4] D.C. Reynolds, D.C. Look and B. Jogai. *Solid State Commun.* **99** (1996) 873.

# Effect of pH on the structural, optical and morphological properties of Ga-doped ZnO nanoparticles prepared by reflux method

Jatani Ungula<sup>1\*</sup>, Francis B. Dejene<sup>1</sup>, Hendrik C. Swart<sup>2</sup>

<sup>1</sup> Department of Physics, University of the Free State (QwaQwa Campus), Private Bag X13, Phuthaditjhaba, 9866, South Africa

<sup>2</sup> Department of Physics, University of the Free State, P.O Box 339, Bloemfontein 9300

\*Corresponding author e-mail address: ungulaj@ufs.ac.za

## 1. Introduction

Group III doped ZnO nanostructures have been intensively studied as a kind of low resistivity n-type semiconductor used for transparent conducting oxide (TCO) applications. Compared to other metals in group III, gallium is a preferred dopant to improve the electrical conductivity, crystal quality and optical transmittance of ZnO in the visible and near UV range [1]. Basically, gallium-doped zinc oxide (GZO) is more stable with respect to oxidation due to gallium's greater electronegativity in comparison with aluminium and because the ionic and covalent radii of Ga are nearly equal to that of Zn. Thus, Ga<sup>3+</sup> can be substituted for Zn<sup>2+</sup> over a larger doping range without any lattice distortion and so has a lower defect induced concentration. The solution pH is known to play a crucial role in influencing the properties of nanostructures. For instance, it was reported that acidic nature prevents the growth of high-quality ZnO nanofilms and solution conditions have a particular effect on ZnO particle size powders [2]. For this reason, in the present study, effect of pH of precursor solution on the structural, optical and luminescence properties of ZnO:Ga (2 mol.%) NPs were studied. We were able to produce better quality GZO NPs with high crystallinity, improved morphology, highly enhanced photoluminescence and largest band gap at pH of 8. This investigation aims for the improvement of the properties of a photo electrode seed layer for a Dye Sensitized Solar Cell based on thin films, where the improvement of conductivity and the decrease of resistivity is the main issue.

## 2. Results

Gallium-doped zinc oxide nanoparticles (GZO NPs) were synthesized by reflux method for different pH values (3, 5, 7 and 8 pH) and a control sample (GZO) was synthesized without adjustment of pH. From the analysis of X-ray diffraction (XRD) spectra, Fig. 1, it was found that the diffraction peak intensities and crystallite sizes of GZO NPs increased with an increase in pH of the precursor solution. The samples synthesized at a pH of 3 and 8 had crystallite sizes of 13 and 27 nm respectively. The control sample had a crystallite size of 11 nm. Scanning electron microscopy micrographs showed agglomerated tiny particles that formed on big slabs of nanorods in acidic conditions, but fine and enlarged particles on nano-spherical bases at higher pH. The cathodoluminescence (CL) analysis of GZO NPs exhibited a decrease in peak full width at half maximum (FWHM) and red shift of peak positions with the increase in pH values. However, the relative intensities of CL increased with the increase in pH in conformity with XRD results. The photoluminescence exciton peak intensities and FWHM of the GZO NPs increased to a maximum at a 5pH and then reduced as the solution became basic. Interestingly, the increase of the deep level peak intensities with the increase in pH followed the XRD and CL results. UV-vis analysis, Fig 2, also demonstrate that the optical properties of GZO NPs improved with the increase of pH as shown by the blue shift of the absorption edge of the reflectance spectra. The band gap energy was tuned from 3.18 eV at a pH of 3 to 3.31 eV at pH of 8.

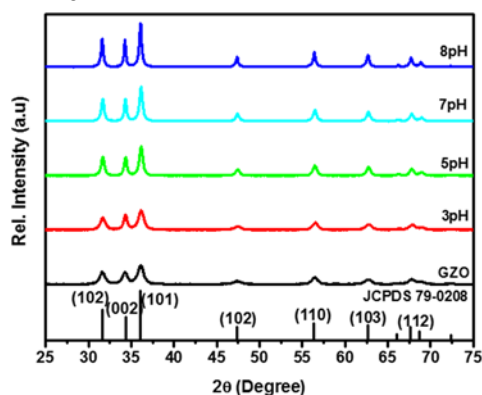


Fig. 1: X-ray diffraction patterns for GZO NPs at different pH values.

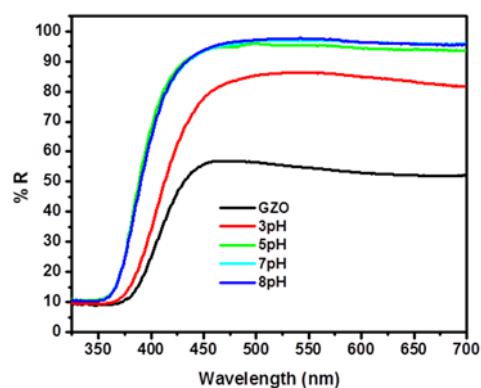


Fig. 2: UV-Vis reflectance % for GZO NPs at different pH values.

## 3. References

- [1] B.E. Sernelius, K.F. Berggren, Z.C. Jin, I. Hamberg, C.G. Granqvist, *Physical Review B* **37** (1988) 10244.
- [2] J.K. Sheu, K.W. Shu, M.L. Lee, C.J. Tun, G.C. Chi, *Journal of the Electrochemical Society* **154**(6) (2007) H521.

# Block copolymer templates for zinc oxide nanorods

**A. Talla<sup>1\*</sup>, C. Kameni Boumenou<sup>1</sup>, S. R. Tankio Djiokap<sup>1</sup>, S. R. Dobson<sup>1</sup>, K. Talla<sup>1</sup>, Z. N. Urgessa<sup>1</sup>, J.R. Botha<sup>1</sup>**

<sup>1</sup>*Department of Physics, Nelson Mandela Metropolitan University, P O Box 77000, Port Elizabeth, 6031, South Africa*  
<sup>\*</sup>*Corresponding author e-mail address: s217063969@live.nmmu.ac.za*

## 1. Introduction

Titanium oxide (TiO<sub>2</sub>) is an important compound which has been used in applications like photovoltaic cells and photocatalysts [1]. Nanoparticles of this compound are often used as electron collectors in dye sensitized solar cells. Because of the grain boundaries between nanoparticles, however, the electron collection becomes inefficient [2]. As the result, the collection of electrons compete with the recombination and leads to a low charge collection efficiency and hence a low solar to electrical conversion efficiency [3]. Nanostructured TiO<sub>2</sub>, such as nanowires/rods and nanotubes have received attention because their geometry facilitates efficient conduction in devices [4]. In order to obtain TiO<sub>2</sub> nanotubes, zinc oxide (ZnO) nanorods can be used as templates [5].

## 2. Results

The growth of ZnO nanorods using solution methods on a lattice mismatched substrate typically suffers from a random orientation of the rods relative to the substrate. In this study, the use of block copolymer films as a template for the oriented growth of ZnO nanorods, which in turn can be used for the growth of TiO<sub>2</sub> nanotubes, is presented. Block copolymers have the tendency to self-assemble into various nanoscopic structures such as lamellae, spheres or cylinders on a nanometer scale. Poly (styrene-block-methylmethacrylate) (PS-b-PMMA) has been investigated as a potential nano-mask for semiconductor growth. For this study, diblock copolymer thin films are grown on a silicon substrate coated with a random polymer (poly (styrene-random-methylmethacrylate) (PS-r-PMMA)), which permits a non-preferential interaction between the diblock constituents and the substrate. Subsequent thermal annealing of PS-b-PMMA of an appropriate thin film thickness leads to perpendicular cylinders of PMMA within a PS matrix. Finally, the vertically oriented PMMA cylindrical micro domains in PS thin films are easily removed, leaving vertically aligned cylinders in which ZnO nanorods is subsequently grown. Samples are characterized using scanning probe microscopy to determine the surface topography and phase morphology of the annealed PS-b-PMMA thin films. Film thicknesses are measured by X-ray reflectometry. Preliminary results on the growth of ZnO nanorods, both before and after coating in TiO<sub>2</sub>, will be presented.

## References

- [1] U. Diebold, *Surf. Sci. Rep.* **48** (2003) 53
- [2] M. Gratzel, *Nature* **414** (2001) 338
- [3] G. Schlichthorl, N.G. Park and A.J. Frank, *J. Phys. Chem. B* **103** (1999) 782
- [4] G.K. Mor, K. Shankar, M. Paulose and C.A. Grimes, *Nano Lett.* **6** (2006) 215
- [5] J. Qiu, W. Yu, X. Gao and X. Li, *Nanotechnology* **17** (2006) 4695

# Sol-gel synthesis and characterization of doped barium titanate nanophosphors

T. L. Lotha<sup>1,2\*</sup>, Martin Onani<sup>1</sup>, B. F. Dejene<sup>2</sup>, H. C. Swart<sup>2</sup>

<sup>1</sup>Department of Chemistry, University of the Western Cape, Private Bag X17, Bellville, Cape Town, South Africa

<sup>2</sup>Department of Physics, University of the Free State, P.O. Box 339, Bloemfontein, 9300, South Africa

\*Corresponding author e-mail address: lothatl@gmail.com

## 1. Introduction

Barium titanate ( $\text{BaTiO}_3$ ) has been of practical interest for more than 60 years because of its attractive and useful properties in electronic and electrical industries.  $\text{BaTiO}_3$  is chemically and mechanically very stable, it is easily prepared and can be used as polycrystalline ceramic samples, and it exhibits ferroelectric properties at room temperature [1]. Due to its high dielectric constant and low loss characteristics, barium titanate has been used in applications, such as capacitors and multilayer capacitors (MLCs). Doped barium titanate has found wide application in semiconductors and piezoelectric devices, and has become one of the most important ferroelectric ceramics.  $\text{BaTiO}_3$  is ceramic material with a perovskite structure are very significant electronic materials. Barium titanate is a member of a large family of compounds with general formula  $\text{ABO}_3$  called perovskite. The general crystal structure is a primitive cube, with the Ba-larger cation in the corner, the Ti-smaller cation in the middle of the cube and oxygen, in the centre of the faces edges [2]. Barium titanate is the first discovered ferroelectric perovskite. Its ferroelectric properties are connected with a series of three structural phase transitions. The most investigated phase transition is from tetragonal ferroelectric to cubic paraelectric structure which occurs at Curie point  $T_C = 120^\circ\text{C}$ . The synthetic methods of  $\text{BaTiO}_3$  nanopowders have attracted extensive attention; in particular, the sol-gel process [3] has been intensively studied, because it provide high crystallinity, high purity, narrow particle size distribution, and well-controlled morphology of the powders, and has become a focus in the last decade in the field of ceramics powders preparation [4] at relatively low temperature.  $\text{BaTiO}_3$  powders synthesized by sol-gel process are easy to form agglomerates, while the organic acids (surfactant) are used to prevent agglomeration of particles.

## 2. Results

Metal titanate of  $\text{BaTiO}_3$  was successfully fabricated by the sol-gel route. Barium titanate ( $\text{BaTiO}_3$ ) with a perovskite structure is one of the most important materials in the electronic industry due to its high piezoelectricity, good dielectric, ferro-electric and optic electric properties. The photoluminescence results show a red emission peak at  $\lambda_{em} = 617 \text{ nm}$  when excited at  $\lambda_{exc} = 310 \text{ nm}$ , which corresponds to the intra-4f transition from the excited state  $^1D_2$  to the ground state  $^3H_4$  of  $\text{Pr}^{3+}$ . The SEM micrographs, fig. 1, show the change in morphology of undoped, doped and co-doped  $\text{BaTiO}_3$ . As the content of ethylene glycol (EG) also known as ethylene alcohol increased, the particle shape changed from non-uniform to a uniform spherical shape. Fig. 2 shows the X-ray diffraction patterns of the obtained phosphor powders. The results indicate that the material crystallised to a cubic phase, the crystallite size of the  $\text{BaTiO}_3$  is within a range of 10-30 nm.

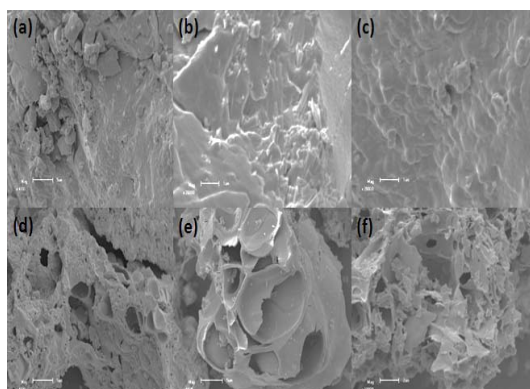


Fig. 1: SEM images for (a-c) undoped,  $\text{Pr}^{3+}$  doped, and  $\text{Al}^{3+}$  co-doped  $\text{BaTiO}_3$  at volume ratio (1:1), (d-f) (2:3) of acetic acid to ethylene alcohol respectively.

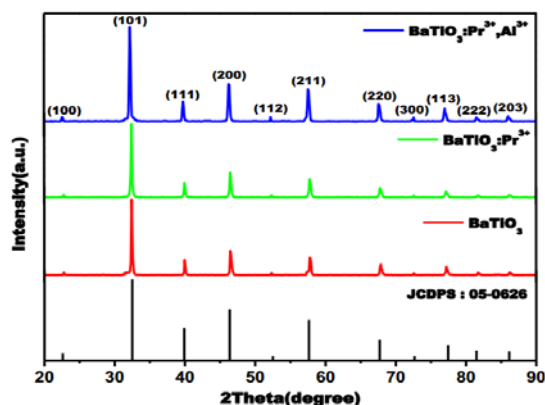


Fig. 2: XRD patterns of pure cubic crystal structures of undoped and doped  $\text{BaTiO}_3$ . The indexed peaks match exactly with the JCPDS card no. 310-174.

## 3. References

- [1] F. Jona, and G. Shirane, Ferroelectric crystals, Dover Publications, INC., New York, 1993
- [2] Y. Wang, H. Xu, X. Wang, X. Zhang, H. Jia, and J. Qiu, *J. Phys. Chem. B*, **110** (2006) 13835.
- [3] Q.Z. Shi, B. Cui, H. Wang, J. Tian, and Z.G. Chang, *Sci. China Ser. B* **48** (2005) 60.

# Magnetic and optical properties of un-doped and Co-doped TiO<sub>2</sub> nanotubes from electrospun carbon fiber templates

**Dickson Andala<sup>1\*</sup>, Francis Dejene<sup>2</sup>, Martin Onani<sup>3\*</sup>**

<sup>1</sup>Multimedia University of Kenya, PO Box 15653-00503, Nairobi-Kenya,

<sup>2</sup>Department of Physics, University of the Free State (Qwa Qwa Campus), Private Bag X 13, Phuthaditjhaba 9866, South Africa

<sup>3</sup>Department of Chemistry, University of the Western Cape, Private Bag X17, Bellville, Cape Town, South Africa

\*Corresponding author e-mail address: dandala@mmu.ac.ke; andalad@gmail.com

## 1. Introduction

Undoped and Co-doped Titanium dioxide nanotubes were fabricated using the Tubes Fiber Templating (TUFT) approach in which electrospun polylactide (PLA) nanofibers were used as exo-templates. **Cobalt (II) ions dissolved in titanium isopropoxide** were deposited as colloidal suspensions onto electrospun polymer fibers to yield PLA-Co-TiO<sub>2</sub> coaxial fibers with diameters ranging between 350 ± 100 nm. Thermal degradation of PLA template core, yielded hollow Co-TiO<sub>2</sub> nanotubes with diameters ranging between 250 ± 100 nm. The walls of the tubes ranged between 100 ± 50 nm based on size difference between coaxial fibers and nanotubes.

## 2. Results

From the optical properties results, maximum absorption occurred at ≈ 325 nm for CoTiO<sub>2</sub> nanotubes which was blue shifted relative to macro-crystalline. Co doping shifted the absorption edge of the TiO<sub>2</sub> nanotubes to longer wavelengths consistent with a charge-transfer transition between the d-electrons of the dopant and the TiO<sub>2</sub> conduction band. The emission spectrum of Co-TiO<sub>2</sub> nanotubes was obtained in the range of 350 – 560 nm following excitation wavelength at 325 nm at room temperature. This spectrum exhibited three emission peaks located at 374 nm, 420 nm and 470 nm in Figure 1. The emission transition at 374 nm and 420 nm were attributed to highest energy direct photoemission band gap and the lowest energy indirect transition respectively. The reduction in intensity observed in Co-TiO<sub>2</sub> nanotubes direct transition with Co doping, is ascribed to the introduction of Co<sup>2+</sup> 3d states in the conduction band. This was due to charge-transfer transition between the d-electrons of the dopant and the TiO<sub>2</sub> conduction band with n-type consistent with n-type doping. Magnetic susceptibility measurements as a function of temperature for Co doped TiO<sub>2</sub> nanotubes were done at different dopant concentrations. Low concentrations of Co below 4 % resulted in a homogeneous solid solution curve A in Figure 2. As the concentration of Co dopant increased a magnetic phase transition was observed at 38 K. This was attributed to formation of CoTiO<sub>3</sub> impurity with a Néel temperature of 38 K, corresponding to antiferromagnetic-paramagnetic transition. The observed transition temperature was independent of Co content and field applied consistent with formation of a magnetically ordered CoTiO<sub>3</sub> phase.

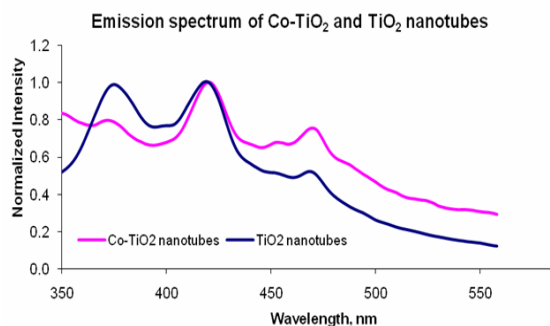


Fig. 1: Photoluminescence spectra of undoped and Co-doped TiO<sub>2</sub> nanotubes.

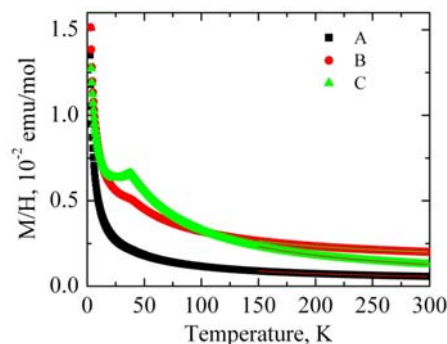


Fig. 2: Magnetic susceptibility curve for Co-TiO<sub>2</sub> nanotubes (Co concentration: A: 4 %; B: 8 %; C: 12 %).

## 3. References

- [1] G. C. Feifei-Tao, Z. Wen, Q. Wang, J. Li, Zheng Xu *Journal of Solid State Chemistry*. **182**, (2009), 1055.
- [2] M. Fleischhammer; M. Panthofer; W. Tremel. *J. Solid State Chem.* **182**(2009) 942.
- [3] F. Ochanda; K. Cho; D. Andala; C. T. Keane; A. Atkinson; W. E. Jones, Jr. *Langmuir*. **25** (2009)7547.

# Photochemical and photophysical properties gold nanoparticles supported on electrospun TiO<sub>2</sub> nanofibers

**Dickson Andala<sup>1\*</sup>, Leah Nyangasi<sup>2</sup>, Francis Dejene<sup>3</sup>, Martin Onani<sup>4</sup>**

<sup>1</sup>Multimedia University of Kenya, PO Box 15653-00503, Nairobi-Kenya.

<sup>2</sup>Kenyatta University, PO Box 43844-00100, Nairobi-Kenya.

<sup>3</sup>Department of Physics, University of the Free State (Qwa Qwa Campus), Private Bag X 13, Phuthaditjhaba 9866, South Africa

<sup>4</sup>Department of Chemistry, University of the Western Cape, Private Bag X17, Bellville, Cape Town, South Africa

\*Corresponding author e-mail address: dandala@mmu.ac.ke or andalad@gmail.com

## 1. Introduction

The net effect depositing metal nanoparticles on the surface of metal oxide nanofibers and their resultant influence on photophysical and photochemical properties of these materials has not been understood. Photoluminescence studies are useful in understanding the mechanism behind the increased photocatalytic efficiency in the photocatalysts. Previous studies show that charge carrier recombination limited the efficiency of TiO<sub>2</sub> as a photocatalyst. This work aims at establishing photochemical and photo-physical interactions between Au nanoparticles deposited on TiO<sub>2</sub> nanofibers. The TiO<sub>2</sub> nanofibers were fabricated via electrospinning polymer infused with titanium isopropoxide followed by calcination. Au nanoparticles were deposited TiO<sub>2</sub> nanofiber surface by wet chemical deposition method.

## 2. Results

The resultant TiO<sub>2</sub> nanofibers had diameters in the range 150±50 nm while the Au nanoparticles had diameters 50±10 nm, Figure 1. The absorption spectra for the TiO<sub>2</sub> nanofibers and the Au/TiO<sub>2</sub> photocatalyst gave an absorption maxima at ~350±2 nm that could be attributed to the optical band gap. These spectra were blue shifted by 30 nm compared to the bulk titania absorption maxima of 380 nm reflecting widening of the band gap as a result of quantum confinement effects. The absorption peak at ~540 nm can be attributed to Au nanoparticles due to surface plasmon resonance effect. The emission spectrum of TiO<sub>2</sub> nanofibers gave a characteristic peak at an emission maximum of 370 nm following excitation at 300 nm in Figure 2. This has been attributed to the band gap emission. It was red shifted relative to the absorption maxima by 20 nm. The emission of Au/TiO<sub>2</sub> photocatalyst was shifted by 35 nm ( $\lambda_{\text{max}}$  405 nm) relative to the pure TiO<sub>2</sub> nanofibers. The decreased Au/TiO<sub>2</sub> photocatalyst band gap emission can be attributed to the presence of surface trap states due to the presence of the Au nanoparticles.

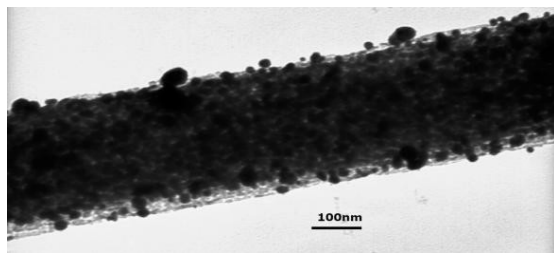


Fig. 1: TEM image of Au/TiO<sub>2</sub>.

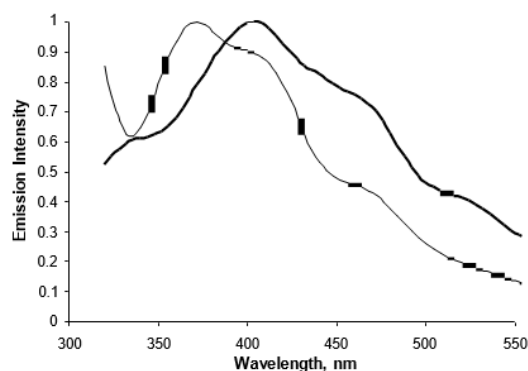


Fig. 2: Emission spectra of TiO<sub>2</sub> (narrow line) and Au/TiO<sub>2</sub> (bold line) photocatalyst at room temperature.

## 3. References

- [1] E. A. Obuya, H. Harrigan, D. Andala, J. Lippens, C.T. Keane, W. E. Jones Jr. *J. Mol. Cat. A: Chem.* **340** (2011) 89.
- [2] S. K. Mohapatra, N. Kondamudi, S. Banerjee, M. Misra. *Langmuir.* **24** (2008) 11276.
- [3] H. Yoshida, K. Hirao, J. I. Nishimoto, K. Shimura, S. Kato, H. Itoh, T. Hattori. *J of Phy. Chem. C.* **112** (2008) 5542.

# Investigation of ZnO:RE<sup>3+</sup> nanostructures for efficient charge transfer in hybrid based P3HT heterostructures

G. L. Kabongo<sup>1,2,3\*</sup>, P. S. Mbule<sup>1</sup>, G. H. Mhlongo<sup>2</sup>, B. M. Mothudi<sup>1</sup>, K. T. Hillie<sup>2</sup>, M. S. Dhlamini<sup>1\*</sup>

<sup>1</sup>Department of Physics, University of South Africa, PO Box 392, 0003, South Africa

<sup>2</sup>CSIR-National Centre for Nano-Structured Materials, PO Box 395, 0001, South Africa

<sup>3</sup>Département de Physique, Université Pédagogique Nationale, 8815, République Démocratique du Congo

\*Corresponding author e-mail address: geekale@gmail.com, dhlamms@unisa.ac.za

## 1. Introduction

Blending of inorganic semiconductor nanostructures with organic conjugated polymers to form hybrid heterostructures for solar cell applications has attracted much attention owing to its cost effective synthesis and tunable photophysical properties. In the current report, we demonstrate a novel hybrid heterostructure of poly(3-hexylthiophene) (P3HT) using inorganic ZnO:RE<sup>3+</sup> electron acceptor. It has been found that the inclusion of the inorganic semiconductor in the organic conjugated polymer harvest light absorption which resulted in an enhancement of the absorption coefficient associated with higher optical conductivity (order of ~2). Moreover, charge-transfer was effectively enhanced as revealed by singlet exciton lifetime analysis performed using time-correlated single photon counting (TCSPC), which correlated very well with photoluminescence quenching. Finally, these results pave the way for the fabrication of novel class of hybrid photoactive layers for organic photovoltaic solar cells with improved chain ordering and tunable photophysical properties.

## 2. Results

Fig. 1 shows typical broad absorption spectra ranging from 350-750 nm of P3HT due to intermolecular  $\pi$ - $\pi^*$  ordering. The ZnO nanocrystals exhibits strong band-to-band absorption peak at about 369 nm. For the samples containing P3HT, both spectra were similar in shape and exhibited three vibronic features at 482, 550 and 604 nm [1,2].

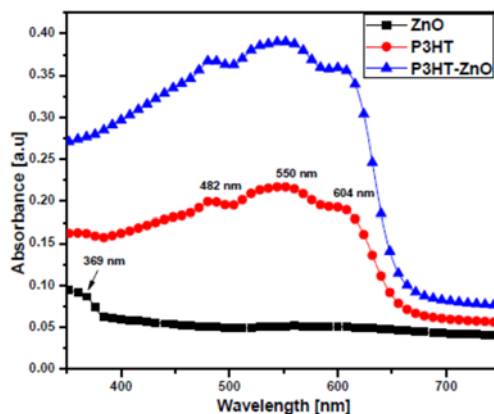


Fig. 1: Absorption spectra.

## 3. References

- [1] Shen W., Tang J., Yang R., Cong H., Bao X., Wang Y., Wang X., Huang Z., Liu J., Huang L., Jiao J., Xu Q., Chen W., Belfiore L.A., *RSC Adv* 4 (2014) 4379.
- [2] Chawla P., Singh S., Sharma S.N., *Beilstein J Nanotechnol* 5 (2014) 1235.



# Enhanced room temperature ferromagnetism in sol-gel derived ZnO:Ho<sup>3+</sup> nanostructures

G. L. Kabongo<sup>1,2,3\*</sup>, G. H. Mhlongo<sup>2</sup>, B. M. Mothudi<sup>1</sup>, K. T. Hillie<sup>2</sup>, M. S. Dhlamini<sup>1\*</sup>

<sup>1</sup>Department of Physics, University of South Africa, PO Box 392, 0003, South Africa

<sup>2</sup>CSIR-National Centre for Nano-Structured Materials, PO Box 395, 0001, South Africa

<sup>3</sup>Département de Physique, Université Pédagogique Nationale, 8815, République Démocratique du Congo

\*Corresponding author e-mail address: geekale@gmail.com, dhlamms@unisa.ac.za

## 1. Introduction

This investigation describes the synthesis of ZnO nanostructures doped with Ho<sup>3+</sup> ions by using a conventional sol-gel synthesis method. The nanostructured produced exhibited a wurtzite hexagonal structure in both ZnO and ZnO:Ho<sup>3+</sup> samples. The change in morphology with addition of Ho<sup>3+</sup> dopants was observed, which was assigned to Ostwald ripening effect occurring during the nanoparticles growth. The photoluminescence emission properties of the doped samples revealed that Ho<sup>3+</sup> was emitting through its electronic transitions. Moreover, reduced surface defects were observed in the Holmium doped samples which analysis was undertaken using X-ray Photoelectron Spectroscopy (XPS) technique. Finally, enhanced room temperature ferromagnetism (RT-FM) for Ho<sup>3+</sup>-doped ZnO samples with a peak-to-peak line width of 452 G was detected and found to be highly correlated to the UV-Vis transmittance results.

## 2. Results

Fig. 1 shows the number of spins ( $N_s$ ) contributing to the ferromagnetic resonance. The calculated values were  $1.576 \times 10^8$ ,  $2.906 \times 10^8$ ,  $3.35 \times 10^8$ ,  $0.284 \times 10^8$  for 0, 0.25, 0.5 and 0.75 mol% Ho<sup>3+</sup> samples, respectively [1].

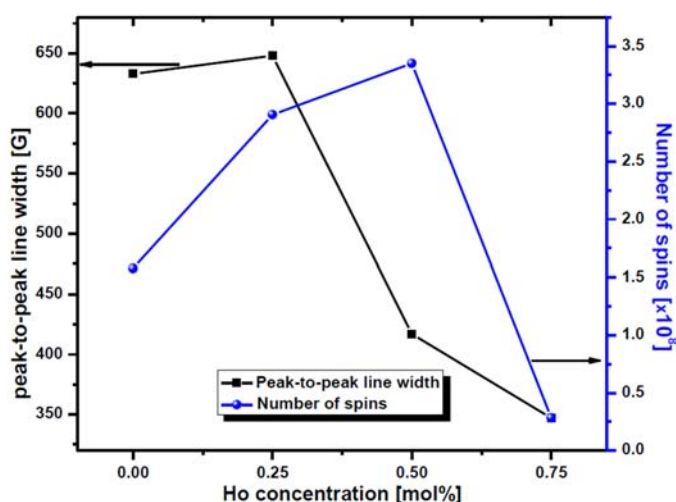


Fig. 1: Peak-to-peak line width and number of spins as a function of Ho<sup>3+</sup> concentration.

## 3. Reference

[1] Rai G.M., Iqbal M.A., Xu Y., Will I.G., Zhang W., *Chin. J Chem Phys* **24** (3) (2011) 353.

# Thickness determination of interfacial SiO<sub>2</sub> ultra-thin films between ZnO based materials and the Si substrate

Fred Joe Nambala<sup>1,2</sup>, **Benard S. Mwankemwa<sup>1</sup>**, Jacqueline M. Nel<sup>1</sup>, Wiets D. Roos<sup>3</sup>, Elizabeth Coetsee-Hugo<sup>3</sup>, R. E. Kroon<sup>3</sup>, Mmantsae Diale<sup>1\*</sup>

<sup>1</sup>Department of Physics, University of Pretoria, Private bag X20, Hatfield, 0028. South Africa.

<sup>2</sup>Department of Physics, University of Zambia, PO Box 32379, Great East Road Campus, Lusaka. Zambia.

<sup>3</sup>Department of Physics, University of the Free State, PO Box 339, Bloemfontein, 9300. South Africa.

\*Corresponding author e-mail address: mmantsae.diale@up.ac.za

## 1. Introduction

The determination of precise thickness of an ultra-thin film of SiO<sub>2</sub> on Si substrate is crucial in the fabrication of high efficiency silicon inversion layer solar cells. XPS can be employed to determine the thickness,  $d_{ox}$  of a thin film less than 2 nm by measuring the Si 2p peak in Si and SiO<sub>2</sub> of a sample using the equation [1]:

$$d_{ox} = \lambda_{ox} \sin \theta \ln \left( \frac{I_{ox}}{\beta I_{Si}} + 1 \right) \quad (1)$$

where  $\lambda_{ox}$  is the attenuation length of the Si 2p photoelectrons in SiO<sub>2</sub>,  $\theta$  is the photoelectron take-off angle  $\beta = I_{ox}^{\infty}/I_{Si}^{\infty}$  (where  $I_{ox}^{\infty}$  and  $I_{Si}^{\infty}$  are the Si 2p intensities of infinitely thick SiO<sub>2</sub> and Si layers, respectively) and  $I_{ox}/I_{Si}$  is the ratio of Si 2p intensities from a film under investigation [1,2].

ZnO and Al doped ZnO thin films were prepared using the sol-gel method and deposited on Si by spin-coating. The films of the device structure samples were pre-heated during deposition and later post-annealed to ensure crystallisation.

## 2. Results

For the 1 at.% Al in ZnO films on Si, the XPS Si 2p peak intensities were positioned at 99.3 and 103.3 eV for Si and SiO<sub>2</sub>, respectively. The resultant thickness of the interfacial SiO<sub>2</sub> ultra-thin film was determined as 0.69 nm. XPS depth profiling was used to obtain the thickness of the undoped and doped ZnO films on Si.

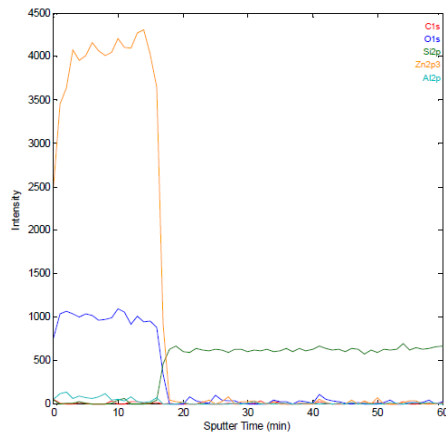


Fig. 1: XPS 1 at.% Al in ZnO on n-Si depth profile.

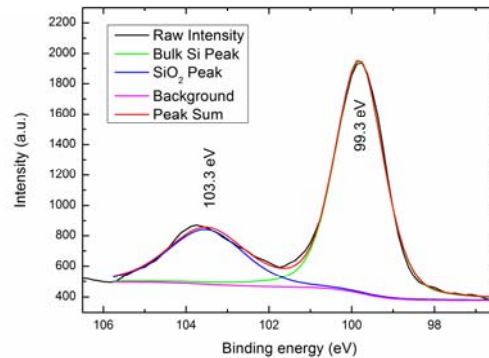


Fig. 2: Si 2p peaks of Si and SiO<sub>2</sub> intensities for calculating thickness.

## 3. References

- [1] S. Geng, S. Zhang and H. Onishi. *Materials Science Forum* **437-438** (2003) 195.
- [2] D. F. Mitchell, K. B. Clark, J. A. Bardwell, W. N. Lennard, G. R. Massoumi and I. V. Mitchell. *Surf. Interf. Anal.* **21** (1994) 44.

# Study on photoluminescence and energy transfer of $\text{Eu}^{3+}/\text{Sm}^{3+}$ single-doped and co-doped $\text{BaB}_8\text{O}_{13}$ phosphors

Mantwa A. Lephoto<sup>1</sup>, Kamohelo G. Tshabalala<sup>1</sup>, Selepe J. Motlounge<sup>1</sup>, Odireleng M. Ntwaaborwa<sup>2\*</sup>

<sup>1</sup>Department of Physics, University of the Free State, QwaQwa campus, Private Bag X13, Phuthaditjhaba, 9866, South Africa

<sup>2</sup>School of physics, University of the Witwatersrand, Private Bag 3, Wits, 2050, South Africa

\*Corresponding author e-mail address: ntwaab@gmail.com

## 1. Introduction

Rare earth (RE) ion doped luminescent materials have been generating interest for many decades due to their wide range of applications as electronic displays, light sources, advertising boards and theft prevention devices. Rare-earths ions possess excellent luminescent characteristics due to their inner shell electronic transitions between the 4f–4f energy levels [1]. In many rare-earths ions, particular attention was always paid to  $\text{Eu}^{3+}$ , which often shows high fluorescence efficiency and its hypersensitive transition of  ${}^5\text{D}_0\text{--}{}^7\text{F}_2$  in the red part of the spectrum. On the other hand,  $\text{Sm}^{3+}$ , whose ionic radius is very similar to that of  $\text{Eu}^{3+}$ , also gives a red emission and sometimes enhance the emission intensity of  $\text{Eu}^{3+}$  when co-doped or even shift their emission peaks to longer wavelengths [2]. This study, is aimed at investigating the ion–ion interactions and energy transfer between  $\text{Eu}^{3+}$  and  $\text{Sm}^{3+}$  ions in borates. During the past years, many borates were chosen as host lattices for phosphors because of their large band gap, high thermal and chemical stability, high luminescence efficiency and low cost [3].

$\text{Eu}^{3+}$ -  $\text{Sm}^{3+}$  co-doped  $\text{BaB}_8\text{O}_{13}$  powder phosphors were prepared by solution combustion method using urea ( $\text{CH}_4\text{N}_2\text{O}$ ) as a fuel. The powders were prepared at  $600^\circ\text{C}$  and annealed for 3 hours in a muffle furnace at  $800^\circ\text{C}$ . The resulting powders were then characterized using different techniques.

## 2. Results

Shown in Fig. 1 are the X-ray diffraction spectra of  $\text{BaB}_8\text{O}_{13}$  single-doped  $\text{Eu}^{3+}/\text{Sm}^{3+}$  and co-doped powder phosphors. Comparing the prepared powders with the literature (JCPDS no: 20-0097), the strong peaks of the XRD patterns can be indexed to the orthorhombic structure with cell parameters  $a = 8.550 \text{ \AA}$ ,  $b = 17.350 \text{ \AA}$  and  $c = 13.211 \text{ \AA}$ . The additional peaks (marked with \*) may be attributed to the unreacted precursors during the combustion reaction. The excitation spectra of  $\text{Ba}_{1-x-y}\text{B}_8\text{O}_{13}: x\text{Eu}; y\text{Sm}$  powder phosphors showed that the phosphors can be excited efficiently by wavelengths of 394 nm and 400 nm due to  ${}^7\text{F}_0\text{--}{}^5\text{L}_6$  and  ${}^6\text{H}_{5/2}\text{--}{}^4\text{K}_{11/2}$  transitions of  $\text{Eu}^{3+}$  and  $\text{Sm}^{3+}$  ions, respectively. Photoluminescence emission (PL) spectra of  $\text{Ba}_{1-x-y}\text{B}_8\text{O}_{13}: x\text{Eu}; y\text{Sm}$  ( $x = 0.05$  and  $y = 0.03$ ) under the excitation of 394 nm and 400 nm is shown in Fig. 2. The emission spectra exhibit both emissions from  $\text{Eu}^{3+}$  and  $\text{Sm}^{3+}$  ions. This can be considered as a clear evidence of energy transfer from  $\text{Sm}^{3+}$  to  $\text{Eu}^{3+}$  ion and from  $\text{Eu}^{3+}$  to  $\text{Sm}^{3+}$ .

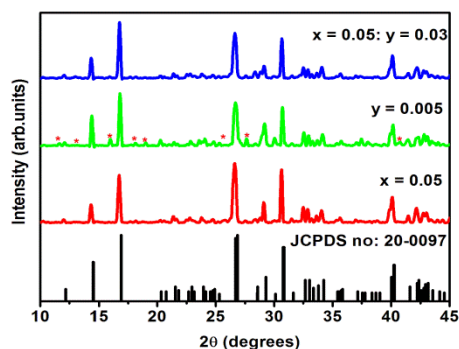


Fig. 1: XRD spectra of  $x\text{mol Eu}^{3+}/y\text{mol Sm}^{3+}$  single-doped and co-doped  $\text{BaB}_8\text{O}_{13}$  powder phosphors.

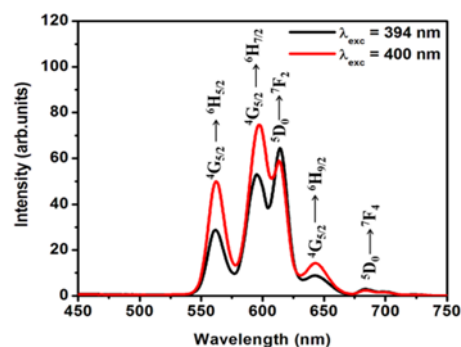


Fig. 2: PL emission spectra of  $\text{Ba}_{1-x-y}\text{B}_8\text{O}_{13}: x\text{Eu}; y\text{Sm}$  ( $x = 0.05$  and  $y = 0.03$ ) powder phosphor.

## 3. References

- [1] L. Wang, H. Guo, Y. Wei, H. Noh, J. H. Jeong. *Opt. Mater.* **42** (2015) 233.
- [2] J. Huang, Q. Li and D. Chen, *Mat. Sci. Eng. B.* **172** (2010) 108.
- [3] Y. Fan, Y. Hu, L. Chen, X. Wang and G. Ju. *Physica B.* **450** (2014) 99.

# A comparison investigation of optical, structural and luminescence properties of $\text{CdO}_x\text{Te}_{1-x}$ and $\text{CdTe}_x\text{Se}_{1-x}$ nanoparticles prepared by a simple one pot method

Sharon Kiprotich<sup>1\*</sup>, Francis B. Dejene<sup>1</sup>, Martin O. Onani<sup>2</sup>

<sup>1</sup> Department of Physics, University of the Free State, (QwaQwa campus), Private Bag X-13, Phuthaditjhaba, 9866, South Africa

<sup>2</sup> Departments of Chemistry, University of the Western Cape, Private Bag X17, Bellville 7535, South Africa

\*Corresponding author e-mail address: KiprotichS@ufs.ac.za

## 1. Introduction

Semiconductor quantum dots (QDs) have attracted much attention over the past decades due to their novel size-dependent optical properties displayed by excellent luminescent properties, broad excitation spectra, narrow emission bandwidth, high quantum yields and reduced tendency to photo bleaching compared with organic dyes [1]. With these enthralling properties QDs devices have been developed targeting applications in biological imaging, optoelectronic, photovoltaic devices and optical amplifier media for telecommunication networks [2]. In varying different parameters such as reaction time, reaction temperature, pH and molar concentration, the nanoparticles (NPs) can be tuned to suit the desired applications. In this study L-cysteine capped  $\text{CdO}_x\text{Te}_{1-x}$  and  $\text{CdTe}_x\text{Se}_{1-x}$  nanoparticles were prepared by a facile wet chemical route using potassium telluride, sodiumselenosulphate as stable tellurium and selenium (Se) sources respectively and L-cysteine as a capping agent. Capping with L-cysteine is intended to enhance the QDs stability and act as antioxidant and impurity removal reagent. The red shift observed in the emission spectra is attributed to the larger particle size [3].

## 2. Results

Fig. 1 shows the spherical monodispersed scanning electron microscope (SEM) images of the representative  $\text{CdO}_x\text{Te}_{1-x}$  NPs prepared at 30 minutes of reaction time. The X-ray diffraction pattern corresponded to the hexagonal structure of the bulk CdTe nanocrystals with some cubic phases of CdO. There was however change in phase to cubic when Se was injected into the CdTe at 60 minutes. The average crystallite sizes of the NPs calculated using Scherrer equation were in the range 10-36 nm. Fig. 2 (a) and (b) display photoluminescence (PL) emission spectra of the as-prepared  $\text{CdO}_x\text{Te}_{1-x}$  and  $\text{CdTe}_x\text{Se}_{1-x}$  NPs respectively. With increase in reaction time the emission band red shifted from approximately 508 to 566 nm. On Se injection, the emission drastically shifted to a region from 650 to 693 nm followed by a continuous decrease in the peak intensity. The emission spectra display a good symmetry and sufficiently narrow full width at half maximum ranging from 41 to 80 nm in both cases. Ultraviolet-visible analysis displayed well-resolved maxima which generally shifted to longer wavelengths for prolonged duration of synthesis. The band gaps of the as-prepared NPs decreased with increase in reaction time.

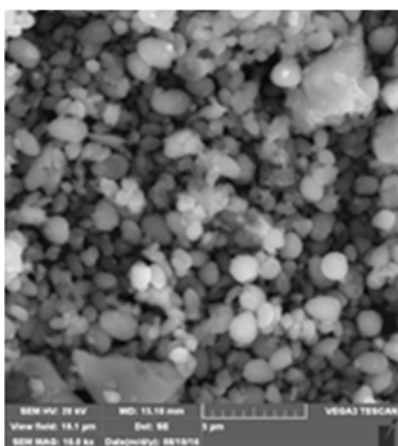


Fig. 1: Representative SEM image of  $\text{CdO}_x\text{Te}_{1-x}$  nanoparticles

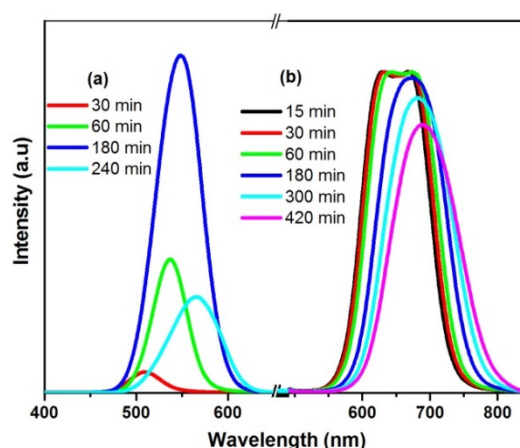


Fig. 2: PL emission spectra of  $\text{CdO}_x\text{Se}_{1-x}$  and  $\text{CdTe}_x\text{Se}_{1-x}$  prepared at different reaction times

## 3. References

- [1] T. Kabashima, Z. Yu, C. Tang, Y. Nakagawa, K. Okumura, T. Shibata, J. Lu and M. Kai, *Peptides* **29** (2008) 356.
- [2] M. T. Harrison, S. V. Kershaw, M. G. Burt, A. L. Rogach, A. Kornowski, A. Eychmuller, and H. Weller, *Pure Appl. Chem.* **72** (2000) 295.
- [3] S.D. Gunjal, Y.B. Khollam, S.R. Jadkar, T. Shripathi, V.G. Sathe, P.N. Shelke, M.G. Takwale and K.C. Mohite, *Sol. Energy* **106** (2014) 56.

# High luminescent L-cystine capped CdTe quantum dots prepared at different reaction times

Sharon Kiprotich<sup>1\*</sup>, Martin O. Onani<sup>2</sup>, Francis B. Dejene<sup>1</sup>

<sup>1</sup>Department of Physics, University of the Free State, (QwaQwa campus), Private Bag X-13, Phuthaditjhaba, 9866, South Africa

<sup>2</sup>Department of Chemistry, University of the Western Cape, Private Bag XI7, Bellville 7535, South Africa

\*Corresponding author e-mail address: KiprotichS@ufs.ac.za

## 1. Introduction

As a new type of fluorescence materials, quantum dots (QDs) have attracted great scientific interests due to their unique properties and advantages over traditional organic fluorophores [1]. It is known that CdTe nanocrystals of different sizes have tuneable emission from green to red due to quantum confinement. They have been widely studied in industrial and biomedical applications such as light-emitting devices, photonic crystals, nonlinear optical devices, biological labels and neuroplastic cells following conjugation with some bio-active moieties. This is due to their optical and chemical properties which include high photoluminescence (PL) intensity, narrow emission or broad excitation band and good photo-chemical stability [2, 3]. Surface coating has been widely used to prevent QD oxidation and thereby reduce the cytotoxicity of the particles. Here in we report L-cystine capped CdTe QDs using potassium telluride as stable tellurium sources while sodium borohydride was used as a reductant. The aim of this work is to produce near-infrared (NIR) emitting CdTe QDs because they possess many superior properties for instance, NIR light traveling in biological tissues is hardly weakened due to the relatively low absorbance of photons by biological tissues [4]. Most importantly the QDs produced using simple and less expensive method is stable and highly crystalline.

## 2. Results

The representative high resolution transmission microscopy (HRTEM) images (Fig. 1), shows that the as-obtained CdTe QDs appeared as spherical particles with excellent monodispersity. From its analysis it showed clear lattice fringes which are an indicative of good crystallinity of the as prepared sample. X-ray diffraction (XRD) pattern correspond well to zinc blende phase of bulk CdTe with diffraction peaks shifting to lower angles as reaction time increase. Increase in reaction time caused increase in crystallinity of the sample as explained by increase in peak intensity of the XRD peak at 120 minutes. For much longer reaction time, the crystallinity of the sample starts to decrease. The crystallite sizes calculated from the Scherrer equation were in the range 8 - 30 nm for different reaction times which were in accord to the particle sizes calculated from HRTEM. This is also supported by the PL emission spectra which show highest intensity at longer growth time. Fig. 2 display PL emission spectra of the as prepared CdTe QDs at different reaction times achieved when excited at single wavelength of 350 nm. It is clearly seen that for prolonged growth time the emission band is shifted to longer wavelength due to increase in particle sizes. Ultra violet visible analysis display well resolved absorption maxima which are red shifted upon increase in reaction time. There was an inverse relation between the bandgap and reaction time. However, the band gap was larger than the bulk band gap of CdTe (1.5 eV).

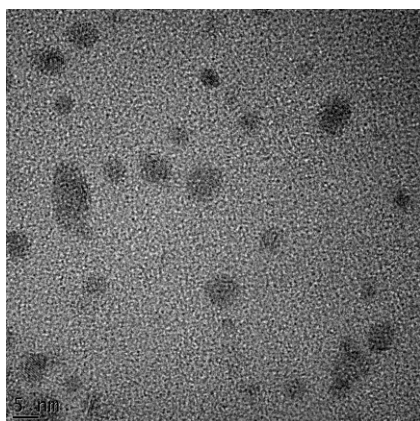


Fig. 1: Representative HRTEM micrograph for CdTe QDs prepared at 30 minutes of reaction time.

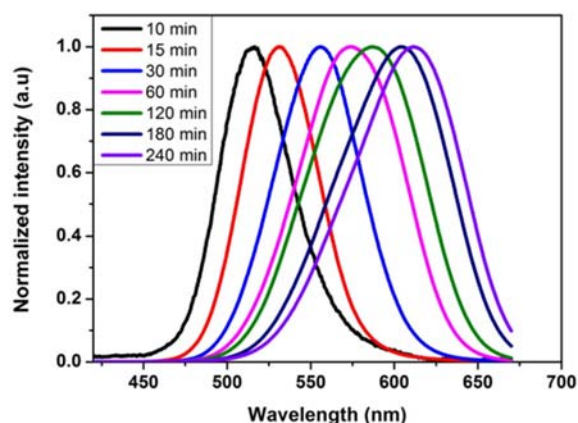


Fig. 2: PL emission spectra for CdTe QDs prepared at different reaction times

## 3. References

- [1] W.R. Algar, K. Susumu, J.B. Delehanty, I.L. Medintz, *Anal. Chem.* **83** (2011) 8826.
- [2] M. Gao, C. Lesser, S. Kirstein, H. Mchwald, A. L. Rogach, H.Weller, *J. Appl. Phys.* **87** (2000) 2297.
- [3] N. N. Mamedova, N. A. Kotov, A. L. Rogach, J. Studer, *Nano Lett.* **1** (2001) 281.
- [4] P. Yang, M. Ando, T. Taguchi, N. Murase, *J. Phys. Chem. C* **115** (2011) 14455.

# Roles of cationic concentration and pH on the structural, morphological and optical band gap of chemically synthesized lead sulphide thin films

Fekadu Gashaw Hone<sup>1\*</sup>, F. B. Dejene<sup>1</sup>

<sup>1</sup>University of the Free State, Department of Physics (QwaQwa Campus), Phuthaditjhaba, South Africa

\*Corresponding author e-mail address: fekeye@gmail.com

## 1. Introduction

Nanocrystalline lead sulphide (PbS) thin films were deposited on glass substrates by chemical bath deposition method from two baths with different compositions. The first bath was complexed by sodium hydroxide (NaOH) and the effects of lead concentrations were investigated, while the second bath was complexed by triethylamin (Et<sub>3</sub>N) and the effects of bath pH were studied. The deposited thin films were characterized by variety of techniques to investigate the influence of lead concentration and pH on the material properties. The X-ray diffraction analyses revealed that all the films were polycrystalline in nature with a face centered cubic crystal structure. The XRD results also verified that the crystalline size decreased with increasing lead concentration. Moreover, pH and lead concentration had strong influences on the preferred orientation of the crystallites as well as other structural parameters such as microstrain, dislocation density and texture of coefficients. The surface roughness and morphology of PbS thin films were examined by AFM and FESEM. The elemental analyses were performed by EDAX and it was confirmed that a better stoichiometric ratio was found for higher pH value. The optical absorption study revealed that the optical band gap of the PbS thin films decreased from 1.15 eV to 0.85 eV when lead concentration increased from 0.1 M to 0.3 M. Room temperature PL was applied to study the emission properties of PbS thin films.

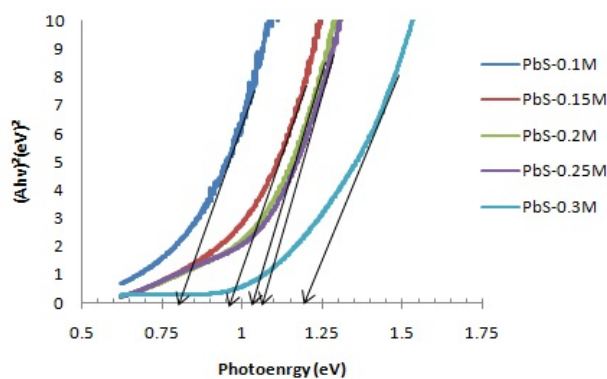


Fig.1: A graph of  $(Ah\nu)^2$  plotted as a function of the photon energy for PbS thin films for various lead concentration

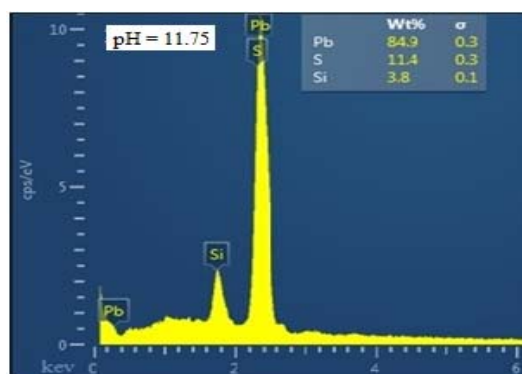


Fig.2: EDAX spectra of PbS thin film at a pH of 11.75

## 3. References

- [1] L. Beddek, M. Messaoudi, N. Attaf, M.S. Aida and J. Bougdira, *J. Alloys. Compd.*, **666** (2016) 327.
- [2] R. Thiagarajan, M.M. Beevi, M. Anusuya and T. Ramesh, *Optoele. and Adv. Matte.*, **6** (2012) 132.
- [3] S. Sengupta, Maayan Perez, Alexander Rabkin and Y. Golan, *CrystEngComm*, **18** (2016) 149.
- [4] K.C. Preetha, K.V. Murali, A.J. Ragina, K. Deepa, T.L. Remadevi, *Curr. Appl. Phys.*, **12** (2012) 53.

# Plasmonic metamaterial-based graphene/TiO<sub>2</sub>/Ag thin film by a simple spray pyrolysis technique

**Promod Kumar<sup>1\*</sup>, H. C. Swart<sup>1\*</sup>**

<sup>1</sup>Department of Physics, University of the Free State, P.O. Box 339, Bloemfontein, ZA 9300, South Africa.

\*Corresponding authors e-mail address: talk2promodthakur@gmail.com, SwartHC@ufs.ac.za

## 1. Introduction

Graphene based hybrid nanostructures have received special attention in both the scientific and technological development due to their unique and unusual physicochemical behavior, which make them attractive in various applications such as, batteries, supercapacitors, fuel cells, solar cells, photovoltaic devices and bio-sensors. Many theoretical and experimental studies have been performed to improve the optical and photocatalytic activity of graphene-based semiconducting oxide-based materials (such as ZnO, SnO<sub>2</sub>, TiO<sub>2</sub>) by doping noble metals, changing the shape and size of nanoparticles. Although the study of the graphene-based hybrid nanostructures materials has achieved much progress, there are still many challenges in this field. Further developments and studies of graphene-based hybrid materials in the field of science and technology are still needed to find the various applications.

## 2. Results

In the present study, the role of plasmonic metamaterials in light trapping photovoltaics for inorganic semiconducting materials by a simple and low cost spray pyrolysis technique has been studied. A glass substrate was used as a matrix for the deposition of silver nanoparticles followed by the deposition of a titanium dioxide (TiO<sub>2</sub>) thin film by a simple thermal pyrolysis method [1]. Then the graphene-TiO<sub>2</sub> based plasmonic metamaterials thin film has been fabricated, figure 1, which has a low resistivity and a low electron-hole recombination probability. Confinement and manipulation of light also occurred at this nanoscale which is beyond the diffraction limit. The localized surface plasmon resonance (LSPR) at the metal-dielectric interface for the silver nanoparticles has been observed at 404 nm with a transmittance of over 70% at a wavelength of 500 nm for the thin film. The results suggest that stacking of Ag-graphene-TiO<sub>2</sub> did not change the band gap of TiO<sub>2</sub> while it changed the conductivity of the film. Thus the diffusion of the noble metals in the glass and TiO<sub>2</sub> matrices based thin films can significantly trap the light of a particular wavelength by mean of plasmonic resonance and may be useful for superior photovoltaic and optoelectronic applications.

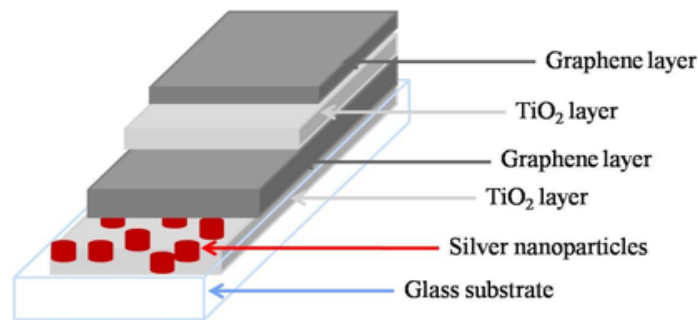


Figure 1: The stacking details of a thin film grown by the spray pyrolysis method.

## 3. Reference

[1] Pham VH, Cuong TV, Hur SH, Shin EW, Kim JS, Chung JS, Kim EJ. *Carbon* 48 (2010) 1945.

# Synthesis, structural, optical and electrical characteristics of nickel oxide thin films by chemical processing methods

**Shadrach Akinkuade<sup>1,2\*</sup>, Jacqueline Nel<sup>1</sup>, Walter Meyer<sup>1</sup>**

<sup>1</sup>Physics Department, University of Pretoria, Pretoria 0002, South Africa

<sup>2</sup>Physics Unit, Science Technology Department, The Federal Polytechnic, Ado-Ekiti, Nigeria

\*Corresponding author e-mail address: u14302552@tuks.co.za

## 1. Introduction

Transparent conductive oxides (TCO) are wide bandgap semiconductors; they are useful in many applications such as transparent electronics, UV photodetectors and solar cells. In these applications, electrical and optical properties of TCOs are combined in a device [1]. Some of the TCOs such as indium tin oxide (ITO) and zinc oxide, which have been studied extensively are n-type semiconductors [2], since it is difficult to achieve p-type conductivity by doping in these materials and rectifying junctions are essential for the study of electrical characteristics of TCOs [3], therefore research efforts are focused on p-type TCO. Nickel oxide (NiO) is a TCO with p-type properties; it has a stable wide bandgap of 3.5 to 4.0 eV [4]. In this work, thin films of NiO are produced from simple and economical methods; chemical bath deposition and spin coating. The films were characterized with scanning electron microscope (SEM) and X-ray Diffraction (XRD) using Co K $\alpha$  radiation. Attempts were made to characterise the heterojunction between NiO and other n-type materials, such ZnO and n-Silicon for optical and electrical properties.

## 2. Results

The porous and wormlike morphology of the film as revealed by SEM is shown in figure 1, figure 2 shows the XRD pattern of the annealed film at different temperatures, this indicates that the films are crystalline. Optical characteristics obtained from Raman spectrometer and UV-VIS spectrophotometer and electrical characteristics of the films will also be discussed.

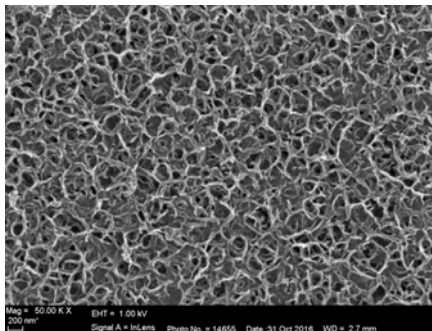


Fig.1 Morphology of NiO thin film with seed layer on glass on glass

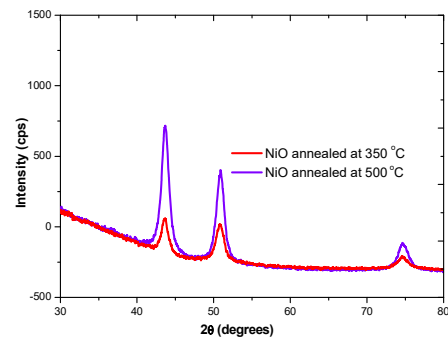


Fig.2 XRD pattern of NiO thin films annealed at different temperatures

## 3. References

- [1] W. Chia-ching and Y. Cheng-fu, *Nanoscale Res. Lett.*, **8(1)** (2013) 1.
- [2] L. Cattin, B. A. Reguig, A. Khelil, M. Morsli, K. Benchouk, and J. C. Bernède, *Appl. Surf. Sci.* **254(18)** (2008) 5814.
- [3] F. D. Auret, L. Wu, W. E. Meyer, J. M. Nel, M. J. Legodi, and M. Hayes, **677(4)** (2004) 674.
- [4] B. A. Reguig, M. Regragui, M. Morsli, A. Khelil, M. Addou, and J. C. Bernède, *Sol. Energy Mater. Sol. Cells* **90(10)** (2006) 1381.



# Structural transformation and enhanced gas sensing characteristics of TiO<sub>2</sub> nanostructures induced by annealing

Zamaswazi Tshabalala<sup>1,2\*</sup>, David Motaung<sup>2</sup>, Hendrik Swart<sup>1</sup>

<sup>1</sup>Department of Physics, University of the Free State, P. O. Box 339, Bloemfontein ZA9300, South Africa

<sup>2</sup>DST/CSIR, National Centre for Nano-structured Materials, Council for Scientific Industrial Research, Pretoria, 0001, South Africa

\*Corresponding author e-mail address: ZTshabalala@csir.co.za

## 1. Introduction

To date, fabrication of low-cost, ultra-sensitive and selective chemiresistive sensors that are able to detect toxic, flammable and explosive gases have become indispensable for environmental monitoring, industrial and biomedical applications [1]. One possible application is an ultra-sensitive gas sensor that can operate at low temperature with high selective to detect the harmful gases, liquids, and chemicals released to the air by industrial wastes, agricultural chemicals, etc. The current promising materials are semiconductor metal oxide-based sensors which have displayed substantial potential by their noticeable change in their electrical resistance upon exposure to either reducing or oxidizing gases. Moreover, metal oxides (MOX) are very stable and they can be easily synthesized in various forms using different synthesis routes (e.g. chemically or in the vapour phase) [2]. Herein, we report on the effect of annealing temperature on the morphology, structure, optical and magnetic properties of TiO<sub>2</sub> nanostructures prepared using microwave assisted hydrothermal method. Upon annealing the nanostructures at various temperatures, their morphology transformed from nanotubes to nanorods. Moreover, their gas sensing behaviour towards NO<sub>2</sub>, H<sub>2</sub>S, CH<sub>4</sub> and CO gases was also investigated and correlated with their defect states and surface area.

## 2. Results

The Focused Ion beam scanning electron microscopy (FIB-SEM) images in Fig.1 display a change in morphology as the annealing temperature was increased to 900 °C. Before annealing (as-synthesized) a web of nanotubes with average diameter of 22 nm was observed. After annealing in air at 900 °C, the nanotubes transformed to “nanorods-like” structures with an average diameter of 87 nm as displayed in the insert of Fig. 1. It was observed that the higher temperature favours the formation of nanorods by virtue of enhanced thermal stability as compared to that of nanotubes. Structural analyses demonstrated a transformation from anatase to rutile upon annealing. Moreover, the rutile percentage improved with annealing temperature. The as-synthesized TiO<sub>2</sub> nanotubes showed a surface area of 124.86 m<sup>2</sup>g<sup>-1</sup>, while those annealed at 450, 700 and 900 °C, disclosed smaller surface areas of 81.73, 13.08 and 2.71 m<sup>2</sup>g<sup>-1</sup> respectively (see Fig. 2). The desorption branch of the isotherm was used to determine the Barrett–Joyner–Halenda (BJH) pore size distributions of the nanostructures, displaying an increase in the pore diameter from 15 nm for the as-synthesized and 24 nm to 74.5 nm for the annealed samples.

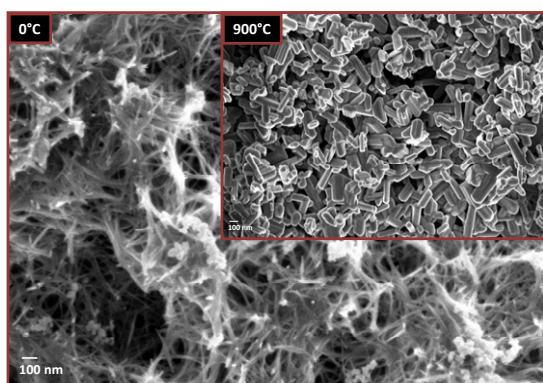


Fig. 1: SEM micrographs of un-annealed TiO<sub>2</sub> nanotubes and those annealed at 900 °C (insert)

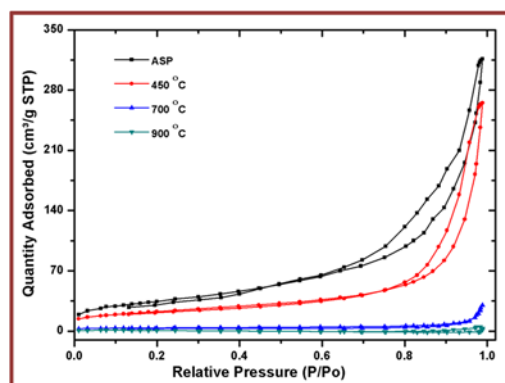


Fig. 2: Nitrogen adsorption isotherms for the TiO<sub>2</sub> nanostructures.

## 3. References

- [1] K. Wetchakun, T. Samerjai, N. Tamaekong, C. Liewhiran, C. Siriwong, V. Kruefu, A. Wisitsoraat, A. Tuantranont, S. Phanichphant. *Sens. Actuators B* **160** (2011) 580.
- [2] Z. Tshabalala, K. Shingange, B. Dhonge, O. Ntwaeaborwa, G. Mhlongo, D. Motaung. *Sens. Actuators B* **238** (2017) 402.

## Abstract number index

Abstract	Delivery	Page				
				#70	Poster 42	p. 84
#2	Oral 1	p. 3		#71	Poster 31	p. 73
#5	Poster 6	p. 48		#72	Poster 69	p. 111
#6	Oral 15	p. 23		#73	Poster 68	p. 110
#7	Invited 8	p. 30		#75	Poster 32	p. 74
#9	Poster 21	p. 63		#76	Poster 44	p. 86
#10	Poster 71	p. 113		#77	Poster 70	p. 112
#11	Invited 5	p. 18		#78	Poster 7	p. 49
#13	Poster 63	p. 105		#79	Poster 52	p. 94
#14	Poster 64	p. 106		#81	Poster 12	p. 54
#15	Invited 2	p. 6		#83	Poster 24	p. 66
#16	Oral 8	p. 12		#84	Poster 17	p. 59
#17	Poster 54	p. 96		#85	Poster 18	p. 60
#19	Poster 47	p. 89		#86	Poster 37	p. 79
#20	Poster 59	p. 101		#88	Poster 8	p. 50
#21	Invited 7	p. 25		#89	Poster 58	p. 100
#22	Oral 4	p. 8		#90	Oral 7	p. 11
#23	Poster 34	p. 76		#91	Poster 15	p. 57
#24	Poster 22	p. 64		#92	Oral 23	p. 36
#25	Poster 3	p. 45		#93	Oral 22	p. 33
#26	Poster 2	p. 44		#94	Poster 13	p. 55
#27	Oral 3	p. 5		#95	Oral 2	p. 4
#31	Oral 10	p. 16		#96	Poster 29	p. 71
#34	Poster 28	p. 70		#97	Poster 50	p. 92
#36	Poster 41	p. 83		#98	Poster 60	p. 102
#37	Poster 27	p. 69		#99	Oral 6	p. 10
#38	Poster 33	p. 75		#100	Poster 55	p. 97
#39	Oral 11	p. 17		#101	Poster 14	p. 56
#40	Poster 74	p. 116		#103	Oral 21	p. 32
#42	Oral 5	p. 9		#105	Poster 40	p. 82
#41	Poster 53	p. 95		#106	Poster 43	p. 85
#44	Poster 51	p. 93		#107	Poster 61	p. 103
#45	Poster 48	p. 90		#108	Oral 17	p. 26
#46	Oral 18	p. 27		#109	Poster 9	p. 51
#48	Poster 5	p. 47		#111	Poster 72	p. 114
#49	Poster 1	p. 43		#112	Oral 14	p. 22
#50	Oral 9	p. 15		#114	Poster 10	p. 52
#51	Poster 49	p. 91		#115	Poster 16	p. 58
#53	Poster 4	p. 46		#116	Poster 65	p. 107
#54	Poster 11	p. 53		#117	Poster 66	p. 108
#55	Poster 19	p. 61		#118	Poster 67	p. 109
#56	Poster 23	p. 65		#119	Oral 12	p. 20
#57	Poster 45	p. 87		#120	Oral 19	p. 28
#58	Poster 38	p. 80		#121	Invited 4	p. 14
#59	Poster 35	p. 77		#122	Poster 39	p. 81
#60	Poster 36	p. 78		#126	Oral 13	p. 21
#61	Poster 57	p. 99		#127	Invited 3	p. 7
#62	Poster 30	p. 72		#128	Invited 10	p. 35
#63	Poster 20	p. 62		#129	Invited 6	p. 19
#64	Poster 73	p. 115		#130	Invited 1	p. 2
#65	Poster 62	p. 104		#131	Invited 9	p. 34
#66	Oral 25	p. 38		#134	Poster 56	p. 98
#67	Oral 20	p. 31		#135	Oral 24	p. 37
#68	Oral 16	p. 24		#136	Poster 25	p. 67
#69	Poster 46	p. 88		#137	Poster 26	p. 68



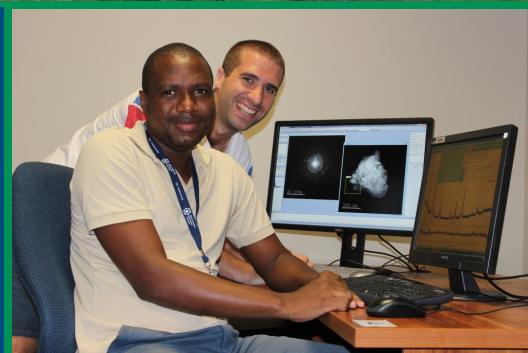
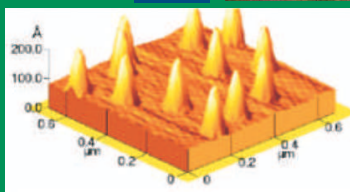
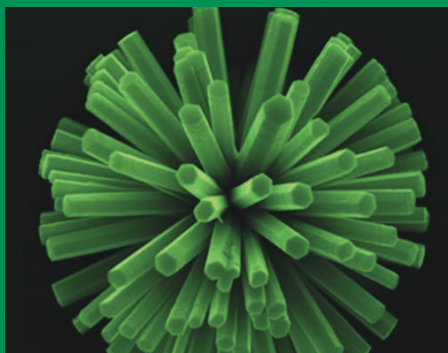
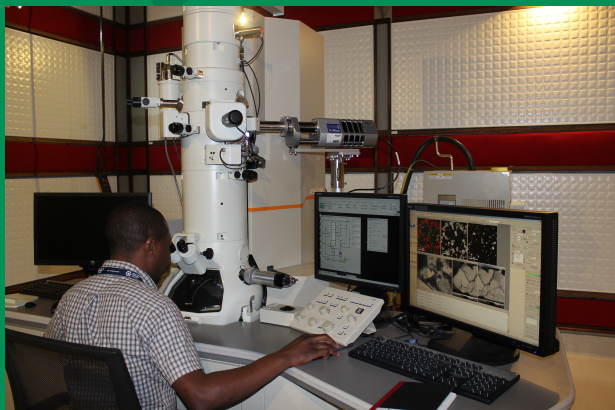
**Nelson Mandela  
Metropolitan  
University**

for tomorrow

Department of

**Physics**

Faculty of Science



### MATERIALS RESEARCH FOR ENERGY TECHNOLOGIES

The Centre for High Resolution Transmission Electron Microscopy (Centre for HRTEM) at NMMU houses four state-of-the-art electron microscopes (EMs) including the only Cs-corrected atomic resolution electron microscope in Africa. The wide range of research projects and MSc and PhD topics include:

- ▶ HRTEM and in situ HRTEM investigation of nanoparticle catalysts
- ▶ Irradiation damage and fission product transport in nuclear reactor fuel cladding materials
- ▶ Accident tolerant coatings on zircaloy nuclear reactor fuel tubes
- ▶ Novel fuel designs for the ESKOM advanced high temperature gas cooled nuclear reactor
- ▶ Refining of weldability limits of creep-aged power plant stainless steel
- ▶ Collaboration with eNtsha (NMMU Mechanical Engineering) for lifetime assessment of high value power plant components
- ▶ Advanced EM characterisation of diamond, Pt, Ti and Al alloys and compound semiconductor structures
- ▶ The Centre collaborates closely with local and international institutions focusing on existing and novel materials for advanced high temperature gas cooled nuclear reactors (AHTRs), pressurised water cooled reactors and coal-fired power plants.

### NANOPHOTONICS

*Nano-sized materials for opto-electronic devices*

- ▶ Nano-science is the major driver of high tech opto-electronics
- ▶ Nano-structures provide novel ways to engineer high efficiency LEDs, laser diodes and sensors
- ▶ "Nano" is "BIG"!

The Physics Department has unique equipment for the synthesis and characterization of semiconductor nano-structures, including a state-of-the-art reactor for semiconductor crystal growth.

We have active collaborations with several local and overseas universities, including groups in Sweden, Germany and the UK.

**WE CURRENTLY DEVELOP:**

- ▶ InAsSb layers and nano-structures for infrared detectors
- ▶ ZnO for high efficiency white LEDs

**EXCITING NEW MASTERS DEGREE IN NANOSCIENCES, PRESENTED JOINTLY BY NMMU AND THREE OTHER SA UNIVERSITIES.**

**CONTACT**

*Prof Jan Neethling*

jan.neethling@nmmu.ac.za

chrtem.nmmu.ac.za

**CONTACT**

*Prof Reinhardt Botha*

reinhardt.botha@nmmu.ac.za

[www.nmmu.ac.za/physics](http://www.nmmu.ac.za/physics)



**Nelson Mandela  
Metropolitan  
University**

for tomorrow

Department of

**Physics**

Faculty of Science



## RENEWABLE ENERGY

### Sustainable Energy for the Future

The Centre for Energy Research is actively involved in various energy research projects, on Photovoltaics, Solar Thermal and Wind Energy. Studies include various renewable energy research projects on different technologies and the development of new characterisation techniques.

The following Applied Physics skills are acquired:

- ▶ LabView programming
- ▶ Data acquisition system design and analysis
- ▶ Computer - equipment interfacing

Future student projects include:

- ▶ Advanced PV characterisation
- ▶ Concentrator PV technology
- ▶ Solar Resource assessment
- ▶ Infrared thermography
- ▶ Electroluminescence studies
- ▶ PV module energy yield monitoring and analysis

#### CONTACT

*Prof Ernest van Dyk*  
ernest.vandyk@nmmu.ac.za

## OPTICAL FIBRE TELECOMMUNICATION RESEARCH

Escalating bandwidth demands fuelled by smartphones, tablet computers, social media, Big data and cloud computing makes Telecommunications an extremely challenging and rewarding field.

The Centre for Broadband Communication at NMMU has one of the best equipped research laboratories in Africa.

We offer an exciting range of MSc and PhD projects featuring:

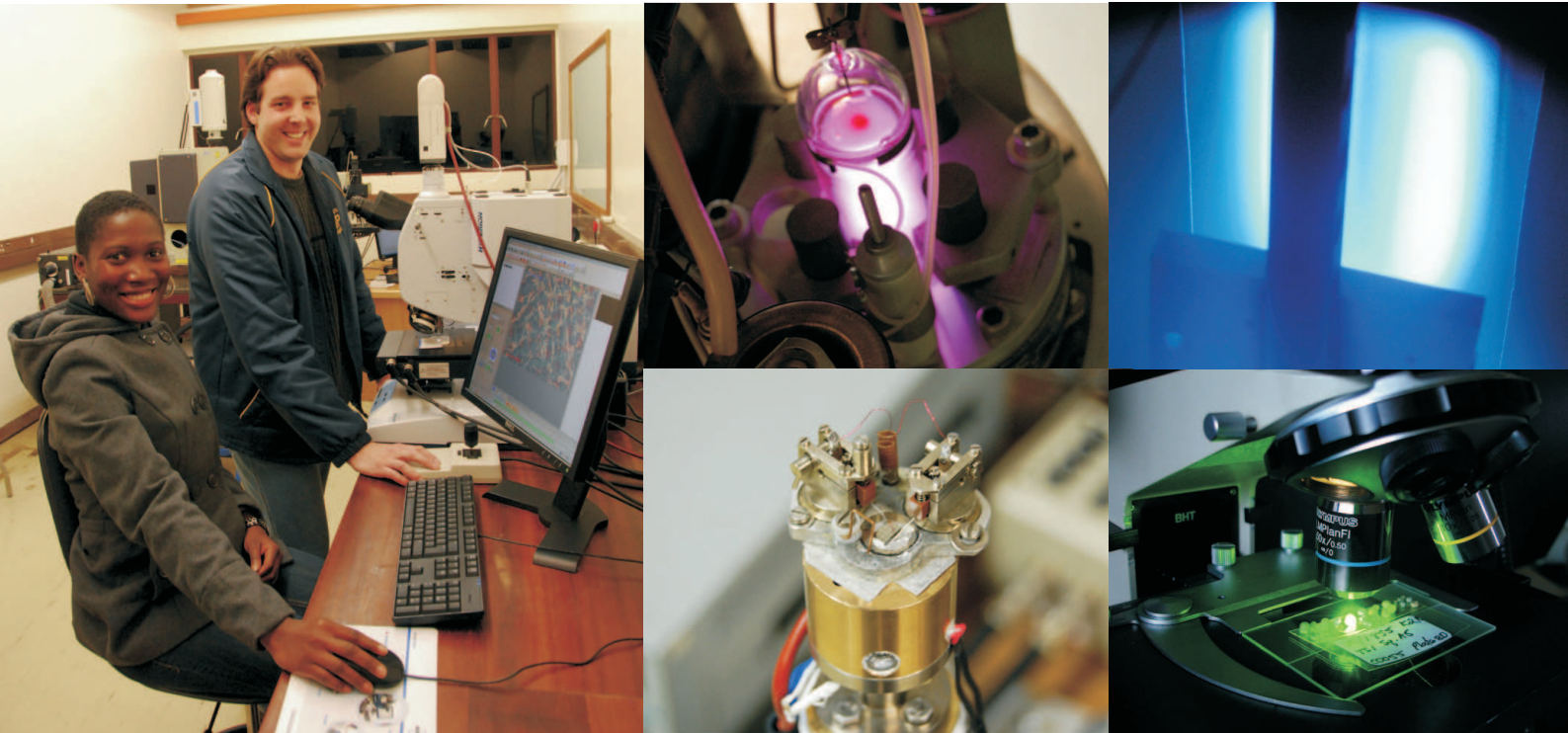
- ▶ Fibre-to-the-home (FTTH) technologies
- ▶ Square Kilometer Array related optical fibre topics
- ▶ Dispersion measurement, compensation and emulation
- ▶ Polarization effects, wavelength division multiplexing, non-linear effects
- ▶ Modelling and simulation, OTDR, fusion splicing, bit error rate testing

Scholarship opportunities are available for good, motivated students.

#### CONTACT

*Prof Tim Gibbon*  
tim.gibbon@nmmu.ac.za

[www.nmmu.ac.za/physics](http://www.nmmu.ac.za/physics)



## We offer postgraduate opportunities in the following research focus areas

### Materials

- Nuclear applications
- Under irradiation
- Solar cells
- Opto-electronics
- Carbon-based
- Nano-magnetism

### Theoretical Physics

- Mathematical physics
- High energy theory
- Quantum resonances theory
- Quantum information theory
- Computational solid state physics
- Symmetries and group theory

### Astronomy

### Biophysics

### Physics Education

### Enquiries about postgraduate studies

Head: Department of Physics  
University of Pretoria  
Private Bag X20, Hatfield, 0028

Email: [Chris.Theron@up.ac.za](mailto:Chris.Theron@up.ac.za)

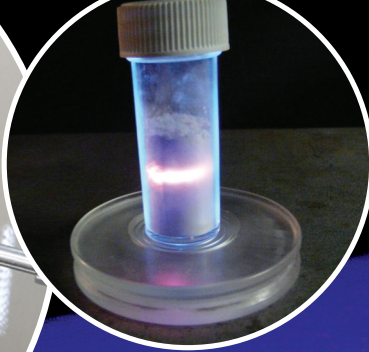
Tel: +27 12 420 2455

Fax: +27 12 362 5288

Web: <http://www.up.ac.za/physics>



UNIVERSITEIT VAN PRETORIA  
UNIVERSITY OF PRETORIA  
YUNIBESITHI YA PRETORIA  
Faculty of Natural and Agricultural Sciences



*Don't stop dreaming.*

# Department of Physics



T: +27(0)51-401 2531 | [natagri@ufs.ac.za](mailto:natagri@ufs.ac.za) | [www.ufs.ac.za/natagri](http://www.ufs.ac.za/natagri)

 UFSUV |  UFSweb |  UFSweb

*Inspiring excellence.  
Transforming lives.*

UNIVERSITY OF THE  
FREE STATE  
UNIVERSITEIT VAN DIE  
VRYSTAAT  
YUNIVESITHI YA  
FREISTATA



UFS·UV

NATURAL AND  
AGRICULTURAL SCIENCES  
NATUUR- EN  
LANDBOUWETENSAPPE